UNIVERSIDADE FEDERAL DO RIO GRANDE DO SUL
GRADUATE PROGRAM IN PHYSICS
DOCTORAL THESIS

Relaxation and quasi-stationary states in systems with long-range interactions *

Fernanda Pereira da Cruz Benetti

Doctoral thesis prepared under the supervision of Professor Yan Levin, co-supervision of Professor Renato Pakter and presented to the Institute of Physics at UFRGS in partial fulfillment of the requirements for obtaining the title of Doctor in Physics.

Porto Alegre
December 2016

*Project financed by the Conselho Nacional de Desenvolvimento Científico e Tecnológico (CNPq) and the Coordenação de Aperfeiçoamento Pessoal de Nível Superior (CAPES).

Acknowledgments

The guidance, patience and encouragement of my supervisors Yan Levin and Renato Pakter is what made this work possible. I sincerely thank them for their help, availability and trust in all aspects of the work.

I owe a great deal to Tarcísio N. Teles, who guided me when I began working on the subject of long-range interactions. Even through times I felt I was locked inside a problem, with no way out, he accompanied my progress to make sure I found a way.

This research has been greatly enriched by my collaboration with Ana Carolina Ribeiro-Teixeira, who I thank for enlightening discussions and who I admire for her dedication to understanding the subjects she applies herself to. Our work together has lead to a friendship which has also contributed, albeit indirectly, to the completion of this thesis.

This work is the culmination not only of four years of PhD research, but of ten years in this University, beginning when I enrolled as an undergraduate student in the Physics course. Therefore, I especially wish to acknowledge the professors whose classes fed my desire to continue in this field and become a researcher: Rita Maria Cunha de Almeida, for my first contact into university-level physics and stimulating my curiosity about science in general; Luiz Fernando Ziebell, for his dedication to teaching thorough and intricate classes, both in the undergraduate and graduate program; Felipe Rizzato, for his wonderfully intuitive classes; Leonardo Brunnet, for introducing me to computational physics (and, memorably, Shannon entropy); Claudio Schneider, whose thermodynamics course was truly engaging and whose words have stuck with me during difficult moments (*aprender dói!*); and Yan Levin for his statistical mechanics course, which was the reason I decided to pursue a graduate degree in this field.

From the Graduate Program, I am grateful to Liane Thier Ruschel for her assistance in navigating through all the necessary procedures and regulamentation during these years. I also thank Samoel Renan Mello da Silva for his crucial and reliable support with the computational clusters.

Outside of UFRGS, I warmly thank Bruno Marcos from the Université Côte d'Azur for having received me with great hospitality at my stay there, and for guiding me and introducing me to a new topic in my research in long-range interacting systems. This project would have suffered without him.

On a personal note, I thank my parents, Antonio and Silvia, for having shown me that the greatest value in life is to try to understand and respect the world around you, whether it be through science, through art, or through music; my sister Lucia, for having chosen the latter while maintaining a passion for science that sometimes surpasses that of her physicist sister, and her courage in following this sometimes tortuous path; my grandmother Enar, who never understood what I was doing but was proud of me anyway.

I am especially grateful to Everton for his companionship and unfaltering encouragement and support; much of this would not have been possible without him. I thank Birba, for her insistant help with my Portuguese; Bibiana, for putting up with me; Beatriz, for her travels; Thales for ten years of good games and great lunches; and Nicole, for reminding me of what's important. For the many small happy moments during these years, I again thank all of the above, as well as Sabrina, Gabriel C., Gabriel M., Tarso, Rafa Rui, and Jessica.

From Nice, I thank Eduard, Liana, and Jean-Baptiste for making me feel at home at the lab, David for the partnership at conferences (and for patiently perusing the Ramanujan Journal) and Lolo for enjoying my adventures; I will always be indebted to their friendship and hospitality.

Finally, I thank Arthur for all of our walking.

Abstract

BENETTI, F. P. C. **Relaxation and quasi-stationary states in systems with long-range interactions**

Thesis (Doctorate) - Physics Institute, Universidade Federal do Rio Grande do Sul, Porto Alegre, 2016.

Systems whose components interact by unscreened long-range forces—for example, stellar systems and non-neutral plasmas—have characteristics that are anomalous with respect to systems with shielded or short-range forces. Besides presenting unique thermodynamic properties such as negative specific heat and inequivalence of ensembles, their dynamics is predominantly collisionless and leads to out-of-equilibrium quasi-stationary states. These states are notoriously difficult to predict given an arbitrary initial condition, and there is still no unified theory to treat them. Thermodynamic equilibrium is reached only after long timescales that increase with the system size and often exceed the lifetime of the universe. Relaxation to equilibrium, therefore, has two timescales: one short, leading to out-of-equilibrium quasi-stationary states, and a second, longer, which leads to thermodynamic equilibrium. In this thesis, we examine these phenomena by applying theoretical models and numerical simulation for different long-range interacting systems, including a model of classical XY-type spins with long-range interactions, and the self-gravitating system in three dimensions. In a second stage we study the collisional relaxation to thermodynamic equilibrium through kinetic equations and numerical simulation. We thus seek to clarify the mechanisms behind the quasi-stationary states and collisional relaxation.

Keywords: Long-range interactions, quasi-stationary states, self-gravitating systems, HMF model, Vlasov equation, Boltzmann equation.

Resumo

BENETTI, F. P. C. **Relaxação e estados quasi-estacionários em sistemas com interações de longo alcance**

Tese (Doutorado) - Instituto de Física, Universidade Federal do Rio Grande do Sul, Porto Alegre, 2016.

Sistemas cujos componentes interagem por meio de forças de longo alcance não-blindadas—por exemplo, sistemas estelares e plasmas não-neutros—têm algumas características anômalas em relação a sistemas com forças blindadas ou de curto alcance. Além de apresentarem características termodinâmicas peculiares como calor específico negativo e inequivalência de ensembles, sua dinâmica é predominantemente não-colisional e leva à estados quasi-estacionários fora de equilíbrio. Esses estados são notoriamente difíceis de prever dada uma condição inicial qualquer, e ainda não existe uma teoria unificada para tratá-los. O equilíbrio termodinâmico é atingido somente após tempos longos que escalam com o tamanho do sistema, muitas vezes excedendo o tempo de vida do universo. A relaxação para o equilíbrio, portanto, tem duas escalas de tempo: uma, curta, que leva a estados quasi-estacionários fora de equilíbrio, e a segunda, longa, que leva ao equilíbrio termodinâmico. Nesta tese de doutorado, examinamos esses fenômenos aplicando modelos teóricos e simulação numérica para diferentes sistemas de interação de longo-alcance, incluindo um modelo de spins clássicos tipo XY com longo alcance, e o sistema auto-gravitante em três dimensões. Em uma segunda etapa, estudamos a relaxação para o equilíbrio termodinâmico, a relaxação colisional, através de equações cinéticas e simulação numérica. Desta forma, buscamos esclarecer os mecanismos por trás dos estados quasi-estacionários e da relaxação colisional.

Palavras-chave: Interações de longo alcance, estados quasi-estacionários, sistemas auto-gravitantes, modelo HMF, equação de Vlasov, equação de Boltzmann.

Contents

List of Publications

This list contains all of the journal articles in which I am a co-author, published (or submitted for publication) during my graduate research.

- BENETTI, F. P. C., Teles, T. N., Pakter, R., and Levin, Y., "Ergodicity breaking and parametric resonances in systems with long-range interactions", *Physical Review Letters* **108** 140601 (2012).[1]

- Teles, T. N., BENETTI, F. P. C., Pakter, R., and Levin, Y., "Nonequilibrium phase transitions in systems with long-range interactions", *Physical Review Letters* **109** 230601 (2012).[1]

- Pikovsky, A., Gupta, S., Teles, T. N., BENETTI, F. P. C., Pakter, R., Levin, Y., and Ruffo, S., "Ensemble inequivalence in a mean-field XY model with ferromagnetic and nematic couplings", *Physical Review E* **90** 062141 (2014).

- Ribeiro-Teixeira, A. C., BENETTI, F. P. C., Pakter, R., and Levin, Y., "Ergodicity breaking and quasistationary states in systems with long-range interactions", *Physical Review E* **89** 022130 (2014).

- Levin, Y., Pakter, R., Rizzato, F. B., Teles, T. N., and BENETTI, F. P. C., "Nonequilibrium statistical mechanics of systems with long-range interactions", *Physics Reports* **535** 1 (2014).

- BENETTI, F. P. C., Ribeiro-Teixeira, A. C., Pakter, R., and Levin, Y., "Nonequilibrium stationary states of 3D self-gravitating systems", *Physical Review Letters* **113** 100602 (2014).

- Antunes, F. L., BENETTI, F. P. C., Pakter, R., and Levin, Y., "Chaos and relaxation to equilibrium in systems with long-range interactions", *Physical Review E* **92** 052123 (2015).

- BENETTI, F. P. C. and Marcos, B., "Collisional relaxation in the inhomogeneous Hamiltonian mean-field model: Diffusion coefficients", *Physical Review E* **95** 022111 (2017).

[1] Works published during my Masters degree, included here for the sake of completeness of the research project

List of Abbreviations

LRI	long-range interaction
QSS	quasi-stationary state
HMF	Hamiltonian Mean Field
LB	Lynden-Bell
IM	integrable model
CH	core-halo
MD	molecular dynamics
WB	water-bag
MLWB	multilevel water-bag
GVC	generalized virial condition
LenBal	Lenard-Balescu
MDfull	Molecular dynamics of full Hamiltonian system
MDbath	Molecular dynamics of test particles in thermal bath

Chapter 1

Introduction

Given a system composed of many bodies and their laws of interaction, the fundamental goal of thermodynamics and statistical mechanics is to determine the stationary state that the system will evolve to, starting from an initially perturbed configuration. Ruelle states that "[...] *the main problem of statistical mechanics is to study the infinite system equilibrium states and their relation to the interactions which give rise to them*" [1]. For most of the systems dealt with by these disciplines, the transitional period from the perturbed state (that is, out of equilibrium) to the stable stationary state (equilibrium) is very fast compared to our macroscopic observation times [2]. This is the case for systems whose particles interact by short-range forces. In fact, Ruelle goes on to declare the restriction "[...] *each subsystem has a negligible interaction with the subsystems which are far away*"[1] [1]. Perturbations quickly die out as neighborhoods thermalise in an exponentially fast process. Naturally, the state of interest for researchers is then the equilibrium state, which is very successfully described by these theories.

In this thesis, on the other hand, we focus on interactions which are *long-ranged*. Typically, a system is defined as having long-range interactions (LRI) if the interaction potential between pairs of particles, ϕ, decays as $\phi \sim 1/r^{\alpha}$, where r is the interparticle distance and α is a constant that satisfies $\alpha < d$, d being the dimension of the embedding space [3]. For example, gravity and Coulomb interactions both have an exponent $\alpha = 1$ for dimension $d = 3$, and are thus long-ranged. The long-range nature of the interaction means that the particles dynamics is dominated by the mean-field, and not by nearest-neighbor interactions, as in the short-range case. This leads to many peculiar characteristics from both a dynamical and statistical equilibrium point of view, including long-lived quasi-stationary nonequilibrium states [3, 4], anomalous diffusion [5, 6], inequivalence of ensembles [7–9], negative specific heat [10–12], and strange critical exponents [13].

Despite being ubiquitous in nature, these systems remain a challenge due to these dynamical and equilibrium features. In recent years, they have been the object of intense interest in the statistical mechanics community, involving work in fields as diverse as stellar and

[1] In his terminology, a *subsystem* is equivalent to a particle moving through space.

galactic dynamics in astrophysics [14–16], non-neutral plasmas [17], vortices in fluid dynamics [18], cold atom clouds [19], and other quantum systems [20, 21]. Furthermore, they are studied using a range of different theoretical methods, from equilibrium statistical mechanics techniques, such as large deviation theory [22, 23] to dynamics, such as analysis of the stability of the Vlasov equation [4, 24, 25]. Only recently have these fields begun to merge under the denomination of statistical mechanics of long-range interactions, resulting in several reviews [3, 26, 27]. Although significant advances have been made, a coherent, unified theory is still lacking.

The greatest obstacle to a unifying theory is the different mechanisms underlying the relaxation process. If interparticle forces are long-ranged, thermalisation is not exponentially fast. Intuitively, we may consider that we can no longer apply the picture of small thermalised neighborhoods of particles, which in turn equilibrate with each other, because each particle interacts with others that can be very far away, leading to collective effects. Due to the predominance of the mean-field over pair interactions, the dynamics becomes effectively collisionless. Only finite size effects, or correlations, drive the system to thermodynamic equilibrium. The greater the number of particles in the system, the longer the time necessary for the equilibrium state to be achieved. Nevertheless, other stable configurations arise, resulting from stationary solutions of the long-range dynamics.

The existence of the nonequilibrium state is due to the collisionless nature of the long-range dynamics. The force on one particle of a many-body system is the result of its interaction with all other particles in the system. These interactions do not shortly die out with distance, as in the short-range case. Therefore, the mean-field becomes much more important to the particle's dynamics than its interactions with its neighbors. A simple illustration of this statement in the context of astrophysics can be found in reference [28]: taking a homogeneous mass distribution inside a certain volume, we can compare the force exerted on a stellar mass at a point a in the volume by masses at different distances from a. Taking the infinitesimal volume element of a solid angle Ω located at a distance r from point a, the amount of mass it encloses is $\mathrm{d}\Omega\, r^2 \mathrm{d}r$. The force that the mass enclosed in the radial interval $[r_1,r_2]$ in the solid angle volume $\mathrm{d}\Omega$ exerts on point a is proportional to $\mathrm{d}\Omega \int_{r_1}^{r_2} r^2/r^2 \mathrm{d}r = \mathrm{d}\Omega(r_2 - r_1)$. As this force grows with interval in r, clearly the mass enclosed in larger distances is more important to the dynamics than close neighbors. In the limit $N \to \infty$, the dynamics is completely dominated by the mean-field, and the particle trajectories can be considered as that of particles evolving in a smooth potential. For finite systems, fluctuations cause correlations between particles, which influence the dynamics on very long timescales.

Typically, these two contributions—*(i)* the mean field and *(ii)* the "collisions", which are, more accurately, the correlation between a particle and its neighbors—scale as 1 and $1/N$, respectively, where N is the number of particles. In the thermodynamic limit, $N \to \infty$, the correlations are completely negligible and the dynamics is collisionless. It therefore cannot be described by the typical collisional Boltzmann equation, and is instead determined by

the collisionless Boltzmann equation (or Vlasov equation, as it is known in plasma physics). The stationary solutions of the collisionless Boltzmann equation are not necessarily Maxwell-Boltzmann equilibrium, and are not described by traditional thermodynamics and statistical mechanics. Dynamical aspects must be taken into account and other tools must be developed.

Eventually, the $1/N$ contributions will drive the system towards thermodynamic equilibrium. This process is known as *collisional* relaxation[2]. For this reason, the nonequilibrium stationary states are known as quasi-stationary states (QSS): for any finite N, the microcanonical entropy will increase. Nevertheless, the lifetime of the QSS scales as N^{δ}, where δ depends on the system under consideration. For many physical systems, such as elliptical galaxies, this timescale can be longer than the age of the universe itself [14]. The QSS is of much higher interest than the thermodynamic equilibrium state in such cases, distinguishing them from the typical short-range systems treated by traditional statistical mechanics.

1.1 Definition and examples of long-range interactions

We have defined long-range interactions as those resulting from potentials that decay as $\phi \sim 1/r^{\alpha}$. The condition $\alpha < d$ ensures that the potential is nonintegrable in the sense that if we integrate a distribution of particles over a volume, the potential energy will diverge as the volume increases.

It is important to note that other definitions of LRI exist. For example, some authors propose the use of the force instead of the potential in order to classify LRI [29,30]. The same argument of nonintegrability can be made using the force. This results in a dynamical classification of LRI, and indicates that $\alpha < d-1$. The objective of the dynamical classification is to emphasize that the QSS is the result of the system's dynamics, and that arguments about nonintegrability of the potential and the resulting nonadditivity of the internal energy are more suited to thermodynamics and equilibrium statistics than to the study of QSS. One advantage of this classification is that it determines how a LRI system is affected by its short-range properties: in the limiting case where $d-1 < \alpha < d$ (that is, thermodynamically long-range but dynamically short-range), the existence of a QSS depends on the characteristics of the interaction at short-range, unlike dynamically long-range systems which always exhibit a QSS.

Yet another definition has been used in spin systems. In this case, long-range potentials have been defined as decaying with $1/r^{d+\sigma}$, with $0 < \sigma < 2$ for $d > 2$ [31]. The critical exponents of systems with these potentials are different from those of short-range systems.

While all the above definitions are valid, and certainly imply in interesting findings, it is the first definition, $\alpha < d$, that we use in this work. It is sufficiently strong for the methods we use and the theory we describe. Many examples of physical systems fall under this definition.

[2] We emphasize that the term collisional can be misleading since there are no hard collisions such as in a hard-sphere gas model, and only interparticle correlations. However, we will use this terminology since it is commonplace in the literature.

Of the fundamental forces, as cited above, both gravitational and Coulomb systems are LR. Under the first category fall galaxies and globular clusters, where the "particles" are stars or groups of stars, and even the dynamics of the large-scale structure of the universe, where the "particles" can be the galaxies themselves, as well as dark matter. For the latter, we may consider any non-neutral plasma, where the Coulomb interaction is not shielded by the presence of particles of opposite charge. This includes magnetically confined ion beams, for example.

Many systems present effective LRI, despite not necessarily having a fundamental long-range force. A fluid with two-dimensional turbulence can be discretized into vortices which interact through an effective logarithmic potential, which is long-range in two dimensions [18]. Another effective logarithmic potential occurs in colloids at interfaces. By deforming the interface, the colloids may induce an effective potential $V(r) \sim \ln(r/\lambda)$ where λ is the capillary length [32]. Both these system thus mimic the behavior of gravitational systems in two dimensions, which have a logarithmic pair potential. In the case of colloids, the analogy may be made between the deformation of the interface and the gravitational potential; the capillary length with a screening of the potential, and the vertical force with the mass. This analogy even results in an analogous "Jeans' length": in a stellar system, the Jeans' length corresponds to the minimum necessary size for it to remain stable, given a certain kinetic energy [28]. For the capillary system, there exists a maximum system size for which perturbations in homogeneous distributions are stable, analogous to the Jeans' length. Yet another gravity analogue is the Bose-Einstein condensate configuration proposed in reference [20], which has an effective $1/r$ attractive potential between atoms.

Other examples of effective long-range forces include wave-particle systems, where the interaction of the particle with a wave can be an effective LRI, and and cold atom clouds, where no long-range potential exists yet long-range forces still emerge. An example of the former includes the free electron laser [33, 34], which has been extensively studied recently by the LRI community [35, 36]. Regarding the latter, cold atoms in cavities and magneto-optical traps can exhibit both an effective Coulomb force due to photon diffusion as well as an effective gravitational force, known as the shadow effect, from the decrease of laser intensity as it enters the atomic cloud [19, 37].

Many spin models are also long-range: long-range Ising models have been used to study the propagation of correlation in quantum systems [21] as well as interactions between excitations in systems of trapped ions [38]. The Hamiltonian-Mean-Field (HMF) model, one of the most thoroughly studied LRI systems, is a long-range XY model [39]. It has been applied as a toy model analogous to the free electron laser [36] and for investigating bar formation in galactic disks [40]. It is also equivalent to the first Fourier mode of a one-dimensional gravitational system [41].

The above examples emphasize the how pervasive LRI systems are in nature. Despite their very different physical origins, they display a universality peculiar to LRI systems, such as steady states with non-Maxwell-Boltzmann momentum distributions.

1.2 Organization of the thesis

The subject of research of this thesis is the collisionless and collisional relaxation of LRI systems. The two following chapters are dedicated to a revision of these processes. In chapter 2, we present the principal ideas of collisionless relaxation and the different characterizations of quasi-stationary states. Chapter 3 contains a description of the collisional relaxation process and characteristics of the thermodynamic equilibrium states of LRI systems.

Following this revision, the next chapters present our published works on the subjects. The chapters are organized by the specific LRI system that was studied. Each begins with an introduction to the system, followed by sections summarizing the published work. At the end of each section is the corresponding paper. Chapter 4 is the Hamiltonian Mean Field (HMF) model, a paradigmatic spin model [39, 42]. The work is a continuation of research done during my Masters degree, in which we found conditions for which certain theories of quasi-stationary states (presented in section 2.3) are valid. This work is shown in section 4.1. The next publication, section 4.2, generalizes this analysis to different initial conditions and further probes the quasi-stationary states by comparing results from a different theory. The publications of the last two sections, 4.3 and 4.4, are dedicated to the collisional relaxation to equilibrium. Chapter 5 is the generalized Hamiltonian Mean Field (GHMF) model, which is a long-range version of an isotropic XY model [43,44]. This chapter contains two sections, corresponding to publications about nonequilibrium (section 5.1) and equilibrium (section 5.2) phase transitions. Chapter 6 corresponds to spherically-symmetric three-dimensional self-gravitating systems, and contains one publication on collisionless quasi-stationary states (section 6.1), in which we perform a similar analysis as that of the HMF model in section 4.2. A review of most of the work on LRI systems done by our group is presented in chapter 7. My research in this review consists of our work done with the HMF and GHMF model. Finally, chapter 8 presents a summary and the conclusions of the thesis.

Chapter 2

Collisionless dynamics and relaxation

The existence of quasi-stationary states and the separation of the relaxation process in two different timescales is due to the collisionless nature of the dynamics of LRI systems. The total force on any given particle is determined by the collective contribution of all other particles, which predominates over the individual contributions of particles in its close neighborhood. The "collisional" relaxation—thus called in analogy with the collisional relaxation of short-range systems—occurs only due to fluctuations, residual correlations and other finite-size effects. The predominance of the mean-field potential in the dynamics can be estimated qualitatively by examining the *coupling parameter* Γ of plasma physics, which is the ratio of the potential energy between neighboring particles, u_{neigh}, and the average kinetic (thermal) energy $\mathcal{K}$ [27],

$$\Gamma = \frac{u_{\text{neigh}}}{\mathcal{K}}. \tag{2.1}$$

For a LR potential $\phi(r)$ as defined in chapter 1,

$$\phi(r) \sim \frac{g}{r^\alpha}, \quad \alpha < d, \tag{2.2}$$

the typical potential energy between two neighboring particles will be proportional to $\lambda^{-\alpha}$, where λ is the typical separation between particles. For N particles occupying a volume V of radius R, we can estimate λ as $\lambda \sim (V/N)^{1/d} = R/N^{1/d}$. Then, u_{neigh} will scale as

$$u_{\text{neigh}} \sim \frac{g}{\lambda^\alpha} = \frac{gN^{\alpha/d}}{R^\alpha} \tag{2.3}$$

where g is the coupling constant, for example the square of the particle mass m or charge q in gravity and Coulomb, respectively. Taking gravity as an example, $g = m^2$, and

$$\Gamma = \frac{u_{\text{neigh}}}{\mathcal{K}} \sim \frac{mN^{\alpha/d}}{R^\alpha \langle v^2 \rangle}. \tag{2.4}$$

As we will see further on in section 2.2, we may estimate how $\langle v^2 \rangle$ scales as a function of R and the total mass $M = mN$ using the virial theorem. According to this theorem, for

gravitational systems in d dimensions $2\langle\mathcal{K}\rangle = \alpha GM^2/R^\alpha$. For example, in three dimensions $\alpha = -1$ and we recover the famous relation $2\mathcal{K} = -U$. Thus, in a stationary state,

$$\begin{aligned}\Gamma &\sim \frac{mN^{\alpha/d}}{R^\alpha}\frac{R^\alpha}{M} \\ &\sim N^{\alpha/d-1}.\end{aligned} \tag{2.5}$$

Since $\alpha < d$, Γ vanishes in the limit $N \to \infty$, meaning that the interactions between pairs of particles is negligible compared to the particle's kinetic energy. In this limit, the mean field dominates completely and pair correlations are unimportant, leading to the "collisionless" dynamics.

The parameter Γ compares the potential energy of the pair interaction with the mean kinetic energy. We may instead also look at the mean potential energy, $\mathcal{U}$. Continuing with the example of gravity, $\mathcal{U}$ scales as M^2/R^α. By increasing the number of particles in the system, the total mass M also grows, and therefore so does $\mathcal{U}$. From the result of the virial theorem seen above, if $\mathcal{U}$ increases, so does $\langle v^2\rangle$, leading to extremely high velocities for $N \to \infty$. Therefore, both $\mathcal{U}$ and $\mathcal{K}$ diverge as $N \to \infty$ in long range systems.

In order to establish a useful scaling in the dynamics, so that the kinetic and potential terms scale similarly without very high velocities, the typical procedure is to rescale the interaction by some factor dependant of N, known as the Kac prescription [45, 46]. For gravitational systems, this consists in simply rescaling the particle mass m by $1/N$[1]. When N tends to infinity, the pair interaction effectively tends to zero, and the only force felt by each particle is that of the mean-field. For finite N, eventually pair correlations will drive the system away from the collisionless steady state, in the *collisional* relaxation process.

In the next sections of this chapter, we will discuss the first of these two processes, in terms of the dynamics and of the stationary solutions. We address why LRI dynamics is collisionless and describe types of quasi-stationary states.

2.1 Collisionless relaxation

Collisionless relaxation is the first step in the relaxation process of LRI systems. It is a consequence of the dynamics governed by the collisionless Boltzmann equation, also known as the Vlasov equation in plasma physics,

$$\begin{aligned}\frac{D}{Dt}f(\mathbf{r},\mathbf{p},t) &= \left(\frac{\partial}{\partial t} + \frac{\mathbf{p}}{m}\cdot\nabla_\mathbf{r} - \nabla\psi(\mathbf{r},t)\cdot\nabla_\mathbf{p}\right) f(\mathbf{r},\mathbf{p},t) = 0, \\ \psi(\mathbf{r},t) &= \int \mathrm{d}\mathbf{r}'\mathrm{d}\mathbf{p}'\phi(\mathbf{r}-\mathbf{r}')\, f(\mathbf{r}',\mathbf{p}',t)\end{aligned} \tag{2.6}$$

[1] Observing the ratio $\Gamma \sim N^{\alpha/d-1}$, the $1/N$ scaling might not seem to be the most appropriate; however, in order to estimate the ratio, we consider a homogeneous particle distribution, which is not usually the case for LRI systems. This scaling will be discussed in more detail in section 3.1

where $f(\mathbf{r},\mathbf{p},t)$ is the smooth one-particle distribution function, or probability density of finding a particle in the $2d$-dimensional infinitesimal phase space volume $dz = \mathrm{d}\mathbf{r}\,\mathrm{d}\mathbf{p}$, $\nabla_{\mathbf{p}} = \frac{\partial}{\partial p_x}\hat{i}+\frac{\partial}{\partial p_y}\hat{j}+\frac{\partial}{\partial p_z}\hat{k}$, $\psi(\mathbf{r},t)$ is the convolution potential and $\phi(\mathbf{r}-\mathbf{r}')$ is the interaction potential. The operator D/Dt on the left hand side of equation (2.6) is the convective derivative. It gives the variation in time of a quantity $a(\mathbf{r},\mathbf{p},t)$, where the coordinates $\mathbf{r}$ and $\mathbf{p}$ are Lagrangian as opposed to Eulerian—they indicate the position and momentum of an element of a as it evolves along the flow of a.

This dynamics differs significantly from that of the usual systems dealt with in statistical mechanics, which obey the collisional Boltzmann equation [47],

$$\frac{D}{Dt}f(\mathbf{r},\mathbf{p},t) = \left(\frac{\partial f(\mathbf{r},\mathbf{p},t)}{\partial t}\right)_{\mathrm{col}}. \tag{2.7}$$

The collisional term $\left(\frac{\partial f(\mathbf{r},\mathbf{p},t)}{\partial t}\right)_{\mathrm{col}}$ is associated with the change in the probability of finding a particle in the phase space volume dz due to hard-sphere collisions. Of course, for a potential $\psi(\mathbf{r},t)$ which decays as a power-law, there are contact collisions are rare. Any change in the probability density at a flow element is caused by correlations with other particles due to discrete pair interactions.

2.1.1 Revision of kinetic theory

To understand why LRI systems obey the Vlasov instead of the Boltzmann equation, we must return to a fundamental description of the Hamiltonian system. Therefore, in this subsection we will present a review of kinetic theory based on reference [48].

Let us take a system of N particles embedded in a d-dimensional space. The particles have canonical coordinates of position and conjugate momentum given by $\{\mathbf{r}_i\}_1^N$ and $\{\mathbf{p}_i\}_1^N$, respectively, where $\mathbf{r}$ and $\mathbf{p}$ are each d-dimensional vectors. The evolution of the system of particles is determined by a Hamiltonian $\mathcal{H}(\{\mathbf{r}_i\}_1^N,\{\mathbf{p}_i\}_1^N;t)$ which gives Hamilton's equations of motion

$$\frac{\partial \mathbf{r}_i}{\partial t} = \frac{\partial \mathcal{H}}{\partial \mathbf{p}_i}, \tag{2.8a}$$

$$\frac{\partial \mathbf{p}_i}{\partial t} = -\frac{\partial \mathcal{H}}{\partial \mathbf{r}_i},. \tag{2.8b}$$

The initial coordinates $\left(\{\mathbf{r}_i(t=0)\}_1^N,\{\mathbf{p}_i(t=0)\}_1^N\right)$ together with the above equations completely determine the state of the system at any time t.

Equivalently, instead of considering the N coordinates of the particles evolving in a $2d$-dimensional phase space, we may take instead Nd-dimensional vectors R and P,

$$\begin{aligned}\mathbf{R} &= \{R_i\}_1^{Nd} = (R_1,\ldots,R_{Nd}),\\ \mathbf{P} &= \{P_i\}_1^{Nd} = (P_1,\ldots,P_{Nd}).\end{aligned} \tag{2.9}$$

When $\mathbf{r}_i = (R_i,\ldots,R_{i+d})$ and $\mathbf{p}_i = (P_i,\ldots,P_{i+d})$ for all $i \in [1,N]$, the vectors $\mathbf{R}$ and $\mathbf{P}$ represent the state of the system at that moment. Now, it is possible to define a probability density $f_N(\mathbf{R},\mathbf{P},t)$ of finding the system at a $2dN$-dimensional infinitesimal volume $\mathrm{d}\mathbf{R}\mathrm{d}\mathbf{P}$ at time t.

For a conservative system, the integral over phase space of $f_N(\mathbf{R},\mathbf{P},t)$ must be equal to one: the system does not lose nor gain any particles, and must be located somewhere in the phase space at all times. Thus,

$$\int \mathrm{d}\mathbf{R}\mathrm{d}\mathbf{P}\, f_N(\mathbf{R},\mathbf{P},t) = 1, \forall t. \tag{2.10}$$

According to Liouville's theorem, this probability is conserved through any trajectory in phase space. Its convective derivative must be equal to zero,

$$\frac{Df_N(\mathbf{R},\mathbf{P},t)}{Dt} = \frac{\partial f_N}{\partial t} + \sum_{i=1}^{N}\left[\frac{\partial f_N}{\partial R_i}\dot{R}_i + \frac{\partial f_N}{\partial P_i}\dot{P}_i\right] = 0, \tag{2.11}$$

where from this point forward we use R_i and P_i as notation representing all the d coordinates of the particle i: $(R_i,\ldots,R_{i+d})$ now becomes simply R_i, and $(P_i,\ldots,P_{i+d})$ is P_i. Using Hamilton's equations of motion, equation (2.11) can be written also as

$$\frac{\partial f_N}{\partial t} = \sum_{i=1}^{N}\left[\frac{\partial \mathcal{H}}{\partial R_i}\frac{\partial f_N}{\partial P_i} - \frac{\partial \mathcal{H}}{\partial P_i}\frac{\partial f_N}{\partial R_i}\right] \tag{2.12}$$

or, more simply,

$$\frac{\partial f_N(\mathbf{R},\mathbf{P},t)}{\partial t} = \mathrm{L}\, f_N(\mathbf{R},\mathbf{P},t), \tag{2.13}$$

where L is the Liouville operator,

$$\mathrm{L} = \sum_{i=1}^{N}\left\{\frac{\partial \mathcal{H}}{\partial R_i}\cdot\frac{\partial}{\partial P_i} - \frac{\partial \mathcal{H}}{\partial P_i}\cdot\frac{\partial}{\partial R_i}\right\}, \tag{2.14}$$

Equation (2.13) is the Liouville equation, and it determines the evolution of the probability density $f_N(\mathbf{R},\mathbf{P},t)$ in phase space. For a Hamiltonian of the form

$$\mathcal{H} = \mathcal{H}_{\mathrm{kin}} + \mathcal{H}_{\mathrm{ext}} + \mathcal{H}_{\mathrm{int}}, \tag{2.15}$$

where $\mathcal{H}_{\mathrm{kin}}$, $\mathcal{H}_{\mathrm{ext}}$ and $\mathcal{H}_{\mathrm{int}}$ are the kinetic, external and interparticle potential terms, respec-

tively, the Liouville operator can be written as

$$\mathrm{L} = \sum_i (\mathrm{L}^i_{\mathrm{kin}} + \mathrm{L}^i_{\mathrm{ext}}) + \sum_i \sum_{j<i} \mathrm{L}^{ij}_{\mathrm{int}}, \tag{2.16}$$

$$\mathrm{L}^i_{\mathrm{kin}} = -\frac{\partial \mathcal{H}_{\mathrm{kin}}}{\partial P_i} \cdot \frac{\partial}{\partial R_i}, \tag{2.17}$$

$$\mathrm{L}^i_{\mathrm{ext}} = \frac{\partial \mathcal{H}_{\mathrm{ext}}}{\partial R_i} \cdot \frac{\partial}{\partial P_i}, \tag{2.18}$$

$$\mathrm{L}^{ij}_{\mathrm{int}} = \frac{\partial \phi(R_{ij})}{\partial R_i} \cdot \left(\frac{\partial}{\partial P_i} - \frac{\partial}{\partial P_j} \right), \tag{2.19}$$

where $\phi(R_{ij})$ is the interaction potential between a particle with $\mathbf{r} = R_i$ and a particle with $\mathbf{r} = R_j$.

The Liouville equation and the probability density $f_N(\mathbf{R},\mathbf{P},t)$ describe the evolution of the N-body system exactly. It is, however, very difficult to deal with, since it describes the evolution of an $2dN$-dimensional function. In an attempt to simplify this treatment, we may define *reduced* distribution functions by integrating over some degrees of freedom. For example, instead of dealing with the probability of finding the N particles in the $2Nd$-dimensional volume $\mathrm{d}\mathbf{R}\mathrm{d}\mathbf{P}$, we can look for the probability of finding *one* particle in the $2d$-dimensional volume $\mathrm{d}\mathbf{r}_1\mathrm{d}\mathbf{p}_1$ by integrating over all degrees of freedom except one,

$$f_1(\mathbf{r}_1,\mathbf{p}_1,t) = N \int \prod_{i=2}^{N} \mathrm{d}\mathbf{r}_i \mathrm{d}\mathbf{p}_i f_N(\mathbf{R},\mathbf{P},t). \tag{2.20}$$

In the same manner, we can define the probability of finding one particle in $\mathrm{d}\mathbf{r}_1\mathrm{d}\mathbf{p}_1$ and a second particle in $\mathrm{d}\mathbf{r}_2\mathrm{d}\mathbf{p}_2$,

$$f_2(\mathbf{r}_1,\mathbf{p}_1,\mathbf{r}_2,\mathbf{p}_2,t) = N(N-1) \int \prod_{i=3}^{N} \mathrm{d}\mathbf{r}_i \mathrm{d}\mathbf{p}_i f_N(\mathbf{R},\mathbf{P},t) \tag{2.21}$$

and so on.

Thus, from the distribution $f_N(\mathbf{R},\mathbf{P},t)$, the s-particle reduced distribution functions $f_s(\{\mathbf{r}\}^s_1,\{\mathbf{p}\}^s_1)$ are defined as

$$f_s(\{\mathbf{r}\}^s_1,\{\mathbf{p}\}^s_1) = \frac{N!}{(N-s)!} \int \mathrm{d}\mathbf{r}_{s+1} \cdots \mathrm{d}\mathbf{r}_N \mathrm{d}\mathbf{p}_{s+1} \cdots \mathrm{d}\mathbf{p}_N f_N \left(\{\mathbf{r}\}^N_1,\{\mathbf{p}\}^N_1; t \right). \tag{2.22}$$

If all particles were uncorrelated, the reduced distribution functions could be written as a product of one-particle distribution functions, $f_s = \prod_{i=1}^{s} f_1$. However, this is not generally true. Instead, they may be written as a product of one-particle distribution functions plus

correlation functions $c_s(\{\mathbf{r}\}_1^s,\{\mathbf{p}\}_1^s)$. For example, for f_2 and f_3 we may write

$$f_2(1,2) = f_1(1)f_1(2) + c_2(1,2), \tag{2.23}$$

$$f_3(1,2,3) = f_1(1)f_1(2)f_1(3) + f_1(1)c_2(2,3) + f_1(2)c_2(1,3) + f_1(3)c_2(1,2) + c_3(1,2,3) \tag{2.24}$$

and so on, where we have abbreviated $(\mathbf{r}_i,\mathbf{p}_i) = i$ for simplicity.

In order to relate the reduced distribution functions with the Liouville equation, equation (2.13) is integrated over the interval $(\{\mathbf{r}\}_{s+1}^N,\{\mathbf{p}\}_{s+1}^N)$. After some manipulation [48], a coupled system of integro-differential equations is obtained, given by

$$\frac{\partial f_s}{\partial t} = \sum_{i=1}^{s}\left[(\mathrm{L}_{\mathrm{kin}}^i + \mathrm{L}_{\mathrm{ext}}^i)f_s + \sum_{j<i}^{s}\mathrm{L}_{\mathrm{int}}^{j,i}f_s + \int \mathrm{d}\mathbf{r}_{s+1}\mathrm{d}\mathbf{p}_{s+1}\mathrm{L}_{\mathrm{int}}^{i,s+1}f_{s+1}\right]. \tag{2.25}$$

This is the BBGKY hierarchy (Bogoliubov-Born-Green-Kirkwood-Yvon). It defines a hierarchy of coupled equations for the reduced distribution functions f_s, since the evolution of f_s depends on f_{s+1}. In the same way as the Liouville equation or the Hamilton equations, the equations of the BBGKY hierarchy contain all information on the evolution of the system.

Using equation (2.23), the first equation of the hierarchy is [49]

$$\frac{\partial f_1(1)}{\partial t} + \mathbf{v}_1\cdot\frac{\partial f_1(1)}{\partial \mathbf{r}_1} - (N-1)\frac{\partial f_1(1)}{\partial \mathbf{p}_1}\int \mathrm{d}\mathbf{r}_2\mathrm{d}\mathbf{p}_2\frac{\partial \phi(r_{12})}{\partial \mathbf{r}_1}f_1(2) = -(N-1)\int \mathrm{d}\mathbf{r}_2\mathrm{d}\mathbf{p}_2\frac{\partial \phi(r_{12})}{\partial \mathbf{r}_1}\frac{\partial c_2(1,2)}{\partial \mathbf{p}_2}. \tag{2.26}$$

This equation is very similar to the Boltzmann equation (2.7), if we interpret the right-hand side (RHS) as the collisional operator. Because of the Kac prescription, in the limit $N \to \infty$ the term on the RHS goes to zero: all terms on the left-hand side (LHS) are of order $\mathcal{O}[1]$, while the correlation term is of order $\mathcal{O}[1/N] on the RHS$[2].

Since the RHS term depends on the correlation $c_2(1,2)$, it depends also on the next equation of the hierarchy, and so on. Therefore, it is still exact. In practice, however, it is impossible to solve exactly due to the hierarchy, which should be truncated at some point.

To do so, an approximation is necessary.

Due to the Kac rescaling, which introduces the small parameter $1/N$, a perturbative approach can be used [3, 50]. The factor $1/N$ has not been explicitly written in the above equations of the BBGKY hierarchy, but for LRI systems it is implicit in the $\mathrm{L}_{\mathrm{int}}^{i,j}$ and correlational terms. The first approximation in $1/N$ corresponds to truncating the hierarchy for $s > 1$ and neglecting the correlational term in f_2, so that $f_2(1,2) = f_1(1)f_1(2)$. By doing so, we neglect the RHS term of equation (2.26), and so only one equation is left in the hierarchy: the Vlasov equation. Thus, the first approximation leads to collisionless dynamics. Taking the next order of approximation, two-body correlational terms appear [51]. At this point, the collisional dynamics, which now we see to be in fact due to correlations and not collisions,

[2] Without the Kac prescription, the LHS would be of order $\mathcal{O}[N]$ and the RHS of order $\mathcal{O}[1]$, and the ratio would still be of order $1/N$. The argument for collisionless dynamics thus remains the same without the Kac prescription, but the terms in the transport equation would diverge in the thermodynamic limit.

begins to be represented. This aspect will be further explored in the following chapter. For now, we focus on the collisionless dynamics of the Vlasov equation.

This approximation, completely neglecting finite N effects, should be exact in the thermodynamic limit $N \to \infty$. Indeed, in 1977 Braun and Hepp demonstrated that for systems with sufficiently smooth long-range interparticle potentials, the Vlasov collisionless description coincides with the system's dynamics for times that scale at least with $\ln N$ [52]. More recently, it was shown that this is a low estimate, and the time should scale with N^γ with $\gamma > 0$ [53]. In the thermodynamic limit $N \to \infty$, the equilibrium state of a LRI system is a stationary solution of the Vlasov equation. For finite N, the collisionless description is incomplete and fluctuations occur, leading the system from one Vlasov solution to another until eventually thermodynamic equilibrium is reached, hence the name *quasi*-stationary state [4].

To find the solution of the Vlasov equation for a given initial condition is not a trivial task. According to the Jeans theorem [28], any stationary solution of the Vlasov dynamics depends on the phase space coordinates only through a function of the integrals of motion of the potential. Equivalently, any functional of an integral of motion of the potential is a stationary solution of Vlasov dynamics. This implies in a serious problem for finding a stationary solution given an arbitrary initial condition, because the Vlasov equation has an infinite number of integrals of motion. More specifically, the integral of any functional of the distribution function is a conserved quantity. These are known as the Casimir invariants [15, 54],

$$C_s[f] = \int \mathrm{d}\mathbf{r}\mathrm{d}\mathbf{p}\, a[f(\mathbf{r},\mathbf{p})], \tag{2.27}$$

where $a[f(x)]$ is any functional of $f(x)$. Therefore, contrary to the collisional Boltzmann equation, whose stationary solution is the Maxwell-Boltzmann distribution, the Vlasov equation has an infinite number of stationary solutions. To fully describe the QSS attained by an LRI system, we would need to determine which of the infinite number of stationary solutions corresponds to the system's initial distribution. This is a very difficult task, given the non-linearity of equation (2.6).

One aspect of the quasi-stationary state can, nevertheless, be determined: the virial condition.

2.2 Virial theorem

When an N-body system is in a stationary state, it obeys the virial theorem. This gives us a clue as to how the stationary configuration should be. It does not, however, fully specify it, since many different distributions can satisfy the virial theorem.

The virial theorem was demonstrated for the first time by Clausius in 1870 [55], who

introduced the quantity known as the virial $\mathcal{G}$, given by

$$\mathcal{G} = -\frac{1}{2N}\sum_{i=1}^{N} \mathbf{r}_i \cdot \mathbf{F}(\mathbf{r}_i), \tag{2.28}$$

where $\mathbf{F}(\mathbf{r})$ is the force on a particle at the position $\mathbf{r}$. Clausius showed that, in a stationary state, the virial should be equal to the mean kinetic energy of the system. This can be demonstrated from the moment of inertia I. For a system of N particles of identical mass m, the average moment of inertia is

$$I = \frac{m}{N}\sum_{i=1}^{N} |\mathbf{r}_i|^2. \tag{2.29}$$

Differentiating twice with respect to time and dividing by two, we have

$$\begin{aligned} \frac{1}{2N}\frac{\mathrm{d}^2 I}{\mathrm{d}t^2} &= \frac{m}{N}\sum_{i=1}^{N}\left(|\dot{\mathbf{v}}_i|^2 + \mathbf{r}_i \cdot \ddot{\mathbf{r}}_i\right) \\ &= 2\mathcal{K} + \frac{1}{N}\sum_{i=1}^{N} \mathbf{r}_i \cdot \mathbf{F}(\mathbf{r}_i), \end{aligned} \tag{2.30}$$

where $\mathcal{K}$ is the mean kinetic energy. In a stationary state, the moment of inertia I should not change and we may set $\mathrm{d}^2 I/\mathrm{d}t^2$ to zero. This leads to the virial theorem,

$$2\mathcal{K} = -\frac{1}{N}\sum_{i=1}^{N} \mathbf{r}_i \cdot \mathbf{F}(\mathbf{r}_i), \tag{2.31}$$

or $\mathcal{K} = \mathcal{G}$.

Let us consider a system in which the interaction between two particles i and j is given by the potential $\phi(|\mathbf{r}_i - \mathbf{r}_j|)$. Given an external potential of the form $\phi_{ext} = \kappa|\mathbf{r}|^\gamma$, the total potential at position $\mathbf{r}$ is

$$\psi(\mathbf{r}) = \sum_{j=1}^{N} \phi(|\mathbf{r} - \mathbf{r}_j|) + \kappa|\mathbf{r}|^\gamma. \tag{2.32}$$

In this case, the virial is

$$\begin{aligned} \mathcal{G} &= \frac{1}{2N}\sum_{i=1}^{N} \mathbf{r}_i \cdot \left.\frac{\partial \psi(\mathbf{r})}{\partial \mathbf{r}}\right|_{\mathbf{r}=\mathbf{r}_i} \\ &= \frac{1}{2N}\sum_{i=1}^{N}\sum_{\substack{j=1 \\ j\neq i}}^{N} \mathbf{r}_i \cdot \left.\frac{\partial \phi(|\mathbf{r} - \mathbf{r}_j|)}{\partial \mathbf{r}}\right|_{\mathbf{r}=\mathbf{r}_i} + \frac{1}{2N}\sum_{i=1}^{N} \kappa\gamma|\mathbf{r}_i|^\gamma \end{aligned} \tag{2.33}$$

The first term of the RHS of equation (2.33) can be written as

$$\begin{aligned}
\sum_{i=1}^{N}\sum_{\substack{j=1\\ j\neq i}}^{N}\mathbf{r}_i\cdot\left.\frac{\partial\phi(|\mathbf{r}-\mathbf{r}_j|)}{\partial\mathbf{r}}\right|_{\mathbf{r}=\mathbf{r}_i} &= \sum_{i=2}^{N}\sum_{j=1}^{i-1}\mathbf{r}_i\cdot\left.\frac{\partial\phi(|\mathbf{r}-\mathbf{r}_j|)}{\partial\mathbf{r}}\right|_{\mathbf{r}=\mathbf{r}_i}+\sum_{i=1}^{N-1}\sum_{j=i+1}^{N}\mathbf{r}_i\cdot\left.\frac{\partial\phi(|\mathbf{r}-\mathbf{r}_j|)}{\partial\mathbf{r}}\right|_{\mathbf{r}=\mathbf{r}_i}\\
&= \sum_{i=2}^{N}\sum_{j=1}^{i-1}\mathbf{r}_i\cdot\left.\frac{\partial\phi(|\mathbf{r}-\mathbf{r}_j|)}{\partial\mathbf{r}}\right|_{\mathbf{r}=\mathbf{r}_i}+\sum_{i=1}^{j-1}\sum_{j=2}^{N}\mathbf{r}_i\cdot\left.\frac{\partial\phi(|\mathbf{r}-\mathbf{r}_j|)}{\partial\mathbf{r}}\right|_{\mathbf{r}=\mathbf{r}_i}\\
&= \sum_{i=2}^{N}\sum_{j=1}^{i-1}\left(\mathbf{r}_i\cdot\left.\frac{\partial\phi(|\mathbf{r}-\mathbf{r}_j|)}{\partial\mathbf{r}}\right|_{\mathbf{r}=\mathbf{r}_i}+\mathbf{r}_j\cdot\left.\frac{\partial\phi(|\mathbf{r}-\mathbf{r}_i|)}{\partial\mathbf{r}}\right|_{\mathbf{r}=\mathbf{r}_j}\right)\\
&= \sum_{i=2}^{N}\sum_{j=1}^{i-1}(\mathbf{r}_i-\mathbf{r}_j)\cdot\left.\frac{\partial\phi(|\mathbf{r}-\mathbf{r}_j|)}{\partial\mathbf{r}}\right|_{\mathbf{r}=\mathbf{r}_i}\\
&= \sum_{i=2}^{N}\sum_{j=1}^{i-1}r_{ij}\frac{\partial\phi(r_{ij})}{\partial r_{ij}},
\end{aligned}\tag{2.34}$$

where $r_{ij}=|\mathbf{r}_{ij}|=|\mathbf{r}_i-\mathbf{r}_j|$ and $\partial/\partial\mathbf{r}_i=(\mathbf{r}_{ij}/r_{ij})(\partial/\partial r_{ij})$.

Depending on the form of the potential $\phi(r_{ij})$, the result of equation (2.34) can be related to the mean potential energy using Euler's homogeneous function theorem. The theorem states that, if $f(\mathbf{r})$ is a homogeneous function of order n, that is, $f(\lambda\mathbf{r})=\lambda^n f(\mathbf{r})$, then $\mathbf{r}\cdot\nabla f(\mathbf{r})=nf(\mathbf{r})$. Therefore, if $\phi(r_{ij})$ is a homogeneous function of order n, the virial theorem is

$$\begin{aligned}
2\mathcal{K} &= \frac{1}{N}\sum_{i=2}^{N}\sum_{j=1}^{i-1}n\phi(r_{ij})+\frac{1}{N}\sum_{i=1}^{N}\kappa\gamma|\mathbf{r}_i|^{\gamma}\\
&= n\mathcal{U}+\kappa\gamma\langle|\mathbf{r}|^{\gamma}\rangle.
\end{aligned}\tag{2.35}$$

where $\mathcal{U}$ is the mean interaction potential energy. For example, for a self-gravitating system in three dimensions, the potential is a homogeneous function of order $n=-1$, because $\phi(\lambda r)=(\lambda r)^{-1}=\phi(r)/\lambda$. Thus, the virial condition is $2\mathcal{K}=-\mathcal{U}$.

We state that an initial condition satisfies the virial condition if the initial distribution has a mean kinetic energy $\mathcal{K}_0$, a mean interaction potential energy $\mathcal{U}_0$, and, if an external potential exists, $\langle|\mathbf{r}_i|^{\gamma}\rangle_0$, that satisfy the equation (2.35). In order to have a measure of a given state's "closeness" to the virial condition, we introduce the virial number $\mathcal{R}$,

$$\mathcal{R}=\frac{\mathcal{K}}{\mathcal{G}}=\frac{2\mathcal{K}}{n\mathcal{U}}\tag{2.36}$$

where the second equality holds for potentials which are homogeneous functions of order n and without external potentials. Taking once again gravity in three dimensions as an example, the virial number is

$$\mathcal{R}_{\mathrm{g3d}}=-\frac{2\mathcal{K}}{\mathcal{U}}.\tag{2.37}$$

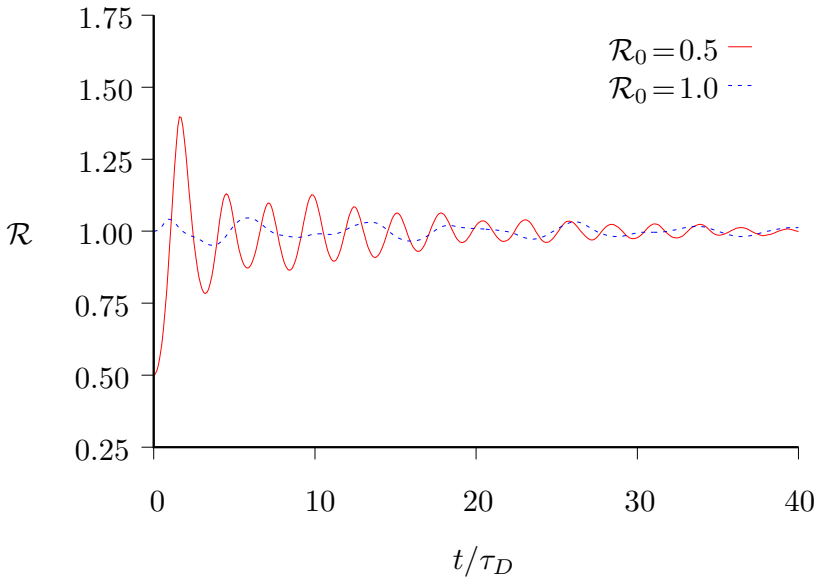

Figure 2.1: *Evolution of the virial number $\mathcal{R}$ of a self-gravitating system in three dimensions, equation* (2.37)*. Two initial conditions are shown: off the virial condition, $\mathcal{R}_0 = 0.5$ (solid line) and on the virial condition $\mathcal{R}_0 = 1.0$ (dashed line). If the initial state does not satisfy the virial condition given by equation* (2.31)*, the distribution undergoes strong mean-field oscillations until it reaches a configuration for which it is satisfied. For $\mathcal{R}_0 = 1.0$, oscillations are minimal, because the system began its evolution already on the virial condition.*

The virial number of the initial distribution is $\mathcal{R}_0 = \mathcal{R}(t = 0)$. For $\mathcal{R}_0 \neq 1$, the virial condition is not satisfied. In this case, the system quickly tends to a configuration which does satisfy it, and $\mathcal{R}$ oscillates around $\mathcal{R} = 1$ until the oscillations are damped and the system remains in the stationary state with $\mathcal{R} = 1$. The closer $\mathcal{R}_0$ is to 1, the smaller will be the amplitude of the initial oscillations. Figure 2.1 shows two initial conditions for a self-gravitating system in three dimensions: $\mathcal{R}_0 = 0.5$ (solid line) and $\mathcal{R}_0 = 1.0$ (dashed line). The virial number of the system with $\mathcal{R}_0 = 0.5$ immediately begins to oscillate around 1. The same happens for the $\mathcal{R}_0 = 1.0$ case, but with much smaller oscillations, seeing as the system already satisfied the virial theorem at $t = 0$.

The potential of the system of interest may not always be a homogeneous function of order n. This is the case for one of the LRI systems which appear in this thesis: the HMF model (chapter 4). The interaction between particles in the HMF model is given by a cosine and so it is not possible to use equation (2.35). In this case, the virial condition must be explicitly calculated from equation (2.31) for each initial particle distribution. This method works very well, and was published in the work presented in chapter 4.

2.3 Characterization of quasi-stationary states

Once the virial condition is known for a given LRI system, we can determine if the initial distribution satisfies it. If it does not, the distribution will necessarily undergo strong mean-field oscillations until it reconfigures itself in such a way that the virial condition is

satisfied. This process, known as *violent relaxation* [56], can cause some particles to gain large amounts of energy through parametric resonances. When this happens, the system tends to a *core-halo* formation: a dense core of low energy surrounded by fewer particles of high energy. Although not a main subject of this thesis, the core-halo (CH) formation was intensively studied previously by our research group, and the next subsection 2.3.1 contains a brief review of its findings.

The CH formation contrasts with another well-known description of the QSS known as Lynden-Bell (LB) statistics. Lynden-Bell introduced the term violent relaxation, and was the first to propose a statistical theory based on this concept. This theory is described in section 2.3.2. However, our work has shown that LB statistics has good results only when the initial distribution satisfies the virial condition; that is, when the mean-field oscillations are minimal and the relaxation is not as "violent" [57].

To understand this apparent paradox, we applied a different approach to describe the QSS when the virial condition is satisfied: a system of uncoupled particles evolving under a self-consistent potential. We refer to this method as the *integrable model* (IM), and describe it in section 2.3.3.

2.3.1 Core-halo model

When a LRI system begins in a configuration that is far from a virialised state, the mean-field oscillations lead to wave-particle interactions that can transfer large amounts of energy from the wave to the resonant particles, in a process similar to Landau-damping [58]. These oscillations should eventually die out as the particles take energy from the waves and compose a high-energy halo surrounding the dense core containing the majority of particles. Figure 2.2 shows the CH configuration for a self-gravitating system in two dimensions, in which mass particles interact through a potential $\phi(r_{ij}) \sim \ln(r_{ij})$.

Supposing that the oscillations are able to transfer all of their free energy to the resonant particles, the core should be completely cold. Due to the phase space incompressibility of Vlasov dynamics, the phase space density cannot surpass that of the initial distribution, since the distribution evolves as the density of an incompressible fluid.

Combining these insights with tools from plasma physics, such as the envelope equation, Levin *et al.* proposed a core-halo distribution [27],

$$f_{CH}(\mathbf{r},\mathbf{p}) = \eta\Theta[\epsilon_c - \epsilon(\mathbf{r},\mathbf{p})] + \chi\Theta[\epsilon(\mathbf{r},\mathbf{p}) - \epsilon_c]\Theta[\epsilon_h - \epsilon(\mathbf{r},\mathbf{p})] \tag{2.38}$$

where ϵ_h and ϵ_c are the energy corresponding to the orbits that delimit the halo and core, respectively, and η and χ are the core and halo densities, respectively. This distribution was proposed for systems with initial distributions of the *water-bag* type; that is, a distribution of constant density η on a compact support in phase space,

$$f_{wb}(\mathbf{r},\mathbf{p}) = \eta\Theta(r_m - |\mathbf{r}|)\Theta(p_m - |\mathbf{p}|). \tag{2.39}$$

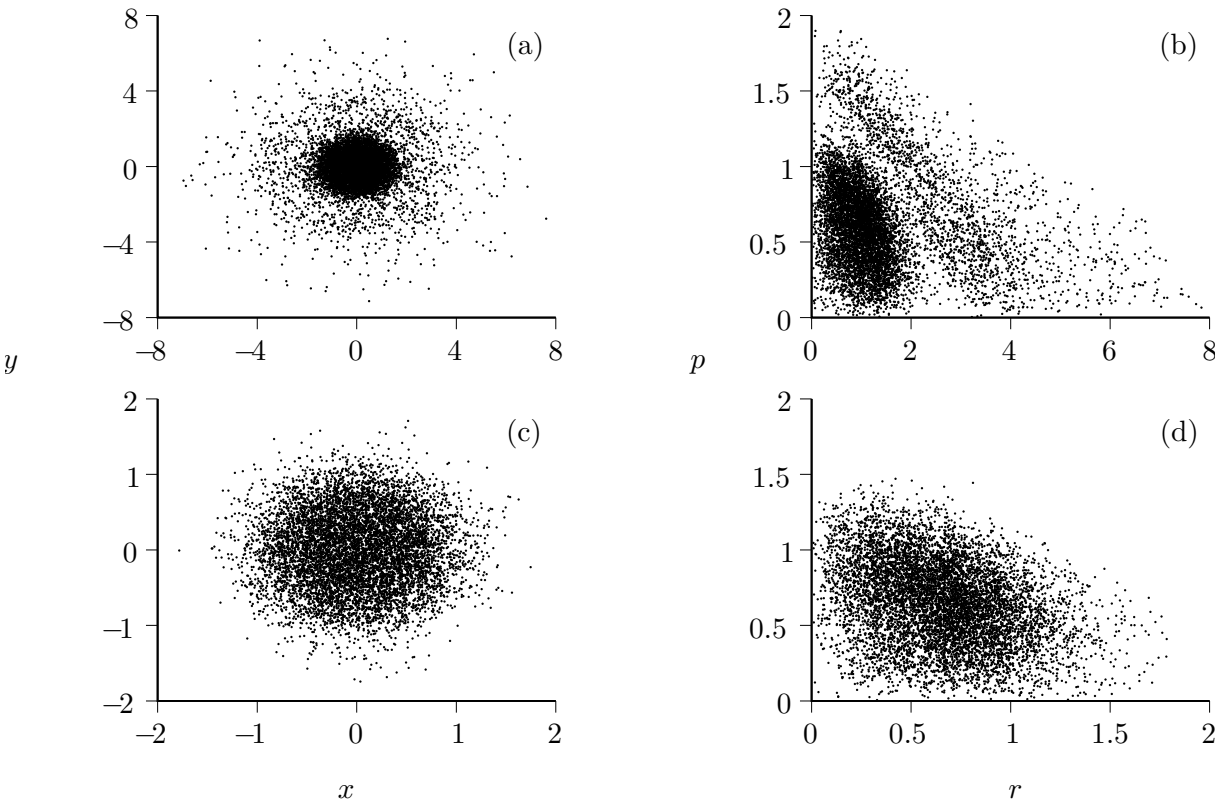

Figure 2.2: *Particles in space —left, panels (a) and (c)— and phase space —right, panels (b) and (d)— of a self-gravitating system in 2 dimensions (interacting through a logarithmic potential). The top, panels (a) and (b), corresponds to a system with $R_0 = 2.5$ (far from the virial condition), while on the bottom, panels (c) and (d), the system was initially virialised ($R_0 = 1$). The CH configuration is clearly shown on the top panels.*

The core density η is the same as the water-bag density due to the incompressibility constraint.

In order to determine the parameter ϵ_h, Levin *et al.* used a technique from plasma physics known as the *envelope equation*. This method involves determining an equation of motion for the spatial "envelope" of the water-bag distribution; that is, the limit of the distribution in $\mathbf{r}$. It is an approximate method, which supposes that the distribution remains uniform during the first few mean-field oscillations. At $t = 0$, the envelope is simply the limit in $\mathbf{r}$ of the water-bag distribution, r_m. Once this equation is determined, it is possible to define a potential corresponding to the uniform distribution that oscillates with the envelope frequency. Then, test particles interact with this potential, and the highest energy achieved by a test particle is thus defined as the halo energy ϵ_h.

The other remaining parameters, ϵ_c and χ, are then determined by the constraints of normalization and mean energy.

This approach has been shown to be very successful for several LRI systems, such as self-gravitation in one and two dimensions [59, 60] and charged particle beams [61]. For three-dimensional self-gravitating systems, the lack of a confining potential means particles that gain enough energy are ejected from the system and do not form the halo. The theory is nevertheless successful in predicting the profile and the number of particles that compose

the core [62].

All of these works show that the core-halo phenomenon occurs in systems which begin their evolution away from the virial condition. Otherwise, the mean-field oscillations do not occur and wave-particle energy gain is minimized. The works show that in this case, Lynden-Bell theory, which we will now discuss, has good results.

2.3.2 Violent relaxation

If the initial distribution is not a stationary solution of Vlasov dynamics, it undergoes strong oscillations until it reaches the QSS. This is a relatively fast process, occurring during a time interval of the order of the crossing time τ_{cr}, the time necessary for a particle to cross the system [4]. It is known as violent relaxation due to the intensity of the mean-field oscillations. This name was introduced by Lynden-Bell in 1967 in his research on the steady states of gravitational systems [56]. In this work, Lynden-Bell developed a statistical theory for describing the stationary states based on the conservation of the density of the distribution function $f(\mathbf{r},\mathbf{p},t)$ under Vlasov dynamics.

Under collisionless dynamics, the distribution function evolves as the density of an incompressible fluid. This means that as the distribution evolves, its local density remains constant along the flow (its convective derivative is zero). As the distribution function evolves, it undergoes a filamentation process on progressively smaller length scales, until eventually the evolution occurs on a length scale so small it is indiscernible to any observation. In this situation, a coarse-grained or macroscopic stationary state is reached, described by the coarse-grained distribution function $\bar{f}$, while the microscopic distribution function f continues to evolve. Figure 2.3 shows an example of the filamentation process of a distribution of particles in phase space of a LRI system.

LB statistics determines an expression for $\bar{f}$ through the maximization of a coarse-grained entropy s_{LB} under constraints of energy and norm conservation. Only the coarse-grained entropy may increase; the fine-grained entropy must be preserved (analogous to the preservation of the Gibbs entropy). The procedure for obtaining the coarse-grained entropy is similar to the process of counting microstates that leads to the Boltzmann entropy of a lattice gas, for example.

Let us consider a uniform initial distribution of density η. The phase space is divided into macrocells, each composed of ν microcells. N microcells are occupied by the initial distribution f_0. This number remains constant during the dynamics, due to the incompressibility of the Vlasov flow. However, the density in each macrocell is not necessarily preserved. A phase element that initially occupies a microcell belonging to macrocell j can move on to a microcell belonging to another macrocell $k \neq j$ (see figure 2.4). Defining $\bar{f}$ as

$$\begin{aligned} \bar{f}(\mathbf{r},\mathbf{p}) &= \eta\rho(\mathbf{r},\mathbf{p}), \\ \rho(\mathbf{r},\mathbf{p}) &= \frac{n_\nu}{\nu}, \end{aligned} \tag{2.40}$$

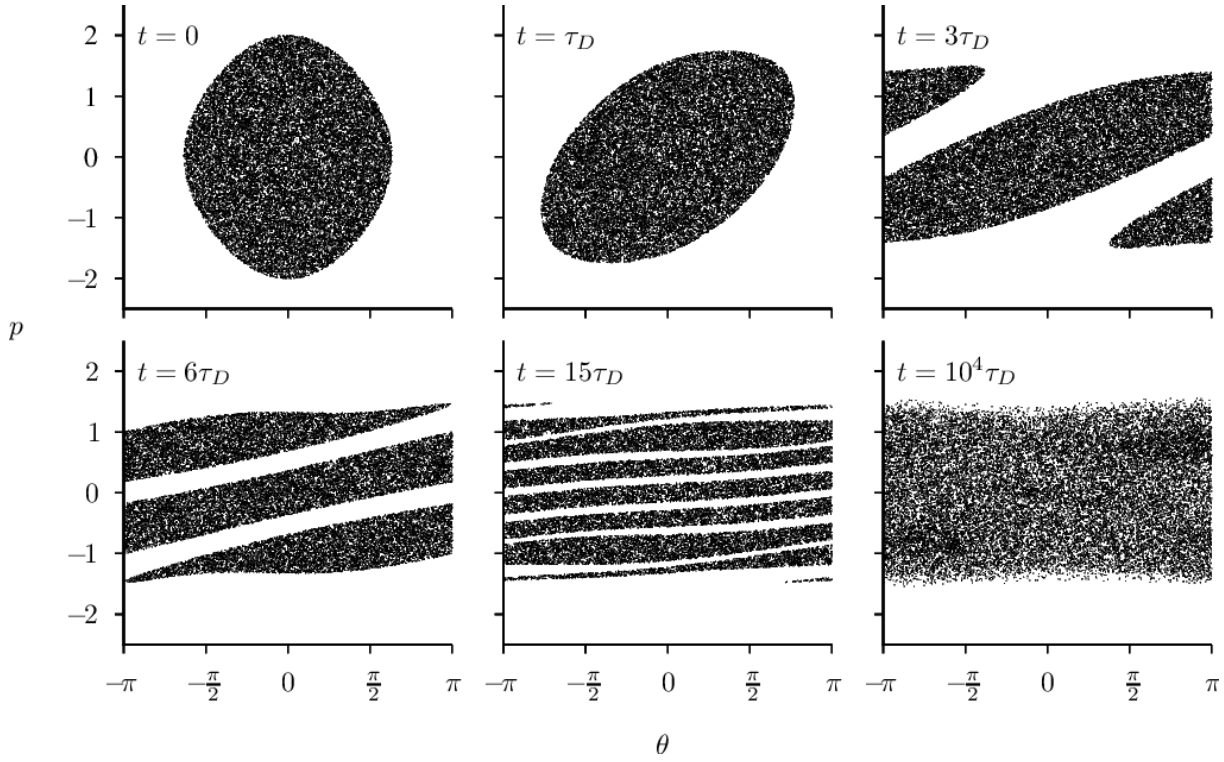

Figure 2.3: *Evolution of a distribution of particles in phase space for an LRI system, specifically, the HMF model which will be presented in chapter 4. The filamentation process of the distribution is clearly shown.*

where n_ν is the number of occupied microcells in the macrocell centered around $(\mathbf{r},\mathbf{p})$, we see that n_ν may vary and therefore the coarse-grained distribution $\bar{f}$ can also change.

The LB entropy is given by $s_{\text{LB}} = k_B \ln W$ where W is the number of ways to distribute the N phase elements. At this point, Lynden-Bell assumes that the flow of $f(\mathbf{r},\mathbf{p})$ is ergodic and mixing in the energy surface of the d-dimensional phase space. This means that the probability of finding $f(\mathbf{r},\mathbf{p})$ in an element $\mathrm{d}\mathbf{r}\mathrm{d}\mathbf{p}$ of the constant energy surface is proportional to the ratio of the area of the element and the area of the surface [63]. It follows that all microcells have an equal probability of being occupied, subject to the appropriate constraints of energy, norm and momentum. Due to the incompressibility of Vlasov dynamics, no more than one phase element may occupy a microcell at the same time. The counting of number of ways to distribute the phase elements is done in the same way as the Boltzmann counting, except in this case phase elements are being distributed instead of particles. The resulting entropy is [27]

$$s_{\text{LB}} = -\int \mathrm{d}\mathbf{r}\mathrm{d}\mathbf{p}\,\{\rho(\mathbf{r},\mathbf{p})\ln[\rho(\mathbf{r},\mathbf{p})] + [1-\rho(\mathbf{r},\mathbf{p})]\ln[1-\rho(\mathbf{r},\mathbf{p})]\}\,. \tag{2.41}$$

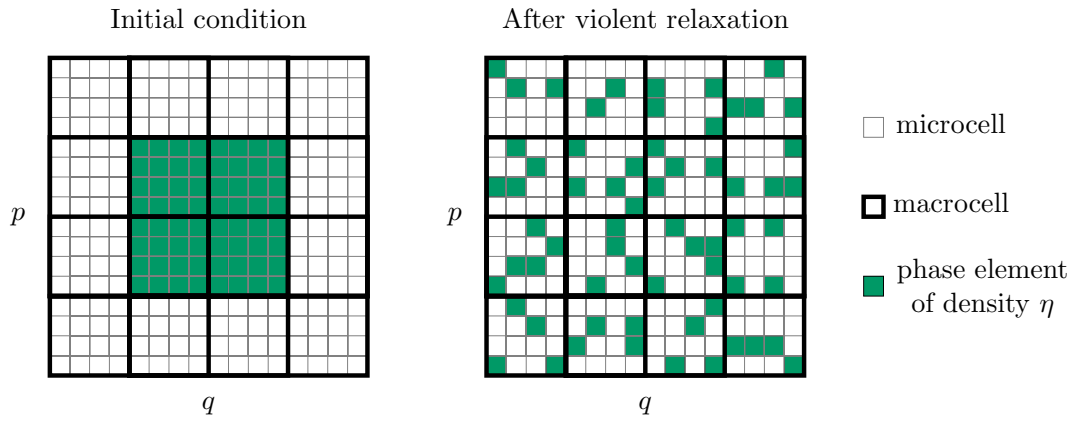

Figure 2.4: *Division of phase space in macrocells which are, in turn, divided into microcells. The left panel shows a representation of a uniform initial distribution of density η which fills some macrocells. Each macrocell has an initial density η or 0. The right panel shows the phase space after a transient time, with phase elements occupying microcells out of the originally occupied macrocells. The total number of microcells occupied by phase elements of density η is preserved, but the macrocell density varies, taking on values between 0 and η. The energy, norm and momentum of the distribution are conserved by Lagrange multipliers.*

Maximizing under the constraints of energy and norm conservation,

$$1 = \int \mathrm{d}\mathbf{r}\mathrm{d}\mathbf{p}\, \bar{f}(\mathbf{r},\mathbf{p}), \tag{2.42a}$$

$$\mathcal{E} = \int \mathrm{d}\mathbf{r}\mathrm{d}\mathbf{p} \left(\frac{p^2}{2m} + \frac{\psi(\mathbf{r})}{2}\right) \bar{f}(\mathbf{r},\mathbf{p}), \tag{2.42b}$$

we obtain the most probable distribution,

$$f_{\mathrm{LB}}(\mathbf{r},\mathbf{p}) = \eta \frac{1}{1 + \exp\left[\beta\epsilon(\mathbf{r},\mathbf{p}) - \mu\right]}, \tag{2.43}$$

where $\epsilon(\mathbf{r},\mathbf{p}) = p^2/2m + \psi(\mathbf{r})$ is the one-particle energy. The form of the expression in equation (2.43) is similar to a Fermi-Dirac distribution. This results from the conservation of the density of f—since the density is preserved, a microcell cannot be filled by more than one phase element, a characteristic analogous to the Pauli exclusion principle for fermions. However, the analogous form is only valid for one-level initial distributions. Considering an initial distribution with L different levels of density η_i, such as the one we used in the work presented in section 4.2, Lynden-Bell showed that the corresponding coarse-grained distribution will be

$$f_{\mathrm{LB}}(\mathbf{r},\mathbf{p}) = \frac{\sum_{i=1}^{L} \eta_i e^{-\beta_i[\epsilon(\mathbf{r},\mathbf{p})-\mu_i]}}{1 + \sum_{i=1}^{L} e^{-\beta_i[\epsilon(\mathbf{r},\mathbf{p})-\mu_i]}} \tag{2.44}$$

LB statistics has had mixed results in describing the QSS of LRI systems. Early comparisons of numerical simulations of astrophysical systems showed, for some initial conditions, a good agreement for low-energy particles and significant deviations in the high-energy tails, or halos, of the distributions [64–66]. More recent numerical simulations have also had di-

verging results. In self-gravitating systems, high-energy regions were not in agreement with the LB distribution [67,68], while for spin models, some initial conditions were well described and others presented halos that did not match LB theory [57,69].

The population of high-energy levels by particles of initially lower energy is explained by the oscillatory dynamics of the mean-field potential $\psi(\mathbf{r})$. Particles that enter in resonance with the collective motion gain energy at the expense of the oscillations, a process known as Landau damping [70, 71]. By taking energy from the collective oscillations, the creation of the high-energy halo damps the oscillations, which should eventually cease. The distribution becomes divided between a dense, low-energy degenerate core and a diffuse high-energy halo [59, 60, 62, 72]. Once the oscillations have died out, there is no longer any way for particles to exchange energy. They remain trapped in their high or low energy state. This is a clear breaking of the ergodicity and mixing condition.

It is therefore reasonable to assume that, for LB statistics to be applicable, the initial condition must be such that the potential does not undergo strong oscillations. Thus, the ergodicity breaking caused by the core-halo formation and the statistically improbable occupation of high energy levels can be avoided. In fact, LB statistics presents better results when the initial distribution satisfies the virial theorem, for then the initial state is already close to a stationary solution [27, 67, 73].

2.3.3 Integrable Model

The virial condition indicates initial distributions that will not undergo strong oscillations. Of course, if the initial distribution is not a stationary solution of Vlasov dynamics, some oscillation will occur even if it does satisfy the virial condition, because the system must still relax to its QSS. Nevertheless, the oscillations should be weak compared to non-virial initial conditions.

Previously, we put forth an argument that if the virial condition is satisfied, LB statistics may be a good approximation for describing the QSS, because the core-halo structure does not form. On the other hand, we have also seen that LB statistics depends on the premise of ergodicity and mixing in phase space, that is, that all regions of phase space have equal probability of being occupied by a phase element of density η. However, for this to be valid, the initial distribution *should* oscillate strongly, hence the name violent relaxation. Then, energy can be exchanged between particles, which can go on to populate different regions of phase space. If the potential is stationary, each particle's dynamics becomes independent of the other particles. The dynamics becomes integrable and no energy is transferred between them [74]. This implies that virialised initial conditions *do not* result in ergodicity and mixing of the distribution function in phase space. If the dynamics is integrable, there is no reason to suppose that LB statistics is appropriate.

A model that seems more adequate to represent LRI systems with potentials that fluctuate weakly is the self-consistent uncoupled dynamics approach introduced by de Buyl *et al.*

in 2011 [75,76]. We refer to it as the "integrable model" (IM) to contrast it with the ergodic approach of Lynden-Bell. De Buyl *et al.* proposed a system with uncoupled particles analogous to the HMF model, a model of continuous spins with long-range interactions [39,42]. In the IM, independent particles interact with an external potential $\psi = H\cos\theta$. In the HMF model, the potential is $\psi = M(t)\cos\theta$ where $M(t) = \langle\cos\theta\rangle$. In order to associate the two models, the value of H is defined as being equal to $\langle\cos\theta\rangle$ of the stationary distribution of the IM pendulums.

A similar treatment can be performed for other LRI systems. In general terms, we consider a system composed of N non-interacting particles, subject to an external potential $\psi_{\mathrm{IM}}(\mathbf{r})$. Since the particles are independent, no energy is exchanged between them. They evolve on orbits defined by their initial energy and other conserved quantities (for example, angular momentum in spherically symmetric potentials). Thus, a distribution function f is conserved, given by

$$f(\varepsilon,\{h_i\}) = \frac{n(\varepsilon,\{h_i\})}{g(\varepsilon,\{h_i\})}, \tag{2.45}$$

where $\{h_i\}, i = 1,\ldots,N_c$ are the N_c quantities conserved by the dynamics, $n(\varepsilon,\{h_i\})$ and $g(\varepsilon,\{h_i\})$ are the number of particles and density of states with energy ε and quantities $\{h_i\}$, respectively. For any given initial distribution $f_0(\mathbf{r},\mathbf{p})$, $n(\varepsilon,\{h_i\})$ is given by

$$n(\varepsilon,\{h_i\}) = \int f_0(\mathbf{r},\mathbf{p})\delta\left[\varepsilon - \epsilon(\mathbf{r},\mathbf{p})\right]\prod_i \delta\left[h_i - \mathsf{h}_i(\mathbf{r},\mathbf{p})\right]\mathrm{d}\mathbf{r}\mathrm{d}\mathbf{p}, \tag{2.46}$$

where $\epsilon(\mathbf{r},\mathbf{p}) = p^2/2m + \psi_{\mathrm{IM}}(\mathbf{r})$ and $\{\mathsf{h}_i(\mathbf{r},\mathbf{p})\}$ are the expressions for the other conserved quantities as a function of the phase space coordinates. The density of states does not depend on the initial distribution,

$$g(\varepsilon,\{h_i\}) = \int \delta\left[\varepsilon - \epsilon(\mathbf{r},\mathbf{p})\right]\prod_i \delta\left[h_i - \mathsf{h}_i(\mathbf{r},\mathbf{p})\right]\mathrm{d}\mathbf{r}\mathrm{d}\mathbf{p}. \tag{2.47}$$

A particle initially in one of the states of an orbit $(\varepsilon,\{h_i\})$ will pass through all other states in the same orbit during its evolution[3]. The time necessary for it to complete the orbit, returning to its initial state, is the orbital period. If the force is non-linear, the orbital periods of particles in initially close orbits will be incommensurable. After a transient time, an orbital shell $\left[(\varepsilon,\{h_i\}),(\varepsilon+\mathrm{d}\varepsilon,\{h_i+\mathrm{d}h_i\})\right]$ will be uniformly occupied by particles, even if not all states in the shell were initially occupied, as illustrated schematically by figure 2.5. Therefore, the marginal distributions $n(\mathbf{r})$ and $n(\mathbf{p})$ can be calculated by integrating over

[3] Of course, since each particle is isolated, its dynamics is ergodic over its own orbit. Considered as an entire distribution, however, it represents a nonergodic version of the LRI system.

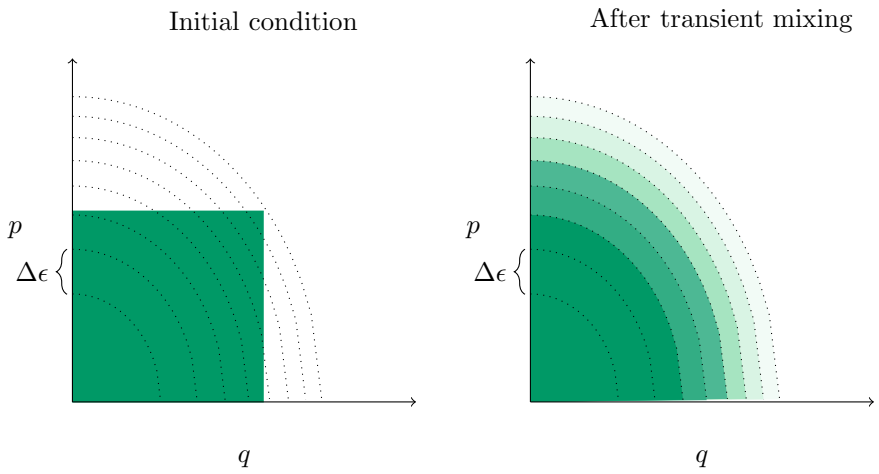

Figure 2.5: *Schematic representation in phase space of a distribution undergoing the uncoupled dynamics of the integrable model. On the left, an initial distribution $f_0(\mathbf{r},\mathbf{p})$ of constant density η; on the right, the stationary state achieved after a transient period in which the distribution spreads itself over constant energy orbits (in this case, we consider that only the particle energy is conserved). Black dotted lines represent constant energy orbits.*

the orbits,

$$n_{\mathrm{IM}}(\mathbf{r}) = \int f(\varepsilon,\{h_i\})\delta\left[\varepsilon - \epsilon(\mathbf{r},\mathbf{p})\right]\prod_i \delta\left[h_i - \mathsf{h}_i(\mathbf{r},\mathbf{p})\right]\mathrm{d}\varepsilon\mathrm{d}h_1\cdots\mathrm{d}h_{N_c}\mathrm{d}\mathbf{p}, \tag{2.48}$$

$$n_{\mathrm{IM}}(\mathbf{p}) = \int f(\varepsilon,\{h_i\})\delta\left[\varepsilon - \epsilon(\mathbf{r},\mathbf{p})\right]\prod_i \delta\left[h_i - \mathsf{h}_i(\mathbf{r},\mathbf{p})\right]\mathrm{d}\varepsilon\mathrm{d}h_1\cdots\mathrm{d}h_{N_c}\mathrm{d}\mathbf{r}. \tag{2.49}$$

The aim of this integrable, non-interacting model is to describe the QSS of a more complex, interacting, long-range system. The IM potential $\psi_{\mathrm{IM}}(\mathbf{r})$ must be related to the pair interaction potential $\phi(\mathbf{r},\mathbf{r}')$ of the LRI system. To do so, the IM potential is defined as the mean-field potential $\psi(\mathbf{r}) = \int \mathrm{d}\mathbf{r} n_{\mathrm{IM}}(\mathbf{r})\phi(\mathbf{r},\mathbf{r}')$ that would be generated by the distribution $n_{\mathrm{IM}}(\mathbf{r})$ in the LRI system. However, we see from equation (2.48) that the distribution $n_{\mathrm{IM}}(\mathbf{r})$ depends on $\psi_{\mathrm{IM}}(\mathbf{r})$. The potential $\psi_{\mathrm{IM}}(\mathbf{r})$ must be solved self-consistently with equations (2.48) and (2.45). How to do this will depend on the specific LRI system being studied. For example, for potentials due to mass or charge, the IM potential must satisfy the Poisson equation $\nabla^2\psi_{\mathrm{IM}} = Cn_{\mathrm{IM}}(\mathbf{r})$ where the constant C depends on the LRI system. Schematically the model is given by figure 2.6.

This approach is radically different from that of LB statistics. It completely decouples particle trajectories in phase space, introducing N isolating integrals into the original Hamiltonian. The flow is then nonergodic. In our work with the HMF model and spherically symmetric gravitational systems, we have shown that this method works very well for initially virialised distributions.

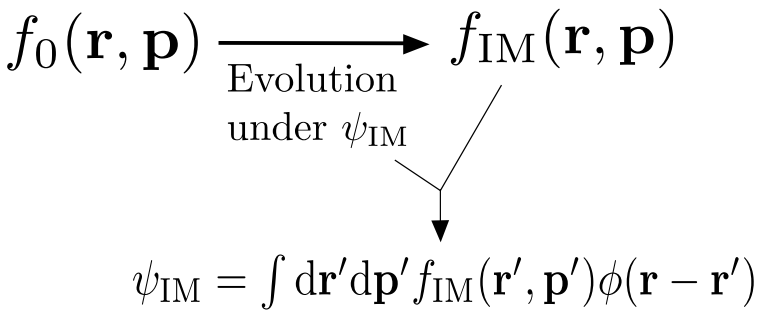

Figure 2.6: *Representation of the integrable model. An initial distribution function $f_0(\mathbf{r},\mathbf{p})$ evolves under the dynamics determined by a constant potential $\psi_{\mathrm{IM}}(\mathbf{r})$ to a stationary distribution $f_{\mathrm{IM}}(\mathbf{r},\mathbf{p})$. The potential ψ_{IM} must, for every $\mathbf{r}$, be equivalent to the mean-field potential generated by the stationary distribution $n_{\mathrm{IM}}(\mathbf{r}) = \int \mathrm{d}\mathbf{p} f_{\mathrm{IM}}(\mathbf{r},\mathbf{p})$ with the interaction potential $\phi(\mathbf{r}-\mathbf{r}')$.*

2.4 Summary and relation to thesis

The CH, IM and LB theories both aim to describe the QSS of Vlasov dynamics, valid in the thermodynamic limit $N \to \infty$. While the CH theory works well in describing the QSS that arise from initially unvirialised water-bag distributions, previous works had shown that LB statistics provided good predictions for the momentum and position marginal distributions for initially virialised water-bag distributions of LRI systems. This was shown in our work with the HMF model, the subject of chapter 4, a long-range XY model. We derived a virial condition for water-bag distributions and showed that when it was satisfied, LB statistics worked better than for initial distributions that were not virialised, in which case a CH distribution occurred [57]. Section 4.1 presents this work.

Subsequently, we applied the IM dynamics to the HMF model for multi-level water-bag distributions: distributions of different density levels on rectangular compact supports in phase space. We then showed that the results of IM were more accurate than LB statistics [73]. This work is discussed in section 4.2.

Finally, we generalized the IM to spherically symmetric three-dimensional self-gravitating systems. These systems are notoriously difficult due to both a short-range divergence and the unbounded potential at large r. For initial conditions that are virialised, we successfully predicted the marginal distributions using the uncoupled dynamics [77]. This is the subject of section 6.1.

The above works deal with the quasi-stationary states of the LR thermodynamic limit, in which $N \to \infty$ while the pair coupling tends to zero. In finite systems, fluctuations and residual correlations lead to collisional relaxation. Consequently, the QSS, corresponding to stationary Vlasov states, have a finite lifetime τ_R. In the next section, we discuss the slow relaxation that takes the LRI system from the QSS to thermodynamic equilibrium.

Chapter 3

Collisional relaxation and thermodynamic equilibrium

In the previous chapter, we examined the BBGKY hierarchy and saw that by taking a zeroth-order approximation in the small parameter $1/N$, we obtain the Vlasov, or collisionless, framework. To see the effects of finite N, we must take the next order of approximation and include terms of order $\mathcal{O}[1/N]$,

$$\frac{Df}{Dt} = c_N[g(\mathbf{R},\mathbf{P})] \tag{3.1}$$

where $c_N[f]$ is the collisional operator. However, by considering these higher-order terms, the equations become complex and difficult to solve. Even so, in some cases it is possible to use kinetic theory to estimate the relaxation time τ_R; for example, for one-dimensional homogeneous states, $\tau_R \sim N^2$ [78].

3.1 Collisional relaxation

A common approach to studying the collisional relaxation is to write equation (3.1) as a Fokker-Planck equation [28]. Using the notation $\mathbf{z} = (\mathbf{r},\mathbf{v})$ to simplify, the approach considers a test particle of probability density $P(\mathbf{z},t)$ evolving in a bath of particles with a stationary distribution function $f(\mathbf{z})$. The equation is given by

$$\frac{DP}{Dt} = \sum_{i,j=1}^{d} \frac{\partial^2}{\partial z_i \partial z_j} \{D[\Delta z_i \Delta z_j] f(\mathbf{z})\} - \sum_{i=1}^{d} \frac{\partial}{\partial z_i} \{D[\Delta z_i] f(\mathbf{z})\} \tag{3.2}$$

where $D[\Delta z_i \Delta z_j]$ and $D[\Delta z_i]$ are the diffusion and friction coefficients, respectively.

To simplify the calculation of the coefficients, it is usual to approximate the system as

homogeneous, so equation (3.2) becomes

$$\frac{DP}{Dt} = \sum_{i,j=1}^{d} \frac{\partial^2}{\partial v_i \partial v_j} \left\{ D[\Delta v_i \Delta v_j] f(\mathbf{v}) \right\} - \sum_{i=1}^{d} \frac{\partial}{\partial v_i} \left\{ D[\Delta v_i] f(\mathbf{v}) \right\}. \tag{3.3}$$

By using the dimensional analysis

$$D[\Delta v^2] \sim \frac{[V]^2}{[\tau]}, \tag{3.4}$$

where $[V]$ and $[\tau]$ are typical velocity and time scales, the relaxation timescale τ_R should scale as $\tau_R \sim [V]^2 / D[\Delta v^2]$.

3.1.1 Two-body encounters and relaxation time

The first estimates of the collisional relaxation time were made for gravitational systems; specifically, the seminal work of Chandrasekhar for stellar systems, in 1941 [79]. In this work, Chandrasekhar associates the relaxation time with the time necessary for the total energy exchanged by stellar encounters to be of the same order of the initial kinetic energy. To do so, he calculated the friction and diffusion coefficients for the stars by supposing that their trajectories took place in a homogeneous and infinite distribution of mass. Under this assumption, stellar orbits are linear, and each orbit is adequately characterized by its velocity v. Then, the stellar encounters between the test and bath particles are estimated to be independent and localized. With these considerations, the variations Δv and Δv^2 corresponding to each individual encounter can be calculated. To find the total variation of the test particle velocity v as it passes through a system of size R, these variations should be integrated over the number of encounters that it undergoes. After some calculations (see e.g. [28] or [80]), the resulting timescale is

$$\tau_R \sim \frac{N}{\ln N} \tau_{cr} \tag{3.5}$$

where τ_{cr} is the *crossing time*—the time necessary for the particle to cross the system.

Many numerical works have also attempted to determine the relaxation time of LRI systems. These suggest a scaling of the form $\tau_R \sim N^\gamma \tau_D$, where the exponent γ varies according to the interaction type. For example, for self-gravitating systems, the exponent was found to be $\gamma = 1$ for the one-dimensional case [81], $\gamma = 1.3$ for a two-dimensional system of interacting shells [68], and $\gamma = 1$ for a two-dimensional system of point masses [82]. For the HMF model, $\gamma = 1.7$ has been found [4], but more recent results suggest that $\gamma = 2$ [83].

Up to this day, Chandrasekhar's approach is used as a starting point for studies on collisional relaxation [28]. However, the approximations used lead to problems such as a logarithmic divergence for stars separated by large distances and errors in the estimate for stars with very high or very low velocities [82]. More complete kinetic treatments, which

take into account inhomogeneity and collective effects, have been successful with respect to eliminating divergences [84]. The equations obtained, however, are complex and it can be impractical to solve them for real systems [49].

The greatest obstacle is the use of the velocity variable to characterize the orbits. For homogeneous systems, this is correct; however, when one approximates a gravitational system as homogeneous to calculate the mean variation of v due to two-body encounters and subsequently invokes the finite size of the system to find the total variation, errors may be introduced. In order to improve this approximation, the "orbit-averaging" method was introduced and used in Fokker-Planck simulations [85–87]. The root of this method consists in taking the expression for the variation in velocity due to an encounter and rewriting it in terms of the particle energy and angular momentum, then integrating over an orbit.

A more realistic orbit-averaging method is to use action-angle variables, which are the appropriate coordinates for inhomogeneous systems [88,89].

The action-angle variables are obtained from a canonical transformation [74],

$$\mathbf{J} = \frac{1}{2\pi} \oint p(\mathbf{q}) \mathrm{d}\mathbf{q} \tag{3.6}$$

where ($\mathbf{q}$,$\mathbf{p}$) are the position and momentum canonical coordinates and $\mathbf{J}$ is the action. For integrable systems, all degrees of freedom decouple and the canonical transformation above leads to a new Hamiltonian that is independent of the angle $\mathbf{w}$, and so

$$\mathbf{w} = \Omega(\mathbf{J})t + \mathbf{w_0} \tag{3.7}$$

where $\Omega(\mathbf{J}) = \partial h/\partial \mathbf{J}$ is the angular frequency. Under the adiabatic approximation, the actions should vary very slowly compared to the timescale of the fluctuations caused by two-body encounters and other perturbations. Therefore, the orbit-averaging procedure can be performed by integrating over the angle variables.

These approaches aim to simplify the calculation of the evolution of f under the rigorous kinetic equations, which have been developed by Lenard, Balescu, and Landau in the field of plasma physics. Heyvaerts applied these equations in action-angle variables in self-gravitating systems [84], and the reviews of Chavanis give a thorough presentation of this kinetic framework, see e.g. [49, 90]. In the next subsection, we give a brief outline of these equations, which are the subject of the work presented in section 4.4.

3.1.2 Kinetic treatment

Besides the BBGKY hierarchy, another intuitive way to understand the finite-size effects is through the Klimontovich equation. Taking again a system of N particles of mass m with coordinates ($\{\mathbf{r}_i\}_{i=1}^N$,$\{\mathbf{p}_i\}_{i=1}^N$) interacting through a long-range potential $\phi(|\mathbf{r}_i - \mathbf{r}_j|)$, we saw that the state of the system could be described by the $2Nd$-dimensional probability

density $f_N(\mathbf{R},\mathbf{P},t)$ (2.11), where $\mathbf{R}$ and $\mathbf{P}$ are Nd-dimensional vectors. The system can also be described by a $2d$-dimensional discrete distribution function $f_d(\mathbf{r},\mathbf{p},t)$ [3],

$$f_d(\mathbf{r},\mathbf{p},t) = \sum_{i=1}^{N} \delta[\mathbf{r} - \mathbf{r}_i(t)]\delta[\mathbf{p} - \mathbf{p}_i(t)]. \tag{3.8}$$

For a conservative system, the total number of particles remains the same so the convective derivative must be equal to zero,

$$\frac{Df_d}{Dt} = \frac{\partial f_d}{\partial t} + \frac{\mathbf{p}}{m} \cdot \nabla f_d - \nabla \psi_d[f_d] \cdot \nabla_{\mathbf{p}} f_d = 0, \tag{3.9a}$$

$$\psi_d[f_d(\mathbf{r},\mathbf{p},t)] = \int \mathrm{d}\mathbf{p}'\mathrm{d}\mathbf{r}' f_d(\mathbf{r}',\mathbf{p}',t)\phi(|\mathbf{r} - \mathbf{r}'|). \tag{3.9b}$$

Equation (3.9) is the Klimontovich equation. It gives the evolution of the N particles in the $2d$-dimensional configuration space, instead of the $2Nd$-dimensional phase space like the Liouville equation.

The discrete distribution function $f_d(\mathbf{r},\mathbf{p},t)$ is uniquely determined for any initial condition $f_0(\mathbf{r},\mathbf{p})$. By taking an average over many different initial conditions corresponding to the same macroscopic parameters, a smooth distribution function $f(\mathbf{r},\mathbf{p},t)$ is obtained,

$$f(\mathbf{r},\mathbf{p},t) = \langle f_d(\mathbf{r},\mathbf{p},t) \rangle \tag{3.10}$$

as well as a smooth mean-field potential,

$$\psi[f] = \int \mathrm{d}\mathbf{p}'\mathrm{d}\mathbf{r}' f(\mathbf{r}',\mathbf{p}',t)\phi(|\mathbf{r} - \mathbf{r}'|). \tag{3.11}$$

The smooth functions differ from the discrete functions by the fluctuations δf and $\delta\psi$, so that $f_d(\mathbf{r},\mathbf{p},t) = f(\mathbf{r},\mathbf{p},t) + \delta f(\mathbf{r},\mathbf{p},t)$ and $\psi_d(\mathbf{r}) = \psi(\mathbf{r}) + \delta\psi(\mathbf{r})$. By definition, $\langle \delta f \rangle = 0$ and $\langle \delta\phi \rangle = 0$.

By taking the same initial condition average over the Klimontovich equation (3.9) and subtracting the result from the unaveraged equation (3.9), one obtains

$$\frac{\partial f}{\partial t} + \frac{\mathbf{p}}{m} \cdot \nabla f - \nabla\psi \cdot \nabla_{\mathbf{p}} f = \nabla_{\mathbf{p}} \cdot \langle \delta f \nabla \delta\psi \rangle \tag{3.12a}$$

$$\frac{\partial \delta f}{\partial t} + \frac{\mathbf{p}}{m} \cdot \nabla \delta f - \nabla\delta\psi \cdot \nabla_{\mathbf{p}} f - \nabla\psi \cdot \nabla_{\mathbf{p}} f = 0. \tag{3.12b}$$

The system of equations (3.12) is known as the quasi-linear approximation, because in the first equation (3.12a) the term on the RHS is of order $\mathcal{O}[1/N]$, while in the second equation only terms of order up to $\mathcal{O}[1/\sqrt{N}]$ have been kept.

After some algebra [49], an important kinetic equation for the evolution of f can be

obtained from the results: the Lenard-Balescu equation

$$\frac{\partial f}{\partial t} = \pi(2\pi)^d m \frac{\partial}{\partial \mathbf{p}} \cdot \int \mathrm{d}\mathbf{k}\mathrm{d}\mathbf{p}'\, \mathbf{k}\, \mathbf{k} \frac{\delta[\mathbf{k}\cdot(\mathbf{p}-\mathbf{p}')]}{|D_{\mathbf{k},\mathbf{p}}|^2} \left(\nabla_{\mathbf{p}} - \nabla_{\mathbf{p}'}\right) f(\mathbf{p},t) f(\mathbf{p}',t) \tag{3.13}$$

where $1/|D_{\mathbf{k},\mathbf{p}}|$ is

$$\frac{1}{|D_{\mathbf{k},\mathbf{p}}|} = \frac{\hat{\phi}(\mathbf{k})}{\epsilon(\mathbf{k},\mathbf{k}\cdot\mathbf{p})}, \tag{3.14}$$

$\hat{\phi}(\mathbf{k})$ is the Fourier transform of the interaction potential $\phi(|\mathbf{r}-\mathbf{r}'|)$ and $\epsilon(\mathbf{k},\omega)$ is a dielectric function given by

$$\epsilon(\mathbf{k},\omega) = 1 - \hat{\phi}(\mathbf{k}) \int \mathrm{d}\mathbf{p} \frac{\mathbf{k}\cdot\partial f(\mathbf{p})/\partial \mathbf{p}}{\mathbf{k}\cdot\mathbf{p} - \omega}. \tag{3.15}$$

Through equation (3.14), we see that in the Lenard-Balescu equation, the interaction potential is "dressed" by the dielectric function given by equation (3.15). This "dressing" is known as collective effects. It is responsible for the polarization clouds that shield the charge of ions in neutral plasmas (Debye shielding), and for the gain in effective mass of stellar particles. It is a result of the field of particles reacting to its own perturbations. In some cases, such as stellar systems, it is argued that the collective effects are not important, and can be neglected [51]. For such cases, one can simply set $\epsilon(\mathbf{k},w) = 1$, which gives the Landau equation. However, other studies of stellar systems showed that the inclusion of collective effects can avoid (or, at least, damp) the occurrence of dynamical friction, corresponding to the drift/friction coefficient obtained from the Fokker-Planck equation (3.3), $D[\Delta v]$ [91,92]. Using the two-body encounter method of Chandrasekhar [93], the drift coefficient becomes

$$D[\Delta v] = 8\pi G m^2 \ln(\Gamma) n(<v) \tag{3.16}$$

where m is the mass of the test and field stars, $\ln\Gamma$ is the Coulomb logarithm and depends on the system size as well as the typical interparticle distance, and $n(<v)$ indicates the density of stars with velocity less than the velocity of the test star. Chandrasekhar's result shows that stars should suffer a friction that depends on their velocity and their mass; physically, it is caused by a density wake of stars that are gathered behind the test star as it moves through the field. His approach of two-body encounters between a test star and field stars does not include collective effects, however; the fields stars do not interact between themselves.

The damping of an important feature such as dynamical friction is an example of how collective effects can affect dynamics. It is still unclear to what extent they can be neglected, and when they should be included. This was one of the motivations of the work of section 4.4, in which B. Marcos and I calculate diffusion coefficients in action-angle variables for inhomogeneous states of the HMF model using Fokker-Planck equations derived from the Lenard-Balescu and the Landau equations. We were therefore able to compare the inclusion and exclusion of collective effects.

In equation (3.13), we see that when the Kac prescription is used and $m = 1/N$, the

timescale of the evolution of f goes at least with $\mathcal{O}[N]$. After such timescales, the system should have evolved sufficiently to approach thermodynamic equilibrium.

3.2 Thermodynamic equilibrium

Collisional relaxation should lead the system to the thermodynamic equilibrium described by Boltzmann-Gibbs statistical mechanics. Even though in this regime we may apply traditional statistical mechanics, certain peculiarities arise. These are mostly caused by two fundamental characteristics of LRI systems: nonadditivity and, to a lesser extent, nonextensivity. The lack of these properties can have important consequences for the thermodynamics of LRI systems.

3.2.1 Nonextensivity

A macroscopic quantity $A(\{x_i\})$ of a system is called *extensive* if, when its variables $\{x_i\}$ are multiplied by a constant λ, the quantity scales as λ, so $A(\lambda\{x_i\}) = \lambda A(\{x_i\})$. In other words, A is extensive if it is a homogeneous function of order 1. The thermodynamic potentials should be extensive. For example, if the temperature T, the volume V and the number of particles N is doubled, the Helmholtz free energy $F(T,V,N)$ should also double. Another example is the Boltzmann entropy $S = k_B \ln W$, where W is the number of states. For continuous systems, the number of states is related to the surface of constant energy in the $2Nd$-dimensional phase space. This clearly grows exponentially with N, and so the entropy must scale linearly with N and is therefore always extensive.

In long-range systems, this is not always the case. To illustrate this, let us look at the Curie-Weiss model, which is a LRI spin system that is commonly used to exemplify this characteristic due to its simplicity [3]. It consists of N spins that can be either "up" ($S = 1$) or "down" ($S = -1$), described by the Hamiltonian

$$\mathcal{H} = \frac{J}{2} \sum_{i=1}^{N} \sum_{\substack{j=1 \\ j \neq i}}^{N} S_i S_j \tag{3.17}$$

where J is the coupling constant (negative for ferromagnetic coupling, and positive for antiferromagnetic coupling).

Since there is a double sum over all N particles, the internal energy $U(N)$ clearly scales with N^2. Therefore, it is nonextensive: if we double the number of particles, the internal energy will be four times its original value. This is inconvenient for studying its thermodynamic properties. In the limit $N \to \infty$, the Helmholtz free energy will be trivially dominated by the internal energy U, since $F(T,V,N) = U(T,V,N) - TS(T,V,N)$ and as we have seen, S always scales with N. The temperature is intensive, that is, it remains unchanged when varying N.

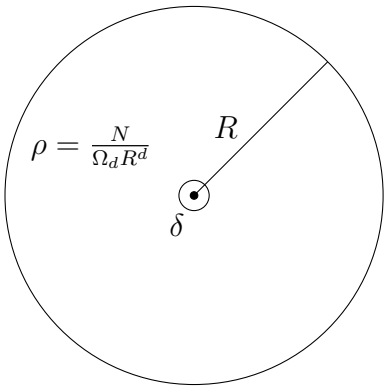

Figure 3.1: *Representation of a d-dimensional volume occupied by a homogeneous particle density ρ. The small radius δ represents a typical interparticle distance. Example taken from [3].*

Thus, in order to systematically study the thermodynamics of LRI systems of different sizes, the common procedure is to rescale the interaction coupling J by a factor $1/N$ (the Kac prescription, which we have seen before in chapter 2) [45, 46]. Equivalently, depending on the system and the parameters one wants to examine, the rescaling can be done with the volume, with a factor $1/V$. This restores extensivity. Other strategies are also possible, such as rescaling the temperature in order to make it extensive instead of intensive [94]. Then, both the U and TS terms would scale as N^2.

The above example of the Curie-Weiss model is simple because it is a lattice model and there is no defined distance measure with which the interaction decays, so the energy clearly scales as N^2. However, for continuous systems with an arbitrary LRI potential, the situation is not as immediately clear. We can still make an estimate by considering a homogeneous distribution of mass inside a d-dimensional volume of radius R (see Figure 3.1). Then, the density ρ is given by

$$\rho = \frac{N}{V} = \frac{N}{\Omega_d R^d} \tag{3.18}$$

where Ω_d is the angular contribution to the volume.

Taking a LR pair potential $\phi(|\mathbf{r} - \mathbf{r}'|)$

$$\phi(|\mathbf{r} - \mathbf{r}'|) = \frac{J}{|\mathbf{r} - \mathbf{r}'|^\alpha}, \tag{3.19}$$

the mean-field potential felt by a particle at the center of the distribution (the black dot in Figure 3.1) is

$$\begin{aligned} \psi &= J\rho\Omega_d \int_\delta^R \mathrm{d}r' r'^{d-1} \frac{1}{r'^\alpha} \\ &= J\rho \frac{\Omega_d}{d-\alpha} \left(R^{d-\alpha} - \delta^{d-\alpha} \right). \end{aligned} \tag{3.20}$$

For short-range systems, the thermodynamic limit consists in taking $N \to \infty$, $V \to \infty$, while $\rho = N/V$ is constant. Then, writing equation (3.20) as

$$\psi \sim J\rho\Omega_d \left(\frac{N^{1-\alpha/d}}{(\Omega_d \rho)^{1-\alpha/d}} - \delta^{\delta-\alpha} \right) \tag{3.21}$$

we see that the term that scales with N will tend to zero in the thermodynamic limit, since in short-range interactions $\alpha > d$. The energy of the particle will depend on its neighboring particles, corresponding to the typical short-range distance δ.

If, however, we consider the long-range case, where $\alpha < d$, the term proportional to $N^{1-\alpha/d}$ does not die out, and the energy of the particle grows with N. The total energy, roughly estimated as

$$U \sim N\psi \sim \frac{JN^2}{R^d}\left(R^{d-\alpha} - \delta^{d-\alpha}\right), \tag{3.22}$$

grows superlinearly with N, and is nonextensive in this thermodynamic limit.

More appropriately, the thermodynamic limit for LRI systems is $N \to \infty$, $J \to 0$, with $\gamma \equiv JN$ constant. Then,

$$U \sim N\gamma\left(\frac{1}{R^\alpha} - \frac{\delta^{d-\alpha}}{R^d}\right). \tag{3.23}$$

Once again, this limit introduces the Kac rescaling $1/N$, restoring extensivity.

3.2.2 Nonadditivity

Although extensivity is restored by rescaling the intensity of the interaction between particles, the system still lacks additivity. A quantity $A(x)$ is *additive* if it satisfies the relation $A(x_1 + x_2) = A(x_1) + A(x_2)$. Taking a system of N particles with short-range interactions and dividing it into two subsystems, we may write its internal energy as $E = E_1 + E_2 + E_{1,2}$, where E_1 and E_2 are the internal energies of subsystems 1 and 2, respectively, and $E_{1,2}$ is the energy of interaction between subsystems 1 and 2. For a short-range system, E_1 and E_2 scale with their respective volumes (or, equivalently, their respective number of particles). The energy of interaction between subsystems only occurs near the surface that separates them, therefore it scales as $V^{(d-1)/d}$; it is an *interfacial* energy. In the typical short-range thermodynamic limit, $N \to \infty, V \to \infty$, $E_{1,2}$ is completely negligible and thus the energy satisfies additivity.

Notwithstanding the Kac prescription, LRI systems remain nonadditive seeing as even the concept of an interfacial energy becomes ill-defined. This is immediately clear with the example of Campa *et al* [3], Hamiltonian (3.17) using the Kac prescription $J \to J/N$. If we split the system into a subsystem of $N/2$ spins with $S = 1$ and another of $N/2$ spins with $S = -1$, clearly $E_1 = E_2 = JN/8$, while the interaction energy is $E_{1,2} = -JN/4$, resulting in a total energy of $E = 0$. The interaction energy is *not* negligible compared to the subsystem energy; in this perfectly mean-field case, it is exactly the same as the negative of their sum. The interaction energy between subsystems is caused by interaction between their bulk, not their interface. Thus, the total energy is not additive.

The lack of additivity allows for the existence of convex regions of the entropy as a function of the energy, the so-called "convex intruders" that occur near first-order phase transitions [3]. In short-range systems, when the system has an energy $\varepsilon*$ corresponding to a convex entropy, it can split into two phases of energies ε_1 and ε_2 out of the convex region

in such a way that the total energy $\varepsilon_1 + \varepsilon_2 = \varepsilon*$ is the same. This is known as the Maxwell construction, and is possible due to additivity. In LRI systems, this separation is not possible and the states corresponding to convex entropies are physically accessible.

3.2.3 Ensemble inequivalence

Without additivity, the LRI system cannot divide into two coexisting phases near critical points. Therefore, when the system has a mean energy corresponding to a convex region of the entropy, its configuration is a valid microcanonical macrostate. These macrostates are not accessible in the canonical ensemble: the Legendre-Fenchel transform of the entropy with respect to the temperature can only be applied in concave regions, so the Maxwell envelope construction must be used. This ensures that the free energy is concave. Therefore, there may be macrostates corresponding to certain values of the internal energy that are accessible in the microcanonical ensemble which are not accessible in the canonical ensemble.

It has been proven that when the entropy is concave, the microcanonical and canonical ensemble are equivalent in the thermodynamic limit [1]. Since LRI systems may present nonconcave intervals of the entropy (which, importantly, are accessible macrostates), they may be inequivalent.

It is important to note that not all LRI systems present "convex" intruders, therefore having LR interactions is not a sufficient condition for this type of inequivalence. Nevertheless, many LRI systems do exhibit nonconcavity in the entropy: the Blume-Emery-Griffiths spin model [95], the Curie-Weiss-Potts model [96], models for turbulence [97], magnetically-confined plasmas [98] and gravitational systems [99]. Dipolar gases in optical lattices exhibit inequivalence between microcanonical and canonical ensembles; this inequivalence is of special interest since, unusually, they are best described experimentally by the microcanonical ensemble [100]. Cohen and Mukamel have shown that inequivalence may occur not only between microcanonical and canonical ensembles, but also between canonical and gran-canonical [9]. A survey on results of ensemble equivalence and inequivalence is given by Touchette in reference [101].

In some systems, the entropy may exhibit gaps in the domain of its thermodynamic parameters. Therefore, the microstates corresponding to the values of the parameter along these gaps are inaccessible, and without additivity the system cannot cross to other valid domains. This leads to a breaking of ergodicity in the microcanonical ensemble, while in the canonical ensemble the system is able to cross these forbidden regions [102, 103].

An interesting consequence of the lack of additivity is that it allows for negative specific heat, which is commonly known in the astrophysical community [10, 11]. To see how an isolated self-gravitating system can have negative heat capacity, it suffices to look at the virial theorem. As we saw in section 2.2, for three-dimensional self-gravitating systems, the virial theorem states that $2\mathcal{K} = -\mathcal{U}$ or $\mathcal{K} = -\mathcal{E}$ where $\mathcal{E} = \mathcal{K} + \mathcal{U}$. Using the equipartition

theorem, $\mathcal{K} = 3Nk_BT/2$, so

$$\frac{\partial \mathcal{E}}{\partial T} = -3Nk_B/2. \tag{3.24}$$

A physical interpretation is that as stars lose kinetic energy, they fall into orbits of lower potential energy, which will now increase their kinetic energy, more than what was initially lost.

Negative specific heat is only possible in the microcanonical ensemble—in the canonical ensemble, the specific heat by definition is positive. Therefore, near phase transitions, ensembles may be inequivalent [7, 104, 105].

3.3 Summary and relation to thesis

In this chapter we have reviewed some basic concepts relating to the second relaxation process of LRI systems, known as collisional relaxation, and the equilibrium properties of the states thereby achieved. The collisional relaxation occurs due to residual correlations between particles. In the thermodynamic limit, these correlations tend to zero and may be neglected. However, in real systems, N is finite and so the correlations will exist and will drive the system to thermodynamic equilibrium, although the typical relaxation timescale τ_R will scale with the system size (usually superlinearly).

In section 4.3 we study the effect of a short-range coupling in a mean-field model. The short-range coupling may induce stronger correlations which should reduce the relaxation timescale τ_R. The coupling also introduces the possibility of chaotic orbits in the mean-field limit, allowing us to examine any possible relation between chaos and collisional relaxation.

Collisional relaxation was also the focus of another work, presented in section 4.4. In this study, we used action-angle variables to find diffusion coefficients for kinetic equations describing the adiabatic evolution of inhomogeneous states of a mean-field spin model, the Hamiltonian-Mean-Field (HMF) model. This enables us to study the corresponding Fokker-Planck equation, which is a future project.

Regarding ensemble inequivalence and the equilibrium states of LRI systems, section 5.2 presents a microcanonical and canonical phase diagram for an XY model with a nematic coupling, the generalized HMF model. This model exhibits first-order phase transitions and ensemble inequivalence. The same model also presents a nonequilibrium phase diagram that is qualitatively and quantitatively different from its equilibrium diagram, in the sense that the transitions are of different orders and occur in different regions of parameter space. These results are presented in section 5.1.

Chapter 4

Hamiltonian Mean Field Model

The Hamiltonian Mean Field (HMF) model, is a one-dimensional model of N particles that interact through a sinusoidal potential. It was introduced in 1992 by Konishi and Kaneko as a symplectic map [39], and was first named HMF model by Antoni and Ruffo in 1995 [42]. In 1994, it was also introduced by Pichon in his doctoral thesis as a model for studying the bar formation in galactic disks [40]. It is a paradigmatic model for the LRI research community due to its computational simplicity while it maintains the representative characteristics of LRI systems, such as the existence of QSS [106]. Although considered a toy model, its dynamics can be representative of many physical phenomena, such as the bar formation cited above, as well as the free electron laser (FEL) [36] and dipole-dipole interactions in Bose-Einstein condensates [107].

The system is described by the Hamiltonian

$$\mathcal{H} = \sum_{i=1}^{N} \frac{p_i^2}{2} + \frac{1}{N} \sum_{i,j=1}^{N} \frac{1 - \cos\left(\theta_i - \theta_j\right)}{2}, \tag{4.1}$$

where (θ_i,p_i) are the canonically conjugate variables of position and momentum, respectively, of the ith particle. It can be interpreted as a system of particles confined to move on a ring of unitary radius, with the positions given by θ; or, equivalently, as a system of classical XY spins, in which all spins interact with all others.

Another form of writing the Hamiltonian given by equation (4.1) is

$$\mathcal{H} = \sum_{i=1}^{N} \frac{p_i^2}{2} + \sum_{i=1}^{N} \frac{1 - M\cos\theta_i}{2}, \tag{4.2}$$

$$M = \langle \cos\theta \rangle, \tag{4.3}$$

where we used $\langle \sin\theta \rangle = 0$, considering only distributions symmetric around $\theta = 0$ [72]. The magnetization M is the order parameter that distinguishes between the ferromagnetic $M > 0$ and the paramagnetic $M = 0$ states.

4.1 Ergodicity breaking and parametric resonances in systems with long-range interactions

The potential of the HMF model is not a homogeneous function of the distance between particles. As described in section 2.2, in these cases there is no virial condition that associates the potential and kinetic energy of a stationary state regardless of the form of the distribution. We can, however, deduce a generalized virial condition (GVC) that depends on the specific initial distribution.

In this work, we present a GVC for initial distributions of the water-bag (WB) type, $f_0(\theta,p) = \eta\Theta(\theta_m - |\theta|)\Theta(p_m - |p|)$. The GVC specifies, for a system with a given mean energy $\mathcal{E}$, the initial magnetization M_0 that minimizes the oscillations of the particle distribution. Besides minimizing the initial mean-field oscillations, the GVC should also predict the QSS magnetization of configurations that start away from the GVC curve. This should occur because any stationary state should satisfy the virial condition. Therefore, even if the initial magnetization does not correspond to the value predicted by our GVC for a given mean energy, the oscillations should be such that they lead to a QSS magnetization that *does* satisfy the GVC.

We showed that this is in fact the case, and that the virialised initial conditions are reasonably well described by LB statistics, while initial conditions off the GVC create high-energy halos that do not appear in LB distributions. This is in agreement with previous works by Levin *et al* that showed that LRI systems such as confined plasmas and self-gravitating systems are reasonably well described by LB statistics when the virial condition is satisfied, and form core-halo configurations when it is not [61, 62].

This work was done as part of my Masters research and was the first step in a project that was continued in my doctoral research. It was published as "Ergodicity breaking and parametric resonances in systems with long-range interactions" in the journal *Physical Review Letters*, volume 108, page 140601 (2012).

Ergodicity Breaking and Parametric Resonances in Systems with Long-Range Interactions

Fernanda P. da C. Benetti, Tarcísio N. Teles, Renato Pakter, and Yan Levin

Instituto de Física, Universidade Federal do Rio Grande do Sul, Caixa Postal 15051, CEP 91501-970, Porto Alegre, RS, Brazil

(Received 14 December 2011; published 3 April 2012)

We explore the mechanism responsible for the ergodicity breaking in systems with long-range forces. In thermodynamic limit such systems do not evolve to the Boltzmann-Gibbs equilibrium, but become trapped in an out-of-equilibrium quasi-stationary-state. Nevertheless, we show that if the initial distribution satisfies a specific constraint—a generalized virial condition—the quasistationary state is very close to ergodic and can be described by Lynden-Bell statistics. On the other hand, if the generalized virial condition is violated, parametric resonances are excited, leading to chaos and ergodicity breaking.

DOI: 10.1103/PhysRevLett.108.140601 PACS numbers: 05.20.−y, 05.45.−a, 05.70.Ln

Statistical mechanics of systems in which particles interact through long-ranged potentials is fundamentally different from the statistical mechanics of systems with short-range forces [1]. In the latter case, starting from an arbitrary initial condition (microcanonical ensemble) systems evolve to a thermodynamic equilibrium in which particle distribution functions are given by the usual Boltzmann-Gibbs statistical mechanics [2]. The state of thermodynamic equilibrium does not depend on the specifics of the initial distribution, but only on the global conserved quantities such as energy, momentum, angular momentum, etc. The situation is very different for systems in which particles interact through long-range potentials, such as gravity or unscreened Coulomb interactions [3–6]. In this case, it has been observed in numerous simulations that these systems do not relax to thermodynamic equilibrium, but become trapped in a quasistationary state (qSS), the lifetime of which diverges with the number of particles [4,6–8]. The distribution functions in this quasistationary state do not obey the Boltzmann-Gibbs statistical mechanics—and, in particular, particle velocities do not follow the Maxwell-Boltzmann distribution, but depend explicitly on the initial condition. It has been an outstanding challenge of statistical mechanics to quantitatively predict the final stationary state reached by systems with unscreened long-range forces, without having to explicitly solve the N-body dynamics or the collisionless Boltzmann (Vlasov) equation.

Some 40 years ago Lynden-Bell (LB) proposed a generalization of the Boltzmann-Gibbs statistical mechanics to treat systems with long-range interactions [9]. Lynden-Bell's construction was based on the Boltzmann counting, but instead of using particles, LB worked directly with the levels of the distribution function. The motivation for this approach was the observation that dynamical evolution of the distribution function for systems with long-range interactions is governed by the Vlasov equation [10]. This equation has an infinite number of conserved quantities, Casimirs—any local functional of the distribution function is a Casimir invariant of the Vlasov dynamics. In particular if the initial distribution function is discretized into levels, the volume of each level must be preserved by the Vlasov flow. For an initially one-level distribution function, Vlasov dynamics requires that the phase-space density does not exceed that of the initial distribution—one-particle distribution function over the reduced phase space (μ-space) evolves as an incompressible fluid. Using this constraint in a combination with the Boltzmann counting, LB was able to derive a coarse-grained entropy, the maximum of which he argued should correspond to the most-probable distribution—the one that should describe the equilibrium state. Numerous simulations, however, showed that, in general, Lynden-Bell statistics was not able to account for the particle distribution in self-gravitating systems, and the theory has been abandoned in the astrophysical context. Recently, however, Lynden-Bell's work has been rediscovered by the statistical mechanics community, which showed that for some systems, specifically the widely studied Hamiltonian mean-field model (HMF), Lynden-Bell's approach could make reasonable predictions about the structure of the phase diagram [11]. The fundamental question that needs to be addressed is: Under what conditions can Lynden-Bell statistics be used to accurately describe systems with long-range interactions? This will be the topic of the present Letter.

To be specific, we will study the HMF model [1], which has become a test bench for theories of systems with long-range forces. However, our results and methods are completely general and can be applied to other systems, such as self-gravitating clusters or confined non-neutral plasmas. The HMF model consists of N particles restricted to move on a circle of radius one. The dynamics is governed by the Hamiltonian

$$H = \sum_{i=1}^{N} \frac{p_i^2}{2} + \frac{1}{2N} \sum_{i,j=1}^{N} [1 - \cos(\theta_i - \theta_j)], \qquad (1)$$

where the angle θ_i is the position of ith particle and p_i is its conjugate momentum [11–13]. The *macroscopic* behavior of the system is characterized by the magnetization vector

$\mathbf{M} = (M_x, M_y)$, where $M_x \equiv \langle \cos\theta \rangle$, $M_y \equiv \langle \sin\theta \rangle$, and $\langle \cdots \rangle$ stands for the average over all particles. The Hamilton equations of motion for each particle reduce to

$$\ddot{\theta}_i = -M_x(t)\sin\theta_i(t) + M_y(t)\cos\theta_i(t). \tag{2}$$

Since the Hamiltonian does not have explicit time dependence, the average energy per particle,

$$u = \frac{H}{N} = \frac{\langle p^2 \rangle}{2} + \frac{1 - M(t)^2}{2}, \tag{3}$$

is conserved.

The failure of LB theory in the astrophysical context was attributed to incomplete relaxation, lack of good mixing, or broken ergodicity [14]. The mechanisms behind this failure have not been elucidated. On the other hand, it has been recently observed that if the initial distribution is virialized—satisfies the virial condition—LB's approach was able to quite accurately predict the stationary state of gravitational and Coulomb systems [3–6]. Unfortunately, the virial theorem can be derived only for potentials which are homogeneous functions. This is not the case for the HMF model. Nevertheless, the fact that LB theory seems to apply under some conditions makes one wonder if such conditions can be found for arbitrary long-range potentials, which are not in general homogeneous functions.

To answer the questions posed above, we note that if the initial distribution is virialized, macroscopic oscillations of observables should be diminished. On the other hand, if the system is far from virial, the mean-field potential that each particle feels will undergo strong oscillations. It is then possible for some particles to enter in resonance with the oscillations of the mean-field, gaining large amounts of energy. The parametric resonances will result in the occupation of regions of the phase space which are highly improbable, from the point of view of Boltzmann-Gibbs or LB statistics [15]. Furthermore, resonant particles will take away energy from collective oscillations producing a form of nonlinear Landau damping [16]. After some time, macroscopic oscillations will die out and each particle will feel only the static mean-field potential. From that point on, particle dynamics will become completely regular, with no energy exchange possible between the different particles. The particles which have gained a lot of energy from the parametric resonances will be trapped forever in the highly improbable regions of the phase space, unable to thermalize with the rest of the system.

To see how the theoretical picture advocated above can be applied to the HMF, we first derive a generalized virial condition for this model. For simplicity we will consider initial distributions of the "water-bag" form in (θ, p). Without loss of generality, we choose a frame of reference where $\langle \theta \rangle = 0$ and $\langle p \rangle = 0$. The one-particle initial distribution function then reads

$$f_0(\theta, p) = \frac{1}{4\theta_0 p_0}\Theta(\theta_0 - |\theta|)\Theta(p_0 - |p|), \tag{4}$$

where Θ is the Heaviside step function, and $|\theta_0|$ and $|p_0|$ are the maximum values of angle and momentum, respectively. Note that from symmetry, $M_y(t) = 0$ at all times. When the dynamics starts, the mean-squared particle position will evolve with time. We define the envelope of the particle distribution as $\theta_e(t) = \sqrt{3\langle \theta^2 \rangle}$, so that $\theta_e(0) = \theta_0$. We next differentiate $\theta_e(t)$ twice with respect to time to obtain the envelope equation of motion,

$$\ddot{\theta}_e = \frac{3\langle p^2 \rangle}{\theta_e} + \frac{3\langle \theta\ddot{\theta} \rangle}{\theta_e} - \frac{9\langle \theta p \rangle^2}{\theta_e^3}. \tag{5}$$

Using the conservation of energy, $\langle p^2 \rangle = 2u + M_x^2(t) - 1$. To calculate, $\langle \theta\ddot{\theta} \rangle$, we use the equation of motion for θ. Supposing that the distribution of angles remains close to uniform on the interval $[-\theta_e, \theta_e]$, we obtain

$$\begin{aligned}\langle \theta\ddot{\theta} \rangle &= \frac{-M_x(t)}{2\theta_e}\int_{-\theta_e(t)}^{\theta_e(t)} \theta\sin\theta d\theta \\ &= M_x(t)\cos\theta_e(t) - M_x^2(t),\end{aligned} \tag{6}$$

where the magnetization $M_x(t)$ is

$$M_x(t) = \frac{1}{2\theta_e}\int_{-\theta_e(t)}^{\theta_e(t)} d\theta\cos\theta = \frac{\sin\theta_e(t)}{\theta_e(t)}. \tag{7}$$

Neglecting the correlations between positions and velocities, $\langle \theta p \rangle = 0$, we finally obtain a dynamical equation for the envelope

$$\ddot{\theta}_e = \frac{3}{\theta_e(t)}(2u + M_x(t)\cos\theta_e(t) - 1), \tag{8}$$

where $u = p_0^2/6 + (1 - M_0^2)/2$ and $M_0 = \sin(\theta_0)/\theta_0$. The generalized virial condition is defined by the stationary envelope, $\ddot{\theta}_e = 0$, which means that along the curve

$$(2u - 1)\theta_0 + \sin\theta_0\cos\theta_0 = 0 \tag{9}$$

magnetization remains approximately invariant. In Fig. 1 we plot Eq. (9) in the M_0-u plane and compare it with the full molecular dynamics simulation of the HMF model. As can be seen, agreement between the theory and simulation is excellent.

Along the generalized virial condition curve, Eq. (9), the magnetization—and, therefore, the mean-field potential acting on each particle of the HMF model—has only microscopic oscillations and the parametric resonances are suppressed. Under these conditions, we expect that LB theory will be valid. The coarse-grained entropy within the LB approach is given by

$$s(f) = -\int dp d\theta\left[\frac{f}{\eta_0}\ln\frac{f}{\eta_0} + \left(1 - \frac{f}{\eta_0}\right)\ln\left(1 - \frac{f}{\eta_0}\right)\right], \tag{10}$$

where $\eta_0 = 1/4\theta_0 p_0$ [17]. Maximizing this entropy under the constraints of energy and particle conservation, we obtain the equilibrium distribution function

$$f(p, \theta) = \frac{\eta_0}{e^{\beta[(p^2/2) - M_x\cos\theta - \mu]} + 1}. \tag{11}$$

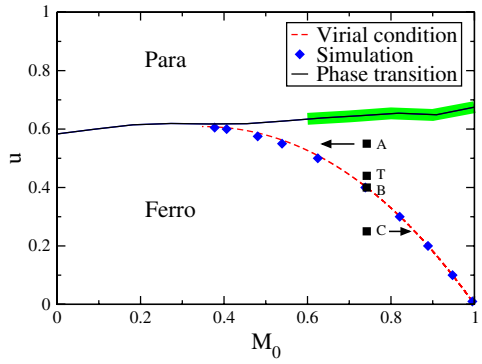

FIG. 1 (color online). Phase diagram of the HMF model obtained using the molecular dynamics simulations. Solid curve is the line of first order phase transitions separating paramagnetic and ferromagnetic phases. This line extends up to $M_0 = 0.6$, after which point the order of the phase transition, shaded region (green line), becomes unclear, with strong dependence on the initial conditions and various reentrant transitions occurring in this region. Dashed curve is the generalized virial condition, Eq. (9). Along this curve oscillations of the envelope are suppressed. Diamonds are the results of simulation. Starting with the initial energy and magnetization along the virial curve, diamonds show the final magnetization to which the system relaxes. For points along this curve, the final magnetization is almost identical to the initial one. Note that the generalized virial curve terminates at $M_0 = 0.34$ slightly below the phase transition line. This small difference, however, is sufficient to invalidate the Lynden-Bell theory, which for $M_0 = 0.4$ predicts a second order phase transition, while the simulations show that the phase transition is of first order [18]. Points (A), (B), and (C) correspond to the initial conditions for the distribution functions shown in Fig. 2. The Poincaré sections of the test particle dynamics for the initial conditions described by the points (B) and (T) are shown in Fig. 3. Finally, we note that since the stationary distribution must satisfy the virial condition and the energy is conserved, Eq. (9) allows us to predict the magnetization to which the system will evolve for initial conditions lying inside the ferromagnetic region, see the arrows for points (A) and (C).

The Lagrange multipliers μ and β are determined by particle and energy conservation,

$$\int dpd\theta f(p,\theta) = 1, \tag{12}$$

$$\int dpd\theta f(p,\theta)\left[\frac{p^2}{2} + \frac{1}{2}(1 - M_x\cos\theta)\right] = u, \tag{13}$$

respectively, and the magnetization by the self-consistency requirement,

$$\int dpd\theta\cos\theta f(p,\theta) = M_x. \tag{14}$$

Solving these equations numerically along the curve Eq. (9), we see that there is an excellent agreement between LB theory and the simulations, Fig. 2. If the macroscopic oscillations are suppressed and the parametric resonances are not excited, the system is able to relax to a quasiergodic equilibrium permitted by the Vlasov dynamics.

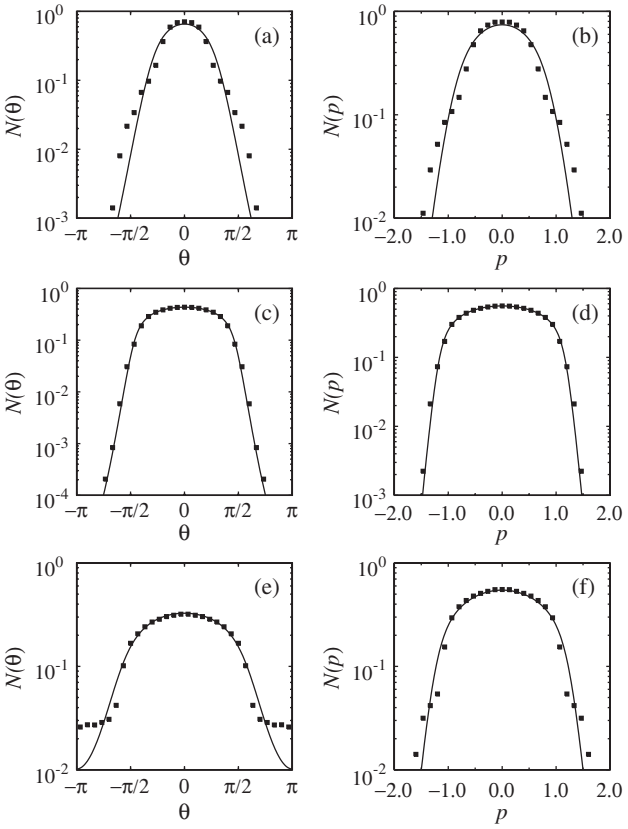

FIG. 2. The angle and velocity distribution functions corresponding to the initial conditions described by points (A), (B) and (C) of Fig. 1, respectively. Symbols are the results of molecular dynamics simulations and solid curves are the predictions of LB theory. The simulated distribution functions for the point (B), lying on the generalized virial curve, are in excellent agreement with the predictions of the LB theory [panels (c) and (d)], demonstrating that the dynamics along the generalized virial curve is quasiergodic. On the other hand, the distribution functions for points (A) and (C) deviate significantly from the predictions of LB theory — showing that away from the generalized virial curve, ergodicity is broken [panels (a),(b) and (e),(f)].

To make clear the role of parametric resonances in ergodicity breaking, in Fig. 3(a) we plot the Poincaré section of a set of noninteracting test particles, which at $t = 0$ are distributed in accordance with Eq. (4). The motion of each particle is governed by Eq. (2) with M_x determined by Eqs. (7) and (8). The position and momentum of each particle are plotted when magnetization is at its minimum. We see that if the energy and the initial magnetization lie on the generalized virial curve—point (B) of Fig. 1—particle trajectories are completely regular. However, when initial conditions do not coincide with the generalized virial curve—point (T) of Fig. 1—parametric resonances appear and dynamics becomes chaotic. Particles enter in resonance with the oscillations of the mean-field potential, gaining sufficient energy to move into statistically improbable regions of the phase space.

The Poincaré section of test particle dynamics is remarkably similar to the final stationary distribution obtained using the complete N-body molecular dynamics simulation of the HMF, Fig. 3. Equation (8) can also be used to calculate the period of the first oscillation of $M(t)$. For example, for point (T) of the phase diagram Fig. 1, we find the period to be $T = 5.0$, while the full molecular dynamics simulations gives $T = 5.4$. For point (C) we find $T = 3.85$, while the simulations give $T = 3.82$.

In conclusion, we have studied the mechanism responsible for the ergodicity breaking in systems with long-range interactions. Ergodicity breaking and the parametric resonances are intimately connected. If the macroscopic oscillations—and the resulting resonances—are suppressed, the system is able to relax to a quasiergodic stationary state. However, when the parametric resonances are excited, some particles are ejected to statistically improbable regions of the phase space, at the same time as the oscillations are damped out. The process of continuous particle ejection, and the resulting decrease of macroscopic oscillations of the envelope, leads to the formation of a static mean-field potential and to asymptotically integrable dynamics. Once the integrability of the equations of motion is achieved, the ergodicity becomes irreversibly broken. Unlike for particles with short-range interaction potentials, ergodicity is the exception rather than the rule for systems with long-range forces—it can only be observed if the initial distribution function satisfies the generalized virial condition derived in this Letter. Finally we note, that since the stationary distribution must satisfy the virial condition and the energy must be conserved, Eq. (9) allows us to predict the magnetization to which the system will evolve for initial conditions lying inside the ferromagnetic region. For example, point (A) of Fig. 1 which has initial magnetization and energy $M_0 = 0.74$ and $u = 0.55$, will evolve to a final stationary state with $M = 0.56$; while the point (C) with $M_0 = 0.74$ and $u = 0.25$, will evolve to a final stationary state with $M = 0.86$, which are precisely the values obtained using the molecular dynamics simulations.

This work was partially supported by the CNPq, FAPERGS, INCT-FCx, and by the US-AFOSR under the grant FA9550-09-1-0283.

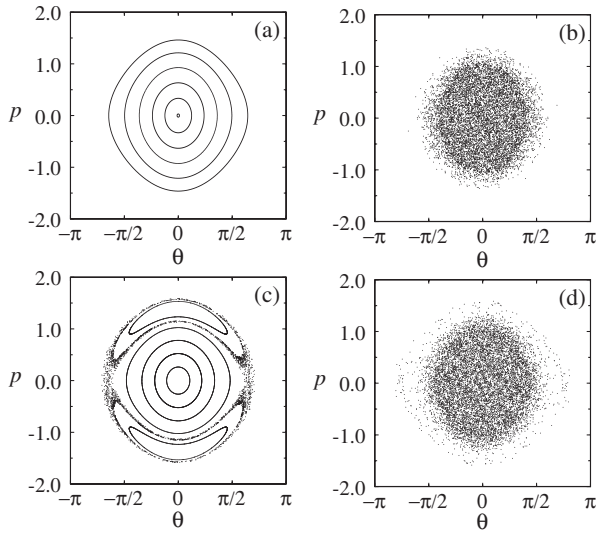

FIG. 3. Poincaré sections of test particles and snapshots of the phase space obtained using molecular dynamics simulation once the system has relaxed to qSS. Panels (a) and (b) correspond to the initial condition lying on the generalized virial curve, point (B) of Fig. 1. In this case the test particle dynamics is completely regular, and the stationary particle distributions are well described by LB theory. Panels (c) and (d) correspond to the initial conditions slightly off the virial curve, point (T) of Fig. 1. Even though we have moved only a little from the virial curve, we see the appearance of resonant islands and the dynamics of some of the test particles becoming chaotic. Such resonances drive some particles of the HMF to statistically improbable—from the point of view of the Boltzmann-Gibbs and LB statistical mechanics—regions of the phase space. Once the envelope oscillations are damped out, particle dynamics becomes completely integrable, and there is no mechanism for the resonant particles to equilibrate with the rest of the distribution. Thus, away from the generalized virial curve, ergodicity becomes broken.

[1] A. Campa, T. Dauxois, and S. Ruffo, Phys. Rep. **480**, 57 (2009).
[2] J. W. Gibbs, *Collected Works* (Longmans, Green and Co., NY, 1928).
[3] Y. Levin, R. Pakter, and T. N. Teles, Phys. Rev. Lett. **100**, 040604 (2008).
[4] T. N. Teles, Y. Levin, R. Pakter, and F. B. Rizzato, J. Stat. Mech. (2010) P05007.
[5] M. Joyce and T. Worrakitpoonpon, Phys. Rev. E **84**, 011139 (2011).
[6] T. N. Teles, and Y. Levin, and R. Pakter, Mon. Not. R. Astron. Soc. **417**, L21 (2011).
[7] J. Barré, D. Mukamel, and S. Ruffo, Phys. Rev. Lett. **87**, 030601 (2001).
[8] K. Jain *et al.*, J. Stat. Mech. (2007) P11008.
[9] D. Lynden-Bell, Mon. Not. R. Astron. Soc. **136**, 101 (1967).
[10] W. Braun and K. Hepp, Commun. Math. Phys. **56**, 101 (1977).
[11] A. Antoniazzi, F. Califano, D. Fanelli, and S. Ruffo, Phys. Rev. Lett. **98**, 150602 (2007); J. Barre, F. Bouchet, T. Dauxois, and S. Ruffo, Phys. Rev. Lett. **89**, 110601 (2002); T. M. Rocha Filho, A. Figueiredo, and M. A. Amato, Phys. Rev. Lett. **95**, 190601 (2005).P. H. Chavanis, Eur. Phys. J. B, **53**, 487 (2006).
[12] A. Antoniazzi, D. Fanelli, S. Ruffo, and Y. Y. Yamaguchi, Phys. Rev. Lett. **99**, 040601 (2007).
[13] A. Antoniazzi, D. Fanelli, J. Barré, P. H. Chavanis, T. Dauxois, and S. Ruffo, Phys. Rev. E **75**, 011112 (2007);
[14] D. Mukamel, S. Ruffo, and N. Schreiber, Phys. Rev. Lett. **95**, 240604 (2005).
[15] R. Bachelard, C. Chandre, D. Fanelli, X. Leoncini, and S. Ruffo, Phys. Rev. Lett. **101**, 260603 (2008).
[16] L. Landau, J. Phys. USSR **10**, 25 (1946).
[17] F. Staniscia, P. H. Chavanis, G. De Ninno, and D. Fanelli, Phys. Rev. E **80**, 021138 (2009).
[18] R. Pakter and Y. Levin, Phys. Rev. Lett. **106**, 200603 (2011).

4.2 Ergodicity breaking and quasi-stationary states in systems with long-range interactions

In the previous paper, we showed that LB statistics showed good results for the marginal distributions in θ and p when the GVC was satisfied. However, as we saw in subsection 2.3.3, a model based on assumptions very different from those of LB statistics was proposed to describe the QSS of the HMF, the integrable model of de Buyl *et al.* [75, 76]. In the QSS, the potential should be almost stationary, and so the particle dynamics can be uncoupled and described by the IM. We predicted that this model should be more successful than LB statistics for initial conditions on the GVC, because for these conditions the mean-field oscillations are minimized and so there is no mechanism for violent relaxation to occur and for particles to exchange energy. Seeing as LB statistics is fundamented on violent relaxation and mixing, the IM seems more appropriate to describe the dynamics.

In the work presented in the following publication, we applied both models, LB statistics and the IM, to describe the QSS of the HMF model. As a continuation of the work presented in the preceding section, we found a GVC for WB distributions of multiple density levels in p, the MLWB (multilevel water-bag) distribution, given by

$$f_0 = \sum_{i=1}^{L} \eta_i \Theta(\theta_m - |\theta|) \left[\Theta(p_i - |p|) - \Theta(|p| - p_{i-1})\right], \tag{4.4}$$

where L is the number of density levels, θ_m is the maximum value of θ of the distribution, p_i is the maximum value of p for the ith density level and $p_0 = 0$. We compared the marginal distributions in θ and p, as well as the energy distribution functions $f(\epsilon)$, of initially virialised conditions with different density levels. For each value of L, the IM results described the QSS distributions of molecular dynamics better than LB statistics. We also saw that, as we increased L, the agreement between molecular dynamics and the results of both theories gets worse. We concluded that the HMF dynamics is in fact closer to an integrable system than a system with ergodicity and mixing in phase space. The decrease in the success of the IM and LB models as L increases can be explained in part by the GVC, which may be insufficient to minimize the oscillations of each density level independently.

Our results were published in the article "Ergodicity breaking and quasi-stationary states in systems with long-range interactions" in *Physical Review E*, volume 89, page 022130 (2014). The article is presented on the following pages.

Ergodicity breaking and quasistationary states in systems with long-range interactions

Ana C. Ribeiro-Teixeira, Fernanda P. C. Benetti, Renato Pakter, and Yan Levin
Instituto de Física, Universidade Federal do Rio Grande do Sul Caixa Postal 15051, CEP 91501-970, Porto Alegre, RS, Brazil
(Received 30 October 2013; published 21 February 2014)

In the thermodynamic limit, systems with long-range interactions do not relax to equilibrium, but become trapped in quasistationary states (qSS), the life time of which diverges with the number of particles. In this paper we will explore the relaxation of the Hamiltonian Mean-Field model to qSS for a class of initial conditions of the multilevel water-bag form. We will show that if the initial distribution satisfies the virial condition, thereby reducing mean field changes, the final distribution in the qSS can be predicted very accurately using a reduced exactly integrable model. The calculated distribution functions obtained using this approach are found to be more accurate than the ones predicted by the Lynden-Bell theory.

DOI: 10.1103/PhysRevE.89.022130 PACS number(s): 05.20.−y, 05.45.−a, 05.70.Ln

I. INTRODUCTION

Long-range interacting (LRI) systems are ubiquitous in nature. They range from the astronomical scale [1–3], to the macroscopic, e.g., non-neutral plasmas [4,5], wave-plasma interacting systems (free-electron lasers) [6,7], and two-dimensional geophysical vortex systems [8], down to the atomic scale, e.g., classical and quantum cold atoms interacting via quasiresonant lasers [9,10]. In spite of their importance, much of the behavior of these systems remains poorly understood (for recent reviews, see, e.g., Refs. [11–13]). It is known that LRI systems can exhibit ergodicity breaking [14–17], anomalous relaxation and diffusion [18,19], quasistationary states (qSS) [20,21], vanishing Lyapunov exponents, inequivalence of ensembles [22–24], negative specific heat (nonconcave microcanonical entropies) [25,26], temperature discontinuities, etc. The thermodynamic anomalies result from the nonadditivity of energy, while the dynamical pathologies arise from the complexity of collisionless relaxation driven by the wave-particle interactions.

In the thermodynamic limit $N \to \infty$, the dynamics of systems with long-range forces is governed by the collisionless Boltzmann, or Vlasov, equation:

$$\frac{\partial f}{\partial t} + \mathbf{p}\cdot\nabla_{\mathbf{q}} f - \nabla_{\mathbf{q}} V[f](\mathbf{q},t)\cdot\nabla_{\mathbf{p}} f = 0, \qquad (1)$$

$$V[f](\mathbf{q},t) \equiv \int\int d\mathbf{q}'\, d\mathbf{p}'\, f(\mathbf{q}',\mathbf{p}',t)\, v(|\mathbf{q}-\mathbf{q}'|), \qquad (2)$$

where $f(\mathbf{q},\mathbf{p},t)$ is the one-particle distribution function and where $v(|\mathbf{q}-\mathbf{q}'|)$ is the two-body microscopic interaction potential. Note that the mean-field potential $V[f](q,t)$ is a functional of the one-particle distribution $f(\mathbf{q},\mathbf{p},t)$. This makes the Vlasov equation (1) nonlinear and very difficult to solve. Equation (2) shows that the mean-field potential and the distribution function dynamics are intertwined.

The dynamics of a large, but finite, N system may also be well approximated by the Vlasov equation up to time $t_{\max}$. Indeed, Braun and Hepp's theorem [27] states that for a two-body smooth long-range potential the "distance" (in the space of all measures) between two initially close solutions of the Vlasov equation increases at most exponentially in time, which establishes a lower bound $t_{\max} = O[\ln(N)]$ for the time up to which the molecular dynamics (MD) evolution of a finite N LRI system will be described by its associated Vlasov flow.[1] In fact, qSS (corresponding to *stable* stationary states of the Vlasov equation) persist for times that grow as a power of N [21]. Therefore, for LRI systems the $\lim N \to \infty$ and $\lim t \to \infty$ do not commute; taking the latter limit before the former, the system should reach thermodynamic equilibrium, while taking the former before the latter, Vlasov dynamics is always valid and thermodynamic equilibrium is not reached.

For LRI systems with a finite number of particles, the strongly oscillating mean-field potential and the resulting parametric resonances lead to a fast relaxation to qSS, on a time scale independent of N. This is known in astrophysics as a *violent relaxation* [28]. The time reversibility of the Vlasov equation implies that the phase space evolution continues indefinitely on progressively smaller scales. Therefore, no invariant fine-grained measure can ever be reached. Filamentation of the distribution function occurs because initially neighboring phase space elements will evolve according to distinct phase velocities. Evolution deforms initial condition support through ever finer filamentations. The coarse-grained distribution function $\bar{f}$, on the other hand, approaches a stationarity. The concept of qSS and of entropy production are valid only on a coarse-grained level $\bar{f}(\mathbf{q},\mathbf{p},t)$. In the limit $N \to \infty$, the mean-field potential in the qSS will become stationary, while for finite N small oscillations will persist indefinitely. These fluctuations will eventually drive a finite system out of the qSS and to the Boltzmann-Gibbs equilibrium. In this paper we will not be interested in the finite N corrections to the Vlasov dynamics, restricting ourselves to the time scale shorter than the lifetime of the qSS.

The determination of stable solutions to the Vlasov dynamics is not an easy task. Besides the usual constants of motion such as energy, linear and angular momentum, Vlasov

[1]The initial error of a large N particle approximation $f_N(\mathbf{q},\mathbf{p},t)$ of a continuous distribution $f(\mathbf{q},\mathbf{p},t)$ is $d_0 = O(1/\sqrt{N})$, on account of the central limit theorem. Hence, since Braun-Hepp's theorem is also valid for weak solutions, the maximum time during which the molecular dynamics discrete distribution may, within an error ϵ, coincide with its associated Vlasov description grows as $\ln(N)$ at least,

$$d(f_N, f) \lesssim d_0\, e^{\alpha t} \leqslant \epsilon \;\; \to \;\; t_{\max} \geqslant O[\ln(N)].$$

dynamics has an infinite number of conserved quantities known as the Casimir invariants or simply the Casimirs [29,30],

$$C_s[f] = \int s[f(\mathbf{q},\mathbf{p},t)]\, d\mathbf{q}\, d\mathbf{p}, \tag{3}$$

where $s(x)$ is an arbitrary functional. Their conservation is equivalent to the conservation of phase space densities, which are a special case of Casimirs. The Casimirs (3) represent an infinity of conserved quantities. A given initial condition will select from the start of the evolution a given invariant submanifold, which will correspond to one of the stable stationary states of the dynamics. Even if we were able to know all solutions (invariant submanifolds) to the Vlasov equation, we would still need to determine to which invariant submanifold a given initial condition would correspond.

The nonlinearity and the infinity of integrals of motion complicate the study of LRI systems. To circumvent the necessity of integrating the Vlasov equation to obtain the final stationary state, Lynden-Bell (LB) proposed a Boltzmann-like statistical approach. LB argued that the qSS should correspond to the maximum of the coarse-grained entropy [28]. For this to work, however, requires that the dynamics of a LRI system must be ergodic and mixing, which in general is not the case. Although simple and elegant, the LB theory *in general* is not able to predict accurately the particle distribution inside the qSS [13,31–38]. It was observed, however, that if the initial distribution satisfies the virial condition, and the oscillations of the mean-field potential are suppressed, the qSS marginal distribution functions predicted by the LB theory are in excellent agreement with the results of molecular dynamics simulations [2,3,5,17,35,39]. The virial theorem establishes a stable stationarity condition for a system of bound interacting particles. For an isolated system starting from an arbitrary initial condition, its kinetic and potential energies will oscillate around the corresponding virial condition, progressively approaching it as the system approaches stationarity. The closer the system is to such virial condition, the smaller is the amplitude of the mean-field potential oscillations.

On the other hand, if the initial distribution does not satisfy the virial condition, the mean-field potential undergoes violent oscillations. Some particles can then enter in resonance with the macroscopic oscillations gaining large amounts of energy, thus populating the regions of the phase space that are highly improbable from the perspective of LB or Maxwell-Boltzmann statistics, forming a thin halo. The particle evaporation produced by the resonances takes away energy from the collective motion leading to Landau damping [40–42] of the macroscopic oscillations of the mean-field potential. If the oscillations die completely, the mean-field potential becomes static and the dynamics of each particle becomes integrable (for systems with one degree of freedom). The final qSS reached by LRI systems is not ergodic, with the particle distribution often characterized by a "cold" dense core and a "hot" tenuous halo of evaporated (resonant) particles [13]. On the other hand, a good agreement between the LB theory and MD simulations for initial distributions satisfying the virial condition has been attributed to the existence of ergodicity and mixing. This, however, is paradoxical. As has been discussed above, the relaxation dynamics of LRI systems is driven by the fluctuations of the mean-field potential. If, on the other hand, the initial distribution function satisfies the virial condition, the oscillations will be suppressed diminishing the mixing of different phase space levels, which should lead to poor mixing and *lack* of ergodicity.

Recently, an approach very different in spirit to LB theory has been proposed to account for the qSS attained by the Hamiltonian Mean-Field (HMF) model [43–45]. Since the qSS are characterized by the virialization of the distribution, i.e., by the stationarity of the mean-field potential and consequent integrability of the model, it might be reasonable, under some conditions, to consider from the start the associated integrable model of uncoupled pendulums subject to an effective external field. The authors of Ref. [43] found that the marginal distributions for this integrable model (IM) fit well the corresponding HMF qSS distributions for some initial conditions. We shall argue here that this will be the case only if the oscillations of the mean-field potential are negligible from the start, i.e., if the initial distribution satisfies the virial condition. The possibility of approximating the dynamics of the HMF by that of an IM further demonstrates that the hypothesis of ergodicity intrinsic to LB statistics is not valid.

In this paper we will compare the predictions of LB statistics and of the IM with extensive MD simulations of the HMF model with initial multilevel water-bag distributions satisfying the virial condition. In addition to the marginal distributions [$P_\theta(\theta)$ and $P_p(p)$], we also calculate the energy distribution $f(\epsilon)$, which provides a sharper distinction among the different approaches [36,38]. With this comparison, we are interested in verifying whether the agreement observed between the LB theory and MD simulations for one-level distributions is fundamental or is simply a coincidence.

The paper is organized as follows: in Sec. II, we introduce the model and calculate the generalized virial condition for the multilevel ICs; in Sec. III we review the LB formalism; in Sec. IV, we present the IM of uncoupled pendula and use it to calculate the distribution functions for the qSS of the HMF; Sec. V is devoted to results and Sec. VI to conclusions.

II. HMF MODEL

The HMF is a paradigmatic model of a system with LRI [46,47]. The model was originally introduced to study the collective behavior observed in plasma and astrophysics. The model describes N interacting particles constrained to move on a unit circle, or N spins interacting through pairwise exchange interaction. The Hamiltonian of the ferromagnetic version of the model is given by (in units of the coupling constant)

$$\mathcal{H} = \sum_i \frac{p_i^2}{2} + \frac{1}{2N}\sum_{i,j=1}^{N}[1-\cos(\theta_i-\theta_j)], \tag{4}$$

where θ_i is the position of the ith particle on the unit circle and p_i is its conjugate momentum. In equilibrium the model has a second-order phase transition between a homogeneous and an inhomogeneous bunched (ferromagnetic) state.

The one-particle energy is

$$\epsilon(\theta,p) = \frac{p^2}{2} + 1 - M_x\,\cos(\theta) - M_y\,\sin(\theta), \tag{5}$$

where $M = M_x + i\,M_y = 1/N \sum_{j=1}^{N} e^{i\,\theta_j}$ is the instantaneous magnetization, i.e., the average mean-field felt by any particle [see Eq. (2)], which in the case of the HMF is a position-independent function of time:

$$M = \int d\theta\, dp\, f(\theta,p,t)\, e^{i\,\theta}. \tag{6}$$

In this work we will explore the microcanonical dynamics of the HMF, which conserves the average energy per particle $u = \frac{\langle p^2\rangle}{2} + \frac{1-|M|^2}{2}$.

A. Virial condition

The determination of the virial condition for the HMF model poses a problem, since its interaction potential is not a homogeneous function of coordinates. This means that one cannot find a relation between the averages of kinetic and potential energy, and instead we are left with a functional equation which depends on the one-particle distribution function. To proceed we observe that in a stationary state the virial $G = \langle \mathbf{p}\cdot\mathbf{q}\rangle$ does not depend on time, so that

$$\frac{d}{dt}\langle \mathbf{p}\cdot\mathbf{q}\rangle = \left\langle \frac{d}{dt}(\mathbf{p}\cdot\mathbf{q})\right\rangle = 0. \tag{7}$$

Rewriting the above equation as

$$\langle p^2\rangle = -\langle \mathbf{q}\cdot\ddot{\mathbf{q}}\rangle \tag{8}$$

and considering a self-averaging system, i.e., that the above time averages are equivalent to averages over the particles, while making use of Hamilton's equations, it is easy to show the previous equation is equivalent to

$$\langle p^2\rangle = -\frac{1}{N}\sum_{i=1}^{N} \mathbf{F}_i\cdot\mathbf{q}_i. \tag{9}$$

Furthermore, in the case that interactions are long range and in the thermodynamic limit, the mean-field limit is exact, and thus the two-particle distribution function factorizes into a (one-particle) density distribution (pair correlations vanish) [2]. The virial theorem in this case reduces to

$$\langle p^2\rangle = -\int d\mathbf{q}'\, d\mathbf{p}'\, f(\mathbf{q}',\mathbf{p}')\left[-\frac{\partial V(\mathbf{q}')}{\partial \mathbf{q}'}\cdot\mathbf{q}'\right], \tag{10}$$

where $V(\mathbf{q}')$ is the mean-field potential, given by (2). The $\langle\cdot\rangle$ denotes the time average, which is equivalent to the ensemble average with a stationary measure. In the case of the HMF model, however, one is still left with a functional equation since the stationary distribution is not known. In Ref. [17], the authors propose a generalized virial condition for a water-bag initial distribution centered at $\theta = 0$ ($M_y = 0$), with the support $[-\theta_m,\theta_m]\times[-p_1,p_1]$ in phase-space. Using Eq. (10), $\langle p^2\rangle = -\frac{\sin(\theta_m)\cos(\theta_m)}{\theta_m} + \frac{\sin^2(\theta_m)}{\theta_m^2}$. For the water-bag initial condition, $\langle p\,\theta\rangle(t=0) = 0$, which implies that $\langle\theta^2\rangle$ remains constant for short times, so that the water-bag domain is not deformed and the relation $M = \frac{\sin(\theta_m)}{\theta_m}$ continues to hold. Replacing $\langle p^2\rangle$ by the corresponding function of u and M, one ends up with the generalized virial condition for the HMF:

$$(2u-1)\theta_m + \cos(\theta_m)\,\sin(\theta_m) = 0. \tag{11}$$

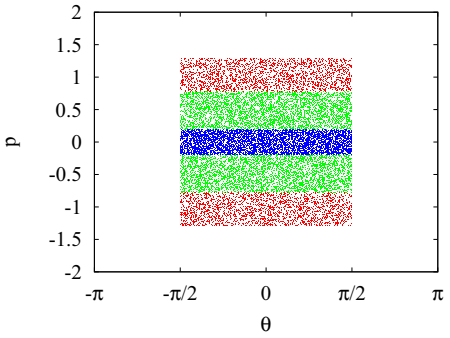

FIG. 1. (Color online) Phase-space representation of a multilevel initial condition. Different colors correspond to different phase space densities.

Equation (11) is only an approximation, since a water-bag distribution is not a stationary solution of the Vlasov equation. Nevertheless, the virial water-bag initial distribution should be "sufficiently close" to the final qSS to suppress any strong oscillations of the magnetization [17].

In this paper we will consider initial conditions uniform in θ, and multilevel in p, given by

$$f_0(\theta,p) = \begin{cases} \left.\begin{cases} \eta_1, & \text{for } 0 \leqslant |p| \leqslant p_1, \\ \eta_2, & \text{for } p_1 < |p| \leqslant p_2, \\ \vdots & \\ \eta_L, & \text{for } p_{L-1} < |p| \leqslant p_L, \end{cases}\right\} & \text{for } |\theta| \leqslant \theta_m, \\ 0, & \text{otherwise,} \end{cases} \tag{12}$$

where $p_1 < p_2 < \cdots < p_{L-1} < p_L$ (see Fig. 1). For these ICs, the initial magnetization is always the same function of the envelope of the distribution, θ_m: $M_0 = \frac{\sin(\theta_m)}{\theta_m}$, so the virial condition will be the same as Eq. (11).

III. LYNDEN-BELL STATISTICS

Lynden-Bell suggested a statistical approach, based on a *coarse-grained* entropy [28], to try to account for the mass distribution in elliptical galaxies. Since the relaxation to qSS of elliptical galaxies is collisionless and is characterized by very strong oscillations of the mean-field potential, LB called this process *violent relaxation*.

A fundamental insight of LB's theory is that Vlasov flow is incompressible. This can be seen by recognizing that the volume in phase space occupied by a given phase space density level,

$$\nu_\eta = \int d\mathbf{q}\, d\mathbf{p}\, \delta[f(\mathbf{q},\mathbf{p},t) - \eta], \tag{13}$$

is a Casimir invariant [Eq. (3)] and is, therefore, preserved by the dynamics. Notice that this implies that the phase space density at later times cannot exceed the maximum of the density at time $t = 0$.

Lynden-Bell argued that variations of the mean gravitational field to which particles (stars) are subjected are so violent that all phase space elements are equally likely to be found at a given energy. This is equivalent to requiring ergodicity and

mixing. The relaxation of such systems should take place under the following constraints:

(1) That the total number of elements of phase with a given mass density (resp. magnetic moment, charge density, etc.) is conserved (incompressibility of Vlasov flow, no sinks, no sources).

(2) That total energy is conserved (isolated system).

(3) No overlap of two elements of phase is allowed by the dynamics, since in this case there would be no conservation of the number of phase elements as stated before (exclusion).

These three assumptions are a direct consequence of the Vlasov equation to which the dynamics of the time-dependent phase space distribution function $f(\mathbf{q},\mathbf{p},t)$ is subjected. However, although very reasonable, the assumption of ergodicity does not have any *a priori* justification. This hypothesis, however, is crucial to LB statistics, since it allows a combinatorial counting of states, i.e., an "ensemble" approach to the distribution function.

LB defines a coarse-grained entropy, which is a functional of the coarse-grained one-particle density distribution $\bar{f}_{LB}(\mathbf{q},\mathbf{p}) = \sum_{\alpha=1}^{L} \bar{f}_\alpha(\mathbf{q},\mathbf{p})$ and must be maximized with respect to $\{\bar{f}_\alpha\}$. The index α runs over the L phase space levels, and $\bar{f}_\alpha(\mathbf{q},\mathbf{p})$ are the respective level distributions. The most probable qSS should be the one which maximizes the entropy subject to the constraints of conservation of the phase space volumes of each level [Eq. (13)] and of the total energy

$$\int \left(\frac{p^2}{2m} + \frac{V(\mathbf{q})}{2}\right) \bar{f}_{LB}(\mathbf{q},\mathbf{p}) d\mathbf{q}\, d\mathbf{p} = u. \tag{14}$$

$V(\mathbf{q})$ is the average mean-field potential at point q [Eq. (2) with $f(\mathbf{q},\mathbf{p},t) = \bar{f}_{LB}(\mathbf{q},\mathbf{p})$]. Since Vlasov dynamics does not lead to entropy production, entropy increase in the LB scheme is the result of coarse graining. Solving the variational problem, we obtain

$$\bar{f}_{LB}(\mathbf{q},\mathbf{p}) = \sum_{\alpha=1}^{L} \eta_\alpha \frac{\exp[-\beta_\alpha(\epsilon(\{q\},\{p\}) - \mu_\alpha)]}{1 + \sum_\gamma \exp[-\beta_\gamma(\epsilon(\{q\},\{p\}) - \mu_\gamma)]}, \tag{15}$$

where the η_α are the respective phase space level densities, and μ_α and $\beta_\alpha = \beta\,\eta_\alpha$ are the effective chemical potentials and the inverse temperatures, which enforce the respective phase space volumes and energy conservation. The "inverse temperature" β gives a measure of how degenerate the system is. In the limit of very low phase space density (high β), i.e., $f_\alpha \ll \eta_\alpha$, the LB distribution tends to a sum of Maxwellians.

The hypothesis of ergodicity "washes out" the memory of the initial condition, except for the conservation of the respective phase space volumes. Using the molecular dynamics simulations, in the forthcoming sections, we will show that conservation of the phase space volumes is not sufficient to predict the particle distribution in the qSS.

IV. INTEGRABLE MODEL ANALOGUE

We now consider an approach that is diametrically opposite from the ergodicity-based LB statistics [43,45]. When the system attains a qSS the mean-field potential must be stationary, $V(\mathbf{q},t) = V(\mathbf{q})$. Conversely, the mean-field potential can be stationary only if the density distribution function, $\rho(\mathbf{q}) \equiv \int d\mathbf{p}\, f(\mathbf{q},\mathbf{p},t)$, is also stationary [see Eq. (2)]. In this limit, particle movements uncouple, and $V(\mathbf{q})$ simply factors out as a constant (in the case of HMF, at least). Motivated by this, the authors in Refs. [43,45] propose that the qSS of the HMF model might be well described by the qSS attained by an associated IM of uncoupled pendulums subject to a fixed external field H, whose single-particle energy function is given by

$$\epsilon(\theta,p) = \frac{p^2}{2} + 1 - H\,\cos(\theta). \tag{16}$$

The value of the field H is then fixed self-consistently to be $H = \langle\cos(\theta)\rangle = \frac{1}{N}\sum_i \cos(\theta_i)$. It was observed, however, that even though for some initial conditions this approximation leads to qSS distributions which are in a good agreement with the MD simulations, in general this is not the case. Indeed, from our previous discussion, we expect that the distribution function of uncoupled pendulums will provide a reasonable approximation to the qSS distribution of the HMF only if the oscillations of the mean-field potential are negligible from the start, i.e., when the initial particle distribution satisfies the virial condition. On the other hand, if the initial condition is far from virial, the parametric resonances will lead to the formation of a qSS with a characteristic core-halo structure [13,17,48].

Determining the stationary distribution attained by the system of uncoupled pendulums is straightforward. Let's consider an arbitrary initial phase space distribution of angles and velocities. Evidently the dynamics of uncoupled pendulums is such that the number of pendulums with energy $[\varepsilon,\varepsilon+d\varepsilon]$ is a constant of motion. Since the force derived from Eq. (16) is nonlinear in angle, the particles on the energy shell $[\varepsilon,\varepsilon+d\varepsilon]$ with slightly distinct energies will have incommensurate orbital frequencies. Therefore, after a transient period, the resulting phase mixing will lead to a uniformity of the particle distribution over the energy shell. Suppose that we start with a distribution of angles and velocities $f_0(\theta,p)$. The number of particles with energy between $[\varepsilon,\varepsilon+d\varepsilon]$ is $n(\varepsilon)d\varepsilon$, where

$$n(\varepsilon) = \iint d\theta\, dp\; f_0(\theta,p)\;\; \delta[\epsilon(\theta,p) - \varepsilon]. \tag{17}$$

The density of states with a given energy $[\varepsilon,\varepsilon+d\varepsilon]$ is

$$g(\varepsilon) = \iint d\theta\, dp\;\; \delta[\epsilon(\theta,p) - \varepsilon]. \tag{18}$$

At $t = 0$, however, not all of these states are occupied. Nevertheless, as the dynamics evolves, the phase mixing will result in a uniform occupation of all the states of a given energy, keeping $n(\varepsilon)$ constant. The coarse-grained distribution function for the stationary state of a system of uncoupled pendulums $\bar{f}(\varepsilon)$ must then satisfy $\bar{f}(\varepsilon)g(\varepsilon) = n(\varepsilon)$, from which we conclude that

$$\bar{f}(\varepsilon) = \frac{\int\int d\theta\, dp\; f_0(\theta,p)\;\; \delta[\epsilon(\theta,p) - \varepsilon]}{\int\int d\theta\, dp\;\; \delta[\epsilon(\theta,p) - \varepsilon]}. \tag{19}$$

The density of states can be calculated explicitly to be [36]

$$g(\varepsilon) = \begin{cases} 4\,K(\kappa^{1/2})/\sqrt{H}, & \text{if } \kappa \leqslant 1, \\ 4\,K(\kappa^{-1/2})/\sqrt{H\kappa}, & \text{if } \kappa > 1, \end{cases} \tag{20}$$

where $\kappa(\varepsilon;H)=(\varepsilon-1+H)/2H$, and $K(x)$ is the complete elliptic integral of the first kind (defined as in Ref. [49]). Again it is important to stress that the formalism above applies only to the IM of uncoupled pendulums. In particular we see that the initial occupation of the energy shells is preserved throughout the dynamics. The initially unpopulated energy shells will remain unpopulated in the stationary distribution derived above. This, in general, is not the case for the HMF model away from the virial condition when the parametric resonances lead to the occupation of the high-energy states not present in the initial distribution. On the other hand, if the virial condition is satisfied, $M(t)$ will remain constant (in the thermodynamic limit) and the parametric resonances will be suppressed. In this case IM with $H=M(0)=M_0$ should provide an accurate description of the stationary distribution.

To calculate the coarse-grained distribution for the stationary state starting from an initial water-bag distribution $f_0(\theta,p)=\frac{1}{4\theta_m p_1}\Theta(\theta_m-|\theta|)\,\Theta(p_1-|p|)$, we must perform the integration over the phase space in the numerator of Eq. (19). Integrating first over momentum, we find

$$2\eta_1\int d\theta\ \Theta(\theta_m-|\theta|)\int_0^{p_1}dp\ \delta\left\{\frac{p^2}{2}-[\varepsilon-1+H\cos(\theta)]\right\}$$
$$=2\sqrt{2}\eta_1\int_0^{\theta_m}d\theta\ \frac{\Theta[\varepsilon-1+H\cos(\theta)]}{\sqrt{\varepsilon-1+H\cos(\theta)}}$$
$$\times\Theta\left\{\frac{p_1^2}{2}-[\varepsilon-1+H\cos(\theta)]\right\}, \tag{21}$$

where $\eta_1=\frac{1}{4\theta_m p_1}$ is the normalization constant of the density distribution function f_0. The theta functions in the integrand above impose restrictions on the domain of integration over θ. Performing the integration in θ, the numerator can then be written as

$$\int\int d\theta\,dp\ f_0(\theta,p)\,\delta[\epsilon(\theta,p)-\varepsilon]$$
$$=\frac{1}{\theta_m p_1}\frac{1}{\sqrt{H\kappa}}\left[F\left(\frac{\theta_{\rm up}^{(1)}}{2},\kappa^{-1/2}\right)-F\left(\frac{\theta_{\rm low}^{(1)}}{2},\kappa^{-1/2}\right)\right], \tag{22}$$

where $F(\phi,x)$ is the incomplete elliptic integral of the first kind, and the appropriate limits of integration $\theta_{\rm low}^{(1)}$ and $\theta_{\rm up}^{(1)}$ are defined below.

The L-level initial conditions defined by Eq. (12) may be considered as a superposition of water bags with different supports. Superposition of result (19) is possible since the pendulums are noninteracting. For these ICs the contribution to the numerator of Eq. (19) from each of the L water bags of the multilevel IC gives

$$I^{(i)}(\varepsilon;H)\equiv\frac{4\sqrt{2}}{\sqrt{H\kappa}}\left[F\left(\frac{\theta_{\rm up}^{(i)}}{2},\kappa^{-1/2}\right)-F\left(\frac{\theta_{\rm low}^{(i)}}{2},\kappa^{-1/2}\right)\right], \tag{23}$$

where the superscript (i) refers to a water bag with domain $[-\theta_m,\theta_m]\times[-p_i,p_i]$. The upper and lower limits of integration are determined by (see Fig. 2)

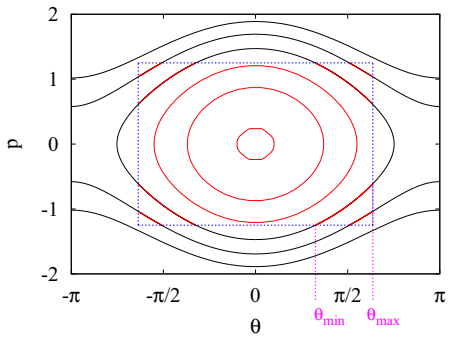

FIG. 2. (Color online) Schematic representation of the construction of the final distribution function for the uncoupled pendulums. Superimposed is the support of the water-bag initial condition. In red are the orbits (chunks of orbits) that contribute to the integral (19).

$$\theta_{\rm up}^{(i)}=\min\{\cos^{-1}(1-2\kappa),\theta_m\}$$
$$\theta_{\rm low}^{(i)}=\begin{cases}0, & \text{for } \epsilon\leqslant p_i^2/2-H,\\ \min\left\{\cos^{-1}\left(\frac{p_i^2}{2H}+1-2\kappa\right),\theta_m\right\}, & \text{for } \epsilon>p_i^2/2-H.\end{cases} \tag{24}$$

Of course, $I^{(i)}(\varepsilon;H)=0$ for energies $\varepsilon\leqslant 1-H$ or $\varepsilon\geqslant\varepsilon_{\rm max}=p_i^2/2+1-H\cos(\theta_m)$ [from Eq. (24)]. The single-particle distribution function is then given by

$$\bar{f}(\varepsilon)=\frac{\eta_L\,I^{(L)}+\sum_{i=1}^{L-1}(\eta_{L-i}-\eta_{L+1-i})\,I^{(L-i)}}{g(\varepsilon)}. \tag{25}$$

V. NUMERICAL RESULTS

To explore the validity of the theory constructed above we have performed molecular dynamics simulations of the HMF model with $N=10^6$ particles. The system is allowed to relax until a qSS is reached. We then compute the position and momentum marginal distribution functions $P_\theta(\theta)$ and $P_p(p)$, as well as the energy distribution $\bar{f}(\varepsilon)$ [36]. In Figs. 3–5 and 8–10 we compare the predictions of LB theory and of IM with the results of MD simulations for water-bag initial distributions with increasing number of levels L.

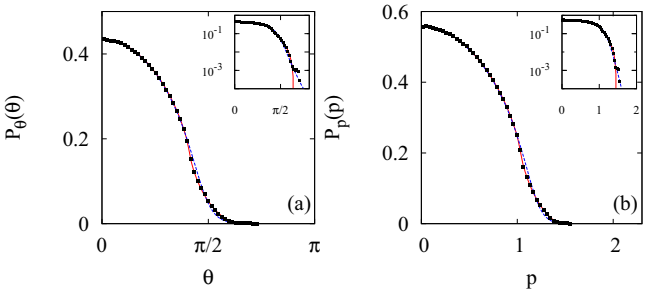

FIG. 3. (Color online) Comparison of the marginal distributions in (a) angles and (b) velocities with the results of MD simulations for the qSS of the HMF. The LB distribution (blue dashed curves) and the IM distribution (red solid curves) for a virial one-level water-bag initial condition with $u=0.4$, $M_0=0.742$.

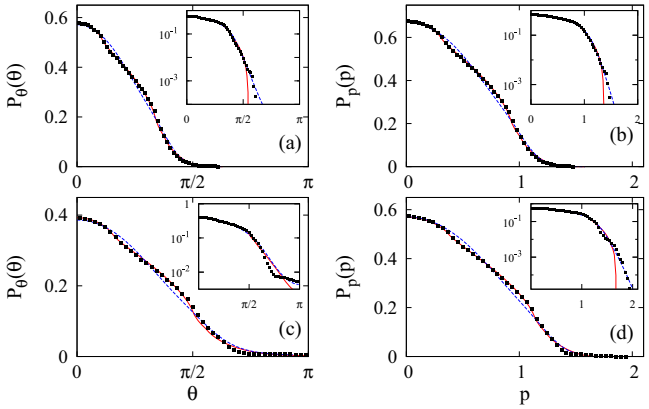

FIG. 4. (Color online) Comparison of the marginal qSS distributions in angle [(a) and (c)] and momentum [(b) and (d)] of the MD (black squares), the corresponding LB stationary distribution (blue dashed curves), and IM distribution (red solid curves), for two sets of virial two-level water-bag initial conditions. (a) and (b) $u = 0.3$, initial magnetization $M_0 = 0.822$, $\theta_m = 1.06$, $p_1 = 1.02$, $\eta_1 = 0.106$; (c) and (d) $u = 0.5$, $M_0 = 0.637$, $\theta_m = 1.58$, $p_1 = 1.24$, $\eta_1 = 0.059$. For both ICs $p_1 = 0.3p_2$, $\eta_2 = 0.5\eta_1$.

A. Marginal distributions

Figures 3–5 show the marginal distributions of angles (left panels) and velocities (right panels), which are calculated from the full single-particle density distribution function $f(\theta, p)$ as

$$P_\theta(\theta) \equiv \int dp\, f(\theta, p); \quad P_p(p) \equiv \int d\theta\, f(\theta, p). \quad (26)$$

Figure 3 is for a one-level water-bag initial condition; Fig. 4, for a two-level IC; and Fig. 5, for a three-level IC. We note the departure of both IM and LB from MD for increasing number of density levels L.

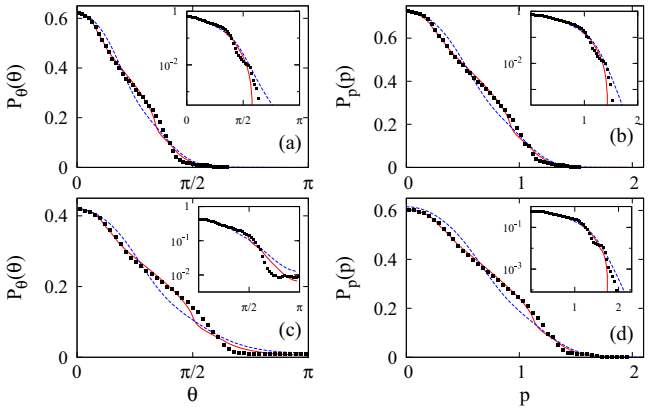

FIG. 5. (Color online) Comparison of the marginal qSS distributions in angle [(a) and (c)] and momentum [(b) and (d)] of the MD (black squares), the corresponding LB stationary distribution (blue dashed curves), and IM distribution (red solid curves), for two sets of virial three-level water-bag initial conditions. (a) and (b) $u = 0.3$, initial magnetization $M_0 = 0.822$, $\theta_m = 1.06$, $p_1 = 1.12$, $\eta_1 = 0.079$; (c) and (d) $u = 0.5$, $M_0 = 0.637$, $\theta_m = 1.58$, $p_1 = 1.35$, $\eta_1 = 0.044$. For both ICs $p_1 = 0.3p_2$, $\eta_2 = 0.5\eta_1$, $p_3 = 0.2p_1$, $\eta_3 = 0.3\eta_1$.

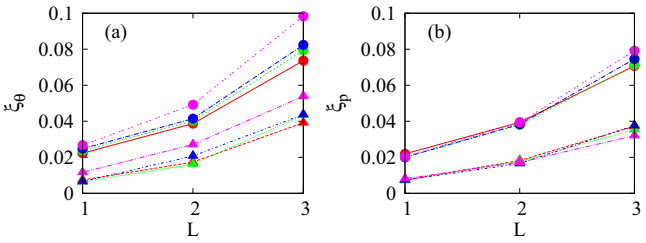

FIG. 6. (Color online) The rms deviations ξ_θ and ξ_p between the LB (IM) marginal distributions in angle and momentum, respectively, and the MD distributions, as a function of number of levels L. Triangles correspond to IM-MD deviation, ξ^{IM}, and circles to IM-MD deviation, ξ^{LB}. Red symbols (triangles and circles) correspond to $u = 0.2$; green symbols, to $u = 0.3$; blue symbols, to $u = 0.4$; and pink symbols, to $u = 0.5$.

Nevertheless, IM accounts very accurately for the MD data; see Figs. 3–5. The differences are noticeable only in the tails of the distributions. Although for one-level initial conditions LB theory provides an accurate description of the marginal distributions, this agreement deteriorates rapidly for multilevel initial conditions. The discrepancy between LB and MD simulations is clearest when one considers the complete distribution function $\bar{f}(\varepsilon)$. In the next section we will see

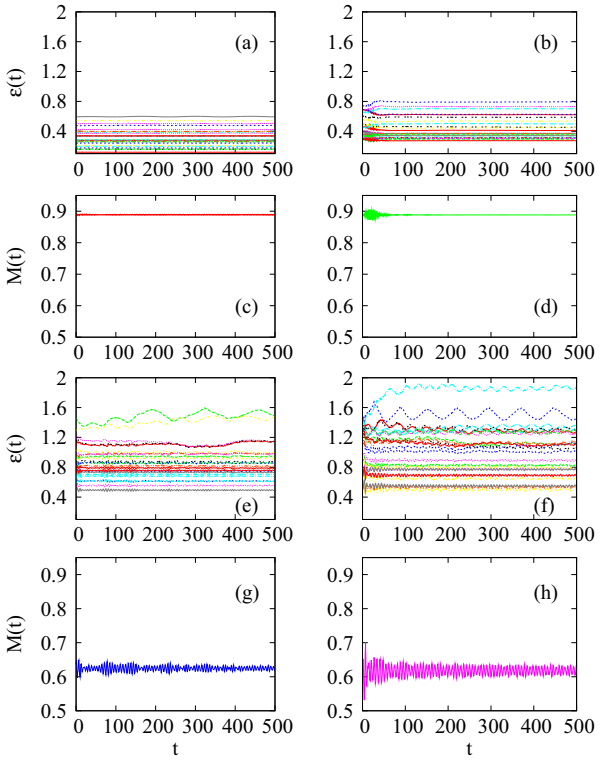

FIG. 7. (Color online) Comparison between the one-particle energies for a few selected particles and corresponding magnetization as a function of time. Panels (a) and (c) correspond to $u = 0.2$, $L = 1$; panels (b) and (d), to $u = 0.2$, $L = 3$; panels (e) and (g), to $u = 0.5$, $L = 1$; panels (f) and (h), to $u = 0.5$, $L = 3$. Note the presence of significant oscillations both in one-particle energy and in magnetization, for multilevel distributions.

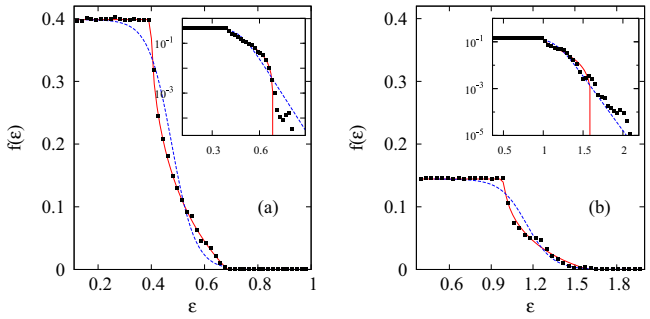

FIG. 8. (Color online) Comparison between MD qSS energy distribution function (black squares), the corresponding LB distribution (blue dashed curve), and IM stationary distribution (red solid curve), for a one-level water-bag IC; (a) $u = 0.2$; (b) $u = 0.5$. Insets are the same curves in log-linear scale. The same IC parameters as in Fig. 3.

that, although the simulations show the existence of a fully degenerate core, LB theory predicts a nondegenerate core characterized by a finite Fermi-Dirac temperature.

To quantify the extent of agreement between the MD simulations and IM and LB theories we define the root-mean-square (rms) deviation of $f_2(x)$ from a reference distribution $f_1(x)$ as

$$\xi_x = \left\{ \frac{\int dx\ [f_2(x) - f_1(x)]^2}{\int dx\ f_1^2(x)} \right\}^{1/2}. \tag{27}$$

In Fig. 6 we plot ξ_x for IM-MD (triangles) and for LB-MD (circles) for marginal distributions in angle and momentum. Although ξ do not exceed 10%, we see that for fixed L, the deviations between LB-MD are always greater than deviations between IM-MD. For given L and u, rms deviation between LB-MD is roughly twice the corresponding deviation between IM-MD. Therefore, the HMF qSS is closer to a completely integrable system than to the ergodicity based LB theory. Furthermore, since both ξ^{IM} and ξ^{LB} (either for P_θ or P_p) increase with increasing number of levels, results suggest that for general ICs, HMF qSS will be neither ergodic nor integrable.

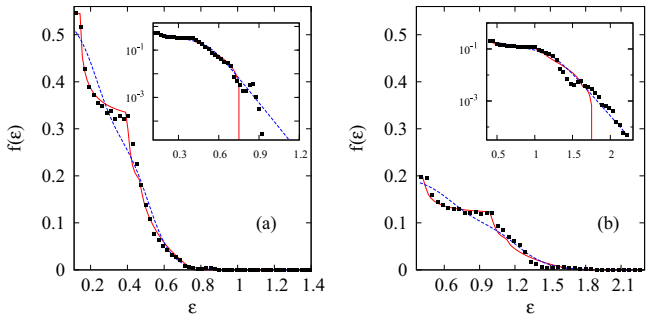

FIG. 9. (Color online) Comparison between MD qSS energy distribution function (black squares), the corresponding LB distribution (blue dashed curve), and IM stationary distribution (red solid curve) for a two-level IC; (a) $u = 0.2$; (b) $u = 0.5$. The same IC parameters as in Fig. 4.

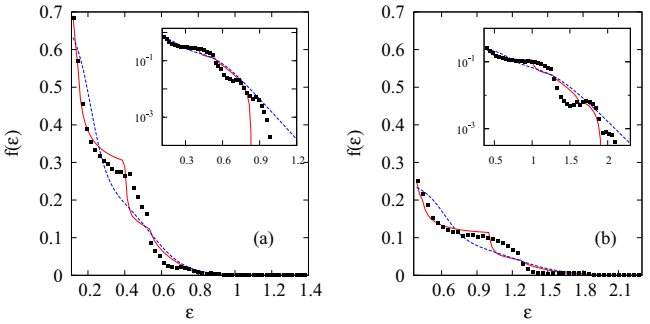

FIG. 10. (Color online) Comparison between MD qSS energy distribution function (black squares), the corresponding LB distribution (blue dashed curve), and IM analog stationary distribution (red solid curve) for a three-level IC; (a) $u = 0.2$; (b) $u = 0.5$. The same IC parameters as in Fig. 5.

The departure from IM predictions, in particular, is a consequence of the fact that, when increasing L, the virial condition (11) does not restrict the stationarity of all the density levels. This is clearly shown in Fig. 7, where we plot, side-by-side, single-particle energies' time evolution (for some selected particles of the system) and the time evolution of the system magnetization. There is a clear relationship between the amplitude of the oscillations of the magnetization and both the variation and variance of the single-particle orbit energies. It demonstrates that for multilevel water-bag distributions satisfying the generalized virial condition, both one-particle energies and magnetization undergo significant oscillations. These oscillations are expected to give rise to parametric resonances which will lead to the halo formation.

B. Energy distributions

The integration over angles (momentums) required to calculate the marginal distributions $P_p\,(P_\theta)$ smoothes out these functions. To explore better the one-particle distribution in the qSS it is, therefore, important to study the full distribution function $\bar{f}(\varepsilon)$:

$$\bar{f}(\varepsilon) = \frac{\int d\theta\, dp\ \ f(\theta,p)\ \ \delta\left[\epsilon(\theta,p) - \varepsilon\right]}{\int d\theta\, dp\ \ \delta\left[\epsilon(\theta,p) - \varepsilon\right]}, \tag{28}$$

where $\epsilon(\theta,p)$ is the single-particle energy function (5) and the denominator is the density of states $g(\varepsilon)$.

Figure 8 shows the comparison between MD, IM, and LB energy distributions for a one-level water-bag IC. Figure 9 shows the same for a two-level IC, and Fig. 10 for a three-level IC. Here again the discrepancy between IM predictions and the MD data is larger in the tails of the distributions. Even though the system starts on the virial curve (11), the water-bag IC is not a fixed point of the Vlasov dynamics. Therefore, for multilevel distributions the magnetization (mean-field potential) may undergo significant oscillations. In this case, some particles may enter in resonance with the mean-field oscillations gaining energy to form a tenuous halo.

For one-level water-bag initial conditions, we see that the MD-obtained energy distribution is in very good agreement

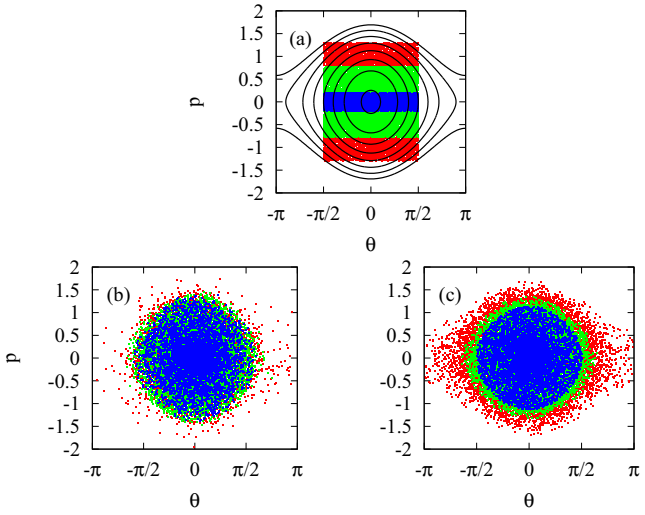

FIG. 11. (Color online) Snapshots of the phase space at (a) $t = 0$ (three-level IC); (b) $t = 1.7 \times 10^4$ time steps after evolution under Eq. (4) (HMF model); (c) $t = 10^3$ time steps after evolution under Eq. (16) (uncoupled pendulums). In both cases (b) and (c) systems have attained stationarity. The number of points is the same in all panels.

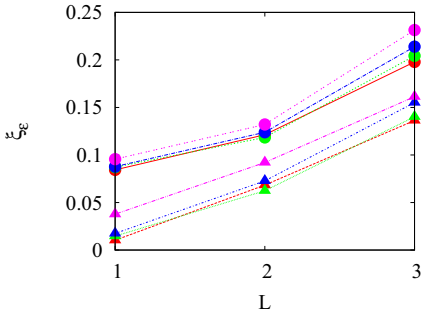

FIG. 12. (Color online) The rms deviations ξ_ε between LB (IM) energy distributions and the corresponding MD distribution, as a function of number of levels L. Triangles correspond to IM-MD rms deviation, ξ_ε^{IM}, and circles to IM-MD rms deviation, ξ_ε^{LB}. Red symbols (triangles and circles) correspond to $u = 0.2$; green symbols, to $u = 0.3$; blue symbols, to $u = 0.4$; and pink symbols, to $u = 0.5$.

with the predictions of IM. On the other hand LB theory is incompatible with MD data (see Fig. 8), while MD shows a *plateau* at the maximum phase-space density, corresponding to a fully degenerate Fermi core [48], LB predicts a smoothly decaying function, corresponding to a Fermi-Dirac distribution with a finite temperature.

For a two-level IC (Fig. 9), we see that the distribution function predicted by the IM deviates from the results of MD simulations. The qualitative structure, however, is maintained. In particular, a small (for the specific set of chosen parameters) plateau persists for low energies, as well as a two-step decay of $\bar{f}(\varepsilon)$, which reflects the two-level IC. While MD shows that the occupation of the lowest energy levels is the same as in the initial distribution, LB predicts a lower maximum density for the qSS. The perfect mixing required by LB allows for initially more energetic levels to decay and penetrate the region originally occupied by the less energetic levels, contrary to what is seen in numerical simulations [36].

For the three-level IC (Fig. 10), we see that the energy distribution starts to deviate significantly from predictions of IM. This is the result of mixing between the different density levels, which within IM is possible only among the initial levels lying on the same trajectory (orbit) (see Fig. 11). Nevertheless, we see that for lower energies, IM and MD curves still coincide. One might think that increased mixing between the different phase space density levels will lead to an improved agreement between LB theory and MD simulations. This, however, is not the case, and, in particular, we see that for three-level distributions LB theory provides an even poorer fit of MD data than for two levels.

One may notice that for higher average energies u [insets in the (b) panels in Figs. 8–10] the tails of the distributions, which lie close to the separatrix energy $\varepsilon_{sx} = 1 + M_0$, are closer to LB distribution. For these values of u, the separatrix is occupied by the initial distribution $f_0(\theta, p)$. Since at the separatrix the resonance criterion is met by mean-field oscillations of any frequency (and infinitesimal amplitude) [50], particles initially at $[\varepsilon_{sx} - \delta\varepsilon, \varepsilon_{sx} + \delta\varepsilon]$ will be excited, and the tails of $\bar{f}(\varepsilon)$ will not coincide with the distribution given by the IM approximation. Even though the LB distribution allows for particle excitation, we argue that similarity with the tails of the numerical data is incidental, since the particles forming the tails of the MD distributions represent a fraction of $\lesssim 0.1\%$ of the total system. Moreover, we argue that the similar behavior observed at the tails of the marginal distributions (Figs. 3–5) should be reminiscent of the same phenomenon, since the marginals $P_\theta(\theta)$ and $P_p(p)$ are derived from the full energy distribution $\bar{f}(\varepsilon)$ through integration over p or θ, respectively.

In Fig. 12 we compare the rms deviation ξ_ε^{IM} (triangles) and ξ_ε^{LB} (circles) as a function of the number of levels in the IC, for different values of the average energy per particle u. Once again we see that for a given L, the rms deviation ξ_ε^{IM} is always below ξ_ε^{LB}. Furthermore, sensitivity to u is much milder than sensitivity to L. Specially for the more complex ICs (two and three levels), the relative departure of LB and IM predictions for the energy distributions is significantly larger than it is for the marginal distributions, being close to 25% for $L = 3$ (ξ_ε^{LB}).

VI. CONCLUSIONS

We have computed, using extensive MD simulations, the qSS distribution functions of the HMF model starting from the multilevel water-bag initial conditions. The distributions were compared with the predictions of the Lynden-Bell theory and a theory based on the coarse-grained dynamics of uncoupled pendulums, the integrable model (IM) [28,44]. To suppress the halo formation all the initial water-bags were chosen to satisfy the generalized virial condition [17].

It is important to stress that LB and IM theories are based on diametrically opposite assumptions. While LB requires ergodicity and good mixing, IM is completely nonergodic. We have verified that for all sets of parameters considered, the HMF model was closer to the integrable limit than to the LB-postulated ergodicity. We have also verified that as

the initial conditions become more complex, i.e., as the number of levels increases, the distribution functions deviate stronger from the predictions of both LB and IM theories. Nevertheless for all the cases investigated, IM remained more accurate than LB theory. The challenge for the future is to understand the structure of the qSS for the multilevel distribution functions, which do not satisfy the virial condition. For one-level water bags the core-halo theory provides a very accurate description of the structure of such qSS [13]. For multilevel systems, however, the complicated mixing between the different phase-space density levels results in a very complex evolution of the core, which so far has escaped any simple characterization.

ACKNOWLEDGMENTS

The authors acknowledge discussions with Bruno Marcos and Tarcísio N. Teles. We also acknowledge support from CFCIF (IF/UFRGS) for computational resources. This work was partially supported by FAPERGS, CAPES, CNPq, and INCT-FCx and by the US-AFOSR under Grant No. FA9550-12-1-0438.

[1] T. Padmanabhan, Phys. Rep. **188**, 285 (1990).
[2] T. N. Teles, Y. Levin, R. Pakter, and F. B. Rizzato, J. Stat. Mech. Theor. Exp. (2010) P05007.
[3] T. Teles, Y. Levin, and R. Pakter, Mon. Not. R. Astron. Soc. **417**, L21 (2011).
[4] B. B. Kadomtsev and O. P. Pogutse, Phys. Rev. Lett. **25**, 1155 (1970).
[5] Y. Levin, R. Pakter, and T. N. Teles, Phys. Rev. Lett. **100**, 040604 (2008).
[6] J. Barré, T. Dauxois, G. De Ninno, D. Fanelli, and S. Ruffo, Phys. Rev. E **69**, 045501 (2004).
[7] A. Antoniazzi, Y. Elskens, D. Fanelli, and S. Ruffo, Eur. Phys. J. B **50**, 603 (2006).
[8] F. Bouchet and A. Venaille, Phys. Rep. **515**, 227 (2012).
[9] M. Chalony, J. Barré, B. Marcos, A. Olivetti, and D. Wilkowski, Phys. Rev. A **87**, 013401 (2013).
[10] E. Shahmoon, I. Mazets, and G. Kurizki, arXiv:1309.0555.
[11] T. Dauxois, S. Ruffo, and L. F. Cugliandolo, editors, *Long-Range Interacting Systems*, Lecture Notes of the Les Houches Summer School, Vol. 90 (Oxford University Press, Oxford, 2008).
[12] A. Campa, T. Dauxois, and S. Ruffo, Phys. Rep. **480**, 57 (2009).
[13] Y. Levin, R. Pakter, F. B. Rizzato, T. N. Teles, and Fernanda P. da C. Benetti, Phys. Rep. **535**, 1 (2014).
[14] T. Tsuchiya, T. Konishi, and N. Gouda, Phys. Rev. E **50**, 2607 (1994).
[15] F. Borgonovi, G. L. Celardo, M. Maianti, and E. Pedersoli, J. Stat. Phys. **116**, 1435 (2004).
[16] D. Mukamel, S. Ruffo, and N. Schreiber, Phys. Rev. Lett. **95**, 240604 (2005).
[17] Fernanda P. da C. Benetti, T. N. Teles, R. Pakter, and Y. Levin, Phys. Rev. Lett. **108**, 140601 (2012).
[18] V. Latora, A. Rapisarda, and S. Ruffo, Phys. Rev. Lett. **83**, 2104 (1999).
[19] V. Latora, A. Rapisarda, and S. Ruffo, Physica A **280**, 81 (2000).
[20] V. Latora, A. Rapisarda, and S. Ruffo, Phys. Rev. Lett. **80**, 692 (1998).
[21] Y. Yamaguchi, J. Barré, F. Bouchet, T. Dauxois, and S. Ruffo, Physica A **337**, 36 (2004).
[22] P. Hertel and W. Thirring, Ann. Phys. **63**, 520 (1971).
[23] J. Barré, D. Mukamel, and S. Ruffo, Phys. Rev. Lett. **87**, 030601 (2001).
[24] O. Cohen and D. Mukamel, J. Stat. Mech. Theor. Exp. (2012) P12017.
[25] W. Thirring, Z. Phys. **235**, 339 (1970).
[26] D. Lynden-Bell, Physica A **263**, 293 (1999).
[27] W. Braun and K. Hepp, Commun. Math. Phys. **56**, 101 (1977).
[28] D. Lynden-Bell, Mon. Not. R. Astr. Soc. **136**, 101 (1967).
[29] P. Chavanis and F. Bouchet, Astron. Astrophys. **430**, 771 (2005).
[30] T. M. Rocha Filho, A. Figueiredo, and M. A. Amato, Phys. Rev. Lett. **95**, 190601 (2005).
[31] Y. Y. Yamaguchi, Phys. Rev. E **78**, 041114 (2008).
[32] S. Goldstein, S. Cuperman, and M. Lecar, Mon. Not. R. Astr. Soc. **143**, 209 (1969).
[33] S. Cuperman, S. Goldstein, and M. Lecar, Mon. Not. R. Astr. Soc. **146**, 161 (1969).
[34] M. Lecar and L. Cohen, Astrophys. Space Sci. **13**, 397 (1971).
[35] M. Joyce and T. Worrakitpoonpon, Phys. Rev. E **84**, 011139 (2011).
[36] R. Pakter and Y. Levin, Phys. Rev. Lett. **110**, 140601 (2013).
[37] R. Pakter and Y. Levin, J. Stat. Phys. **150**, 531 (2013).
[38] A. Campa and P.-H. Chavanis, Eur. Phys. J. B **86**, 170 (2013).
[39] Y. Levin, R. Pakter, and F. B. Rizzato, Phys. Rev. E **78**, 021130 (2008).
[40] C.-S. Wu, Phys. Rev. **127**, 1419 (1962).
[41] D. Sagan, Am. J. Phys. **62**, 450 (1994).
[42] L. D. Landau, J. Phys. (USSR) **10**, 25 (1946).
[43] P. de Buyl, D. Mukamel, and S. Ruffo, Philos. Trans. R. Soc. London, Ser. A **369**, 439 (2011).
[44] P. de Buyl, D. Mukamel, and S. Ruffo, Phys. Rev. E **84**, 061151 (2011).
[45] X. Leoncini, T. L. Van Den Berg, and D. Fanelli, Europhys. Lett. **86**, 20002 (2009).
[46] T. Konishi and K. Kaneko, J. Phys. A **25**, 6283 (1992).
[47] M. Antoni and S. Ruffo, Phys. Rev. E **52**, 2361 (1995).
[48] R. Pakter and Y. Levin, Phys. Rev. Lett. **106**, 200603 (2011).
[49] I. S. Gradshteyn and I. M. Ryzhik, *Table of Integrals, Series and, Products* (Academic Press, New York, 2007).
[50] A. Lichtenberg and A. Lieberman, *Regular and Chaotic Dynamics, Applied Mathematical Sciences* (Springer, New York, 2010).

4.3 Chaos and relaxation to equilibrium in systems with long-range interactions

The objective of this work was to see the effect that a short-range coupling could have on the dynamics of the HMF model. Depending on the intensity of the coupling, the relaxation to equilibrium could be accelerated. With this in mind, we proposed a system composed of two coupled HMF models,

$$\mathcal{H}(\{\theta_i\},\{\phi_i\},\{p_{\theta_i}\},\{p_{\phi_i}\}) = \mathcal{H}_{\mathrm{HMF}}(\{\theta_i\},\{p_{\theta_i}\}) + \mathcal{H}_{\mathrm{HMF}}(\{\phi_i\},\{p_{\phi_i}\}) + \epsilon \sum_{i=1}^{N} \cos(\theta_i - \phi_i) \quad (4.5)$$

where $\mathcal{H}_{\mathrm{HMF}}$ is regular HMF model Hamiltonian given by equation (4.1), and the order parameters are given by

$$\begin{aligned} M_\theta &= \frac{1}{N}\sum_{i=1}^{N} \cos\theta_i, \\ M_\phi &= \frac{1}{N}\sum_{i=1}^{N} \cos\phi_i. \end{aligned} \quad (4.6)$$

The last term on the RHS of equation (4.5) gives the short-range coupling, with the intensity controlled by the parameter ϵ. Each pair of coordinates (θ_i,ϕ_i) are coupled. The θ, ϕ subsystems are internally mean-field, but coupled through the short-range coupling between each pair of coordinates of same index i. Figure 4.1 illustrates the model for $N = 5$, showing a ladder-type structure. Hence, we call this system the HMF-Ladder model.

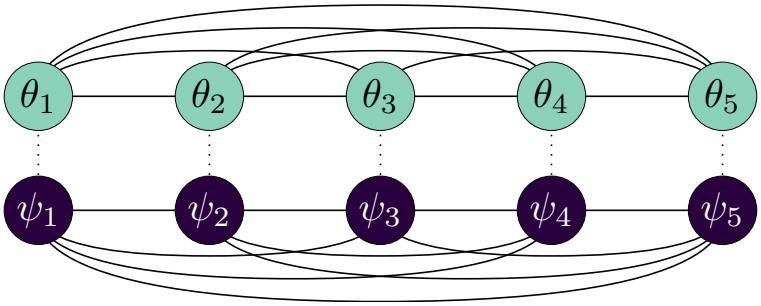

Figure 4.1: *Illustration of the interactions in the HMF-ladder model. Circles on the top (bottom) line represent particles of the θ (ψ) subsystem. The dotted lines between pairs of particles with same index i represent the short-range coupling $\epsilon\cos(\theta_i - \phi_i)$, while the solid lines represent the mean-field coupling between all particles in each subsystem. In this illustration, $N = 5$.*

The coupling between two degrees of freedom also introduces the possibility of chaotic orbits in the mean-field dynamics. In the QSS, oscillations of the magnetization should be very weak, and the dynamics can be approximated as that of independent rotors evolving under a stationary field M. For the normal HMF model, this means that the dynamics is integrable (the degrees of freedom in the Hamiltonian uncouple) [74]. However, in the HMF ladder model, even with stationary magnetizations M_θ and M_ϕ, the orbits can be chaotic

due to the coupling of the θ_i,ϕ_i variables. This allows us to also explore the role of chaos in the collisional relaxation process. To quantify the presence of chaotic orbits, we calculated the Lyapunov exponents λ of test particles evolving under stationary magnetizations.

To see the effect of the short-range coupling on the relaxation time, we simulated the molecular dynamics for different values of ϵ and controlled their approach to equilibrium with the kurtosis κ, given by

$$\kappa = \frac{\langle p^4 \rangle}{\langle p^2 \rangle^2}. \tag{4.7}$$

The value of the kurtosis for a Maxwell-Boltzmann distribution in 2 dimensions is $\kappa = 2$. By monitoring the value of κ, we can see how fast the system is relaxing to the equilibrium distribution. For each ϵ, we performed the MD simulations for different values of N and saw that the curves in κ scaled in time as $t \sim N^{\delta}$, where δ depends on ϵ.

Our expectation was that the value of δ should decrease as a function of ϵ: the short-range coupling should reduce the lifetime of the QSS. We also expected that the average Lyapunov exponent $\langle \lambda \rangle$ of the test particles evolving under the analogous QSS stationary magnetizations should increase as a function of ϵ: the short-range coupling should make orbits more chaotic. On the other hand, if the coupling is very strong, $\epsilon \sim 1$, both subsystems can synchronize and behave as one single HMF system. In this case, we expect that δ should tend to its value at $\epsilon = 0$.

The increase in $\langle \lambda \rangle$ as a function of ϵ was validated, as well as the decrease of δ for weak coupling $\epsilon \ll 1$. Thus, we found a correlation between increasing $\langle \lambda \rangle$ and decreasing δ, but only for weak coupling. In fact, δ begins to grow again at a surprisingly low value of $\langle \lambda \rangle$, indicating that the relation between chaotic orbits and the collisional relaxation time is unclear.

This work was published in the article "Chaos and relaxation to equilibrium in systems with long-range interactions" in the journal *Physical Review E*, volume 92, page 052123 (2015).

Chaos and relaxation to equilibrium in systems with long-range interactions

Felipe L. Antunes, Fernanda P. C. Benetti, Renato Pakter, and Yan Levin
Instituto de Física, Universidade Federal do Rio Grande do Sul, Caixa Postal 15051, CEP 91501-970, Porto Alegre, RS, Brazil
(Received 24 June 2015; revised manuscript received 17 September 2015; published 17 November 2015)

In the thermodynamic limit, systems with long-range interactions do not relax to equilibrium, but become trapped in nonequilibrium stationary states. For a finite number of particles a nonequilibrium state has a finite lifetime, so that eventually a system will relax to thermodynamic equilibrium. The time that a system remains trapped in a quasistationary state (QSS) scales with the number of particles as N^{δ}, with $\delta > 0$, and diverges in the thermodynamic limit. In this paper we will explore the role of chaotic dynamics on the time that a system remains trapped in a QSS. We discover that chaos, measured by the Lyapunov exponents, favors faster relaxation to equilibrium. Surprisingly, weak chaos favors faster relaxation than strong chaos.

DOI: 10.1103/PhysRevE.92.052123 PACS number(s): 05.20.−y, 05.45.−a, 05.70.Ln

I. INTRODUCTION

Systems in which particles interact through long-range (LR) forces remain an outstanding challenge to statistical physics. Such systems are characterized by an interparticle potential that decays with distance as $1/r^{\alpha}$, where $\alpha < d$ and d is the dimensionality of the embedding space [1–3]. Into this category fall galaxies and globular clusters [4,5], two-dimensional fluid models [6], confined plasmas [7], quantum spin models [8], dipolar systems [9], cold atoms models [10], and colloidal particles at interfaces [11]. LR interacting systems are found to have a complex relaxation process, with distinct time scales. Unlike systems in which particles interact by short-range potentials, in the thermodynamic limit LR systems do not relax to equilibrium but become trapped in out-of-equilibrium quasistationary states (QSS), the lifetime of which diverges with the number of particles. Once a system is trapped in a QSS, two outcomes are possible: if the system has a finite number of particles N, residual correlations will eventually drive it to thermodynamic equilibrium (if such equilibrium exists, which is not the case for 3D gravitational systems) after a time $t_{\times}$, which scales with N as $t_{\times} \sim N^{\delta}$, where δ is a system-specific exponent [12–14]. On the other hand, in the thermodynamic limit, $N \to \infty$, the system will remain trapped in a stationary state forever. In this collisionless limit, the relaxation to stationarity is a result of Landau damping [15–18], which transfers the energy of collective oscillations to the individual particles. Once the oscillations of the mean-field potential die out, the particles will move in a static mean-field potential. If a system has sufficient symmetry, the motion of particles in a static potential will be integrable, and the ergodicity will be irrevocably broken. This is often the case for gravitational systems whose initial particle distribution has a spherical symmetry and satisfies the generalized virial condition. On the other hand, if the initial distribution is spherically symmetric, but far from virial, strong density oscillations during the process of violent relaxation can lead to symmetry breaking [19–21]. This means that even if the initial distribution is spherically symmetric, the particle distribution and the static mean-field potential of the QSS will lack this symmetry. In general, equations of motion of a particle in a nonspherically symmetric potential are nonintegrable and chaotic orbits may be present. A natural question that arises is: will presence of chaos diminish the lifetime of a QSS, i.e., speed up the relaxation to thermodynamic equilibrium of a gravitational system [22]? That is, will a gravitational system in which spherical symmetry is spontaneously broken relax to thermodynamic equilibrium faster than a system in which this symmetry remains preserved, as suggested by Refs. [23] and [24]? Unfortunately, slow dynamics makes it very difficult to address this question in the context of self-gravitating systems. We are, therefore, forced to study simpler models that exhibit the same phenomenology as self-gravitating systems. However, even for simplified models it is very difficult to arrive at any analytical results. One possibility is to explore the Lenard-Balescu equation from plasma physics [25]. However, in order to be minimally tractable, this equation requires integrable one-particle dynamics [26], ruling out the possibility of studying the effects of chaos due to broken symmetry. In this paper we will, therefore, rely on molecular dynamics simulations to explore the effect of chaos on collisional relaxation of QSS to thermodynamic equilibrium.

II. HAMILTONIAN MEAN-FIELD MODEL

A paradigmatic model of a system with LR interactions is the Hamiltonian mean-field (HMF) model of particles moving on a circle. The Hamiltonian for this system is

$$H = \sum_{i=1}^{N} \frac{p_i^2}{2} + \frac{1}{2N} \sum_{i,j=1}^{N} [1 - \cos(\theta_i - \theta_j)], \tag{1}$$

where p_i and θ_i are the conjugate momenta and positions. If the initial particle distribution is symmetric, i.e., for each particle exists a particle in a symmetric position in phase space, the order parameter of the system—the magnetization per particle **M**—has only one nonzero vector component and can be written as

$$M = \langle \cos\theta \rangle, \tag{2}$$

where the brackets denote average over the particle distribution. The average energy per particle, $\varepsilon = H/N$, can then be expressed as

$$\varepsilon = \frac{\langle p^2 \rangle}{2} + \frac{1 - M(t)^2}{2}, \tag{3}$$

and the one-particle energy, $u_i = u(\theta_i, p_i)$, as

$$u_i = \frac{p_i^2}{2} + 1 - M(t)\cos(\theta_i), \tag{4}$$

corresponding to the energy of a single simple pendulum in a time-dependent potential. Introduced by Konishi and Kaneko as a symplectic map [27], modified to a continuous time system by Inagaki and Konishi [28], and, subsequently, presented by Antoni and Ruffo as a dynamical mean-field version of the XY spin model [29], the HMF model has been extensively studied in the literature. Depending on the overall energy of the system, the HMF has two phases: a high-energy paramagnetic (uniform) phase and a low-energy ferromagnetic (clustered) phase. The HMF model exhibits properties such as long-lived QSS, out-of-equilibrium phase transitions, and slow relaxation to thermodynamic equilibrium [1,2]. Like other LR interacting systems, the HMF model first reaches an out-of-equilibrium, nonmixed [30], QSS through a process of violent relaxation stabilized by Landau damping [31,32]. In the thermodynamic limit, $N \to \infty$, and in the ferromagnetic (clustered) phase, after the initial mean-field oscillations die out, the dynamics of spins (particles) becomes equivalent to noninteracting pendulums and chaos is absent. Integrable dynamics in the QSS prevents us from using this model to explore the role of chaos in relaxation to equilibrium. To address this question we, therefore, introduce a new model—the HMF-ladder—composed of two coupled HMFs interacting through a short-range sinusoidal potential. Since this model has two degrees of freedom, we expect that the spin dynamics of its QSS will be nonintegrable, allowing us to explore the role of chaos in relaxation to thermodynamic equilibrium.

III. HMF-LADDER MODEL

The dynamics of the conjugate momenta $\mathbf{p}_i = \{p_{\theta_i}, p_{\phi_i}\}$ and positions $\mathbf{q}_i = \{\theta_i, \phi_i\}$ of the HMF-ladder model is governed by the Hamiltonian

$$H = H_\theta + H_\phi + \epsilon \sum_{i=1}^{N} \cos(\theta_i - \phi_i), \tag{5}$$

where

$$H_\theta = \sum_{i=1}^{N} \frac{p_{\theta_i}^2}{2} + \frac{N}{2}\left(1 - M_\theta^2\right), \tag{6}$$

$$H_\phi = \sum_{i=1}^{N} \frac{p_{\phi_i}^2}{2} + \frac{N}{2}\left(1 - M_\phi^2\right), \tag{7}$$

and

$$M_\alpha = \langle \cos\alpha \rangle, \quad \alpha = \{\theta, \phi\}. \tag{8}$$

The terms given by Eqs. (6) and (7) correspond to the usual HMF model, Eq. (1). The mean energy per "particles," $\mathcal{E}$, is given by

$$\mathcal{E} = \varepsilon_\theta + \varepsilon_\phi + \epsilon \langle \cos(\theta - \phi) \rangle, \tag{9}$$

where

$$\varepsilon_\alpha = \frac{\langle p_\alpha^2 \rangle}{2} + \frac{1 - M_\alpha^2}{2}, \quad \alpha = \{\theta, \phi\}. \tag{10}$$

Unlike a simple HMF model in which particles have only one degree of freedom θ_i, positions of the "particles" of the HMF-ladder are described by a 2D vector $\mathbf{q}_i = \{\theta_i, \phi_i\}$. The dynamics of the HMF-ladder in general, therefore, will not be integrable even in a stationary state. The Hamilton equations of motion of the HMF-ladder are

$$\ddot{\theta}_i = -M_\theta \sin(\theta_i) + \epsilon \sin(\theta_i - \phi_i), \tag{11a}$$

$$\ddot{\phi}_i = -M_\phi \sin(\phi_i) - \epsilon \sin(\theta_i - \phi_i), \tag{11b}$$

where M_θ and M_ϕ are given by Eq. (8) where time is measured in units of $\tau_D = 1$. In this case, the one-particle energy, $\mathcal{U}_i = \mathcal{U}_i(\theta_i, \phi_i, p_{\theta_i}, p_{\phi_i})$, can be written as

$$\mathcal{U}_i = \frac{p_{\theta i}^2}{2} + \frac{p_{\phi_i}^2}{2} - M_\theta(t)\cos(\theta_i) - M_\phi(t)\cos(\phi_i) + \epsilon\cos(\theta_i - \phi_i) + 2, \tag{12}$$

corresponding to the energy of two coupled pendulums in a time-dependent potential.

IV. GENERALIZED VIRIAL CONDITION

In general, the dynamics of the HMF-ladder prior to its relaxation to QSS is very complicated, driven by various resonances arising from the particle-wave interactions. This makes the study of arbitrary initial conditions very difficult. There is, however, a class of initial conditions—called virial initial conditions [2]—for which the relaxation to QSS is adiabatic. Such initial distributions are particularly useful for exploring the relaxation to equilibrium, since in these cases the initial and QSS magnetizations will remain approximately the same. In this paper we will, therefore, explore the role of chaotic dynamics on the relaxation of virial initial conditions to thermodynamic equilibrium.

The virial theorem requires that in a stationary state

$$\langle p^2 \rangle = -\int d\mathbf{q}\, d\mathbf{p}\, f(\mathbf{q}, \mathbf{p}) \left[-\frac{\partial V(\mathbf{q})}{\partial \mathbf{q}} \cdot \mathbf{q} \right], \tag{13}$$

where $V(\mathbf{q})$ is the mean-field potential [2]. We expect that if the initial distribution satisfies the generalized virial condition (GVC), the macroscopic oscillations of magnetizations will be suppressed. Note that the fact that the distribution satisfies the generalized virial condition does not mean that it is already stationary. To be stationary it must be a time-independent solution of the collisionless Boltzmann (Vlasov) equation. Nevertheless, if the initial distribution satisfies the GVC, relaxation to QSS should be gentler, and strong oscillations of magnetizations should be suppressed. Furthermore, we expect that for such distributions the initial and final magnetizations will be almost the same.

The virial theorem for the HMF-ladder model is given by Eq. (13) with $\partial V(\theta, \phi)/\partial\theta = -\ddot{\theta}$, $\partial V(\theta, \phi)/\partial\phi = -\ddot{\phi}$, and $\langle p^2 \rangle = \langle p_\theta^2 \rangle + \langle p_\phi^2 \rangle$. That is,

$$\langle p_\theta^2 \rangle + \langle p_\phi^2 \rangle = -\int d\theta\, d\phi\, dp_\theta\, dp_\phi \times (\theta\ddot{\theta} + \phi\ddot{\phi}) f(\theta, \phi, p_\theta, p_\phi), \tag{14}$$

with $\ddot{\theta}$ and $\ddot{\phi}$ given by Eqs. (11). For weak coupling $\epsilon \ll |M_{\theta,\phi}|$, we use an ansatz that the virial theorem can be applied

independently to θ and ϕ subsystems, so that

$$\langle p_\theta^2 \rangle = \int d\theta\, d\phi\, dp_\theta\, dp_\phi [M_\theta \theta \sin\theta - \epsilon\theta \sin(\theta-\phi)] f(\theta,\phi,p_\theta,p_\phi), \quad (15)$$

$$\langle p_\phi^2 \rangle = \int d\theta\, d\phi\, dp_\phi\, dp_\theta [M_\phi \phi \sin\phi + \epsilon\phi \sin(\theta-\phi)] f(\theta,\phi,p_\theta,p_\phi). \quad (16)$$

Since the coupling ϵ is antiferromagnetic, the QSS magnetizations should obey $M_\theta = -M_\phi$. We, therefore, consider an initial distribution $f_0(\theta,\phi,p_\theta,p_\phi)$ composed of two antisymmetric water bags, that is,

$$f_0(\theta,\phi,p_\theta,p_\phi) = f_0^\theta(\theta,p_\theta) f_0^\phi(\phi,p_\phi), \quad (17)$$

with

$$f_0^\theta(\theta,p_\theta) = \eta_\theta \Theta(\theta_m - |\theta|)\Theta(p_m - |p_\theta|), \quad (18a)$$

$$f_0^\phi(\phi,p_\phi) = \eta_\phi \Theta(\phi_m - |\phi-\pi|)\Theta(p_m - |p_\phi|). \quad (18b)$$

The water-bag distributions in θ and ϕ are identical in momentum and have the same kinetic energy. Normalization requires that $\eta_\theta = 1/4\theta_m p_m$ and $\eta_\phi = 1/4\phi_m p_m$. The distributions are antisymmetric: f_0^ϕ is centered around π, while f_0^θ is centered on zero, with $\theta_m = \phi_m$ so $M_\theta = -M_\phi$. If the GVC is satisfied, the QSS magnetizations M_θ and M_ϕ should remain close to their initial values,

$$M_\theta = \frac{\sin\theta_m}{\theta_m}, \quad (19a)$$

$$M_\phi = -\frac{\sin\phi_m}{\phi_m}. \quad (19b)$$

Carrying out the integration in Eqs. (15) and (16) using the WB distribution Eqs. (18), we find

$$\langle p_\theta^2 \rangle = M_\theta^2 - M_\theta \cos(\theta_m) + \epsilon M_\phi \cos(\theta_m) - \epsilon M_\phi M_\theta, \quad (20a)$$

$$\langle p_\phi^2 \rangle = M_\phi^2 + M_\phi \cos(\phi_m) - \epsilon M_\theta \cos(\phi_m) - \epsilon M_\phi M_\theta, \quad (20b)$$

where we have used Eqs. (19).

The QSS magnetizations of systems whose initial distributions satisfy the GVC should be approximately the same as their initial values. We also suppose that, for a weak coupling $\epsilon \ll |M_{\theta,\phi}|$, the subsystems should remain roughly independent. Thus, we may approximate $\epsilon\langle\cos(\theta-\phi)\rangle \approx \epsilon M_\theta M_\phi$ (its initial value). Under these constraints, by conservation of energy $\langle p^2\rangle = \langle p_\theta^2\rangle + \langle p_\phi^2\rangle$ should also be preserved, and $\langle p_\theta^2\rangle = \langle p_\phi^2\rangle$ from symmetry. Therefore, we may use Eq. (9) to write

$$\langle p_{\theta,\phi}^2 \rangle = \mathcal{E} - 1 + \frac{M_\theta^2 + M_\phi^2}{2} - \epsilon M_\theta M_\phi. \quad (21)$$

Inserting the last expression in Eq. (20), and using $M_\phi = -M_\theta$, $\phi_m = \theta_m$, we obtain the GVC for the HMF-ladder, which can be written in terms of θ,

$$\mathcal{E} - 1 + M_\theta \cos\theta_m (1+\epsilon) = 0, \quad (22)$$

or of ϕ,

$$\mathcal{E} - 1 - M_\phi \cos\phi_m (1+\epsilon) = 0. \quad (23)$$

Both expressions are equivalent. Equations (22) and (23) can also be written in terms of each subsystem's mean "energy" (without the interaction term) ε_θ or ε_ϕ, given by Eq. (10). For the GVC described above, the two should be approximately equal, so we may define $\varepsilon = \varepsilon_\theta = \varepsilon_\phi$. Then, $\mathcal{E} = 2\varepsilon + \epsilon M_\theta M_\phi = 2\varepsilon - \epsilon M_\alpha^2$, $\alpha = \{\theta,\phi\}$, and the GVC reduces to

$$2\varepsilon - \epsilon M_\theta^2 - 1 + M_\theta \cos\theta_m (1+\epsilon) = 0, \quad (24a)$$

$$2\varepsilon - \epsilon M_\phi^2 - 1 - M_\phi \cos\phi_m (1+\epsilon) = 0. \quad (24b)$$

For $\epsilon = 0$, Eqs. (24) are the same as the GVC found for the HMF model [33,34].

In Fig. 1 we show the evolution of magnetizations for two initial WB distributions, calculated using molecular dynamics simulations, one of which satisfies GVC and the other one does not. As expected the oscillations of magnetization of a system that does not satisfy GVC are much more violent and the final QSS magnetization differs significantly from the initial value. On the other hand, for the WB distribution that satisfies GVC, the initial and final magnetizations are approximately the same.

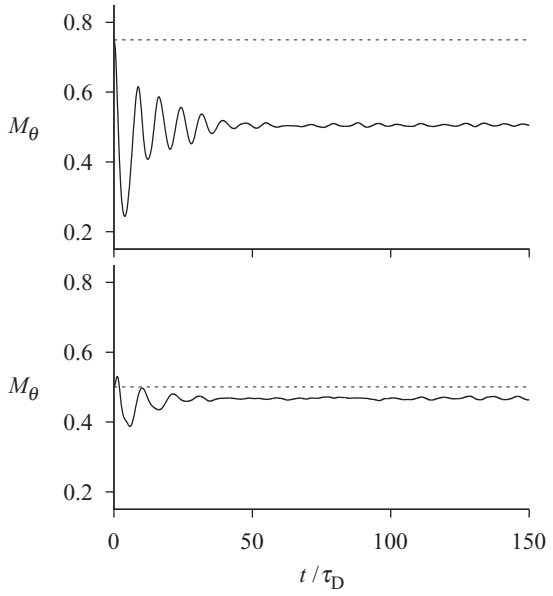

FIG. 1. Results of molecular dynamics simulations showing the short-time oscillations of the magnetization M_θ for two initial WB distributions. The top curve (solid line) is for the distribution that does not satisfy the GVC. The bottom curve (solid line) is for the initial distribution that satisfies the GVC. The horizontal dashed lines show the value of the initial magnetization for each case. Notice that for the distribution that satisfies the GVC, strong oscillations are suppressed and the final magnetization is close to the initial one. In both cases, $\epsilon = 0.1$ and $\varepsilon_\theta = \varepsilon_\phi = 0.6$, and the corresponding virial magnetization is $\sim$0.5. Due to symmetry, we show only M_θ and not M_ϕ ($M_\phi \approx -M_\theta$).

V. PARTICLE DYNAMICS

To explore the particle dynamics in a QSS we will consider Poincaré sections of test particles moving in a *fixed* mean-field potential determined by the generalized magnetizations. We are interested to study how the chaotic dynamics influences the relaxation of a QSS to thermodynamic equilibrium.

Lyapunov exponents

The central property of chaos is sensitivity to initial conditions (SIC). For a dynamical system, SIC implies that all "nearby" initial conditions result in orbits that separate exponentially fast from the original orbit. Suppose a one-dimensional dynamical system whose equation of motion is

$$\dot{x} = F(x). \tag{25}$$

Consider a given orbit, labeled a, and a second, nearby orbit, labeled b. For both orbits, we can write

$$\begin{aligned} \dot{x}_a(t) &= F(x_a), \\ \dot{x}_b(t) &= F(x_b). \end{aligned} \tag{26}$$

The distance between these orbits as a function of time is $d(t) = x_a(t) - x_b(t)$, which follows the time evolution

$$\dot{d}(t) = \dot{x}_a(t) - \dot{x}_b(t) = F(x_a) - F(x_b). \tag{27}$$

Since the second orbit begins very close to the first, we can expand $F(x_b)$ about the nearby position x_a, keeping only the first order term:

$$F(x_b) \approx F(x_a) + \left.\frac{\partial F}{\partial x}\right|_{x_a} (x_b - x_a), \tag{28}$$

$$= F(x_a) - \left.\frac{\partial F}{\partial x}\right|_{x_a} d(t). \tag{29}$$

Therefore, we can write Eq. (27) as

$$\dot{d}(t) = \left.\frac{\partial F}{\partial x}\right|_{x_a} d(t). \tag{30}$$

The largest Lyapunov exponent (LLE) λ_1 is a measure of this rate of separation: $\lambda_1 = \lim_{t\to\infty} \frac{1}{t} \ln \frac{d(t)}{d_0}$, where $d_0 = d(0)$ is the initial separation. If $\lambda_1 > 0$, the two nearby orbits will separate rapidly, and we have SIC and chaos [35,36]. Computationally, we cannot wait an infinitely long integration time, so we calculate an instantaneous Lyapunov exponent (LE) and wait long enough for this exponent to settle approximately to its asymptotic value. A strictly positive maximum Lyapunov exponent is synonymous to exponential instability [37]. A simple method of calculating the λ_1 based on its instantaneous value are provided by Benettin *et al.* [38]. In the case of the HMF-ladder, there are $4N$ Lyapunov exponents. But, for Hamiltonian flows, the Lyapunov exponent distribution (LED) has a symmetry $\lambda_i = -\lambda_{4N-i+1}$ and, since phase-space volume must be preserved, $\sum_{i=1}^{4N} \lambda_i = 0$. In addition in a QSS we have a conservation of particle energy, which, by symmetry, gives two zeros to the LED for each particle. Therefore, it is sufficient to calculate only the N largest LE, since the other exponents will be either zero or negative.

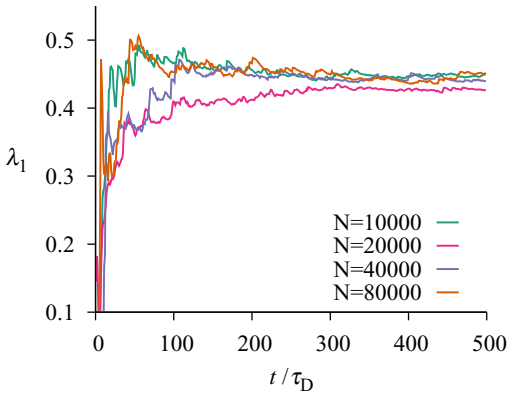

FIG. 2. (Color online) Evolution of the largest Lyapunov exponent (LLE), λ_1, to its stationary value, for the HMF model. The convergence to the same value, $\lambda_1 \simeq 0.45\,\tau_D^{-1}$, was found for different numbers of particles. This result is in agreement with the previous studies where the same behavior was observed and attributed to the instability of particles near a separatrix [40].

VI. NUMERICAL RESULTS

We have integrated the equations of motion using the fourth-order symplectic Position-Extended-Forest-Ruth-Like (PEFRL) algorithm [39] with a time step $dt = 0.1$ [38].

A. Molecular dynamics simulation

For molecular dynamics (MD) simulations of the HMF-ladder, we adopted the antisymmetric WB distribution, Eq. (18), with energy $\varepsilon_\theta = \varepsilon_\phi = 0.6$ that satisfies the GVC, Eq. (24). In Fig. 2 we first show the convergence of the LLE for the usual HMF model with the number of particles N, ranging from $N = 10^5$ to 8×10^5. We see that the final value is approximately the same for all N, $\lambda_1 \simeq 0.45\,\tau_D^{-1}$. This is a surprising result, since we expect that the particle dynamics of HMF in a QSS should be completely integrable, with LLE equal to zero. To understand better the positive value of the LLE of the HMF, we have performed a test particle dynamics simulation in which each particle moves in a *fixed, time independent,* mean-field potential determined by the initial particle distribution. We then calculated the LLE of *each* test particle. As expected, for all the particles, the LLE is zero, except for the particle near the separatrix, for which $\lambda_1 \simeq 0.28\,\tau_D^{-1}$. This result suggests that the nonvanishing LLE value found for the HMF model may be due to unstable behavior of particles near the separatrix, as was also suggested in Ref. [40]. Therefore, the LLE does not provide us with an accurate measure of the degree of chaos present in a many-body system, since its value is dominated by one unstable particle near a separatrix. Unfortunately, it is practically impossible to calculate the exact LED for $N = 10^5$ particles. We expect, however, that for initial conditions that satisfy GVC this spectrum should be similar to the spectrum of noninteracting test-particles moving in a fixed mean-field potential. The LED of test particles can be easily obtained by simply calculating the LLE of *each* test-particle of the initial distribution.

B. Test particle model simulation

To calculate the LED, we numerically integrated Eqs. (11) for the initial particle distribution of WB form satisfying

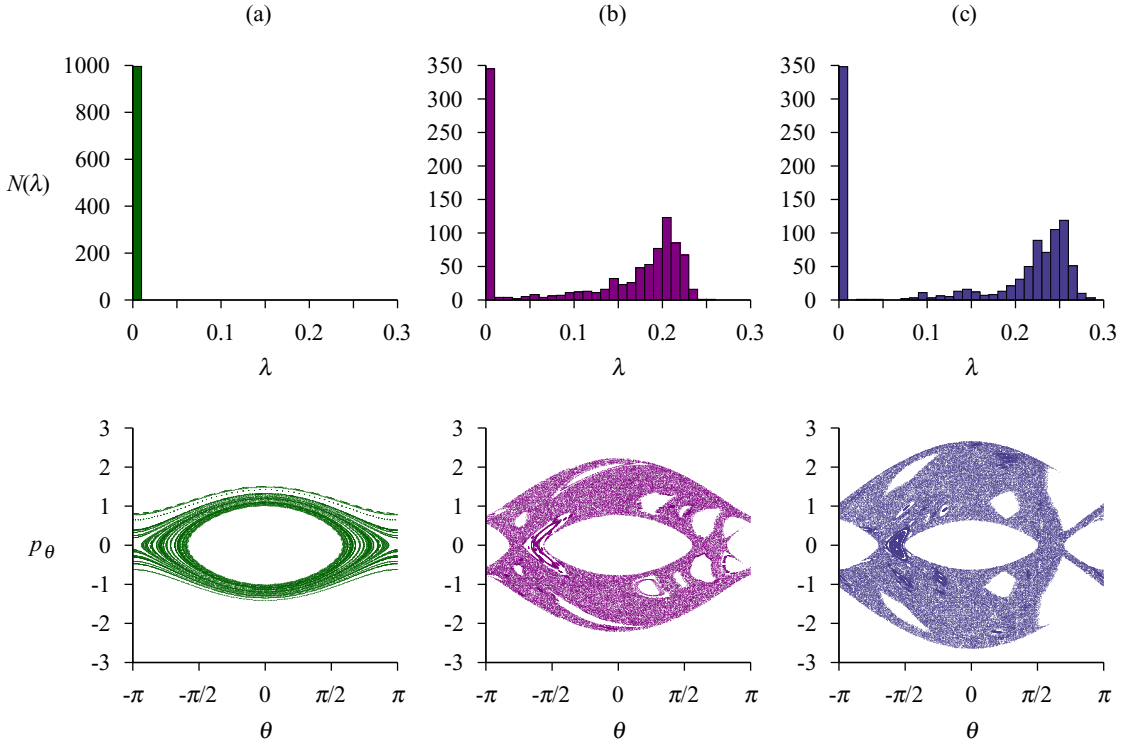

FIG. 3. (Color online) Lyapunov exponent distribution (top) and Poincaré sections (bottom) of the test-particle model for $\epsilon = 0.0$ (left column), $\epsilon = 0.5$ (middle column), and $\epsilon = 1.0$ (right column). The Poincaré sections corresponding to $\epsilon = 0.0$, $\epsilon = 0.5$, and $\epsilon = 1.0$ are of 50 test particles with energy 2.5, 2.8, and 3.2, respectively, taken when $p_\phi = 0$. We see a correlation between Poincaré sections with nonchaotic regular orbits and LED dominated by low exponents.

the GVC. The test-particles move in a time-independent mean-field potential determined by the initial magnetizations, M_θ and M_ϕ. The largest LE for each particle was obtained using the method proposed by Benettin *et al.* In the upper row of Fig. 3, we present a histogram of the LED obtained using test particle dynamics with $N = 10^5$ and different values of the coupling parameter ϵ. In the lower row, we show the characteristic Poincaré sections for the most chaotic particles near the separatrix. We see that there is a strong correlation between the LED and the Poincaré plots.

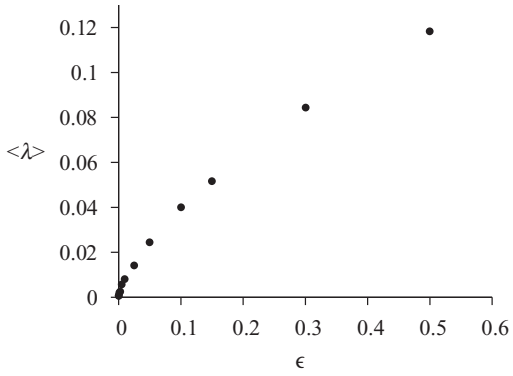

FIG. 4. Average value of the LED, $\langle\lambda\rangle$, vs. the coupling parameter ϵ. As expected, stronger coupling is related with presence of more chaos in the test-particle dynamics.

In Fig. 4 we plot the average value of the LED, as a function of the coupling parameter ϵ. For larger values of ϵ, we see that the orbits become more chaotic.

C. Relaxation exponent

To explore the relaxation to equilibrium, we study the characteristic time scale on which a system evolves from a QSS to thermodynamic equilibrium in MD simulations. As discussed previously, the crossover time scales with the number of particles as $t_\times \sim N^\delta$. We expect that the value

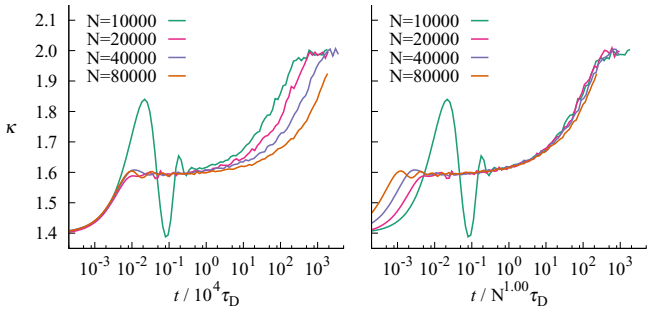

FIG. 5. (Color online) Evolution of the kurtosis for the HMF model ($\epsilon = 0.0$) with different numbers of particles, with time rescaled by $10^4 \tau_D$ (left) and N^δ (right), $\delta = 1.0$. The initial particle distribution satisfied the GVC, with magnetization $M_0 = 0.431\,852$ and mean energy $\varepsilon_\theta = \varepsilon_\phi = 0.6$. The collapse suggests δ equal to 1.0, as predicted by the kinetic equation analysis developed in Ref. [41] for the HMF model.

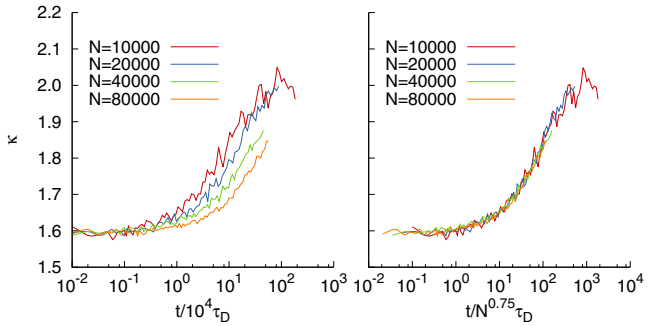

FIG. 6. (Color online) Evolution of the kurtosis for the HMF-ladder model with different numbers of particles, with time rescaled by $10^4\tau_D$ (left) and N^δ (right), $\delta = 0.75$. The initial condition satisfied the GVC, with magnetization $M_0 = 0.440\,772$, subsystem energy $\varepsilon_\theta = \varepsilon_\phi = 0.6$, and a coupling of $\epsilon = 0.01$.

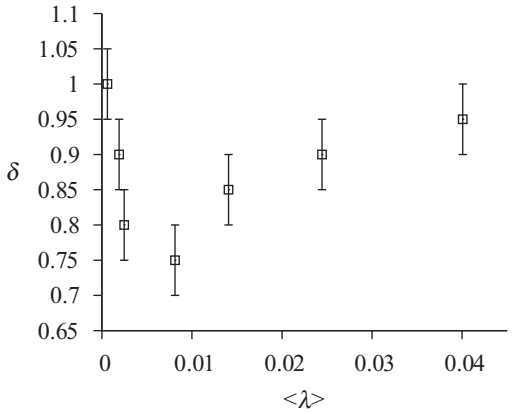

FIG. 7. Exponent δ (from the relaxation time $\tau_\times \sim N^\delta$) vs. average value of the LED, $\langle\lambda\rangle$. Each pair $(\delta, \langle\lambda\rangle)$ corresponds to a different value of the coupling parameter ϵ (see Fig. 4). We see that weak chaos favors relaxation to equilibrium more than strong chaos. Error bars restrict the range of reasonable data collapse.

of the exponent δ should be correlated with the degree of chaos present in the HMF-ladder. To calculate δ, we monitor the crossover from a QSS to thermodynamic equilibrium by measuring the momentum kurtosis given by

$$\kappa = \frac{\langle p^4 \rangle}{\langle p^2 \rangle^2}. \tag{31}$$

For the HMF-ladder in thermodynamic equilibrium, kurtosis has a universal value of two. In Figs. 5 and 6, we show the temporal evolution of kurtosis for $N = 10^3, 2 \times 10^3, 4 \times 10^3$, and 8×10^3 particles. When the time is scaled with $t_\times$ all the curves for different N and the same value of ϵ collapse onto one curve. The exponent δ is obtained by requiring the best possible data collapse; see Figs. 5 and 6. In Fig. 7 we plot the value of δ as a function of the average Lyapunov exponent. We see that the exponent δ is not a monotonic function of the amount of chaos present in a system. This is contrary to our naive expectation that the rate of relaxation to equilibrium should be proportional to the amount of chaos present in a QSS.

VII. CONCLUSIONS

We have explored the role of chaotic dynamics on the time that a system with long-range interactions remains trapped in a QSS before relaxing to thermodynamic equilibrium. The motivation for the study is provided by self-gravitating systems, which during the process of violent relaxation can suffer spontaneous symmetry breaking. When such systems relax to QSS, the resulting mean-field potential will lack spherical symmetry and the particle dynamics will be nonintegrable. The question that we wanted to address in this paper is if presence of chaotic dynamics in a nonequilibrium QSS speeds up the collisional relaxation to thermodynamic equilibrium. Unfortunately, a very slow dynamics of self-gravitating systems makes it very difficult to explore this issue. To overcome this difficulty we introduced a HMF-ladder model, which has a much simpler QSS than a self-gravitating system, characterized only by two magnetizations, M_θ and M_ϕ. With the help of this model, we have discovered that a small degree of chaos, measured by the average of LED, favors relaxation of QSS to thermodynamic equilibrium. Surprisingly, a large amount of chaos is not as efficient at driving a system to equilibrium as a small amount of chaos. Clearly chaotic dynamics of noninteracting particles cannot by itself be responsible for the relaxation to equilibrium. Nevertheless, our results suggest that there is an optimum amount of chaos that helps the residual two-body correlations drive the system toward equilibrium. At the moment we do not have any explanation for this curious behavior.

ACKNOWLEDGMENT

This work was partially supported by the CNPq, INCT-FCx, and by the US-AFOSR under Grant No. FA9550-12-1-0438.

[1] A. Campa, T. Dauxois, and S. Ruffo, Phys. Rep. **480**, 57 (2009).
[2] Y. Levin, R. Pakter, F. B. Rizzato, T. N. Teles, and F. P. C. Benetti, Phys. Rep. **535**, 1 (2014).
[3] A. Gabrielli, M. Joyce, and B. Marcos, Phys. Rev. Lett. **105**, 210602 (2010).
[4] T. Padmanabhan, Phys. Rep. **188**, 285 (1990).
[5] J. Binney and S. Tremaine, *Galactic Dynamics* (Princeton University Press, Princeton, NJ, 1987).
[6] P. H. Chavanis, J. Sommeria, and R. Robert, Astrophys. J. **471**, 385 (1996).
[7] Y. Levin, R. Pakter, and T. N. Teles, Phys. Rev. Lett. **100**, 040604 (2008).
[8] M. Kastner, Phys. Rev. Lett. **106**, 130601 (2011).
[9] O. L. Berman, R. Y. Kezerashvili, G. V. Kolmakov, and Y. E. Lozovik, Phys. Rev. B **86**, 045108 (2012).
[10] S. Slama, G. Krenz, S. Bux, C. Zimmermann, and P. W. Courteille, AIP Conf. Proc. **970**, 319 (2008).

[11] M. Oettel and S. Dietrich, Langmuir **24**, 1425 (2008).
[12] M. Joyce and T. Worrakitpoonpon, J. Stat. Mech. (2010) P10012.
[13] B. Marcos, Phys. Rev. E **88**, 032112 (2013).
[14] T. M. Rocha Filho, A. E. Santana, M. A. Amato, and A. Figueiredo, Phys. Rev. E **90**, 032133 (2014).
[15] L. Landau, J. Phys. USSR **10**, 25 (1946).
[16] D. Sagan, Am. J. Phys. **62**, 450 (1994).
[17] C.-S. Wu, Phys. Rev. **127**, 1419 (1962).
[18] C. Mouhot and C. Villani, Acta Math. **207**, 29 (2011).
[19] L. A. Aguilar and D. Merritt, Astrophys. J. **354**, 33 (1990).
[20] R. Pakter, B. Marcos, and Y. Levin, Phys. Rev. Lett. **111**, 230603 (2013).
[21] W. Simeoni, Jr., F. B. Rizzato, and R. Pakter, Phys. Plasmas **13**, 063104 (2006).
[22] Strictly speaking, for 3D gravitational systems thermodynamic equilibrium is impossible, since in infinite space particles will keep evaporating. Thermodynamic equilibrium, however, is possible for 2D gravitational systems in which particles interact by a logarithmic potential .
[23] D. Pfenniger, Astron. Astrophys. **165**, 74 (1986).
[24] H. E. Kandrup and D. E. Willmes, Astron. Astrophys. **283**, 59 (1994).
[25] P.-H. Chavanis, Astron. Astrophys. **556**, A93 (2013).
[26] P.-H. Chavanis, Eur. Phys. J. Plus **128**, 126 (2013).
[27] T. Konishi and K. Kaneko, J. Phys. A. **25**, 6283 (1992).
[28] S. Inagaki and T. Konishi, Publicat. Astron. Soc. Jpn. **45**, 733 (1993).
[29] M. Antoni and S. Ruffo, Phys. Rev. E **52**, 2361 (1995).
[30] A. Figueiredo, T. M. Rocha Filho, and M. A. Amato, Europhys. Lett. **83**, 30011 (2008).
[31] J. Barré, A. Olivetti, and Y. Y. Yamaguchi, J. Stat. Mech. (2010) P08002.
[32] J. Barré, A. Olivetti, and Y. Y. Yamaguchi, J. Phys. A **44**, 405502 (2011).
[33] F. P. C. Benetti, T. N. Teles, R. Pakter, and Y. Levin, Phys. Rev. Lett. **108**, 140601 (2012).
[34] A. C. Ribeiro-Teixeira, F. P. C. Benetti, R. Pakter, and Y. Levin, Phys. Rev. E **89**, 022130 (2014).
[35] M. Viana, *Lectures on Lyapunov Exponents* (Cambridge University Press, Cambridge, 2014).
[36] K. T. Alligood, T. D. Sauer, J. A. Yorke, and J. D. Crawford, *Chaos: An Introduction to Dynamical Systems* (Springer-Verlag, New York, 1996).
[37] With some exceptions, see the so-called Perron effect [42] .
[38] G. Benettin, L. Galgani, and J. Strelcyn, Phys. Rev. A **14**, 2338 (1976).
[39] I. P. Omelyan, I. M. Mryglod, and R. Folk, Comput. Phys. Commun. **146**, 188 (2002).
[40] F. Ginelli, K. A. Takeuchi, H. Chaté, A. Politi, and A. Torcini, Phys. Rev. E **84**, 066211 (2011).
[41] P.-H. Chavanis, J. Stat. Mech. (2010) P05019.
[42] G. A. Leonov and N. V. Kuznetsov, Int. J. Bifurcat. Chaos **17**, 1079 (2007).

4.4 Collisional relaxation in the inhomogeneous Hamiltonian-mean-field Model: Diffusion coefficients

Continuing on the topic of relaxation to equilibrium, in this work we studied the kinetic equations of the HMF model including terms of order $\mathcal{O}[1/N]$. Our goal with this work was to study the relaxation dynamics of inhomogeneous systems. This was motivated by previous works in astrophysics, which usually approximate self-gravitating systems as homogeneous in order to calculate their diffusion coefficients and subsequently use a Fokker-Planck formalism. For this approach to work, the three different dynamical timescales should scale appropriately:

- τ_{enc}, the time related to the duration of a binary encounter;
- τ_{cr}, the crossing time (the time necessary for a star to cross the stellar background); and
- τ_R, the relaxation time, associated with the time necessary for the entire system to lose memory of its initial state.

In the framework of space and velocity variables (r,v), the homogeneous approximation requires that $\tau_{enc} \ll \tau_{cr} \ll \tau_R$. While the second inequality is satisfied, the first is a somewhat uncontrolled approximation.

However, by using a canonical framework of angle-action variables ($\mathbf{w}$,$\mathbf{J}$), the Hamiltonian is transformed in such a way that it is independent of the angle (at least adiabatically). Therefore, it becomes homogeneous in angle. The only timescale assumption we need is the second, $\tau_{cr} \ll \tau_R$, to guarantee an adiabatic evolution of the one-particle distribution in angle-action coordinates, $f(\mathbf{J})$.

The kinetic equations for the evolution of generic, inhomogeneous LRI systems in action-angle variables have been developed by Heyvaerts [84] and Chavanis [90]. As we have seen in subsection 3.1.2, starting from the Klimontovich equation, the next order of approximation gives the Lenard-Balescu equation. This equation contains a dielectric function which represents *collective effects*; that is, the response of the system to its own internal perturbations. If the collective effects are ignored, the dielectric function can be set to one and the Lenard-Balescu equation becomes the Landau equation.

Although the demonstration and form of these equations has been shown, their application to actual LRI systems is quite a difficult task. It is necessary to calculate the action given a mean-field potential $\psi(r)$ which is not known beforehand. Sometimes it can be achieved by representing the potential in a biorthogonal basis (Kalnajs matrix method [108]), for example in the work of Fouvry *et al* with tepid galactic disks [109]. Luckily, in the HMF model, the mean-field limit with an adiabatically evolving mean magnetization M consists in uncoupled oscillators, so we can write the action variable explicitly. Previous work on the

stability of Vlasov solutions with angle-action variables also provided useful identities for writing the Fourier transforms of the mean-field potential [25, 89, 110].

Both the Landau and Lenard-Balescu equations can be written in the form of a Fokker-Planck equation,

$$\frac{\partial f}{\partial t} = \frac{\partial^2}{\partial J^2}\{D_{dif}[J^2]f(J)\} - \frac{\partial}{\partial J}\{D_{fric}[J]f(J)\} \tag{4.8}$$

where $D_{dif}[J^2]$ and $D_{fric}[J]$ are the diffusion and friction coefficients, respectively. Their form depends on whether or not collective effects are included. We were able to numerically calculate these diffusion coefficients and showed that they are both qualitatively and quantitatively very different for the two cases (neglecting or including collective effects). For highly inhomogeneous states ($M \to 1$), we also obtained analytical expressions for the coefficients.

Molecular dynamics of the HMF model provided an "experimental" test of our results. The diffusion coefficient of the HMF model matches very well the Lenard-Balescu diffusion coefficient, showing that collective effects are very important in its dynamics. To test the Landau diffusion coefficient, on the other hand, we needed to somehow isolate the collective effects from the HMF model. In order to do so, we set up a system composed of N_b bath particles who do not interact between themselves, and N_{tp} test particles who interact with the oscillations of the bath. This new system, which we call MDbath, is therefore composed of:

Bath N_b particles who are initially distributed according to a Vlasov-stable distribution $f_0^b(\theta,p)$. This initial distribution defines the stationary magnetization (corresponding to the adiabatically evolving magnetization)

$$M_0 = \int \mathrm{d}\theta \mathrm{d}p \cos\theta f_0^b(\theta,p). \tag{4.9}$$

The bath particles then evolve according to

$$\ddot{\theta}_i^b = -M_0 \sin\theta_i. \tag{4.10}$$

Test particles N_{tp} particles who do not interact between themselves, but only with the true, instantaneous magnetization of the bath particles, given by

$$\begin{aligned} M_x^b &= \frac{1}{N_b}\sum_{i=1}^{N_b} \cos\theta_i, \\ M_y^b &= \frac{1}{N_b}\sum_{i=1}^{N_b} \sin\theta_i. \end{aligned} \tag{4.11}$$

The test particles evolve according to

$$\ddot{\theta}_i^{tp} = -M_x \sin\theta_i + M_y \cos\theta_i. \tag{4.12}$$

The diffusion coefficients of the MDbath setup are calculated from the test particles only, not the bath particles. This allows us to eliminate the collective effects from the system: the test particles interact only with the fluctuations around M_0 caused by the finite number of bath particles, and not their self-interaction. The resulting diffusion coefficients matched very well the Landau diffusion coefficients, validating the results without collective effects. Of course, since the true HMF model is completely self-interacting, the adequate diffusion coefficient is the Lenard-Balescu one.

This work was published in *Physical Review E* as a regular article, titled "Collisional relaxation in the Hamiltonian Mean-Field Model: Diffusion coefficients", volume 95, page 022111 in February 2017. It is the result of a collaboration with Bruno Marcos, done during a six-month stay at the Université de Nice – Sophia Antipolis (now Université Côte d'Azur) financed by CAPES.

Collisional relaxation in the inhomogeneous Hamiltonian mean-field model: Diffusion coefficients

F. P. C. Benetti[1,2,*] and B. Marcos[2,†]
[1]*Instituto de Física, Universidade Federal do Rio Grande do Sul, Brazil*
[2]*Université Côte d'Azur, CNRS UMR 7351, LJAD, France*
(Received 12 October 2016; published 8 February 2017)

Systems of particles with long-range interactions present two important processes: first, the formation of out-of-equilibrium quasistationary states (QSS) and, second, the collisional relaxation towards Maxwell-Boltzmann equilibrium in a much longer time scale. In this paper, we study the collisional relaxation in the Hamiltonian mean-field model using the appropriate kinetic equations for a system of N particles at order $1/N$: the Landau equation when collective effects are neglected and the Lenard-Balescu equation when they are taken into account. We derive explicit expressions for the diffusion coefficients using both equations for any magnetization, and we obtain analytic expressions for highly clustered configurations. An important conclusion is that in this system collective effects are crucial in order to describe the relaxation dynamics. We compare the diffusion calculated with the kinetic equations with simulations set up to simulate the system with or without collective effects, obtaining a very good agreement between theory and simulations.

DOI: 10.1103/PhysRevE.95.022111

I. INTRODUCTION

Systems with long-range interactions present the generic evolution in two distinct stages: first, the evolution to a quasistationary state in a process called *collisionless (or violent) relaxation* [1] in a time scale $\tau_{\rm dyn}$, and, second, the evolution towards thermodynamic equilibrium in the so-called *collisional relaxation process*, in a time scale of order $\tau_{\rm coll} \sim N^{\delta}\tau_{\rm dyn}$, where $\delta > 0$ depends on the system considered. The mechanism of collisional relaxation is qualitatively well known since the seminal work of Chandrasekhar [2]: The main elements are *two-body* collisions, which randomizes the velocity of the particles, leading to a Maxwell-Boltzmann velocity distribution. Using simple calculations and approximating the system as spatially homogeneous, Chandrasekhar was able to determine that, for gravitational systems in three dimensions, $\tau_{\rm coll} \sim \tau_{\rm dyn} N/\ln N$. This approach was subsequently used by other authors, notably Hénon in the 1960s (see, e.g., Ref. [3]), and led to the development of Fokker-Planck techniques. All these methods share the same feature of approximating the system as homogeneous. For example, in the *orbit-averaging* approach (see, e.g., Ref. [4]), diffusion coefficients are computed approximating the system as homogeneous, and then they are averaged over the actual orbits of the particles. This method is used because it is technically difficult to compute diffusion coefficients for inhomogeneous configurations, essentially because the trajectories of the unperturbed particles (i.e., in the mean-field limit) would need to be computed, which is generally a very difficult task. Moreover, using this approach, it is not possible to take into account *collective effects*, which can be important for some systems and configurations, which we will see it is the case in the present work.

At the same time, a rigorous kinetic theory for (repulsive, neutral) plasmas was being developed first by Landau (introducing, notably, the concept of *Landau damping*) and subsequently by other authors such as Lenard, Balescu, etc. (see, e.g., Ref. [5]). When the system is neutral, the mean-field configuration is homogeneous, and it is therefore possible to attack the problem in an essentially analytical way, including even collective effects.

Over the past few years a rigorous kinetic theory for inhomogeneous configurations has been developed by different authors [6–10]. In these works, the general procedure in order to compute kinetic equations at order $1/N$ has been described. There are, however, many practical difficulties when trying to compute quantities of interest such as the diffusion coefficients, and this for various reasons. The natural way to write these equations is to use *angle-action* variables (see, e.g., Ref. [11]). To compute them as a function of the natural variables (x,v) is technically equivalent to solving the equations of motion for the unperturbed ($N \to \infty$) potential, which is in general impossible analytically. The subsequent calculation of the diffusion coefficient (which involves, e.g., Fourier transform about the angle variable) becomes (even numerically) very difficult. For this reason, we are only aware of the study of self-gravitating tepid disks [12,13]. In this case, it is possible to make controlled approximations, which makes the semianalytical calculations feasible.

In this paper we have chosen to study *exactly* a sufficiently simple model in order to compute the diffusion coefficients without approximations (up to order $1/N$). To do so, we use the popular *Hamiltonian mean-field model* (HMF) [14], which has widely been used to study long-range systems. Its simplicity permits us to compute some analytical and numerical quantities which would be impossible in more realistic models such as three-dimensional gravity. For this reason, the diffusion coefficients have already been studied in the much simpler spatially homogeneous configuration [15]. Our work has two main objectives: On one side, it will permit us to compare the diffusion coefficients with numerical simulations in order to check the validity of the assumptions made deriving the kinetic equations in the case of spatially inhomogeneous distributions. On the other side, it will set up the method to solve numerically the Lenard-Balescu equation not only for the HMF but also for other more complicated models, as self-gravitating systems.

*Caixa Postal 15051, CEP 91501-970, Porto Alegre, RS, Brazil.
†Parc Valrose, 06108 Nice, Cedex 02, France.

The paper is organized as follows: In the first section we summarize the kinetic theory we will apply in the paper. In the next section, we apply the equations for the HMF to compute the diffusion coefficients, giving also analytical results for some cases. Then we compare the theoretical predictions with molecular dynamics simulations, including or not collective effects, and then we give conclusions and perspectives.

II. KINETIC THEORY

The evolution of an N-body system under Hamiltonian dynamics can be described using kinetic theory. The approach outlined in this section follows that of several previous works (see Introduction) and is summarized in, e.g., Ref. [16].[1] The problem addressed by this kinetic approach is the following: Given a set of N particles of mass m with initial positions $\{\mathbf{r}_i\}$ and velocity $\{\mathbf{v}_i\}$ and their Hamiltonian equations of motion, how and to what steady state will they evolve? We start with the discrete distribution function $f_d(\mathbf{r},\mathbf{v},t)$, which contains all the information of the state of the system at a given time t,

$$f_d(\mathbf{r},\mathbf{v},t) = m\sum_{i=1}^{N}\delta[\mathbf{r}-\mathbf{r}_i(t)]\delta[\mathbf{v}-\mathbf{v}_i(t)]. \tag{1}$$

The evolution of the discrete distribution function is given exactly by the Klimontovich equation [17]

$$\frac{\partial f_d}{\partial t}+\mathbf{v}\cdot\frac{\partial f_d}{\partial \mathbf{r}}-\frac{\partial \phi_d}{\partial \mathbf{r}}\cdot\frac{\partial f_d}{\partial \mathbf{v}}=0, \tag{2}$$

$$\phi_d(\mathbf{r},t)=\int u(|\mathbf{r}-\mathbf{r}'|)f_d(\mathbf{r}',\mathbf{v}',t)d\mathbf{r}'d\mathbf{v}', \tag{3}$$

where $\phi_d(\mathbf{r},t)$ is the discrete convolution potential, $u(\mathbf{r}-\mathbf{r}')$ is the pair interaction potential between particles at positions $\mathbf{r}$ and $\mathbf{r}'$, and $\frac{\partial f}{\partial \mathbf{u}}=\sum_{i=1}^{d}\frac{\partial f}{\partial u_i}\mathbf{e}_i$ and d is the spatial dimension.

For a given initial distribution $f_0^d(\mathbf{r},\mathbf{v})=m\sum_{i=1}^{N}\delta[\mathbf{r}-\mathbf{r}_i(t=0)]\delta[\mathbf{v}-\mathbf{v}_i(t=0)]$, the discrete distribution is determined at all future times t. A smooth distribution function can be obtained by averaging over an ensemble of initial conditions,

$$f(\mathbf{r},\mathbf{v},t)=\langle f_d(\mathbf{r},\mathbf{v},t)\rangle \tag{4}$$

and thus $f_d(\mathbf{r},\mathbf{v},t)=f(\mathbf{r},\mathbf{v},t)+\delta f(\mathbf{r},\mathbf{v},t)$.

The same smoothing process can be done for the Klimontovich equation. Since averages over the fluctuations are zero, this leads to

$$\frac{\partial f}{\partial t}+\mathbf{v}\cdot\frac{\partial f}{\partial \mathbf{r}}-\frac{\partial \phi}{\partial \mathbf{r}}\cdot\frac{\partial f}{\partial \mathbf{v}}=\frac{\partial}{\partial \mathbf{v}}\cdot\left\langle \delta f\frac{\partial \delta\phi}{\partial \mathbf{r}}\right\rangle. \tag{5}$$

The above equation gives the evolution of the smooth distribution due to correlation between its own fluctuations and the fluctuation of the smooth potential $\phi(\mathbf{r},t)$, determined by $\phi_d(\mathbf{r},t)=\phi(\mathbf{r},t)+\delta\phi(\mathbf{r},t)$, where

$$\phi(\mathbf{r},t)=\int u(|\mathbf{r}-\mathbf{r}'|)f(\mathbf{r}',\mathbf{v}',t)d\mathbf{r}'d\mathbf{v}', \tag{6}$$

$$\delta\phi(\mathbf{r},t)=\int u(|\mathbf{r}-\mathbf{r}'|)\delta f(\mathbf{r}',\mathbf{v}',t)d\mathbf{r}'d\mathbf{v}'. \tag{7}$$

Subtracting Eq. (5) from the Klimontovich equation and keeping only terms of order lower than $\mathcal{O}(1/N)$ gives the linearized Klimontovich equation,

$$\frac{\partial \delta f}{\partial t}+\mathbf{v}\cdot\frac{\partial \delta f}{\partial \mathbf{r}}-\frac{\partial \delta\phi}{\partial \mathbf{r}}\cdot\frac{\partial f}{\partial \mathbf{v}}-\frac{\partial \phi}{\partial \mathbf{r}}\cdot\frac{\partial \delta f}{\partial \mathbf{v}}=0. \tag{8}$$

The system of Eqs. (5) and (8) are known as the quasilinear approximation, since in the first equation the correlation term on the right-hand side is of order $1/N$, while in the second equation all terms of order $1/N$ or higher have been neglected.

A. Homogeneous systems

We will first give a brief derivation of the kinetic equations for the spatially homogeneous case. It is technically simpler than the inhomogeneous one while sharing the same ideas. In this case $f=f(\mathbf{v},t)$, so Eqs. (5) and (8) become

$$\frac{\partial f}{\partial t}=\frac{\partial}{\partial \mathbf{v}}\cdot\left\langle \delta f\frac{\partial \delta\phi}{\partial \mathbf{r}}\right\rangle, \tag{9a}$$

$$\frac{\partial \delta f}{\partial t}+\mathbf{v}\cdot\frac{\partial \delta f}{\partial \mathbf{r}}-\frac{\partial \delta\phi}{\partial \mathbf{r}}\cdot\frac{\partial f}{\partial \mathbf{v}}=0. \tag{9b}$$

The fluctuation terms are more easily dealt with by using the Fourier-Laplace transforms

$$\widetilde{\delta f}(\mathbf{k},\mathbf{v},\omega)=\frac{1}{(2\pi)^d}\int d\mathbf{r}\int_0^\infty dt\, e^{-i(\mathbf{k}\cdot\mathbf{r}-\omega t)}\delta f(\mathbf{r},\mathbf{v},t) \tag{10}$$

and

$$\widetilde{\delta\phi}(\mathbf{k},\omega)=\frac{1}{(2\pi)^d}\int d\mathbf{r}\int_0^\infty dt\, e^{-i(\mathbf{k}\cdot\mathbf{r}-\omega t)}\delta\phi(\mathbf{r},t). \tag{11}$$

Taking the Fourier-Laplace transform of Eq. (9b), we have

$$\widehat{\delta f}(\mathbf{k},\mathbf{v},0)-i(\mathbf{k}\cdot\mathbf{v}-\omega)\,\widetilde{\delta f}(\mathbf{k},\mathbf{v},\omega)+i\mathbf{k}\cdot\frac{\partial f}{\partial \mathbf{v}}\widetilde{\delta\phi}(\mathbf{k},\omega)=0, \tag{12}$$

where

$$\widehat{\delta f}(\mathbf{k},\mathbf{v},0)=\int\frac{d\mathbf{r}}{(2\pi)^d}\,e^{-i\mathbf{k}\cdot\mathbf{r}}\delta f(\mathbf{r},\mathbf{v},0). \tag{13}$$

From the above equation, we can isolate $\widetilde{\delta f}$ and thus find an expression relating the fluctuations of the distribution function and the fluctuations of the potential and the initial condition,

$$\widetilde{\delta f}=\underbrace{\frac{\mathbf{k}\cdot\frac{\partial f}{\partial \mathbf{v}}\widetilde{\delta\phi}(\mathbf{k})}{\mathbf{k}\cdot\mathbf{v}-\omega}}_{\substack{\text{collective}\\ \text{effects}}}+\underbrace{\frac{\widehat{\delta f}(\mathbf{k},\mathbf{v},0)}{i(\mathbf{k}\cdot\mathbf{v}-\omega)}}_{\substack{\text{initial}\\ \text{conditions}}}. \tag{14}$$

Because collective effects are difficult to compute analytically, a common approximation found in the literature consists in neglecting them (see, e.g., Ref. [9]). In this paper we

[1] Here we use the Klimontovich formulism; the same equations may be obtained from the Born-Bogoliubov-Green-Klimontovich-Yvon (BBGKY) hierarchy, see, i.e., Ref. [8].

will consider the complete problem, and we will study their importance in the inhomogeneous HMF.

The next step in the derivation consists in expressing the Fourier transform of the fluctuation of the potential $\widetilde{\delta\phi}(\mathbf{k},\omega)$ as a function of the fluctuation $\widetilde{\delta f}(\mathbf{k},w)$. To do so, we integrate Eq. (14) over $\mathbf{v}$, and, using the Fourier transform of Eq. (7), we get

$$\int_{-\infty}^{\infty} d\mathbf{v}\widetilde{\delta f}(\mathbf{k},\mathbf{v},\omega) = \frac{1}{\epsilon(\mathbf{k},\omega)}\int_{-\infty}^{\infty} d\mathbf{v}\frac{\widehat{\delta f}(\mathbf{k},\mathbf{v},0)}{i(\mathbf{v}\cdot\mathbf{k}-\omega)}, \tag{15}$$

where we have defined the plasma response dielectric function

$$\epsilon(\mathbf{k},\omega) = 1 - \hat{u}(\mathbf{k})\int d\mathbf{v}\frac{\mathbf{k}\cdot\partial f(\mathbf{v})/\partial\mathbf{v}}{\mathbf{v}\cdot\mathbf{k}-\omega}. \tag{16}$$

Using again Eqs. (7) and (15), we get

$$\begin{aligned}\widetilde{\delta\phi}(\mathbf{k},\omega) &= \hat{u}(\mathbf{k})\int_{-\infty}^{\infty} d\mathbf{v}\widetilde{\delta f}(\mathbf{k},\mathbf{v},\omega)\\ &= \frac{\hat{u}(\mathbf{k})}{\epsilon(\mathbf{k},\omega)}\int_{-\infty}^{\infty} d\mathbf{v}\frac{\widehat{\delta f}(\mathbf{k},\mathbf{v},0)}{i(\mathbf{p}\cdot\mathbf{k}-\omega)}.\end{aligned} \tag{17}$$

Inserting Eqs. (14) and (17) into Eq. (9a), after some algebra, we get the Lenard-Balescu equation (using the notation [17]):

$$\begin{aligned}\frac{\partial f}{\partial t} &= \pi(2\pi)^d m\sum_{i,j=1}^{d}\frac{\partial}{\partial v_i}\int d\mathbf{k}d\mathbf{v}' k_i k_j\frac{\hat{u}(\mathbf{k})^2}{|\epsilon(\mathbf{k},\mathbf{k}\cdot\mathbf{v})|^2}\\ &\times\delta[\mathbf{k}\cdot(\mathbf{v}-\mathbf{v}')]\left(\frac{\partial}{\partial v_j}-\frac{\partial}{\partial v'_j}\right)f(\mathbf{v},t)f(\mathbf{v}',t).\end{aligned} \tag{18}$$

When collective effects are neglected, i.e., the first term of Eq. (14) is neglected, it is simple to see from Eq. (16) that $\epsilon(\mathbf{k},\omega) = 1$.

B. Inhomogeneous systems

In inhomogeneous systems, the strategy is to use, instead of the variables $(\mathbf{r},\mathbf{v})$, the angle-action variables $(\mathbf{w},\mathbf{J})$ corresponding to the Hamiltonian $\mathcal{H}$ of smooth dynamics (i.e., the one corresponding to the limit $N\to\infty$) [18]. Using these variables, particles described by the Hamiltonian $\mathcal{H}$ keep their action $\mathbf{J}$ constant during the dynamic and their angle evolves with time as $\mathbf{w} = \Omega(\mathbf{J})t + \mathbf{w}_0$, where $\mathbf{w}_0$ is the angle at $t = 0$ and $\Omega(\mathbf{J}) = \partial\mathcal{H}/\partial\mathbf{J}$ is the angular frequency [19]. The system thus becomes "homogeneous" in the new coordinates [20].

The equations for evolution of smooth distribution function f and its fluctuation δf are [7,10]

$$\frac{\partial f(\mathbf{J})}{\partial t} + [\mathcal{H}(\mathbf{J}), f(\mathbf{J})] = -\langle[\delta\phi,\delta f(\mathbf{J})]\rangle, \tag{19a}$$

$$\frac{\partial\delta f(\mathbf{J})}{\partial t} + [\mathcal{H}(\mathbf{J}),\delta f(\mathbf{J})] + [\delta\phi, f(\mathbf{J})] = 0, \tag{19b}$$

where ϕ is the smooth mean-field potential and $\delta\phi$ is its fluctuation, and $[\mathcal{H},B] = \frac{\partial\mathcal{H}}{\partial\mathbf{J}}\frac{\partial B}{\partial\mathbf{w}} - \frac{\partial\mathcal{H}}{\partial\mathbf{w}}\frac{\partial B}{\partial\mathbf{J}}$ are Poisson brackets with action-angle variables as the canonical coordinates.

Since by construction $\partial\mathcal{H}/\partial\mathbf{w} = 0$ and $\partial f/\partial\mathbf{w} = 0$, the terms in Poisson brackets reduce to

$$[\mathcal{H},\delta f] = \frac{\partial\mathcal{H}}{\partial\mathbf{J}}\frac{\partial\delta f}{\partial\mathbf{w}} = \Omega(\mathbf{J})\cdot\frac{\partial\delta f}{\partial\mathbf{w}}, \tag{20}$$

$$[\delta\phi, f] = -\frac{\partial\delta\phi}{\partial\mathbf{w}}\cdot\frac{\partial f}{\partial\mathbf{J}}. \tag{21}$$

Substituting the above in Eq. (19) and averaging over angles $\mathbf{w}$,

$$\frac{\partial\overline{f}}{\partial t} = \frac{\partial}{\partial\mathbf{J}}\cdot\left\langle\overline{\delta f\frac{\partial\delta\phi}{\partial\mathbf{w}}}\right\rangle, \tag{22a}$$

$$\frac{\partial\overline{\delta f}}{\partial t} + \Omega(\mathbf{J})\cdot\frac{\partial\overline{\delta f}}{\partial\mathbf{w}} - \overline{\frac{\partial\delta\phi}{\partial\mathbf{w}}\cdot\frac{\partial f}{\partial\mathbf{J}}} = 0, \tag{22b}$$

where $\overline{A}$ represents the angle-averaging of A. From now on, we disregard this notation and write $\overline{A} = A$ for simplicity, but we emphasize that the equations from this point further correspond to the angle-averaged quantities.

Observe that Eq. (22) have the same structure as their homogeneous counterpart equation (9) identifying the action $\mathbf{J}$ with the velocity $\mathbf{v}$ and the angle $\mathbf{w}$ with the spatial variable $\mathbf{r}$. The only difference appears in the second term of Eq. (22b) in which the velocity $\mathbf{v}$ is substituted by the frequency of the unperturbed orbit $\Omega(\mathbf{J})$. Following then the same procedure as the one described in the homogeneous case, we get the Lenard-Balescu-type kinetic equation (with collective effects) in action-angle variables [8,10],

$$\begin{aligned}\frac{\partial f}{\partial t} &= \pi(2\pi)^d m\frac{\partial}{\partial\mathbf{J}}\cdot\sum_{\mathbf{k},\mathbf{k}'}\int d\mathbf{J}'\mathbf{k}\frac{\delta[\mathbf{k}\cdot\Omega(\mathbf{J})-\mathbf{k}'\cdot\Omega(\mathbf{J}')]}{|D_{\mathbf{k},\mathbf{k}'}(\mathbf{J},\mathbf{J}',\mathbf{k}\cdot\Omega(\mathbf{J}))|^2}\\ &\times\left(\mathbf{k}\cdot\frac{\partial}{\partial\mathbf{J}}-\mathbf{k}'\cdot\frac{\partial}{\partial\mathbf{J}'}\right)f(\mathbf{J},t)f(\mathbf{J}',t),\end{aligned} \tag{23}$$

where

$$\frac{1}{D_{\mathbf{k},\mathbf{k}'}(\mathbf{J},\mathbf{J}',\omega)} = \sum_{\alpha,\alpha'}\hat{\Phi}_\alpha(\mathbf{k},\mathbf{J})(\epsilon^{-1})_{\alpha,\alpha'}(\omega)\hat{\Phi}^\star_{\alpha'}(\mathbf{k}',\mathbf{J}'), \tag{24}$$

and $\epsilon_{\alpha\alpha'}(\omega)$ is the dielectric tensor

$$\begin{aligned}\epsilon_{\alpha\alpha'}(\omega) &= \delta_{\alpha\alpha'} + (2\pi)^d\sum_{\mathbf{k}}\int d\mathbf{J}\frac{\mathbf{k}\cdot\partial f/\partial\mathbf{J}}{\mathbf{k}\cdot\Omega(\mathbf{J})-\omega}\\ &\times\hat{\Phi}^\star_\alpha(\mathbf{k},\mathbf{J})\hat{\Phi}_{\alpha'}(\mathbf{k},\mathbf{J}).\end{aligned} \tag{25}$$

The indices (α,α') are labels for the biorthogonal basis $\{\rho_\alpha,\Phi_\alpha\}$, where $\rho(\mathbf{r}) = \int f(\mathbf{r},\mathbf{v},t)d\mathbf{v}$, which satisfies [21]

$$\int u(|\mathbf{r}-\mathbf{r}'|)\rho_\alpha(\mathbf{r}')d\mathbf{r}' = \Phi_\alpha, \tag{26}$$

$$\int\rho_\alpha(\mathbf{r})\Phi^\star_{\alpha'}(\mathbf{r})d\mathbf{r} = -\delta_{\alpha,\alpha'}. \tag{27}$$

The terms $\hat{\Phi}_\alpha$ are the Fourier transforms of the potential in the biorthogonal representation with respect to the angles,

$$\hat{\Phi}_\alpha(\mathbf{k},\mathbf{J}) = \frac{1}{(2\pi)^d}\int d\mathbf{w}e^{-i\mathbf{k}\cdot\mathbf{w}}\Phi_\alpha(\mathbf{w},\mathbf{J}). \tag{28}$$

The Lenard-Balescu equation (23) gives the evolution of f due to the inclusion of a finite-N correction to the collisionless

(Vlasov) kinetic equation. From Eq. (23), we see that the evolution, which slowly deforms the orbits of constant $\mathbf{J}$, is driven by resonances between orbital frequencies, $\mathbf{k}\cdot\Omega(\mathbf{J}) = \mathbf{k}'\cdot\Omega(\mathbf{J}')$. This differs from the homogeneous case, Eq. (18), where f evolves due to the resonances $\mathbf{v} = \mathbf{v}'$.

Using the chain rule, the Lenard-Balescu-type equation (23) can be written in the form of a Fokker-Planck equation,

$$\frac{\partial f}{\partial t} = \sum_{i,j=1}^{d} \frac{\partial^2}{\partial J_i \partial J_j} D^{ij}_{\rm dif}(\mathbf{J},t) f(\mathbf{J},t) - \frac{\partial}{\partial \mathbf{J}} \cdot \mathbf{D}_{fr}(\mathbf{J},t) f(\mathbf{J},t), \tag{29}$$

where

$$D^{ij}_{\rm dif}(\mathbf{J},t) = \pi(2\pi)^d m \sum_{\mathbf{k},\mathbf{k}'} \int d\mathbf{J}' k_i k_j \frac{1}{|D_{\mathbf{k},\mathbf{k}'}(\mathbf{J},\mathbf{J}',\mathbf{k}'\cdot\Omega(\mathbf{J}'))|^2} \times \delta[\mathbf{k}\cdot\Omega(\mathbf{J}) - \mathbf{k}'\cdot\Omega(\mathbf{J}')] f(\mathbf{J}',t) \tag{30}$$

is the diffusion coefficient and the friction coefficient is

$$\mathbf{D}_{fr}(\mathbf{J},t) = \pi(2\pi)^d m \sum_{\mathbf{k},\mathbf{k}'} \int d\mathbf{J}' f(\mathbf{J}') \mathbf{k} \left(\mathbf{k}\frac{\partial}{\partial \mathbf{J}} - \mathbf{k}'\frac{\partial}{\partial \mathbf{J}'} \right) \times \frac{\delta[\mathbf{k}\cdot\Omega(\mathbf{J}) - \mathbf{k}'\cdot\Omega(\mathbf{J}')]}{|D_{\mathbf{k},\mathbf{k}'}(\mathbf{J},\mathbf{J}',\mathbf{k}'\cdot\Omega(\mathbf{J}'))|^2}. \tag{31}$$

The ith component of the friction coefficient (31) can also be written as the sum of the derivative of the diffusion coefficient, plus a polarization force [10],

$$D^{i}_{fr}(\mathbf{J},t) = \frac{\partial}{\partial J_i} D^{ij}_{\rm dif}(\mathbf{J},t) + D^{i}_{\rm pol}(\mathbf{J},t), \tag{32}$$

where the i component of the polarization force is

$$D^{i}_{\rm pol}(\mathbf{J},t) = \pi(2\pi)^d m \sum_{\mathbf{k},\mathbf{k}'} \int d\mathbf{J}' k_i \mathbf{k}' \frac{1}{|D_{\mathbf{k},\mathbf{k}'}(\mathbf{J},\mathbf{J}',\mathbf{k}'\cdot\Omega(\mathbf{J}'))|^2} \times \delta[\mathbf{k}\cdot\Omega(\mathbf{J}) - \mathbf{k}'\cdot\Omega(\mathbf{J}')] \frac{\partial f(\mathbf{J}',t)}{\partial \mathbf{J}'}. \tag{33}$$

When collective effects are not considered, we have

$$\epsilon_{\alpha\alpha'} = \delta_{\alpha\alpha'}, \tag{34}$$

and therefore the Landau equation is obtained using the *bare*, undressed Fourier transforms of the potential,

$$\frac{1}{\left|D^{\rm bare}_{\mathbf{k},\mathbf{k}'}(\mathbf{J},\mathbf{J}',\mathbf{k}'\cdot\Omega(\mathbf{J}'))\right|^2} = |\hat{\Phi}_\alpha(\mathbf{k},\mathbf{J})\hat{\Phi}^\star_\alpha(\mathbf{k}',\mathbf{J}')|^2. \tag{35}$$

III. KINETIC EQUATIONS FOR THE HAMILTONIAN MEAN-FIELD MODEL

We will compute explicitly the diffusion coefficients for the HMF model. It is given by the Hamiltonian

$$H = \sum_{i=1}^{N} \frac{p^2}{2} - \frac{1}{2N} \sum_{i,j=1}^{N} \cos(\theta_i - \theta_j). \tag{36}$$

The energy of one particle can be written as

$$h(\theta,p) = \frac{p^2}{2} + \phi(\theta) = \frac{p^2}{2} - \frac{1}{N}\sum_{i=1}^{N} \cos(\theta_i - \theta). \tag{37}$$

The potential $\phi(\theta) = -1/N \sum_i \cos(\theta_i - \theta)$ can be rewritten as

$$\phi(\theta) = -\frac{\sum_{i=1}^N \cos\theta_i}{N}\cos\theta - \frac{\sum_{i=1}^N \sin\theta_i}{N}\sin\theta = -M_x\cos\theta - M_y\sin\theta, \tag{38}$$

where $\mathbf{M} = (M_x, M_y)$ is the magnetization vector. Its modulus quantifies how bunched, or clustered, the particles are. Shifting all angles by a phase $\alpha = \arctan(M_y/M_x)$, we can write the potential simply as a function of the modulus of the magnetization M,

$$\phi(\theta^\star) = -M\cos\theta^\star, \tag{39}$$

where $\theta^\star = \theta - \alpha$ and $M = M_x = \sum_{i=1}^N \cos\theta_i^\star$. For simplicity, henceforth we denote $\theta^\star$ as θ.

A. Action-angle variables

Inhomogeneous states of the HMF model have previously been studied using action-angle variables in the case of Vlasov stability [22,23]. We define our action angle variables in the same way as these references. The action J is defined as

$$J = \frac{1}{2\pi}\oint p\,d\theta$$

with $p = \sqrt{2[h - \phi(\theta)]}$, where energy h is the one-particle energy and $\phi(\theta)$ is the mean-field potential, Eq. (39). The potential can be fully specified with a single scalar quantity, the modulus of the magnetization M. It is possible to write simply and in a generic way an expression for the action which depends only on the energy of the particle h and the adiabatic, static magnetization M_0 (see Appendix A),

$$J(\kappa) = \frac{4\sqrt{M_0}}{\pi}\begin{cases} 2[E(\kappa) - (1-\kappa^2)K(\kappa)], & \kappa < 1 \\ \kappa E\left(\frac{1}{\kappa}\right), & \kappa > 1 \end{cases}, \tag{40}$$

where

$$\kappa = \sqrt{\frac{h + M_0}{2M_0}}. \tag{41}$$

The action J is discontinuous at the separatrix $\kappa = 1$, the boundary between rotating and librating orbits (see Fig. 1). Figure 2 shows the action as a function of κ and the discontinuity at the separatrix.

The frequency $\Omega(J)$ is $\Omega(J) = \partial h/\partial J$. Due to the frequency being noninjective in J, and J being a function of elliptical integrals of κ, it is easier to treat all expressions directly as a function of κ. We use the Jacobian $\partial\kappa/\partial J$ to change variables,

$$\left[\frac{\partial J}{\partial \kappa}\right] = \frac{4\sqrt{M_0}}{\pi}\begin{cases} 2\kappa K(\kappa), & \kappa < 1 \\ K\left(\frac{1}{\kappa}\right), & \kappa > 1. \end{cases} \tag{42}$$

Thus the frequency is given by $\Omega(J) = (\partial\kappa/\partial J)(\partial h/\partial\kappa)$,

$$\Omega(\kappa) = \pi\sqrt{M_0}\begin{cases} \frac{1}{2K(\kappa)}, & \kappa < 1 \\ \frac{\kappa}{K\left(\frac{1}{\kappa}\right)}, & \kappa > 1 \end{cases}. \tag{43}$$

The explicit expressions for the action-angle variables is a great advantage of the HMF model for the investigating

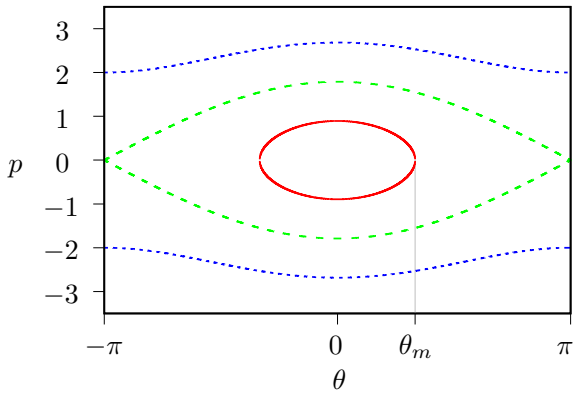

FIG. 1. Examples of a librating orbit (red solid line), for which $\kappa < 1$, a rotating orbit (blue dotted line), for which $\kappa > 1$, and the separatrix orbit (green dashed line), for which $\kappa = 1$. For the librating orbit, $\theta_m = \arccos(1-2\kappa^2)$, while for the other orbits $\theta_m = \pi$.

inhomogeneous states. For most systems, this is not possible, a few exceptions in astrophysics being spherical potentials and flat axisymmetric potentials such as razor-thin and tepid disks, as well as some nonaxisymmetric potentials such as Stäckel potentials [18].

B. Kinetic equations

For the HMF model, the pair potential $u(\theta-\theta') = -\cos(\theta-\theta')$ can be written in the two-dimensional biorthogonal representation as $\Phi_c = -\cos[\theta(w,\kappa)]$ and $\Phi_s = -\sin[\theta(w,\kappa)]$, and its Fourier transforms are

$$\begin{aligned}\hat{\Phi}_c(m,\kappa) &= -c_m(\kappa) = \frac{-1}{2\pi}\int_{-\pi}^{\pi}\cos[\theta(w,\kappa)]e^{-imw}dw,\\ \hat{\Phi}_s(m,\kappa) &= -s_m(\kappa) = \frac{-1}{2\pi}\int_{-\pi}^{\pi}\sin[\theta(w,\kappa)]e^{-imw}dw.\end{aligned} \tag{44}$$

These can be written more simply as (see Appendix B)

$$c_n(\kappa) = \begin{cases} \frac{\pi^2}{K(\kappa)^2}\frac{|n|q(\kappa)^{|n|/2}}{1-q(\kappa)^{|n|}} & \kappa<1,\ n \text{ even},\\ 0 & \kappa<1,\ n \text{ odd},\\ \frac{2\pi^2\kappa^2}{K\left(\frac{1}{\kappa}\right)^2}\frac{|n|q\left(\frac{1}{\kappa}\right)^{|n|}}{1-q\left(\frac{1}{\kappa}\right)^{2|n|}} & \kappa>1,\end{cases} \tag{45}$$

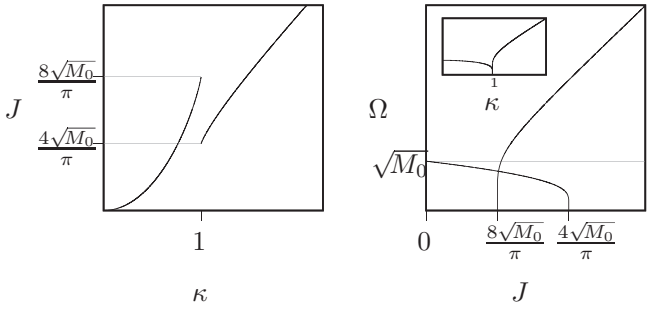

FIG. 2. Action as a function of κ for the HMF model (left), and frequency Ω versus J (inset: Ω vs κ) (right) for the HMF model.

and

$$s_n(\kappa) = \begin{cases} 0 & \kappa<1,\ n \text{ even},\\ -i\frac{\pi^2}{K(\kappa)^2}\frac{nq(\kappa)^{|n|/2}}{1+q(\kappa)^{|n|}} & \kappa<1,\ n \text{ odd},\\ -i\frac{2\pi^2\kappa^2}{K\left(\frac{1}{\kappa}\right)^2}\frac{nq\left(\frac{1}{\kappa}\right)^{|n|}}{1+q\left(\frac{1}{\kappa}\right)^{2|n|}} & \kappa>1,\ p>0,\\ i\frac{2\pi^2\kappa^2}{K\left(\frac{1}{\kappa}\right)^2}\frac{nq\left(\frac{1}{\kappa}\right)^{|n|}}{1+q\left(\frac{1}{\kappa}\right)^{2|n|}} & \kappa>1,\ p<0,\end{cases} \tag{46}$$

where $q(k) = \exp[-\pi K(\sqrt{1-k^2})/K(k)]$. To switch variables from J to κ, we use the Dirac δ identity $\delta[f(x)] = \sum_{x^*}\delta(x-x^*)/|\partial f/\partial x|_{x^*}$ [where x^* are the roots of $f(x)$]. Thus, the Lenard-Balescu equation for the HMF model is

$$\begin{aligned}\frac{\partial f}{\partial t} = {}& \frac{2\pi^2}{N}\left|\frac{\partial J}{\partial\kappa}\right|^{-1}\frac{\partial}{\partial\kappa}\sum_{n,n'=-\infty}^{\infty}\int\frac{d\kappa' n|\partial J'/\partial\kappa'|}{|D_{nn'}(\kappa,\kappa',n\Omega(\kappa))|^2}\\ &\times\sum_{\kappa^\star}\frac{\delta(\kappa'-\kappa^\star)}{\left|n'\frac{\partial\Omega}{\partial\kappa'}\right|_{\kappa^\star}}\left(n\left|\frac{\partial J}{\partial\kappa}\right|^{-1}\frac{\partial}{\partial\kappa}-n'\left|\frac{\partial J'}{\partial\kappa'}\right|^{-1}\frac{\partial}{\partial\kappa'}\right)\\ &\times f(\kappa,t)f(\kappa',t),\end{aligned} \tag{47}$$

where $\kappa^\star$ are the roots of the equation $m\Omega(\kappa)-m'\Omega(\kappa')=0$, the Jacobian $|\partial J/\partial\kappa|$ is given by Eq. (42), and $\partial\Omega/\partial\kappa$ is

$$\frac{\partial\Omega}{\partial\kappa} = \pi\sqrt{M_0}\begin{cases}\frac{E(\kappa)+(\kappa^2-1)K(\kappa)}{2\kappa(\kappa^2-1)K^2(\kappa)}, & \kappa<1,\\ \frac{\kappa^2 E\left(\frac{1}{\kappa}\right)}{(\kappa^2-1)K^2\left(\frac{1}{\kappa}\right)}, & \kappa>1.\end{cases} \tag{48}$$

The associated diffusion coefficient is

$$D_{\rm dif}(\kappa) = \frac{2\pi^2}{N}\sum_{n,n'=\infty}^{\infty}\sum_{\kappa^\star}\frac{n^2|\partial J/\partial\kappa|_{\kappa^\star}}{|D_{nn'}(\kappa,\kappa^\star,n\Omega(\kappa))|^2}\frac{f(\kappa^\star,t)}{\left|n'\frac{\partial\Omega}{\partial\kappa'}\right|_{\kappa^\star}} \tag{49}$$

and the polarization coefficient is

$$D_{\rm pol}(\kappa) = \frac{2\pi^2}{N}\sum_{n,n'=-\infty}^{\infty}\sum_{\kappa^\star}\frac{n\,n'}{|D_{nn'}(\kappa,\kappa^\star,n\Omega(\kappa))|^2}\frac{\partial f/\partial\kappa'|_{\kappa^\star}}{\left|n'\frac{\partial\Omega}{\partial\kappa'}\right|_{\kappa^\star}}. \tag{50}$$

Equation (24), which determines $D_{nn'}(\kappa,\kappa',\omega)$, becomes

$$\frac{1}{D_{nn'}(\kappa,\kappa',\omega)} = \frac{c_n(\kappa)c_{n'}(\kappa')}{\epsilon_{cc}(\omega)} - \frac{s_n(\kappa)s_{n'}(\kappa')}{\epsilon_{ss}(\omega)}. \tag{51}$$

If collective effects are neglected, then $\epsilon_{cc}=\epsilon_{ss}=1$, and we get simply

$$\frac{1}{D^{\rm bare}_{nn'}(\kappa,\kappa')} = c_n(\kappa)c_{n'}(\kappa') - s_n(\kappa)s_{n'}(\kappa'). \tag{52}$$

If collective effects are not neglected, then it is necessary to compute numerically the dielectric tensor, with the procedure we detail below.

C. Numerical computation of the dielectric tensor

The cc and ss components of the dielectric tensor are

$$\epsilon_{cc}(\omega) = 1 + 2\pi\sum_{\ell=-\infty}^{\infty}\int_0^\infty d\kappa\frac{g^{cc}_\ell(\kappa)}{\Omega(\kappa)-\omega/\ell} \tag{53}$$

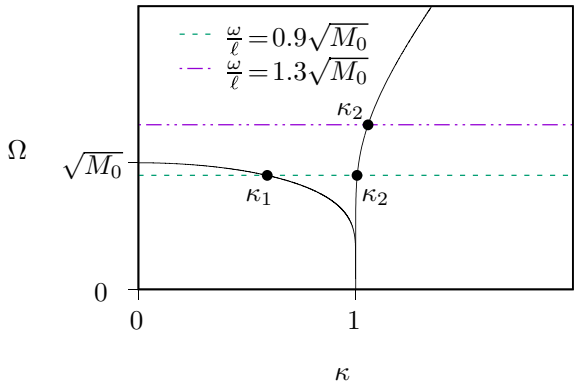

FIG. 3. Poles of integral in the dielectric tensor components (53) and (54). For $\omega/\ell > \Omega_0$ (dash-dotted line), only one pole occurs (κ_2), while for $0 < \omega/\ell < \Omega_0$ (dashed line), there are two (κ_1 and κ_2).

and

$$\epsilon_{ss}(\omega) = 1 + 2\pi \sum_{\ell=-\infty}^{\infty} \int_0^{\infty} d\kappa \frac{g_\ell^{ss}(\kappa)}{\Omega(\kappa) - \omega/\ell}, \tag{54}$$

respectively, where, to simplify the notation, we have defined

$$g_\ell^{cc}(\kappa) = |c_\ell(\kappa)|^2 \partial f/\partial\kappa, \tag{55a}$$

$$g_\ell^{ss}(\kappa) = |s_\ell(\kappa)|^2 \partial f/\partial\kappa. \tag{55b}$$

The off-diagonal terms, involving products of the type $c_n(\kappa)s_{n'}(\kappa')$, are zero after integration.

The integrals in Eqs. (53) and (54) must be performed carefully due to the poles at $\omega = \ell\Omega(\kappa)$. Poles can only occur if ℓ and ω are of the same sign. Moreover, the number of poles depends on the value of ω, since $\Omega(\kappa)$ can have the same value at two different values of κ for $\Omega(\kappa) < \Omega_0$ where $\Omega_0 = \Omega(0) = \sqrt{M_0}$. Therefore, we distinguish among the following cases (see Fig. 3):

(1) $\omega/\ell < 0$: no poles;

(2) $0 < \omega/\ell < \Omega_0$: one pole $\kappa_1 < 1$ and one pole at $\kappa_2 > 1$;

(3) $\omega/\ell > \Omega_0$: one pole at $\kappa_2 > 1$.

For each case, the integrals must be separated into different regions. In all cases we separate between the regions $\kappa \in (0,1)$ and $\kappa \in (1,\infty)$, due to the different expressions of $\Omega(\kappa)$, $c_n(\kappa)$, and $s_n(\kappa)$ in the two domains. Therefore, for case 1, the integrals in Eqs. (53) and (54) are

$$\int d\kappa \frac{g_\ell^{cc/ss}(\kappa)}{\Omega(\kappa) - \omega/\ell} = \int_0^1 d\kappa \frac{g_\ell^{cc/ss}(\kappa)}{\Omega(\kappa) - \omega/\ell} + \int_1^{\infty} d\kappa \frac{g_\ell^{cc/ss}(\kappa)}{\Omega(\kappa) - \omega/\ell}. \tag{56}$$

For case (2), we must use the Landau contour in both regions,

$$\int d\kappa \frac{g_\ell^{cc/ss}(\kappa)}{\Omega(\kappa) - \omega/\ell} = \mathcal{P}\int_0^1 d\kappa \frac{g_\ell^{cc/ss}(\kappa)}{\Omega(\kappa) - \omega/\ell} + i\pi Res\kappa_1 + \mathcal{P}\int_1^{\infty} d\kappa \frac{g_\ell^{cc/ss}(\kappa)}{\Omega(\kappa) - \omega/\ell} + i\pi Res\kappa_2, \tag{57}$$

and, for case (3), only in the second region,

$$\int d\kappa \frac{g_\ell^{cc/ss}(\kappa)}{\Omega(\kappa) - \omega/\ell} = \int_0^1 d\kappa \frac{g_\ell^{cc/ss}(\kappa)}{\Omega(\kappa) - \omega/\ell} + \mathcal{P}\int_1^{\infty} d\kappa \frac{g_\ell^{cc/ss}(\kappa)}{\Omega(\kappa) - \omega/\ell} + i\pi Res\kappa_2, \tag{58}$$

where $\mathcal{P}\int$ denotes the Cauchy principal value and $Resx$ is the residue of the integrand at x.

Equations (49), (51), (53), and (54), with $\Omega(\kappa)$, $s_m(\kappa)$, and $c_m(\kappa)$ determined by equations (43), (45), and (46), respectively, enable us to calculate the diffusion coefficient of the HMF model in action-angle variables, with collective effects. The same can be done neglecting collective effects, using the same equations with $\epsilon_{cc} = \epsilon_{ss} = 1$. The inclusion or exclusion of collective effects greatly affects the resulting diffusion coefficient. This is shown in Fig. 6, where we present diffusion coefficients considering a thermal bath,

$$f(\kappa,t) = C\exp[-\beta M_0(2\kappa^2 - 1)], \tag{59}$$

for two equilibrium configurations (β, M_0), where $C = \sqrt{\beta/(2\pi)^3}/I_0(\beta M_0)$ and $I_n(z)$ is the nth-order modified Bessel function of the first kind. For the numerical results, all sums over n, n', and ℓ are truncated at $n_{\max} = 6$ and $\ell_{\max} = 6$, respectively (although normally $n_{\max} = 4$ and $\ell_{\max} = 2$ suffice).

From the forms of equations of the diffusion coefficients (49), we see that the contributions to the diffusion of a particle with a parameter κ come from its resonances with particles of parameter $\kappa^\star$, where $\kappa^\star$ and κ satisfy $n\Omega(\kappa) = n'\Omega(\kappa^\star)$ and n,n' are integers. In order to see how each resonance contributes to the diffusion coefficient, in Fig. 4 we plot maps showing the normalized contribution of each term in the $\kappa^\star$ sum, for a given κ, for a thermal distribution function corresponding to $M_0 = 0.05$ (top) and $M_0 = 0.9$ (bottom). In other words, if we write the diffusion coefficient as

$$D_{\rm dif}(\kappa) = \sum_{\kappa^\star} \gamma(\kappa,\kappa^\star), \tag{60}$$

then the color map shows $\gamma(\kappa,\kappa^\star)/D_{\rm dif}(\kappa)$.

In the highly inhomogeneous case, $M_0 = 0.9$, almost all the contribution comes from $\kappa^\star < 1$ (inside the separatrix). This is mainly due to the distribution being highly clustered, so most particles are below the separatrix. Consequently, for most particles, the main contribution to their diffusion comes from resonances with particles at their same frequency. This is represented by the strong yellow line at $\kappa^\star < 1$. For the almost-homogeneous case, $M_0 = 0.05$, the particles are not so clustered and so particles with $\kappa^\star \neq \kappa$ also contribute, as demonstrated by the presence of other curves in the top panel.

D. Examples of numerical calculations

In this section we show the predictions for the diffusion coefficients both including or neglecting collective effects. Note that, near the separatrix ($\kappa = 1$), we do not plot the value of the diffusion coefficient. This is because the calculation becomes numerically unstable in this region. Indeed, the

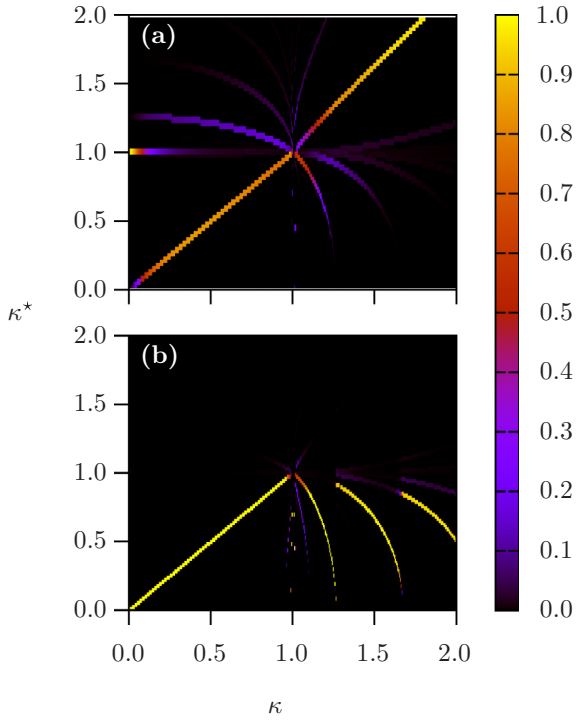

FIG. 4. Normalized contribution to the Lenard-Balescu diffusion coefficient $D_{\rm dif}(\kappa)$, Eq. (49), as a function of $\kappa^\star$. Both panels correspond to thermal equilibrium distributions but with different magnetizations: (a) almost homogeneous, $M_0 = 0.05$, and (b) highly inhomogeneous, $M_0 = 0.9$. In the latter case, most of the contribution comes from resonances at $\kappa^\star < 1.0$ (below the separatrix), while for the nearly homogeneous system this is not the case.

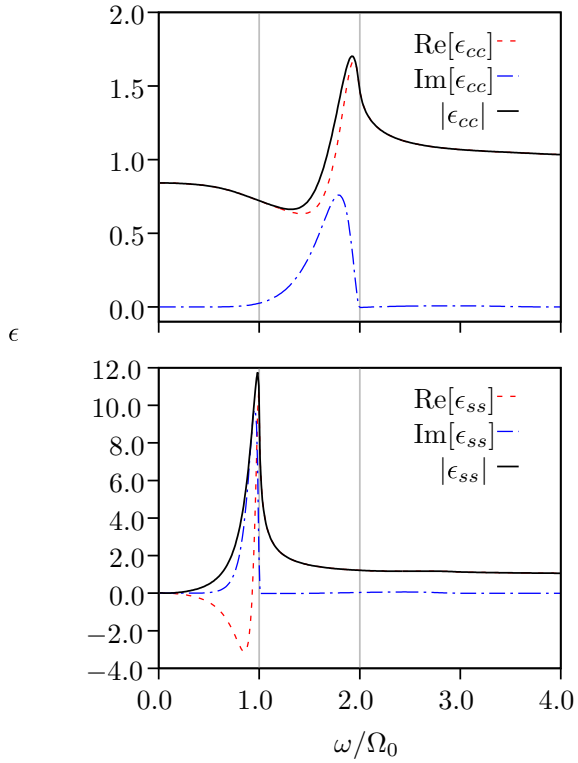

FIG. 5. Cosine (top) and sine (bottom) components of the dielectric tensor $\epsilon(\omega)$, given by Eqs. (53) and (54), respectively. The equilibrium parameters are $(u, M_0) = (-0.1, 0.728)$. The vertical lines show $\omega = \Omega_0$ and $\omega = 2\Omega_0$.

perturbative approach we have used may not be valid [24,25] for particles crossing the separatrix. Since it does not seem to play an important role in the diffusion, we neglect the point $\kappa \approx 1$. First, we notice that, as in the homogeneous case [15], collective effects are very important in this system. To illustrate this behavior, we plot the components of the dielectric tensor in Fig. 5. We observe a characteristic frequency (materialized by a "bump") at a frequency of order $n\Omega_0$, with $n = 1$ for sine perturbations and $n = 2$ for cosine ones. We observe that collective effects are very important for frequencies $\omega \lesssim n\Omega_0$ in this case, i.e., the modulus of the components of the dielectric tensor differs considerably from 1. Inspecting the kinetic equation (47), we see that this implies that for values of κ which correspond to these frequencies (which correspond mainly to librating particles) collective effects are important. However, particles with larger frequencies do not present strong collective effects, because they have frequencies $\omega \gg \Omega_0$ for which the components of the dielectric tensor is close to 1.

This fact is apparent in the computation of the diffusion coefficients for two different magnetizations shown in Fig. 6. For both small magnetization (i.e., system very close to homogeneity) as well as magnetization closer to 1, the diffusion coefficients predicted by the Landau equation (no collective effects) and the Lenard-Balescu equation (collective effects) difrer completely except, as expected, for $\kappa > 1$, which corresponds to particles with frequencies for which the modulus of the components of the dielectric tensor tends to 1.

E. Analytical results for highly magnetized states

It is possible to obtain analytical expressions for the diffusion coefficients for highly magnetized configurations. In this case, all the particles have $\kappa < 1$ and it suffices to perform the sums in the kinetic equations up to $|n| = |n'| = 2$ to obtain a good approximation to the dielectric tensor and the diffusion coefficients. This implies that the position of the resonances are $\kappa^\star = \kappa$, simply.[2] If the system is less magnetized, then there are resonances with particles which are outside the separatrix, and in this case it is necessary to solve numerically the resonance condition $n\Omega(\kappa) = n'\Omega(\kappa^*)$. We will study the case in which collective effects are neglected, and then when collective effects are considered for two paradigmatic cases: a core-halo distribution and a Maxwell-Boltzmann distribution. These two distributions can be considered as prototypes of the two classes of distributions which appears after the violent relaxation process. When initial condition leads to a very "violent" violent relaxation, it results in a core-halo quasiequilibrium, while when the initial condition leads to a "gentle" violent relaxation, a compact distribution similar to a Gaussian one forms [26].

[2]Note that in this approximation the flux associated with Eq. (23) is zero, and hence f does not vary with time.

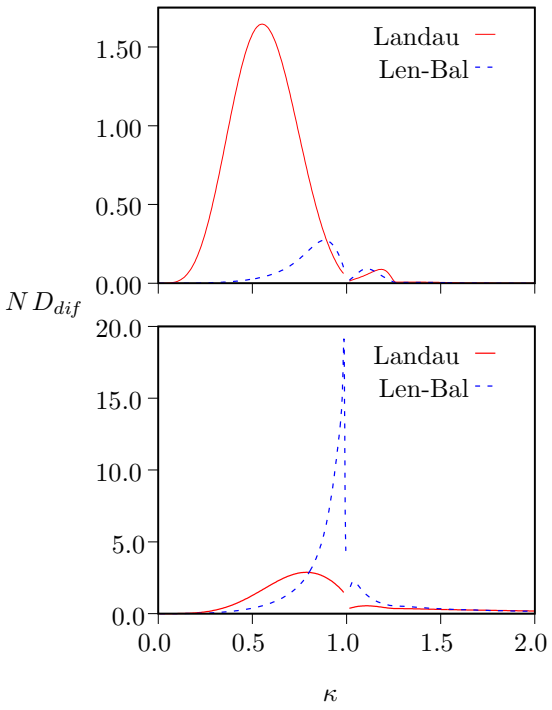

FIG. 6. Diffusion coefficient $D_{\rm dif}(\kappa)$ for two different equilibrium configurations: $(u,M_0)=(-0.1,0.7285)$ (top) and $(u,M_0)=(0.2475,0.0632)$ (bottom). Solid (red) lines show the diffusion coefficient with collective effects, Eqs. (49) and (51), while the dashed (blue) lines show the result without collective effects, Eqs. (49) and (52). Both curves are cut off near $\kappa=1$ due to numerical instability at the separatrix.

1. Without collective effects

When collective effects are neglected, $\epsilon_{cc}=1$ and $\epsilon_{ss}=1$, a very good approximation is given by taking only the first term of Eqs. (49) and (50) (taking higher terms is straightforward). We obtain therefore

$$D_{\rm dif}(\kappa)=\frac{4\pi^8\kappa^2(1-\kappa^2)\mathrm{sech}^4\left[\frac{\pi K(\sqrt{1-\kappa^2})}{2K(\kappa)}\right]}{NK(\kappa)^5[(\kappa^2-1)K(\kappa)+E(\kappa)]}f(\kappa), \tag{61a}$$

$$D_{\rm pol}(\kappa)=\frac{\pi^9\kappa(\kappa^2-1)\mathrm{sech}^4\left[\frac{\pi K(\sqrt{1-\kappa^2})}{2K(\kappa)}\right]}{2N\sqrt{M_0}K(\kappa)^6[(\kappa^2-1)K(\kappa)+E(\kappa)]}\frac{\partial f}{\partial\kappa}(\kappa). \tag{61b}$$

If M_0 is very close to 1, then most of the particles have small κ. It is possible to expand Eq. (61) around $\kappa=0$, giving the following simple results:

$$D_{\rm dif}(\kappa)=\frac{1}{N}[32\pi^2\kappa^4+\mathcal{O}(\kappa^6)]f(\kappa), \tag{62a}$$

$$D_{\rm pol}(\kappa)=\frac{1}{N\sqrt{M_0}}[8\pi^2\kappa^3+\mathcal{O}(\kappa^5)]\frac{\partial f}{\partial\kappa}(\kappa). \tag{62b}$$

2. With collective effects

We will first consider the core-halo distribution. It can be modeled by the sum of two step functions,

$$f_{\rm ch}(\kappa)=\eta_1\Theta[\mu_1-h]+\eta_2\Theta[\mu_2-h], \tag{63}$$

where we have assumed that μ_1 and μ_2 corresponds to the energy of particles which are inside the separatrix. Using the definition of $h=M_0(2\kappa^2-1)$, we can express Eq. (63) as a function of κ

$$f_{\rm ch}(\kappa)=\eta_1\Theta\left[2M_0\left(\kappa_1^2-\kappa^2\right)\right]+\eta_2\Theta\left[2M_0\left(\kappa_2^2-\kappa^2\right)\right], \tag{64}$$

where $\kappa_i=\sqrt{\mu_i/M_0+1}$ and $\kappa_1<1$ and $\kappa_2<1$.

Computing the dielectric tensor is straightforward because the derivative of $f_{\rm ch}$ about κ involves Dirac δ functions:

$$\frac{\partial f_{\rm ch}}{\partial\kappa}=-2\kappa M_0\left\{\eta_1\delta\left[M_0\left(\kappa_1^2-\kappa^2\right)\right]+\eta_2\delta\left[M_0\left(\kappa_2^2-\kappa^2\right)\right]\right\}. \tag{65}$$

The dielectric tensor is purely real, and it can be calculated inserting Eq. (64) into Eqs. (53) and (54):

$$\epsilon_{cc/ss}(\omega)=1+2\pi\sum_{\ell=-\infty}^{\infty}\left\{\frac{g_\ell^{cc/ss}(\kappa_1)}{\Omega(\kappa_1)-\omega/\ell}+\frac{g_\ell^{cc/ss}(\kappa_2)}{\Omega(\kappa_2)-\omega/\ell}\right\}+(\omega\to-\omega), \tag{66}$$

where $(\omega\to-\omega)$ means to sum the same expression with ω replaced by $-\omega$. Using Eqs. (49) and (50) with Eq. (64) and $\kappa^*=\kappa$, it is straightforward to compute the diffusion coefficients.

It is interesting to compare the diffusion coefficients for an idealized core-halo distribution (64) with a more realistic, smoother version of it, which is the kind of distribution we simulated (see Sec. IV):

$$f_{\mathrm{ch}_i^*}(h)=\frac{\eta_1}{1+\exp[\beta_1(h-\mu_1)]}+\frac{\eta_2}{1+\exp[\beta_2(h-\mu_2)]}. \tag{67}$$

For a given mean energy u and magnetization M_0, plus the normalization constraints, three of the six parameters $\eta_1,\eta_2,\beta_1,\beta_2,\mu_1,\mu_2$ are determined. We have chosen the coefficients $\eta_1=0.298$, $\eta_2=0.05$, $\mu_1=-0.517$, and $\mu_2=0.19$ for $i=1,2$; $\beta_1=70$ and $\beta_2=70$ for $i=1$; and $\beta_1=30$ and $\beta_2=10$ for $i=2$. As the coefficients β_i increase, the step functions become steeper. We observe in the top row of Fig. 7 that for the steeper case ch_1^* the two-step core-halo (64) describes very well both the components of the dielectric tensor and the diffusion coefficient. For the softer case ch_2^*, we observe a correct agreement for the components of the dielectric tensor for most of the frequencies. The disagreement is responsible for the differences observed in the diffusion coefficient for some ranges of κ.

For the case of distributions like the Maxwell-Boltzmann one, the main difficulty consists of computing the dielectric tensor. It is possible to do it analytically for a wide class of functions taking the advantage that if $M_0\to1$, most of the particles have small κ. We can thus expand in Taylor series the different quantities which appear in the kinetic equations. We

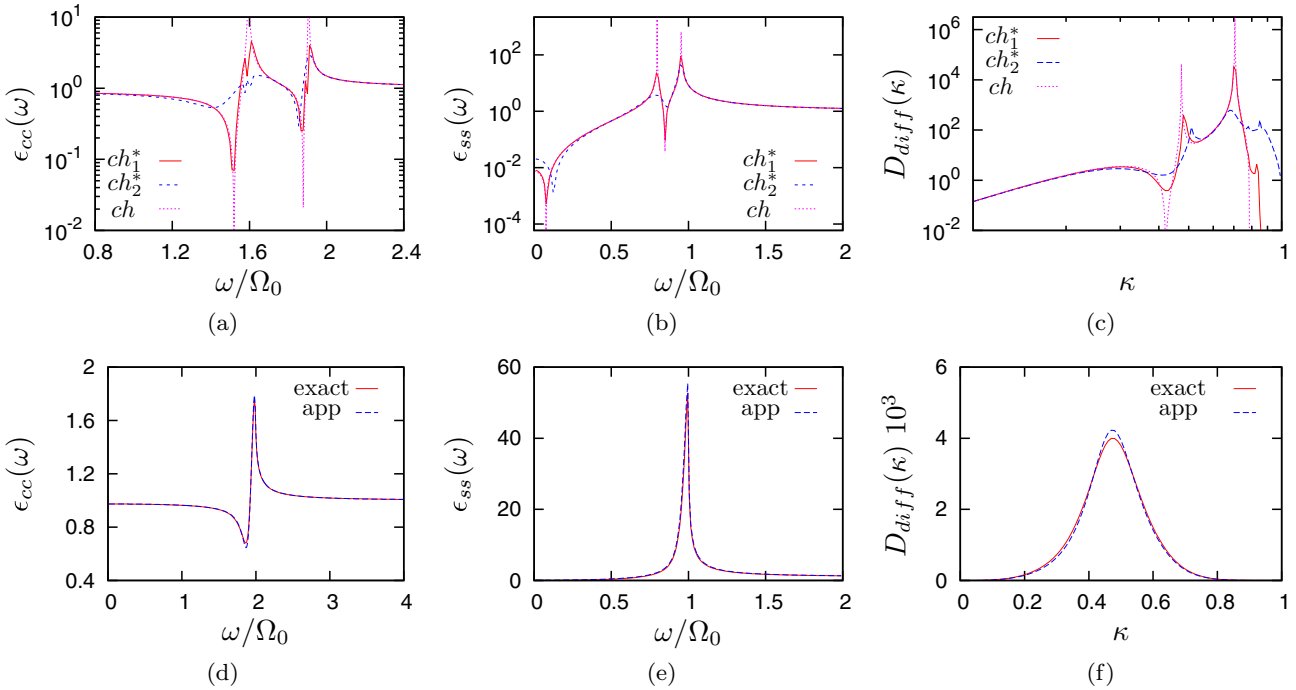

FIG. 7. [(a)–(c)] Comparison of the approximate expressions (C1) and (C2) and the diffusion coefficient for a core-halo system (see text for details), and [(d)–(f)] the same quantities at Maxwell-Boltzmann equilibrium for magnetization $M_0 = 0.95$.

need therefore (valid for $\kappa \leqslant 1$):

$$J(\kappa) = 2\sqrt{M_0}\kappa^2 + \mathcal{O}(\kappa^4), \tag{68a}$$

$$\Omega(\kappa) = \sqrt{M_0}\left[1 - \frac{\kappa^2}{4} + \mathcal{O}(\kappa^4)\right], \tag{68b}$$

$$c_2(\kappa) = \frac{\kappa^2}{2} + \mathcal{O}(\kappa^4), \tag{68c}$$

$$s_1(\kappa) = -i\kappa + \mathcal{O}(\kappa^3). \tag{68d}$$

The components of the dielectric tensor can be approximated as

$$\epsilon_{cc}(\omega) \simeq 1 + \frac{\pi}{2}\int_0^1 d\kappa \frac{\kappa^4 \partial f_{MB}/\partial\kappa}{\sqrt{M_0}\left(1-\frac{\kappa^2}{4}\right) - \omega/2} + (\omega \to -\omega), \tag{69a}$$

$$\epsilon_{ss}(\omega) \simeq 1 + 2\pi\int_0^1 d\kappa \frac{\kappa^2 \partial f_{MB}/\partial\kappa}{\sqrt{M_0}\left(1-\frac{\kappa^2}{4}\right) - \omega} + (\omega \to -\omega). \tag{69b}$$

Taking as the distribution function the thermal equilibrium one (59), the integrals can be expressed in terms of trigonometric and exponential integrals (for the explicit expressions, see Appendix C). Using the approximations (C1) and (C2) and the terms of Eqs. (49) and (50) corresponding to n and n' taking the values from -2 to $+2$ we get, for large M_0, a lengthy but analytical approximation (which we do not explicitly write here) of the diffusion coefficients which is very accurate for M_0 close to 1. In the bottom row of Fig. 7 we show the diffusion coefficients for $M_0 = 0.95$.

IV. COMPARISON WITH SIMULATIONS

The previous subsection presents the application of the kinetic equations to the HMF model. In order to compare those analytical results with the Hamiltonian dynamics of the N-body system, we use molecular dynamics, integrating the equations of motion of N particles and tracking their orbits through time.

In order to compare the theoretical results with simulation we adopt the point of view of the Fokker-Planck equation. The idea is to study a test particle evolving in a field composed of the other particles. The effect of the field on the test particle is taken into account by the diffusion and friction coefficients. The mean-field properties of the field evolve adiabatically compared to the time scale of the fluctuations which lead to the test particle's relaxation. In the case of the HMF model, this means that the field's magnetization is $M = M_0 + \delta M$, where M_0 evolves very slowly compared to δM. The test particle's base orbit is thus determined by M_0, whereas the fluctuations δM drive its relaxation. The collective effects represent the reaction of the field to its own perturbations, that is, the field particles are also affected by δM. If we disregard collective effects, the field particles should evolve subject only to the mean magnetization M_0. Therefore, a possible way of testing the importance of collective effects in the HMF model is to simulate two types of N-body dynamics.

The first, which we will refer to as "MD(bath)," is a dynamics *without* collective effects. The system is composed of N_b particles which form a thermal bath and evolve with the adiabatic, static magnetization M_0 (corresponding to the smooth potential),

$$\ddot{\theta}_i^{\,b} = -M_0 \sin\theta_i, \quad i = 1, \ldots, N_b \tag{70}$$

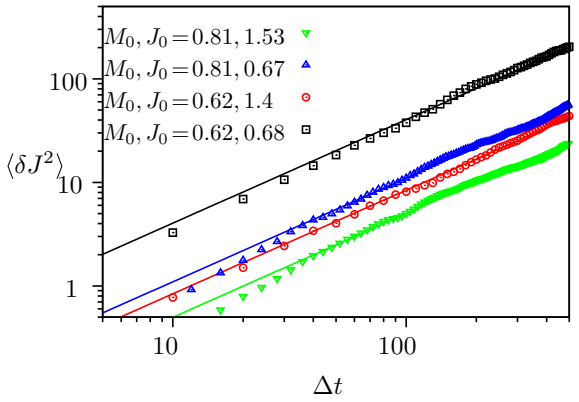

FIG. 8. Variation of J^2, Eq. (75), as a function of time for different values of J_0 and different thermal distributions. Points are molecular dynamics results of the regular HMF model and lines are linear fits. For longer times, the diffusion becomes sublinear.

and N_{tp} independent test particles which evolve under the potential due to the oscillating magnetization of the bath particles,

$$\ddot{\theta}_i^{tp} = -M_x^b \sin\theta_i + M_y^b \cos\theta_i, \quad i = N_b + 1, \ldots, N_b + N_{tp} \tag{71}$$
$$M_x^b = \frac{1}{N_b}\sum_{i=1}^{N_b} \cos\theta_i, \quad M_y^b = \frac{1}{N_b}\sum_{i=1}^{N_b} \sin\theta_i.$$

The bath particles are set up with any initial positions and velocities corresponding to the Vlasov-stable distribution for which we want to measure the diffusion coefficients, e.g., (59) or (67). We detail the procedure for the former case: The initial particle positions and velocities must be distributed according to

$$f_{\rm eq}(\theta, p) = \sqrt{\frac{\beta}{(2\pi)^3}} I_0^{-1}(\beta M_0) \exp\left[-\beta\left(\frac{p^2}{2} - M_0 \cos\theta\right)\right]. \tag{72}$$

For each M_0, β must be determined self-consistently by

$$M_0 = \frac{I_1(\beta M_0)}{I_0(\beta M_0)}. \tag{73}$$

Second, we simulate the full N-body simulation of the HMF model—hence *with* collective effects—which we shall refer to as "MD(full)." All N particles in the system evolve according to

$$\ddot{\theta}_i = -M_x \sin\theta_i + M_y \cos\theta_i, \quad i = 1, \ldots, N \tag{74}$$
$$M_x = \frac{1}{N}\sum_{i=1}^{N} \cos\theta_i, \quad M_y = \frac{1}{N}\sum_{i=1}^{N} \sin\theta_i.$$

We have seen from the analytical calculations that collective effects are important in the HMF model. Therefore, these two N-body methods should result in very different diffusion coefficients. We measure the diffusion coefficients of test particles as follows: First, we calculate the initial action $J_i(t_0)$ of each test particle—or simply each particle, in the case of MD(full)—and separate them accordingly into L bins of size ΔJ_0. Then we calculate the mean-square variation of J for each J_0 as a function of Δt,

$$\langle \delta J^2 \rangle_\ell = \frac{1}{N_\ell}\sum_{i=1}^{N_\ell} [J_i(t_0 + \Delta t) - J_0]^2, \quad \ell = 1, \ldots, L \tag{75}$$

where the sum, for each bin ℓ, is over all N_ℓ particles with $J(t_0) \in [(\ell - 1/2)\Delta J_0, (\ell + 1/2)\Delta J_0)$. The diffusion

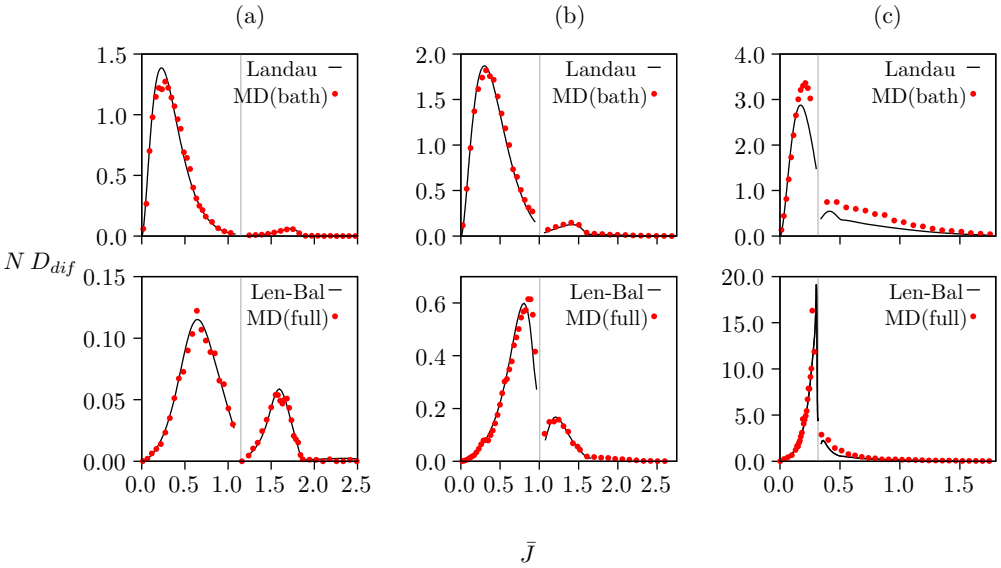

FIG. 9. Diffusion coefficients calculated by molecular dynamics, Eq. (76), compared to the theoretical results, for an equilibrium distribution with parameters (a) $(u, M_0) = (-0.2, 0.816)$, (b) $(u, M_0) = (0.0, 0.622)$, and (c) $(u, M_0) = (0.2475, 0.06)$. On the bottom, MD simulations without collective effects with the prediction of the Landau equation (49). On the top, MD simulations with collective effects with the theoretical curve predicted by the Lenard-Balescu (Len-Bal) equation, using condition (34), and the molecular dynamics given by the regular HMF model, MD(full). The gray vertical line represents the separatrix.

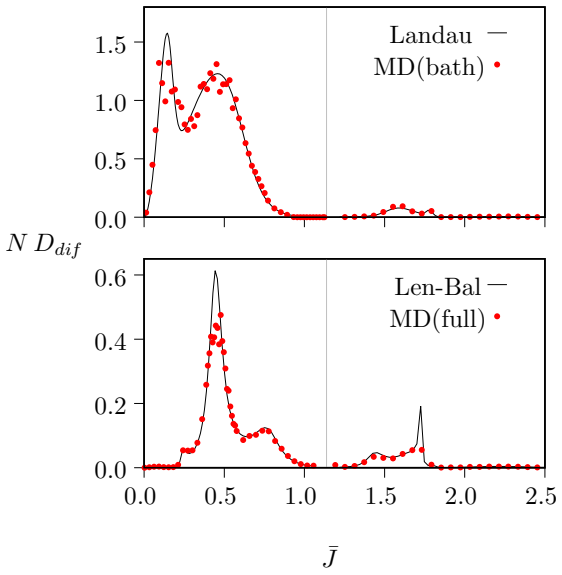

FIG. 10. Diffusion coefficients for a system in a "core-halo" type distribution, given by Eq. (67). On the top, without collective effects: simulation of test particles interacting with the distribution [MD(bath)] and the theoretical curve (Landau). The gray vertical line represents the separatrix. On the bottom, MD simulation results of the regular HMF [MD(full)] with the theoretical curve with collective effects (Len-Bal). The parameters for the distribution are $\beta_1 = 30$, $\beta_2 = 10$, $\eta_1 = 0.298$, $\eta_2 = 0.051$, $\mu_1 = -0.517$, and $\mu_2 = 0.19$, which gives $M_0 = 0.8$.

coefficient for a given J_0 (or, equivalently, for a given bin ℓ), is half of the slope of the linear part of the curve $\langle \delta J^2(\Delta t)\rangle_\ell$,

$$D_{\rm dif}^{\rm MD}(J_0) = \frac{\langle \delta J^2\rangle_\ell}{2\Delta t}. \tag{76}$$

For some values of J_0, care must be taken to calculate the coefficient in the full HMF molecular dynamics: If the magnetization is sufficiently high, then there are little to no particles for higher values of J_0. Therefore, to calculate the coefficient in these regions, we simulate the dynamics of test particles with high J_0 that interact with the full HMF.

Examples of the linear fit are shown in Fig. 8, for two values of J_0. Typically, the fit is done over a time range of $t \in [100,500]$, although this may vary depending on the value of J_0 and M_0. On average, choosing different time ranges does not greatly affect the outcome. For the fits, we took averages of $\langle \delta J^2(\Delta t)\rangle_\ell$ over many time intervals of the dynamics, that is, for many values of t_0. Typically, we used 100 intervals.

In Fig. 9, we compare the molecular dynamics results with the kinetic theory diffusion coefficients for systems in thermal baths.[3]

The top panels show the case without collective effects [MD(bath)] and the Landau diffusion coefficient calculated with (49) and (34), while the bottom panels show the case with collective effects [MD(full)] and the Lenard-Balescu diffusion coefficient (49). Each kind of simulation has been performed with $N = 500\,000$ particles, except for the lowest magnetization case, which was performed with $N = 1\,000\,000$. We see that for magnetizations not close to zero [Figs. 9(a) and 9(b)] the MD fit matches very well the result from the corresponding kinetic equation. In the case of magnetization close to zero [Fig. 9(c)] the match is only reasonably good. This can be explained because in this case the linear diffusion regime is very short and, consequently, the fluctuations larger.

We test also the theoretical results for a core-halo distribution ch_2^* equation (67). For both without collective effects (top) and with collective effects (bottom), the results match very well, see Fig. 10.

V. CONCLUSION

In this paper we have studied the diffusion coefficients corresponding the collisional relaxation in the inhomogeneous HMF model. To perform these calculations we have used the Landau and the Lenard-Balescu equations expressed in action-angle variables. We have described precisely how to perform the calculations and showed that the diffusion coefficients can be easily computed in a very reduced computer time with high precision. Moreover, we have given analytical expressions for the dielectric tensor and the diffusion coefficients for systems with magnetization close to 1, which agree very well with the exact ones.

One of the conclusions of the paper is that, for the cases for which we have calculated the diffusion coefficients, collective effects are very important in the dynamics independently of how much the system is clustered (i.e., magnetized). We note that this is also the case in the homogeneous case [15].

We have also studied which particles "talk to each other" in the collisional relaxation process. For highly clustered systems (i.e., magnetization close to one), the contribution of the relaxation of a given particle comes almost exclusively from particles in the same orbit (i.e., with the same κ). This is a similar behavior than in the homogeneous case, for which it is simple to show that for any long-range one-dimensional system the contribution for the relaxation comes from particles with the same velocity [17]. As the system becomes less clustered, the situation becomes more complicated, and particles in different orbits start to "interact" with one another (see Fig. 4).

In order to test the theoretical predictions, we have computed numerically the diffusion coefficients using molecular dynamics simulations. To check our calculations when the collective effects are neglected, we have set up a simple method to perform simulations in which collective effects are absent. We have found a very good agreement between the theoretical calculations and the simulations both for the dynamics with and without collective effects. We have performed these tests for baths at Maxwell-Boltzmann equilibrium as well as out of equilibrium (core-halo distributions).

The next natural step of this work is to use the diffusion coefficients to compute the whole evolution of the HMF model up to thermalization. With the methods developed in the paper, it is a relatively simple task to compute the evolution with the

[3]For clarity, in the plots of the diffusion coefficients in which the abscissa is the action, we use instead a rescaled action $\bar{J}$,

$$\bar{J} = \begin{cases} J/2 & \kappa < 1 \\ J & \kappa > 1 \end{cases}.$$

Landau or the Lenard-Balescu equation. The magnetization should be computed self-consistently at each time step and then the diffusion coefficient. We stress that the evolution of Eq. (47) could present interesting features because it is nonlinear. This subject will be presented in a forthcoming paper.

We note also that the analytical expressions for the dielectric tensor can be used to study analytically the stability and the mean-field evolution of the HMF model for highly clustered states, computing in an appropriate but straightforward way the pole contributions to the dielectric tensor (see Ref. [22] for a detailed study on the subject).

The extension of our calculations to more complicated interactions, e.g., one-dimensional gravity, is in principle feasible. There are, however, two complications to the calculations compared to the HMF model: first, the biorthogonal basis is not constituted by only two functions but by a infinite number of them. There is, however, the hope that with a suitable choice of family of functions for a given shape of the QSS a reduced number of elements of the basis is sufficient to obtain a good accuracy in the calculations, similarly to the case studied in Refs. [27,28]. Second, we do not expect to have an analytical expression for the Fourier transform of the angle of the element of the basis [Eq. (44)]. These calculations should be performed numerically, which is feasible with a modest computer.

ACKNOWLEDGMENTS

The authors warmly thank J. Barré, D. Chiron, T. M. R. Filho, J. B. Fouvry, A. Galligo, D. Métivier, and T. N. Teles for interesting discussions. This work was partially funded by the Brazilian agencies Conselho Nacional de Desenvolvimento Científico e Tecnológico (CNPq) and Coordenação de Aperfeiçoamento de Pessoa de Nível Superior (CAPES). This work was granted access to the HPC and visualization resources of the Centre de Calcul Interactif hosted by Université Nice Sophia Antipolis, the Mesocentre SIGAMM machine hosted by the Observatoire de la Côte d'Azur, and the Center of Computational Physics CFCIF of the Universidade Federal do Rio Grande do Sul.

APPENDIX A: ACTION-ANGLE VARIABLES OF THE PENDULA

In this Appendix, we present action-angle variables for a pendulum with the Hamiltonian

$$h(\theta,p)=\frac{p^2}{2}-M_0\cos\theta, \tag{A1}$$

using the same conventions as Refs. [22] and [29]. The action J is given by

$$J=\frac{1}{2\pi}\oint p\,d\theta. \tag{A2}$$

If the energy h is greater than the magnetization M_0, then the orbit is rotating: Its momentum will never reach zero. In such cases, the integration over θ will only go from $-\pi$ to π, for positive momentum, or π to $-\pi$, for negative momentum. For librating orbits, which have energy h less than the magnetization M_0, the orbit completes a loop in phase space (see Fig. 1 in the main text), reaching zero momentum at the extreme value of θ, $\pm\theta_m$. The integration starts with positive momentum at $-\theta_m$ and then goes to θ_m and then back to $-\theta_m$ with negative momentum. The action is thus given by

$$J=\frac{1}{2\pi}\begin{cases}2\int_{-\theta_m}^{\theta_m}\sqrt{2(h+M_0\cos\theta)}d\theta & h<M_0,\\ \int_{-\pi}^{\pi}\sqrt{2(h+M_0\cos\theta)}d\theta & h>M_0.\end{cases} \tag{A3}$$

Using the transformation $x=\theta/2$ and $\cos\theta=1-2\sin^2(\theta/2)$, Eq. (A3) can be written as

$$J=\frac{4\sqrt{M_0}}{\pi}\begin{cases}2\int_0^{\frac{\theta_m}{2}}\sqrt{\kappa^2-\sin^2 x}\,dx & \kappa<1,\\ \kappa\int_0^{\frac{\pi}{2}}\sqrt{1-\frac{1}{\kappa^2}\sin^2 x}\,dx & \kappa>1,\end{cases} \tag{A4}$$

where

$$\kappa=\sqrt{\frac{h+M_0}{2M_0}} \tag{A5}$$

and $\theta_m=2\arcsin(\kappa)$. For $\kappa>1$, the integral in Eq. (A4) is the complete Legendre elliptic integral of the second kind $E(1/\kappa)=E(\pi/2,1/\kappa)$, where

$$E(\phi,k)=\int_0^{\phi}\sqrt{1-k^2\sin^2\theta}\,d\theta,\quad k<1. \tag{A6}$$

For $\kappa<1$, switching variables with $\sin\theta=\kappa\sin x$, the corresponding integral in Eq. (A4) becomes

$$\int_0^{\theta_m/2}\sqrt{\kappa^2-\sin^2 x}\,dx=E(\kappa)-(1-\kappa^2)K(\kappa), \tag{A7}$$

where $K(k)$ is the complete elliptic integral of the first kind,

$$K(k)=\int_0^{\pi/2}\frac{d\theta}{\sqrt{1-k^2\sin^2\theta}}. \tag{A8}$$

Therefore, the action is

$$J=\begin{cases}\frac{8\sqrt{M_0}}{\pi}[E(\kappa)-(1-\kappa^2)K(\kappa)], & \kappa<1,\\ \frac{4\sqrt{M_0}}{\pi}\kappa E\left(\frac{1}{\kappa}\right), & \kappa>1.\end{cases} \tag{A9}$$

The angle variables, w, satisfy [20]

$$w=\Omega t, \tag{A10}$$

where $\Omega=\partial h/\partial J$ is the angular frequency and t is the time of the pendulum at position θ,

$$t=\int_0^{\theta}\frac{d\theta'}{\sqrt{2(h+M_0\cos\theta')}}. \tag{A11}$$

Integrating $\int dt=\int d\theta/p(\theta,\kappa)$ gives

$$t(\theta,\kappa)=\frac{1}{\sqrt{M_0}}\begin{cases}F(\phi,\kappa) & \kappa<1,\ p>0,\\ 2K(\kappa)-F(\phi,\kappa) & \kappa<1,\ p<0,\\ \frac{1}{\kappa}F\left(\frac{\theta}{2},\frac{1}{\kappa}\right) & \kappa>1,\ p>0,\\ \frac{1}{\kappa}F\left(\frac{\theta}{2},\frac{1}{\kappa}\right) & \kappa>1,\ p<0,\end{cases} \tag{A12}$$

where $\phi = \arcsin\left(\frac{1}{\kappa}\sin\frac{\theta}{2}\right)$. Multiplying by $\Omega(\kappa)$ as given by Eq. (43), we find the angle variables

$$w = \pi \begin{cases} \frac{F(\phi,\kappa)}{2K(\kappa)} & \kappa < 1,\ p > 0, \\ 1 - \frac{F(\phi,\kappa)}{2K(\kappa)} & \kappa < 1,\ p < 0, \\ \frac{F\left(\frac{\theta}{2},\frac{1}{\kappa}\right)}{K\left(\frac{1}{\kappa}\right)} & \kappa > 1,\ p > 0, \\ \frac{-F\left(\frac{\theta}{2},\frac{1}{\kappa}\right)}{K\left(\frac{1}{\kappa}\right)} & \kappa > 1,\ p < 0. \end{cases} \tag{A13}$$

APPENDIX B: ELLIPTIC IDENTITIES FOR FOURIER TRANSFORMS

In this appendix, we show how to obtain the expressions for the Fourier transforms of the orthogonal components of the potential, proportional to $c_n(\kappa)$ and $s_n(\kappa)$ [Eq. (44)], as obtained in Ref. [29]. First, we must find $\cos[\theta(w,\kappa)]$ and $\sin[\theta(w,\kappa)]$ as functions of w and κ directly. These can be obtained from the angle variable (A13), which depends on θ through incomplete elliptic integrals [22]. For the incomplete elliptic integral of the first kind $F(\alpha,k)$, α can be expressed in terms of the Jacobi elliptic functions $sn(u,k)$, $cn(u,k)$, and $dn(u,k)$. In particular, if $F(\alpha,k) = u$, then $\sin\alpha = sn(u,k)$. Applying to Eq. (A13) gives

$$\cos[\theta(w,\kappa)] = \begin{cases} 1 - 2\kappa^2 sn^2\left[\frac{2K(\kappa)w}{\pi},\kappa\right] & \kappa < 1, \\ 1 - 2sn^2\left[\frac{K(1/\kappa)w}{\pi},1/\kappa\right] & \kappa > 1, \end{cases} \tag{B1}$$

and

$$\begin{aligned} &\sin[\theta(w,\kappa)] \\ &= \begin{cases} 2\kappa sn\left[\frac{2K(\kappa)w}{\pi},\kappa\right]dn\left[\frac{2K(\kappa)w}{\pi},\kappa\right] & \kappa < 1, \\ 2sn\left[\frac{K(\frac{1}{\kappa})w}{\pi},\frac{1}{\kappa}\right]cn\left[\frac{K(\frac{1}{\kappa})w}{\pi},\frac{1}{\kappa}\right] & \kappa > 1,\ p > 1, \\ -2sn\left[\frac{K(\frac{1}{\kappa})w}{\pi},\frac{1}{\kappa}\right]cn\left[\frac{K(\frac{1}{\kappa})w}{\pi},\frac{1}{\kappa}\right] & \kappa > 1,\ p < 1, \end{cases} \end{aligned} \tag{B2}$$

where the properties $sn^2(u,k) + cn^2(u,k) = 1$ and $dn(u,k) = \sqrt{1 - k^2 sn^2(u,k)}$ were used. Finally, (B1) and (B2) can be expressed in terms of the following expansions involving the elliptic functions [30],

$$\begin{aligned} sn^2(u,k) &= \frac{K(k) - E(k)}{k^2 K(k)} \\ &\quad - \frac{2\pi^2}{k^2 K(k)^2}\sum_{n=1}^{\infty}\frac{nq(k)^n}{1 - q(k)^{2n}}\cos\frac{\pi nu}{K(k)}, \end{aligned} \tag{B3}$$

$$\begin{aligned} sn(u,k)dn(u,k) &= \frac{2\pi^2}{kK(k)^2}\sum_{n=1}^{\infty}\frac{\left(n - \frac{1}{2}\right)q(k)^{n-\frac{1}{2}}}{1 + q(k)^{2n-1}} \\ &\quad \times \sin\frac{\pi\left(n - \frac{1}{2}\right)u}{K(k)}, \end{aligned} \tag{B4}$$

$$sn(u,k)cn(u,k) = \frac{2\pi^2}{k^2 K(k)^2}\sum_{n=1}^{\infty}\frac{nq(k)^n}{1 + q(k)^{2n}}\sin\frac{\pi nu}{K(k)}, \tag{B5}$$

where $q(k) = \exp[-(\sqrt{1-k^2})/K(k)]$.

To find $c_n(\kappa)$ and $s_n(\kappa)$, the above expansions should be applied in the equations for $\cos[\theta(w,\kappa)]$ and $\sin[\theta(w,\kappa)]$. This gives the results of Eqs. (45) and (46).

APPENDIX C: DIELECTRIC TENSOR FOR A MAXWELL-BOLTZMANN DISTRIBUTION FOR $M_0 \to 1$

Taking as the distribution function the thermal equilibrium one (59), the components of the dielectric tensor can be approximated as

$$\begin{aligned} \epsilon_{cc}(\omega) &\simeq 1 + \frac{\pi}{2}\int_0^1 d\kappa\,\frac{\kappa^4\partial f_{MB}/\partial\kappa}{\sqrt{M_0}\left(1 - \frac{\kappa^2}{4}\right) - \omega/2} + (\omega \to -\omega) \\ &= 1 + \frac{16\pi\beta C(\omega - 2\sqrt{M_0})^2\alpha_1[Ei(x_1) - Ei(x_2)]}{\sqrt{M_0}} \\ &\quad + \frac{2\pi C[\alpha_2\sinh(\beta M_0) - \beta M_0\cosh(\beta M_0)]}{\beta M_0^{3/2}} \\ &\quad + i\frac{16\pi^2 bC(w - 2\sqrt{M_0})^2\alpha_1\Theta\left(\sqrt{M_0} - \frac{w}{2}\right)\Theta(\omega)}{\sqrt{M_0}} \\ &\quad + (\omega \to -\omega). \end{aligned} \tag{C1}$$

$$\begin{aligned} \epsilon_{ss}(\omega) &\simeq 1 + 2\pi\int_0^1 d\kappa\,\frac{\partial f/\partial\kappa}{\sqrt{M_0}\left(1 - \frac{\kappa^2}{4}\right) - \omega}\kappa^2 + (\omega \to -\omega) \\ &\simeq 1 + 64\pi\frac{\sinh(bM_0)}{\sqrt{M_0}} \\ &\quad - 64\pi b(\sqrt{M_0} - w)\alpha_3[Ei(x_3) - Ei(x_4)] \\ &\quad + i16\pi^3 bC(\sqrt{M_0} - w)\alpha_3\Theta(\sqrt{M_0} - w)\Theta(\omega) \\ &\quad + (\omega \to -\omega), \end{aligned} \tag{C2}$$

where $\alpha_1 = e^{4\beta\sqrt{M_0}\omega - 7\beta M_0}$, $\alpha_2 = -4\beta\sqrt{M_0}\omega + 9\beta M_0 + 1$, $\alpha_3 = e^{8b\sqrt{M_0}w - 7bM_0}$, $x_1 = 6\beta M_0 - 4\beta\sqrt{M_0}\omega$ $x_2 = 8\beta M_0 - 4\beta\sqrt{M_0}\omega$, $x_3 = 8b(M_0 - \sqrt{M_0}w)$, $x_4 = 6bM_0 - 8b\sqrt{M_0}w$, $\Theta(x)$ is the Heaviside step function and $(\omega \to -\omega)$ to sum to the expressions written the same with ω replaced by $-\omega$.

[1] D. Lynden-Bell, Mon. Not. R. Astron. Soc. **136**, 101 (1967).

[2] S. Chandrasekhar, *Principles of Stellar Dynamics* (University of Chicago Press, Chicago, 1942).

[3] M. Henon, in *Saas-Fee Advanced Course 3: Dynamical Structure and Evolution of Stellar Systems*, edited by G. Contopoulos, M. Henon, and D. Lynden-Bell (Observatoire de Genève, Sauverny, Switzerland, 1973), p. 183.

[4] J. Binney and S. Tremaine, *Galactic Dynamics* (Princeton University Press, Princeton, NJ, 2008).

[5] R. Balescu, *Statistical Mechanics: Matter out of Equilibrium* (Imperial College Press, London, 1997).

[6] H. Kandrup, Astrophys. J. **244**, 316 (1981).

[7] J. F. Luciani and R. Pellat, J. Phys. **48**, 591 (1987).

[8] J. Heyvaerts, Mon. Not. R. Astron. Soc. **407**, 355 (2010).

[9] P.-H. Chavanis, Astron. Astrophys. **556**, A93 (2013).
[10] P.-H. Chavanis, Physica A **391**, 3680 (2012).
[11] P. Valageas, Phys. Rev. E **74**, 016606 (2006).
[12] J. B. Fouvry, C. Pichon, and P. H. Chavanis, Astron. Astrophys. **581**, A139 (2015).
[13] J. B. Fouvry, C. Pichon, J. Magorrian, and P. H. Chavanis, Astron. Astrophys. **584**, A129 (2015).
[14] M. Antoni and S. Ruffo, Phys. Rev. E **52**, 2361 (1995).
[15] F. Bouchet and T. Dauxois, Phys. Rev. E **72**, 045103 (2005).
[16] A. Campa, T. Dauxois, and S. Ruffo, Phys. Rep. **480**, 57 (2009).
[17] P. H. Chavanis, Eur. Phys. J. Plus **127**, 19 (2012).
[18] J. Binney and S. Tremaine, *Galactic Dynamics*, 2nd ed. (Princeton University Press, Princenton, NJ, 2008).
[19] H. Goldstein, *Classical Mechanics* (Pearson Education, London, 2002).
[20] A. Lichtenberg and A. Lieberman, *Regular and Chaotic Dynamics*, Applied Mathematical Sciences (Springer, Berlin, 2010).
[21] A. J. Kalnajs, Astrophys. J. **205**, 745 (1976).
[22] J. Barré, A. Olivetti, and Y. Y. Yamaguchi, J. Stat. Mech. (2010) P08002.
[23] S. Ogawa, Phys. Rev. E **87**, 062107 (2013).
[24] J. R. Cary, D. F. Escande, and J. L. Tennyson, Phys. Rev. A **34**, 4256 (1986).
[25] A. I. Neishtadt, Sov. J. Plasma Phys. (Fiz. Plazmy) **12**, 992 (1986).
[26] Y. Levin, R. Pakter, F. B. Rizzato, T. N. Teles, and F. P. C. Benetti, Phys. Rep. **535**, 1 (2014).
[27] J.-B. Fouvry, C. Pichon, and S. Prunet, Mon. Not. R. Astron. Soc. **449**, 1967 (2015).
[28] J.-B. Fouvry and C. Pichon, Mon. Not. R. Astron. Soc. **449**, 1982 (2015).
[29] J. Barré, D. Métivier, and Y. Y. Yamaguchi, Phys. Rev. E **93**, 042207 (2016).
[30] S. C. Milne, Ramanujan J. **6**, 7 (2002).

Chapter 5

Generalized Hamiltonian Mean Field Model

The generalized Hamiltonian Mean Field model (GHMF) is composed of N spins interacting by a ferromagnetic coupling (like the HMF model), plus a nematic coupling,

$$\mathcal{H}(\{\theta_i\},\{p_i\}) = \sum_{i=1}^{N} \frac{p_i^2}{2} + \frac{1}{2N} \sum_{i,j=1}^{N} \{1 - \Delta \cos(\theta_i - \theta_j) - (1-\Delta)\cos[q(\theta_i - \theta_j)]\}\,, \qquad (5.1)$$

where $q \in \mathbb{N}$ and the parameter $\Delta \in (0,1)$ gives the weight of the ferromagnetic compared to the nematic term. For $q = 1$ or $\Delta = 1$, the HMF model is recovered. For $\Delta = 0$, the coupling between spins becomes purely nematic. This spin model is a long-range version of the one used in Refs [43, 44].

The presence of two different types of coupling results in a richer phase diagram than the HMF model, which only has two phases: paramagnetic ($M = 0$) and ferromagnetic ($M > 0$), where M is the modulus of the magnetization, $M = \langle \cos\theta \rangle$. For the GHMF, we may define two order parameters, the magnetizations

$$M_1 = \langle \cos\theta \rangle \quad \text{and} \quad M_q = \langle \cos(q\theta) \rangle. \qquad (5.2)$$

Then, we have three possible phases: *(i)* the paramagnetic phase ($M_1 = M_q = 0$), *(ii)* the nematic phase, ($M_q > 0$, $M_1 = 0$), and *(iii)* the ferromagnetic phase ($M_1 > 0$, $M_q > 0$) (Figure 5.1).

The two following works study the transitions between these different phases for $q = 2$, in both the nonequilibrium case (section 5.1) and the equilibrium case (section 5.2).

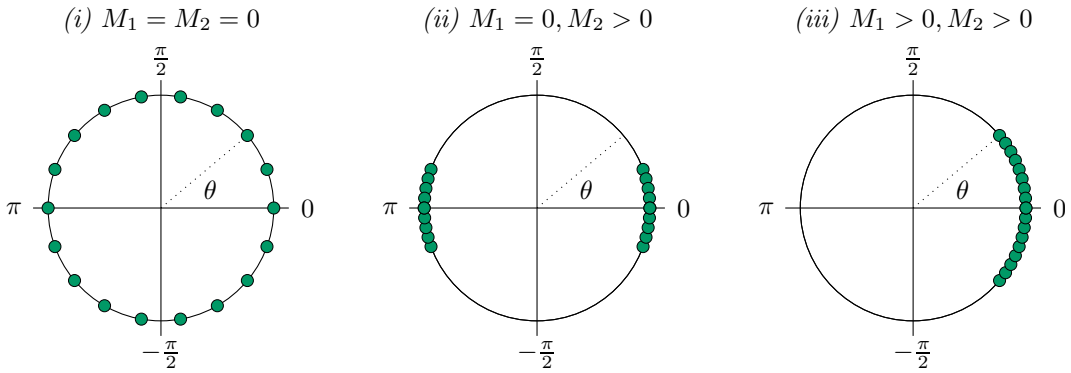

Figure 5.1: *Illustration of the different phases for the GHMF model with $q = 2$: (i) paramagnetic, (ii) nematic and (iii) ferromagnetic. Dots represent particles constrained to move on a circle of unitary radius (black circle), with position given by the coordinate θ, or equivalently as particles with spin θ.*

5.1 Nonequilibrium phase transitions in systems with long-range interactions

The three possible phases of the GHMF model with $q = 2$ are the paramagnetic phase, where particles are homogeneously distributed in angle in the interval $(-\pi,\pi]$, the ferromagnetic phase, with particles clumped around $\theta = 0$, and the nematic phase, with a clump of particles around $\theta = 0$ and another around $\theta = \pi$; see Figure 5.1 for an illustration. These phases can be formed in both equilibrium and nonequilibrium states. In this work, we developed a nonequilibrium phase diagram using nonlinear stability analysis of homogeneous states and compared its predictions with the QSS of molecular dynamics. Finally, we compared it to the microcanonical equilibrium phase diagram obtained by Boltzmann-Gibbs statistical mechanics.

For the molecular dynamics, since we want to discover the QSS of a system that is initially homogeneous, we distribute N particles with random angles and momenta in the intervals $\theta \in [-\pi,\pi]$ and $\theta \in [-p_0,p_0]$. Then, we numerically evolve their Hamilton equations of motions,

$$\begin{aligned} \dot{\theta}_i &= p_i, \\ \dot{p}_i &= -\Delta M_1 \sin\theta_i - 2(1-\Delta) M_2 \sin(2\theta_i), \end{aligned} \tag{5.3}$$

until the system reaches a steady state.

The system is Hamiltonian, and so it conserves the mean energy ε, which is given by

$$\varepsilon = \frac{p_0}{6} + 1, \tag{5.4}$$

for the initial distribution cited above. We then build the "experimental" MD phase diagram on the (ε,Δ) plane.

To construct the dynamical phase diagram, first we observe that homogeneous states

are always possible solutions of Vlasov dynamics; however, they are not necessarily stable. We tested the stability of the initial homogeneous distribution by expanding p_m, the maximum momentum of the distribution, as a Fourier series, $p_m(t) = p_0 + \sum A_n(t)\cos n\theta$, $n \in \mathbb{Z}$. These perturbations are incorporated into the expressions for the magnetizations, $M_q = \int \mathrm{d}p\mathrm{d}\theta f(\theta,p,t)\cos(q\theta)$. By writing time derivatives of the M_q, we analyzed their linearised solutions to find the limits where the homogeneous (i.e., paramagnetic) state becomes unstable compared to the nematic or ferromagnetic state. To find the nematic-ferromagnetic transition, a nonlinear analysis is necessary. We define the transition line as that in which the growth of M_1 and M_2 are equal. The results of MD and the dynamical analysis matched very well.

Finally, we compare this nonequilibrium phase diagram to the one predicted by equilibrium statistical mechanics. To construct the equilibrium diagram, we first calculate the microcanonical entropy $S(\mathcal{E},N) = k_B \ln \Omega(\mathcal{E},N)$, where

$$\Omega(\mathcal{E},N) = \int \prod_i \mathrm{d}\theta_i \int \prod_i \mathrm{d}p_i \, \delta[\mathcal{E} - \mathcal{H}(\{\theta_i\},\{p_i\})] \tag{5.5}$$

and $\mathcal{E} = N\varepsilon$. Maximizing the entropy, we find the most likely values of M_1 and M_2, and thus construct the phase diagram. As expected, the equilibrium phase diagram is very different from the nonequilibrium phase diagram.

These results were published in the paper "Nonequilibrium Phase Transitions in Systems with Long-Range Interactions" in the journal *Physical Review Letters*, volume 109, page 230601 (2012) [104]. This work was part of my Masters research, and lead to the development of the work described in the next section, 5.2.

Nonequilibrium Phase Transitions in Systems with Long-Range Interactions

Tarcísio N. Teles, Fernanda P. da C. Benetti, Renato Pakter, and Yan Levin
Instituto de Física, Universidade Federal do Rio Grande do Sul,
Caixa Postal 15051, CEP 91501-970, Porto Alegre, Rio Grande do Sul, Brazil
(Received 1 June 2012; published 4 December 2012)

We introduce a generalized Hamiltonian mean field model—an XY model with both linear and quadratic coupling between spins and explicit Hamiltonian dynamics. In addition to the usual paramagnetic and ferromagnetic phases, this model also possesses a nematic phase. The generalized Hamiltonian mean field model can be solved explicitly using Boltzmann-Gibbs statistical mechanics, in both canonical and microcanonical ensembles. However, when the resulting microcanonical phase diagram is compared with the one obtained using molecular dynamics simulations, it is found that the two are very different. We will present a dynamical theory which allows us to explicitly calculate the phase diagram obtained using molecular dynamics simulations without any adjustable parameters. The model illustrates the fundamental role played by dynamics as well the inadequacy of Boltzmann-Gibbs statistics for systems with long-range forces in the thermodynamic limit.

DOI: 10.1103/PhysRevLett.109.230601 PACS numbers: 05.70.Ln, 05.20.−y, 05.45.−a

A fundamental concept in statistical mechanics, taught in a typical course, is the equivalence of ensembles [1]. One also learns that mean field theory becomes exact for systems with long-range (LR) interactions [2,3]. However, in order to have a well-defined thermodynamic limit, in this case, special care must be taken. The usual approach is to scale the strength of the two-body interaction potential with the number of particles in the system, N. This is the, so-called, Kac prescription—it makes the infinitely long-range two-body interaction infinitesimally weak [2]. The thermodynamic limit becomes well-defined, since both the kinetic and the potential contributions to the total energy now scale linearly with N, making the energy extensive. Over the last decade, however, it has become clear that both the ensemble equivalence and the exactness of mean field theory may fail for systems with LR interactions [4–6]. The phase-diagrams calculated using Boltzmann-Gibbs (BG) statistics in canonical and microcanonical ensembles do not always coincide [4]. Furthermore, molecular dynamics simulations, show that isolated LR interacting systems become trapped in quasistationary states (qSS), the lifetime of which diverges with the number of particles [7–15]. These qSS depend explicitly on the initial particle distribution.

The inapplicability of BG statistics to systems with LR forces in thermodynamic limit is a consequence of the ergodicity breaking. Scaling of two-body potentials with the number of particles—essential for the existence of a well-defined thermodynamic limit—destroys the correlations (collisions) between the particles [16] that drive normal short-range interacting systems towards the thermodynamic equilibrium. Relaxation to the stationary state of an LR system is, therefore, fundamentally different from the collisional (correlational) relaxation of normal gases and fluids. Collisionless relaxation relies on the collective excitations and evaporative cooling driven by Landau damping [12,17]. The final stationary state reached by a collisionless system is intrinsically nonergodic [13,18]. It does not correspond to the maximum of the Boltzmann entropy. To exemplify this dichotomy, in this Letter, we introduce a new generalized Hamiltonian mean field model (GHMF)—a LR version of the model studied in Refs. [19,20]—which can be solved exactly using BG statistical mechanics. We will show that the equilibrium phase diagram predicted by the BG statistics in the microcanonical ensemble is very different from the one obtained using the molecular dynamics (MD) simulations. We will then construct a dynamical theory that correctly predicts the location and the order of the phase transitions observed in MD simulations.

The GHMF is described by the Hamiltonian

$$H(\theta_i, p_i) = \sum_{i=1}^{N} \frac{p_i^2}{2} + \frac{1}{2N} \sum_{i,j=1}^{N} [1 - \Delta \cos(\theta_i - \theta_j) - (1 - \Delta)\cos(2\theta_i - 2\theta_j)], \quad (1)$$

where $\Delta \in [0, 1]$. The model can be thought of as either XY spins confined to a line, or as particles restricted to move on a circle. The latter interpretation is perhaps more convenient when discussing MD simulations with equations of motion given by: $\dot{\theta}_i = \partial H/\partial p_i$ and $\dot{p}_i = -\partial H/\partial \theta_i$.

We define the ferromagnetic and nematic order parameters as $m_1 = \frac{1}{N}\sum_{i=1}^{N} \cos\theta_i$ and $m_2 = \frac{1}{N}\sum_{i=1}^{N} \cos 2\theta_i$, respectively. Using the usual statistical mechanics approach [5], we first calculate the microcanonical entropy for the GHMF.

Within BG statistical mechanics, all the thermodynamic information is encoded in the phase space volume accessible to the system with the total energy E

$$\Omega(E,N)=\int_{-\pi}^{\pi}\prod d\theta_i\int_{-\infty}^{\infty}\prod dp_i\delta(E-H(\theta_i,p_i)). \quad (2)$$

The integral in Eq. (2) can be divided into two parts—kinetic and configurational,

$$\Omega(E,N)=\int dK\Omega_{\rm kin}(K)\Omega_{\rm conf}(E-K), \quad (3)$$

where

$$\Omega_{\rm kin}(K)=\int_{-\infty}^{\infty}\prod dp_i\delta\Big(K-\frac{\sum p_i^2}{2}\Big), \quad (4)$$

$$\Omega_{\rm conf}(E-K)=\int_{-\pi}^{\pi}\prod d\theta_i\delta(E-K-U(\{\theta_i\})), \quad (5)$$

and U is the potential energy, second term in Eq. (1). Integrating over the momentum degrees of freedom, in the thermodynamic limit we obtain

$$\Omega_{\rm kin}(K)=\exp\Big[\frac{N}{2}\Big(\ln\pi+\ln 2K-\ln\frac{N}{2}+1\Big)\Big]. \quad (6)$$

The microcanonical entropy per particle is $s(\varepsilon)=\frac{1}{N}\ln\Omega(E,N)$,

$$s(\varepsilon)=\frac{1}{2}\ln 2\pi+\frac{1}{2}+\sup_{\kappa}\Big[\frac{1}{2}\ln 2\kappa+\frac{1}{N}\ln\Omega_{\rm conf}(N(\varepsilon-\kappa))\Big], \quad (7)$$

where $\kappa\equiv K/N=(E-U)/N=\varepsilon-u$. Since the potential energy depends only on m_1 and m_2, we define

$$\Omega_m(m_1,m_2)=\int_{-\pi}^{\pi}\prod d\theta_i\delta\Big(\sum\cos\theta_i-Nm_1\Big)\times\delta\Big(\sum\cos 2\theta_i-Nm_2\Big), \quad (8)$$

which using the Fourier representation of the delta function can be written as

$$\Omega_m(m_1,m_2)=\frac{1}{(2\pi)^2}\int_{-\infty}^{\infty}dx\int_{-\infty}^{\infty}dy\exp\Big\{N\Big[-ixm_1-iym_2+\ln\Big(\Big(\int d\theta\exp(ix\cos\theta+iy\cos 2\theta)\Big)\Big)\Big]\Big\}. \quad (9)$$

The integral can be evaluated using the saddle-point method. The extremum corresponds to $(x^\star, y^\star)$, which must satisfy

$$m_1=\frac{\int d\theta\cos\theta\exp[ix\cos\theta+iy\cos 2\theta]}{\int d\theta\exp[ix\cos\theta+iy\cos 2\theta]}, \quad (10)$$

$$m_2=\frac{\int d\theta\cos 2\theta\exp[ix\cos\theta+iy\cos 2\theta]}{\int d\theta\exp[ix\cos\theta+iy\cos 2\theta]}. \quad (11)$$

Defining $a=ix^\star$ and $b=iy^\star$ and neglecting terms of order lower than N,

$$\frac{1}{N}\ln\Omega_m(m_1,m_2)=-m_1a(m_1,m_2)-m_2b(m_1,m_2)+\ln\Big(\int d\theta\exp[a(m_1,m_2)\cos\theta+b(m_1,m_2)\cos 2\theta]\Big). \quad (12)$$

In the thermodynamic limit, we may replace $\ln\Omega_{\rm conf}(E-K)$ by $\ln\Omega_m(m_1,m_2)$ in Eq. (7). Furthermore, noting that $\kappa=\varepsilon-u$, where $u=(1-\Delta m_1^2-(1-\Delta)m_2^2)/2$, the maximization can be taken with respect to m_1, m_2 instead of κ. The entropy per particle then becomes

$$s(\varepsilon)=\frac{1}{2}\ln 2\pi+\frac{1}{2}+\sup_{m_1,m_2}\Big\{\frac{1}{2}\ln[(2\varepsilon-1+\Delta m_1^2+(1-\Delta)m_2^2)]-m_1a(m_1,m_2)-m_2b(m_1,m_2)+\ln\Big[\int d\theta\exp(a(m_1,m_2)\cos\theta+b(m_1,m_2)\times\cos 2\theta)\Big]\Big\}. \quad (13)$$

with the equilibrium values of the order parameter $(m_1^\star, m_2^\star)$ given by

$$\frac{\Delta m_1^\star}{2\varepsilon-1+\Delta m_1^{\star 2}+(1-\Delta)m_2^{\star 2}}=a(m_1^\star,m_2^\star), \quad (14)$$

$$\frac{(1-\Delta)m_2^\star}{2\varepsilon-1+\Delta m_1^{\star 2}+(1-\Delta)m_2^{\star 2}}=b(m_1^\star,m_2^\star). \quad (15)$$

Substituting these expressions into Eqs. (10) and (11), we find the equilibrium values of the order parameters

$$m_1=\frac{\int_{-\pi}^{\pi}d\theta\cos\theta\exp\Big[\frac{\Delta m_1\cos\theta+(1-\Delta)m_2\cos 2\theta}{2\varepsilon-1+\Delta m_1^2+(1-\Delta)m_2^2}\Big]}{\int_{-\pi}^{\pi}d\theta\exp\Big[\frac{\Delta m_1\cos\theta+(1-\Delta)m_2\cos 2\theta}{2\varepsilon-1+\Delta m_1^2+(1-\Delta)m_2^2}\Big]}, \quad (16)$$

$$m_2=\frac{\int_{-\pi}^{\pi}d\theta\cos 2\theta\exp\Big[\frac{\Delta m_1\cos\theta+(1-\Delta)m_2\cos 2\theta}{2\varepsilon-1+\Delta m_1^2+(1-\Delta)m_2^2}\Big]}{\int_{-\pi}^{\pi}d\theta\exp\Big[\frac{\Delta m_1\cos\theta+(1-\Delta)m_2\cos 2\theta}{2\varepsilon-1+\Delta m_1^2+(1-\Delta)m_2^2}\Big]}, \quad (17)$$

where for notational simplicity, we have dropped $\star$. In the case of a first order phase transition—more than one solution of Eqs. (16) and (17)—the equilibrium values of m_1 and m_2 will correspond to the ones that lead to the maximum entropy. The resulting microcanonical phase diagram is shown in Fig. 1.

Equation (2) requires that the system described by the Hamiltonian [Eq. (1)] is ergodic—has equal probability of visiting all possible microstates. To see if this is the case, we use MD simulations to study its dynamics. For the GHMF, we are interested to understand how an ordered (ferromagnetic or nematic) state can arise from an originally disordered homogeneous (paramagnetic) particle distribution $f_0(\theta,p)=\frac{1}{4\pi p_0}\Theta(\pi-|\theta|)\Theta(p_0-|p|)$. The

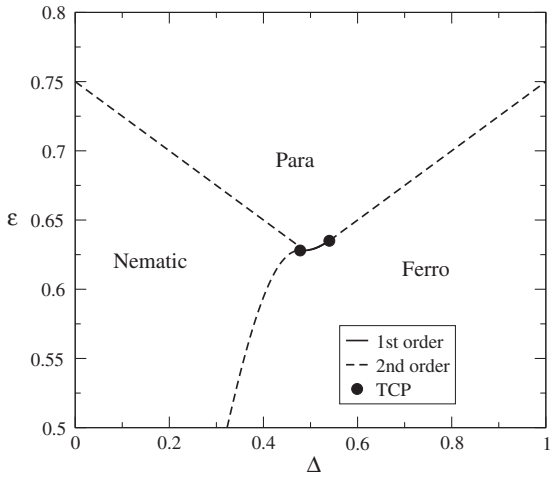

FIG. 1. Microcanonical phase diagram obtained using BG statistics. Solid circles are the two tricritical points.

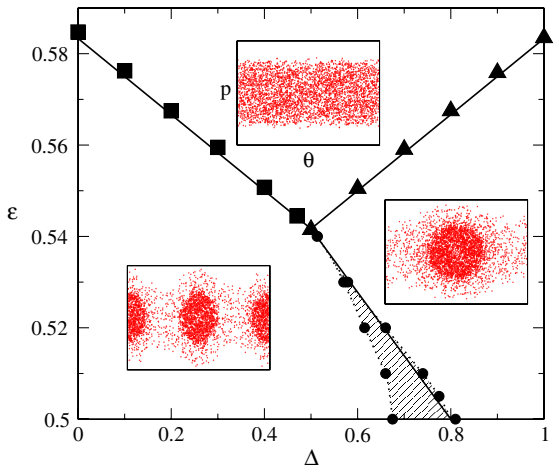

FIG. 2 (color online). The out-of-equilibrium phase diagram of the GHMF. The squares and triangles are simulation results for the qSS nematic-paramagnetic and para-ferromagnetic phase transitions, respectively. The shaded area represents the nematic-ferromagnetic transition region in which either phase occurs with equal probability. To the right of this region, the order is ferromagnetic, and to the left, nematic. Black solid lines are the theoretical predictions for the transitions. All transitions are first order. Insets show the phase space particle distribution in different phases. Notice the characteristic core-halo structure [15] inside both nematic and ferromagnetic phases. The simulations were performed with 2×10^6 particles for the paramagnetic-nematic and paramagnetic-ferromagnetic transition, and with 2×10^7 particles to locate the instability region between the nematic and ferromagnetic phases.

Hamilton's equations of motion reduce to a second order differential equation for θ_i,

$$\ddot{\theta}_i = F(\theta_i) \equiv -\Delta m_1(t)\sin\theta_i(t) - 2(1-\Delta)m_2(t)\sin 2\theta_i(t), \quad (18)$$

where $F(\theta)$ is the force acting on a particle located at θ, and where we have used the fact that $\langle\sin\theta(t)\rangle = \langle\sin 2\theta(t)\rangle = 0$, throughout the dynamical evolution [15,21]. Comparing the phase diagram obtained using MD simulations, we see that it is very different from the prediction of the microcanonical BG statistical mechanics, see Fig. 2.

Besides occurring in different regions of the (ε, Δ) plane, the phase transitions predicted by the BG statistics are of the wrong order. While the transitions from paramagnetic to ferromagnetic or nematic phases are found to be of second order, MD simulations show that these transitions are of first order. Furthermore, the second order phase transition line between the nematic and the ferromagnetic phase disappears completely and is replaced by a region of instability in which either phase can occur with equal probability.

To understand the results of MD simulations, one must forget equilibrium statistical mechanics and return to kinetic theory. In the thermodynamic limit, the dynamical evolution of the one-particle distribution function $f(\theta, p, t)$ of a system with long-range interactions is governed exactly by the Vlasov equation [22]. Vlasov dynamics is collisionless—the relaxation to equilibrium comes from Landau damping, a dynamical process in which individual particles gain energy from collective oscillations, while the oscillations are damped out. The one-particle energy of the GHMF is $\epsilon = p^2/2 + 1 - \Delta m_1\cos(\theta) - (1-\Delta)m_2\cos(2\theta)$. Note that the initial particle distribution $f_0(\theta, p)$ has $m_1 = m_2 = 0$, so that it can be expressed as a function of ϵ. This means that $f_0(\theta, p)$ is a stationary solution of the Vlasov equation. A phase transition in GHMF, therefore, can occur only after a dynamical instability. To explore the nonlinear stability of the GHMF, we consider a perturbation of the initial distribution, such that the maximum momentum $p_0 \to p_m(t) = p_0 + \sum_{n=0}^{\infty} A_n(t)\cos(n\theta)$. We define the generalized order parameters as

$$m_n(t) \equiv \langle\cos(n\theta)\rangle \equiv \int f(\theta, p, t)\cos(n\theta)dpd\theta, \quad (19)$$

where $f(\theta, p, t) = \frac{1}{4\pi p_0}\Theta(\pi - |\theta|)\Theta(p_m(t) - |p|)$. Note that this distribution preserves the phase space density, as is required by the Vlasov equation. Performing the integration in Eq. (19), we find that $m_n(t) = A_n(T)/2p_0$. Taking two temporal derivatives of $m_n(t)$, we obtain,

$$\ddot{m}_n = -n^2\langle p^2\cos(n\theta)\rangle - n\langle F(\theta)\sin(n\theta)\rangle, \quad (20)$$

where we have used the equation of motion, Eq. (18). Performing the averages using the distribution function $f(\theta, p, t)$, we obtain the equations of motion for the generalized order parameters,

$$\ddot{m}_1 + \left(\frac{12\varepsilon - 6 - \Delta}{2}\right)m_1 = f_1(m_1, m_2, m_3, m_4), \quad (21)$$

$$\ddot{m}_2 + 2(12\varepsilon + \Delta - 7)m_2 = f_2(m_1, m_2, m_3, m_4), \quad (22)$$

$$\ddot{m}_3 + 27(2\varepsilon - 1)m_3 = f_3(m_1, m_2, m_3, m_4), \quad (23)$$

$$\ddot{m}_4 + 48(2\varepsilon - 1)m_4 = f_4(m_1, m_2, m_3, m_4), \quad (24)$$

where

$$f_1 = m_1 m_2\left(1 - \frac{3\Delta}{2}\right) + (\Delta - 1)m_2 m_3 - 3(2\varepsilon - 1) \times \{m_1^3 + m_1^2 m_3 + m_3[m_2(2 + m_2) + 2(1 + m_2)m_4] + 2m_1[m_2 + m_2^2 + m_3^2 + m_2 m_4 + m_4^2]\}, \quad (25)$$

$$f_2 = \Delta(m_1^2 - m_1 m_3 + 2m_2 m_4) - 2m_2 m_4 - 12(2\varepsilon - 1)[m_2^3 + m_3^2 m_4 + 2m_1 m_3(1 + m_2 + m_4) + m_1^2(1 + 2m_2 + m_4) + 2m_2(m_3^2 + m_4 + m_4^2)], \quad (26)$$

$$f_3 = \frac{3m_1}{2}[(2 - \Delta)m_2 - \Delta m_4] - 9(2\varepsilon - 1)\{m_1^3 + 6m_1^2 m_3 + 3m_1[m_2(2 + m_2) + 2(1 + m_2)m_4] + 3m_3[m_3^2 + 2(m_2^2 + m_2 m_4 + m_4^2)]\}, \quad (27)$$

$$f_4 = 2\Delta m_1 m_3 - 4(\Delta - 1)m_2^2 - 48(2\varepsilon - 1)[2m_1(1 + m_2)m_3 + m_2(m_2 + m_3^2) + 2(m_2^2 + m_3^2)m_4 + m_4^3 + m_1^2(m_2 + 2m_4)]. \quad (28)$$

We have restricted ourselves to the first four generalized order parameters, since these are already sufficient to understand the phase diagram obtained using MD simulations. Note that the right hand sides of Eqs. (21)–(24) are nonlinear functions, so that the transition from paramagnetic-to-ferromagnetic or paramagnetic-to-nematic phases is determined by the linear stability of these equations. Furthermore, all the order parameters with $n > 2$ are linearly stable. Equations (21) and (22) show that the paramagnetic phase becomes unstable to ferromagnetic ordering when $12\varepsilon - 6 - \Delta < 0$ and to nematic ordering when $12\varepsilon + \Delta - 7 < 0$. The two stability lines agree perfectly with the results of MD simulations, see Fig. 2. It is important to note that m_3 and m_4 always remain linearly stable (recall that $\varepsilon > 0.5$ for the initial distribution).

Linear stability analysis, however, is not sufficient to determine the order of the phase transitions for which the full nonlinear equations must be considered. We first note that Eqs. (21)–(24) are conservative, they do not account for the Landau damping that is responsible for the relaxation to equilibrium and formation of the core-halo structures [15], like the ones shown in the insets of Fig. 2. Phenomenologically, Landau damping can be included in Eqs. (21)–(24) by introducing terms linear in $\dot{m}_n$. The relaxation will then proceed towards the fixed points of Eqs. (21)–(24) which can be calculated explicitly. We find that when either transition line is crossed, the system evolves either to nematic ($m_1 = 0$, $m_2 \neq 0$) or ferromagnetic ($m_1 \neq 0$, $m_2 \neq 0$) fixed points. When crossing the paramagnetic-nematic phase transition line, ($\Delta < 0.5$), the order parameter m_1 remains zero, while m_2 jumps by $\sqrt{\frac{5\sqrt{43}}{18} - \frac{29}{18}} \approx 0.459$, independent of Δ. This theoretical prediction is in excellent agreement with the results of MD simulation which see a jump in the nematic order parameter of 0.45, characterizing a strong first-order phase transition, see Fig. 3. When the paramagnetic-ferromagnetic line is crossed ($\Delta > 0.5$), both m_1 and m_2 experience a jump. For $\Delta = 0.6$, the theory predicts the jumps to be 0.5102 and -0.1861, for the ferromagnetic and nematic parameters, respectively, while the simulations find 0.41 and -0.10. For $\Delta = 1$, the theory predicts the respective jumps to be 0.555391 and -0.1129, while the simulations find 0.45 and -0.07. It is interesting to note that while for the nematic transition the jump in m_2 is universal—independent of Δ—for the ferromagnetic transition, this is not the case.

What will determine the transition between nematic and ferromagnetic phases? Deep inside the nematic and ferromagnetic phases, Eqs. (21)–(24) possess both stable nematic ($m_1 = 0$, $m_2 \neq 0$) and ferromagnetic fixed points ($m_1 \neq 0$, $m_2 \neq 0$). Which of these fixed points is reached first will depend on the initial condition. Starting from a paramagnetic distribution f_0, in the unstable region of the phase diagram, both m_1 and m_2 will grow with time. Equations (21) and (22) show that the rate of growth of the two order parameters are, in general, very different, while $m_1 \sim e^{\lambda_1 t}$, where $\lambda_1 = \sqrt{(6 + \Delta - 12\varepsilon)/2}$, the nematic order parameter grows as $m_2 \sim e^{\lambda_2 t}$, with $\lambda_2 = \sqrt{14 - 24\varepsilon - 2\Delta}$. If the nematic order parameter first

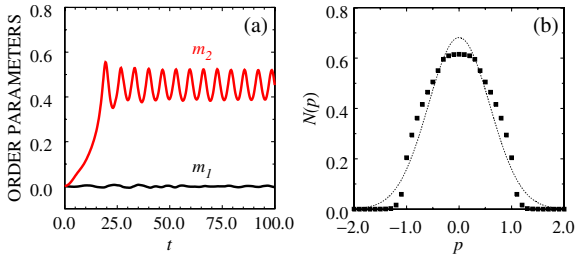

FIG. 3 (color online). Panel (a) shows the growth and saturation of the order parameter m_2 across the paramagnetic-nematic transition obtained using MD simulations. The predicted theoretical value is $m_2 = 0.459$, which is in excellent agreement with the simulations. In panel (b), the symbols are the momentum distribution in the qSS obtained using MD, while the solid line depicts the corresponding Maxwell—Boltzmann distribution to which the systems should relax in the infinite time limit. The parameters are $\Delta = 0.2$ and $u = 0.567$.

reaches the value characteristic of the nematic fixed point, then nematic order will be established, otherwise the phase will be ferromagnetic. Therefore, we expect that the nematic-ferromagnetic transition line should be given by $\lambda_1 = \lambda_2$ (solid line between nematic and ferromagnetic phases in Fig. 2). This is indeed where the instability characterizing nematic-to-ferromagnetic region is found to be, see Fig. 2.

We have introduced a generalized Hamiltonian mean field model. In addition to the usual paramagnetic and ferromagnetic phases, this model also possesses a nematic phase. We have obtained the phase diagram of the GHMF using three different methods: BG statistical mechanics, MD simulations, and a new dynamical theory introduced in this Letter. The model exemplifies the failure of BG statistics to describe isolated systems with LR interactions, in the thermodynamic limit. This is the first time that a complex (multiphase) out-of-equilibrium phase diagram for quasistationary states has been calculated analytically for a system with LR interactions.

This work was partially supported by the CNPq, FAPERGS, INCT-FCx, and by the US-AFOSR under the grant FA9550-12-1-0438.

[1] K. Huang, *Statistical Mechanics* (John Wiley & Sons, New York, 1987), 2nd ed.; L. E. Reichl, *A Modern Course In Statistical Physics* (Wiley-Interscience, New York, 1998), 2nd ed.

[2] M. Kac, Phys. Fluids **2**, 8 (1959); M. Kac, G. E. Uhlenbeck, and P. C. Hemmer, J. Math. Phys. (N.Y.) **4**, 216 (1963); G. A. Baker, Phys. Rev. **130**, 1406 (1963).

[3] H. E. Stanley, *Introduction to Phase Transitions and Critical Phenomena* (Oxford University Press, New York, 1971).

[4] J. Barré, D. Mukamel, and S. Ruffo, Phys. Rev. Lett. **87**, 030601 (2001).

[5] A. Campa, T. Dauxois, and S. Ruffo, Phys. Rep. **480**, 57 (2009).

[6] T. M. R. Filho, M. A. Amato, and A. Figueiredo, J. Phys. A **42**, 165 001 (2009).

[7] V. Latora, A. Rapisarda, and S. Ruffo, Phys. Rev. Lett. **83**, 2104 (1999).

[8] Y. Y. Yamaguchi, J. Barré, F. Bouchet, T. Dauxois, and S. Ruffo, Physica (Amsterdam) **337**, 36 (2004).

[9] A. Antoniazzi, D. Fanelli, S. Ruffo, and Y. Y. Yamaguchi, Phys. Rev. Lett. **99**, 040601 (2007).

[10] M. Joyce and T. Worrakitpoonpon, Phys. Rev. E **84**, 011139 (2011).

[11] K. Jain, F. Bouchet, and D. Mukamel, J. Stat. Mech. (2007) P11008.

[12] Y. Levin, R. Pakter, and T. N. Teles, Phys. Rev. Lett. **100**, 040604 (2008).

[13] T. N. Teles, Y. Levin, R. Pakter, and F. B. Rizzato, J. Stat. Mech. (2010) P05007.

[14] T. N. Teles, Y. Levin, and R. Pakter, Mon. Not. R. Astron. Soc. **417**, L21 (2011).

[15] R. Pakter and Y. Levin, Phys. Rev. Lett. **106**, 200603 (2011).

[16] Y. Levin, Rep. Prog. Phys. **65**, 1577 (2002).

[17] L. Landau, J. Phys. (Moscow) **10**, 25 (1946).

[18] F. P. da C. Benetti , T. N. Teles, R. Pakter, and Y. Levin, Phys. Rev. Lett. **108**, 140601 (2012).

[19] F. C. Poderoso, J. J. Arenzon, and Y. Levin, Phys. Rev. Lett. **106**, 067202 (2011).

[20] D. H. Lee and G. Grinstein, Phys. Rev. Lett. **55**, 541 (1985).

[21] T. M. R. Filho, M. A. Amato, and A. Figueiredo, Phys. Rev. E **85**, 062103 (2012).

[22] W. Braun and K. Hepp, Commun. Math. Phys. **56**, 101 (1977).

5.2 Ensemble inequivalence in a mean-field XY model with ferromagnetic and nematic couplings

In this work, we focused on the equilibrium phase diagram of the GHMF model. As in the previous section, we consider only $q = 2$, so the three phases are paramagnetic, nematic and ferromagnetic. We calculated the microcanonical phase diagram in the (ε,Δ) plane in the same manner as before, as well as the canonical phase diagram in the (T,Δ) plane, where T is the temperature.

To calculate the canonical phase diagram, we integrated the canonical partition function

$$Z(\beta,N) = \int \prod_i \mathrm{d}\theta_i \int \prod_i \mathrm{d}p_i e^{-\beta\mathcal{H}(\{\theta_i\},\{p_i\})}, \tag{5.6}$$

where $\beta = 1/T$ is the inverse temperature and $\mathcal{H}(\{\theta_i\},\{p_i\})$ is the Hamiltonian given by equation (5.1). This gives us the free energy $F(\beta,N) = -\ln Z(\beta,N)/\beta$. The order parameters M_1 and M_2[1] are determined using the canonical measure $\exp[-\beta\mathcal{H}(\{\theta_i\},\{p_i\})]\prod_i \mathrm{d}\theta_i\mathrm{d}p_i$. Then, we have all the necessary equations to construct the canonical phase diagram, minimizing the free energy to find M_1 and M_2 for a given T and Δ.

The resulting phase diagrams, both in the microcanonical and canonical cases, show that the transition is of second-order along most of the transition curves. Notably, it is of first-order near the region where the three transition lines meet, around $\Delta \approx 0.5$. As stated previously in subsection 3.2.3, ensemble inequivalence may exist in first-order phase transitions. This occurs because there are two values of the order parameters that correspond to the same mapping variable. For example, in the first-order phase transition between paramagnetic and ferromagnetic phases in the microcanonical ensemble, two values of M_1 and M_2 result in the same free energy, for the same temperature T and parameter Δ. The transition line is then mapped onto the microcanonical phase diagram by finding the mean energy ε as a function of the temperature and the magnetizations. Unlike the temperature, however, this will give two different values of the mean energy, resulting in two different transition curves. The area between these curves is thus inaccessible in the canonical ensemble, since they do not correspond to macrostates that minimize the free energy.

Our results thus expose a strong ensemble inequivalence in the GHMF model.

This work, entitled "Ensemble inequivalence in a mean-field XY model with ferromagnetic and nematic couplings", was published in the journal *Physical Review E*, volume 90, page 062141 (2014).

[1] In the published paper, the notation for the order parameters differs: $R_1 \equiv M_1$ and $R_2 \equiv M_2$.

Ensemble inequivalence in a mean-field XY model with ferromagnetic and nematic couplings

Arkady Pikovsky,[1,2] Shamik Gupta,[3] Tarcisio N. Teles,[4] Fernanda P. C. Benetti,[4] Renato Pakter,[4]
Yan Levin,[4] and Stefano Ruffo[5]

[1]*Department of Physics and Astronomy, Potsdam University, Karl-Liebknecht-Strasse 24, D-14476 Potsdam, Germany*
[2]*Department of Control Theory, Nizhni Novgorod State University, Gagarin Avenue 23, 606950 Nizhni Novgorod, Russia*
[3]*Laboratoire de Physique Théorique et Modèles Statistiques (CNRS UMR 8626), Université Paris-Sud, 91405 Orsay, France*
[4]*Instituto de Física, Universidade Federal do Rio Grande do Sul, Caixa Postale 15051, CEP 91501-970 Porto Alegre, Rio Grande do Sul, Brazil*
[5]*Dipartimento di Fisica e Astronomia and CSDC, Università di Firenze, INFN and CNISM, Via Sansone 1, 50019 Sesto Fiorentino, Italy*

(Received 8 October 2014; published 31 December 2014)

We explore ensemble inequivalence in long-range interacting systems by studying an XY model of classical spins with ferromagnetic and nematic coupling. We demonstrate the inequivalence by mapping the microcanonical phase diagram onto the canonical one, and also by doing the inverse mapping. We show that the equilibrium phase diagrams within the two ensembles strongly disagree within the regions of first-order transitions, exhibiting interesting features like temperature jumps. In particular, we discuss the coexistence and forbidden regions of different macroscopic states in both the phase diagrams.

DOI: 10.1103/PhysRevE.90.062141 PACS number(s): 05.70.Fh, 05.20.Gg

Recent years have seen extensive studies of systems with long-range interactions that have the two-body potential in d dimensions decaying at large separation r as $1/r^\alpha$, $0 \leqslant \alpha \leqslant d$ [1–4]. Examples span a wide variety, from bacterial population [5], plasmas [6], and dipolar ferroelectrics and ferromagnets [7], to two-dimensional geophysical vortices [8] and self-gravitating systems [9]. A striking feature of long-range systems distinct from short-range ones is that of nonadditivity, whereby thermodynamic quantities scale superlinearly with the system size. Nonadditivity manifests in static properties like negative microcanonical specific heat [10,11], inequivalence of statistical ensembles [12–19], and other rich possibilities [20]. As for the dynamics, long-range systems often exhibit broken ergodicity [16,21] and slow relaxation towards equilibrium [8,16,22–25].

Here, we demonstrate ensemble inequivalence in a model of long-range systems that has mean-field interaction (i.e., $\alpha = 0$) and two coupling modes. This so-called generalized Hamiltonian mean-field (GHMF) model, a long-range version with added kinetic energy of the model of Ref. [26], has N interacting particles with angular coordinates $\theta_i \in [0, 2\pi]$ and momenta $p_i, i = 1, 2, \ldots, N$, which are moving on a unit circle [27]. The GHMF Hamiltonian is

$$H = \sum_{i=1}^{N} \frac{p_i^2}{2} + \frac{1}{2N} \sum_{i,j=1}^{N} [1 - \Delta \cos\theta_{ij} - (1-\Delta)\cos 2\theta_{ij}], \tag{1}$$

where $\theta_{ij} \equiv \theta_i - \theta_j$. Here, $\cos\theta_{ij}$ is an attractive interaction minimized by the particles forming a cluster, so that $\theta_{ij} = 0 \pmod{2\pi}$, while $\cos 2\theta_{ij}$ with two minima at $\theta_{ij} = 0, \pi \pmod{2\pi}$ promotes a two-cluster state. The parameter $\Delta \in [0,1]$ sets the relative strength of the two coupling modes. The potential energy in Eq. (1) is scaled by N to make the energy extensive, following the Kac prescription [28], but the system remains nonadditive. In terms of the XY-spin vectors $\mathbf{S}_i \equiv (\cos\theta_i, \sin\theta_i)$, the interactions have the form of a mean-field ferromagnetic interaction $\sim -\Delta \mathbf{S}_i \cdot \mathbf{S}_j$, and a mean-field coupling $\sim -(1-\Delta)(\mathbf{S}_i \cdot \mathbf{S}_j)^2$ promoting nematic ordering. For XY lattice models with this type of ferro-nematic coupling, see Refs. [26,29–31]. The system (1) has Hamilton dynamics: $d\theta_i/dt = p_i$, $dp_i/dt = -\partial H/\partial\theta_i$. For $\Delta = 1$, when no nematic ordering exists, the GHMF model becomes the Hamiltonian mean-field (HMF) model [22], a paradigmatic model of long-range systems [1].

In this work, we report on striking and strong inequivalence of statistical ensembles for the GHMF model. The system has three equilibrium phases: ferromagnetic, paramagnetic, and nematic, with first- and second-order transitions. Let us note that Ref. [32] studied another model with long-range interactions, which also shows paramagnetic, ferromagnetic, and nematic-like phases. For the GHMF model, by comparing the phase diagrams in the canonical and microcanonical ensembles (the latter is derived in Ref. [27]), we show in the regions of first-order transitions that the phase diagrams differ significantly. We analyze the inequivalence in two ways, by mapping the microcanonical phase diagram onto the canonical one, as is usually done [13–19], and also by doing the inverse mapping of the canonical onto the microcanonical one; in particular, we discuss the coexistence and forbidden regions of different macroscopic states. This study demonstrates the subtleties and intricacies of the presence of different stability regions of macroscopic states in long-range systems in microcanonical and canonical equilibria. It is worth noting that compared to the pure para-ferro transition, the phenomenology here due to the presence of the additional nematic phase is much richer. We show that the region where the three phases meet, within both microcanonical and canonical ensembles, is the one exhibiting ensemble inequivalence.

We now turn to derive our results. Rotational symmetry of the Hamiltonian (1) allows us to choose, without loss of generality, the ordering direction in the equilibrium stationary state to be along x (there are no stationary states with a nonzero angle between the directions of ferromagnetic and nematic order) and to define as order parameters the equilibrium averages

$$R_m \equiv \langle \cos m\theta \rangle, \quad m = 1, 2, \tag{2}$$

where $m = 1$ (2) stands for the ferromagnetic (nematic) order. The canonical partition function is $Z = \prod_i \int dp_i d\theta_i \exp(-\beta H)$, with $\beta = 1/T$ being the inverse of the temperature T measured in units of the Boltzmann constant. Since Eq. (1) is a mean-field system, in the thermodynamic limit $N \to \infty$, one follows the standard Hubbard-Stratonovich transformation and a saddle-point approximation to evaluate Z [1]. One then obtains expressions for R_m's, and the average energy per particle, given by $\langle\varepsilon\rangle = \partial(\beta f)/\partial\beta$, where f is the free energy per particle. One has, with $m = 1,2$,

$$R_m = \frac{\int d\theta \cos m\theta e^{\beta[\Delta R_1 \cos\theta + (1-\Delta)R_2 \cos 2\theta]}}{\int d\theta e^{\beta[\Delta R_1 \cos\theta + (1-\Delta)R_2 \cos 2\theta]}}, \tag{3}$$

$\langle\varepsilon\rangle = 1/(2\beta) + 1/2 - (1/2)(\Delta R_1^2 + (1-\Delta)R_2^2)$, and

$$f = -\frac{1}{2\beta}\ln\left(\frac{2\pi}{\beta}\right) + \frac{1}{2} + \frac{1}{2}\left(\Delta R_1^2 + (1-\Delta)R_2^2\right) - \frac{1}{\beta}\ln\left(\int d\theta e^{\beta[\Delta R_1 \cos\theta + (1-\Delta)R_2 \cos 2\theta]}\right). \tag{4}$$

The canonical phase diagram in the Δ-T plane is obtained by plotting the equilibrium values of R_1 and R_2 that solve Eq. (3) and minimize the free energy (4).

We now describe a practical way to obtain the canonical phase diagram, by introducing auxiliary variables R, α as

$$R \equiv \sqrt{(\beta\Delta R_1)^2 + (\beta(1-\Delta)R_2)^2}, \quad \cos\alpha \equiv \beta\Delta R_1/R, \quad \sin\alpha \equiv \beta(1-\Delta)R_2/R. \tag{5}$$

Then, the argument of the exponential in Eq. (3) becomes $R(\cos\alpha\cos\theta + \sin\alpha\cos 2\theta)$, and the integrals on the right hand side of Eq. (3) evaluate to two quantities $C_m(R,\alpha)$ that depend on the introduced auxiliary variables. Using $R_m = C_m(R,\alpha)$ we obtain, by virtue of Eq. (5), all the parameters in a parametric form in terms of the introduced auxiliary variables:

$$\beta = \frac{R\cos\alpha}{C_1} + \frac{R\sin\alpha}{C_2}, \quad \Delta = 1 - T\frac{R\sin\alpha}{C_2}. \tag{6}$$

Once $R_{1,2}$, β, and Δ are determined, one can use Eq. (4) to find the free energy of the solution. Varying $R \geqslant 0$ and $\alpha \in [0,\pi/2)$ gives all solutions of Eq. (3), while Eq. (4) yields the stable branches. We note that in Ref. [33], studying a nonequilibrium version of our model, a different and more useful method of finding $C_{1,2}$, based on the Fourier mode representation of an equivalent Fokker-Planck equation, is used; in our equilibrium setup, however, exploiting the integrals (3) is simpler. For the pure nematic phase (that has $R_1 = 0$), one sets $\alpha = \pi/2$, so that the only auxiliary parameter is R; one finds $R_2 = C_2(R)$ from Eq. (3), and the temperature from $\beta = R/(R_2(1-\Delta))$.

In contrast to Eq. (3), the order parameters within a microcanonical ensemble, derived in Ref. [27], satisfy

$$R_m = \frac{\int d\theta \cos m\theta \exp\left[\frac{\Delta R_1 \cos\theta + (1-\Delta)R_2 \cos 2\theta}{q(\varepsilon)}\right]}{\int d\theta \exp\left[\frac{\Delta R_1 \cos\theta + (1-\Delta)R_2 \cos 2\theta}{q(\varepsilon)}\right]}. \tag{7}$$

Here, ε is the energy per particle, and $q(\varepsilon) \equiv 2\varepsilon - 1 + \Delta R_1^2 + (1-\Delta)R_2^2$. For given values of ε and Δ, the equilibrium values of R_1 and R_2 are obtained as a particular solution of Eq. (7) that maximizes the entropy [27]:

$$s(\varepsilon) = \frac{1}{2}\ln 2\pi + \frac{1}{2} + \frac{\ln q(\varepsilon)}{2} - \frac{1}{2}\left(\frac{\Delta R_1^2 + (1-\Delta)R_2^2}{q(\varepsilon)}\right) + \ln\int d\theta \exp\left[\frac{\Delta R_1 \cos\theta + (1-\Delta)R_2 \cos 2\theta}{q(\varepsilon)}\right]. \tag{8}$$

The averages (7) are the same as Eq. (3) on making the identification of the microcanonical energy ε with the average energy $\langle\varepsilon\rangle$ in the canonical ensemble, so that the inverse temperature β in Eq. (3) is

$$\beta^{-1} = q(\varepsilon) = 2\varepsilon - 1 + \Delta R_1^2 + (1-\Delta)R_2^2. \tag{9}$$

This constitutes a link between the phase diagrams in the two ensembles. Using then the integrals (3), we get the following parametric representation in the Δ-ε plane for the microcanonical ensemble: After finding $R_1 = C_1(R,\alpha)$ and $R_2 = C_2(R,\alpha)$, we get $R\cos\alpha = \Delta R_1/q(\varepsilon)$, $R\sin\alpha = (1-\Delta)R_2/q(\varepsilon)$, or, explicitly,

$$\Delta = \frac{R_2\cos\alpha}{R_2\cos\alpha + R_1\sin\alpha}, \quad \varepsilon = \frac{1}{2}\left[\frac{(1-\Delta)R_2}{R\sin\alpha} - \Delta R_1^2 - (1-\Delta)R_2^2 + 1\right]. \tag{10}$$

Once $R_{1,2}, \varepsilon, \Delta$ have been determined, one can use Eq. (8) to find the entropy of the solution. For the pure nematic phase, $\alpha = \pi/2$, and $R_2^2 = 1 + (1-2\varepsilon)/(1-\Delta)$.

Summarizing, expressions (3), (6), (7), and (10) provide self-consistent stationary state solutions for the order parameters in the canonical and the microcanonical ensembles, respectively. Stable branches of these solutions correspond respectively to the minimum of the free energy (4) and to the maximum of the entropy (8).

We now present results of the phase diagrams for the two ensembles in Fig. 1. Both diagrams are qualitatively similar, with three phases: paramagnetic, ferromagnetic, and nematic. For large values of the parameter Δ, on decreasing the energy or temperature, one observes a second-order transition from the paramagnetic to the ferromagnetic phase; only at lower values of Δ does this phase transition become of first order. For low values of Δ, decreasing the energy or temperature results in a second-order transition from the paramagnetic to the purely nematic phase for which R_1 is zero; a further decrease results in either a second-order transition (for very small values of Δ) or a first-order transition (for $\Delta \approx 1/2$) to the ferromagnetic phase that has nonzero R_1.

While the phase diagrams in Fig. 1 look simple, their mappings onto each other (Fig. 2) reveal nontrivial inequivalence between the canonical and microcanonical descriptions. This inequivalence is because while the self-consistent solutions (3), (6), (7), and (10) are the same for both ensembles and transform onto one another by using Eq. (9), they are nevertheless stable in different parameter regimes. Thus, using the mapping, Eq. (9), two situations can arise: either a gap, i.e., a region of inaccessible states, or an overlap, i.e., a region of multiple stable solutions. Note that the second-order transition to the nematic phase is the same in both descriptions.

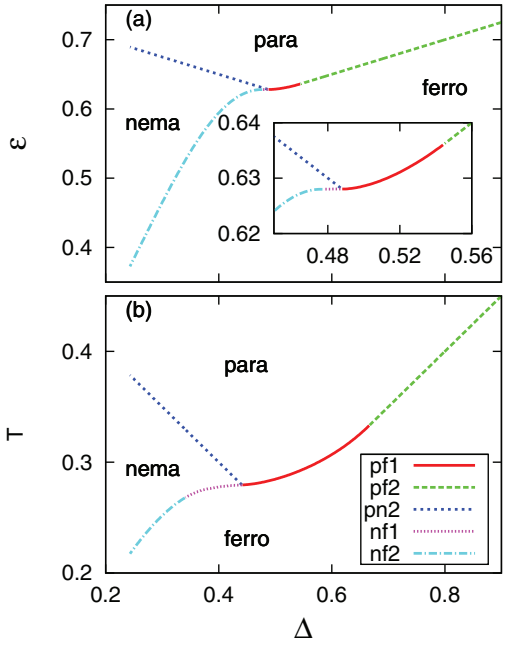

FIG. 1. (Color online) Comparison of the canonical and the microcanonical phase diagrams. Here, pf1 means first-order para-ferro transition, etc. (a) Phase diagram in the Δ-ε plane in the microcanonical ensemble, Eqs. (7) and (8). The two tricritical points are at $\Delta \approx 0.545$, $\varepsilon \approx 0.636$, and at $\Delta \approx 0.477$, $\varepsilon \approx 0.628$, while there is a critical end point at $\Delta \approx 0.487$, $\varepsilon \approx 0.628$. The inset shows a zoom into the central part. (b) Phase diagram in the Δ-T plane in the canonical ensemble, Eqs. (3) and (4). There are two tricritical points, at $\Delta \approx 0.667$, $T \approx 0.333$, and at $\Delta \approx 0.34$, $T \approx 0.267$. The critical end point is at $\Delta \approx 0.441$, $T \approx 0.279$.

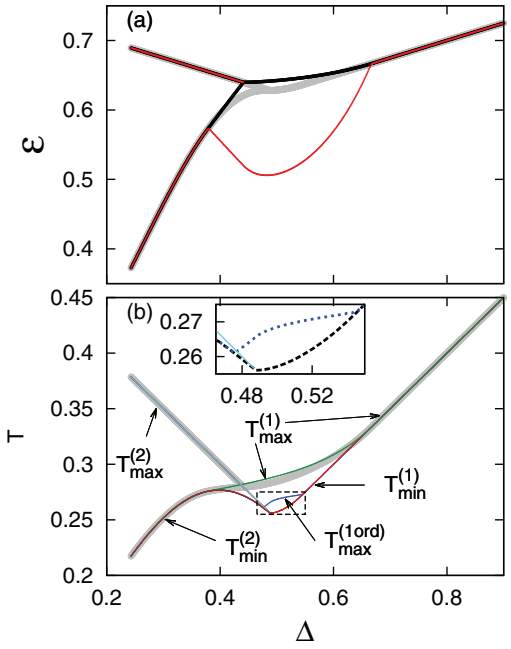

FIG. 2. (Color online) Inequivalence of phase diagrams in the two ensembles. (a) Canonical phase diagram Fig. 1(b) mapped onto the Δ-ε plane (the microcanonical diagram is in the background in gray). Between the bold black and the thin red lines, there is no canonical equilibrium state possible. (b) Microcanonical phase diagram Fig. 1(a) mapped onto the Δ-T plane (the canonical diagram is in the background in gray). $T^{(1)}_{\rm min}$ (red) is the minimal temperature at which the paramagnetic phase exists. $T^{(1)}_{\rm max}$ (green) is the maximum temperature at which the ferromagnetic phase exists. $T^{(2)}_{\rm max}$ (cyan) ($T^{(2)}_{\rm min}$, brown)] is the maximum (minimum) temperature at which the nematic phase exists. The blue line for $T^{(1{\rm ord})}_{\rm max}$ shows the splitting of the first-order microcanonical transition in the region $0.477 < \Delta < 0.545$ (another line that belongs to this splitting is masked by $T^{(1)}_{\rm min}$ and $T^{(2)}_{\rm min}$). The inset shows a zoom into this middle region, where black dashed and blue dotted lines correspond to the two values of the temperature at the microcanonical jump.

As Fig. 2(a) shows, mapping of the canonical phase diagram onto the Δ-ε plane yields a gap. In the domain of Δ where a first-order canonical transition occurs, the canonical transition line splits into two lines when mapped onto the Δ-ε plane. Between these lines, there is no stable canonical state for a given ε (cf. Fig. 3).

A more nontrivial situation arises due to the mapping of the microcanonical phase diagram onto the Δ-T plane, as shown in Fig. 2(b). Here, two features are evident. First, in regions where the microcanonical transition is of second order but the canonical transition is of first order, there are three microcanonically stable values of $R_{1,2}$ at temperatures between the lines $T^{(1)}_{\rm max}$ (green line) and $T^{(1)}_{\rm min}$ (red line), and those between the lines $T^{(1)}_{\rm max}$ and $T^{(2)}_{\rm min}$ (brown line). Second, in regions of a first-order microcanonical transition, the transition line splits into two lines, denoted $T^{(1{\rm ord})}_{\rm max}$ (blue line) and $T^{(1{\rm ord})}_{\rm min}$ (black dashed line), with the latter coinciding with either $T^{(1)}_{\rm min}$ or $T^{(2)}_{\rm min}$, such that for temperatures in between there are two microcanonically stable values of $R_{1,2}$; see the inset of Fig. 2(b) and cuts of the Δ-T phase diagram at fixed values of Δ in Fig. 3. Thus, in the whole domain of Δ where the canonical transition is of first order, one observes a multiplicity of microcanonically stable states in the Δ-T plane. Remarkably, the tricritical points are different in the two ensembles.

In Fig. 4, we employ relation (9) to draw the temperature-energy relation $T(\varepsilon)$ for $\Delta = 0.5$. For both microcanonical and canonical ensembles, this curve has two branches: a high-energy branch and a low-energy branch. At the point where the two branches intersect, the two entropies in the microcanonical ensemble and the two free energies in the canonical ensemble become equal. In the region where the canonical curve shows a jump in the energy at a given temperature, characteristic of a first-order transition that here occurs between the paramagnetic and the ferromagnetic phase [see Fig. 1(b)], the microcanonical curve shows a region of negative specific heat ($\partial T/\partial \varepsilon < 0$). Since the canonical specific heat is always positive, being given by the fluctuations in the energy of the system, the negative microcanonical specific heat is a further indication of ensemble inequivalence for the model under study.

To conclude, we addressed the issue of ensemble inequivalence in long-range interacting systems by studying an XY model of classical spins with linear and quadratic coupling, and evolving under Hamilton dynamics. In this so-called generalized Hamiltonian mean-field model, we compared exact equilibrium phase diagrams in the microcanonical and canonical ensembles. We showed that, within the region of

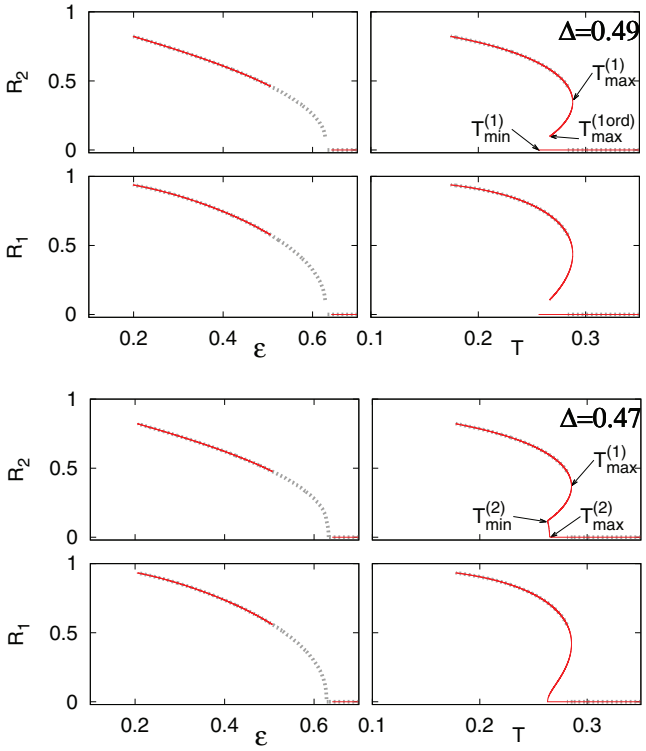

FIG. 3. (Color online) Stable solutions of $R_{1,2}$ vs temperature T in the canonical ensemble and energy ε in the microcanonical ensemble (dotted grey lines); red solid lines are stable "imports" from another ensemble (canonically stable states on left column panels and microcanonically stable states on right column panels); Δ equals 0.49 (top) and 0.47 (bottom). The values of $T^{(1)}_{\max}$, $T^{(1)}_{\min}$, $T^{(2)}_{\max}$, $T^{(2)}_{\min}$, and $T^{(1\mathrm{ord})}_{\max}$ marked by arrows coincide with those in Fig. 2.

first-order transitions, the two ensembles show very different behaviors. Nevertheless, let us remark that when plotted using appropriate variables, the arrangement of critical points and transition lines is similar in the phase diagrams of the two ensembles. One may study how the relaxation to equilibrium differs in the two ensembles, a behavior investigated earlier in the microcanonical ensemble in Ref. [27]. In that paper, it was shown that an isolated system described by the Hamiltonian (1) relaxes to quasistationary states (QSSs) which also have paramagnetic, ferromagnetic, and nematic phases. The phase diagram of a QSS, however, is very different from the one

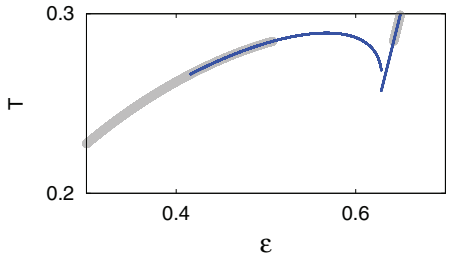

FIG. 4. (Color online) Plot of the dependence ε-T for $\Delta = 0.5$, showing regions of microcanonical energies that are inaccessible canonically. Bold grey lines, canonically stable states; blue solid lines, microcanonically stable states.

predicted by the equilibrium statistical mechanics in the microcanonical ensemble, Fig. 1. Nevertheless, we expect that since the lifetime of the QSS scales with the number of particles in the system, a finite system will eventually relax to the Boltzmann-Gibbs equilibrium. In the thermodynamic limit, however, this relaxation might take longer than the age of the universe. It will be of interest to explore such dynamical behavior in the canonical ensemble.

Finally, we mention that an overdamped nonequilibrium version of the GHMF is a Kuramoto-type model of synchronization of globally coupled oscillators (just as an overdamped nonequilibrium version of the HMF model is the standard Kuramoto model [34,35]), where transitions to synchronization are of major interest. In the context of synchronization, nematic and ferromagnetic phases correspond respectively to two-cluster and one-cluster synchronization patterns (see Ref. [33]), but their stability is obtained from dynamical and not from free energy or entropy considerations.

A.P. is supported by the Grant No. 02..49.21.0003 between the Ministry of Education and Science of the Russian Federation and the Lobachevsky State University of Nizhni Novgorod. S.G. is supported by the CEFIPRA Project No. 4604-3. The authors thank the Galileo Galilei Institute for Theoretical Physics, Florence, Italy, for the hospitality and the INFN for partial support during the completion of this work. S.G. and A.P. acknowledge useful discussions with M. Komarov. This work was partially supported by the CNPq, FAPERGS, INCT-FCx, and by the US-AFOSR under Grant No. FA9550-12-1-0438.

[1] A. Campa, T. Dauxois, and S. Ruffo, Phys. Rep. **480**, 57 (2009).
[2] F. Bouchet, S. Gupta, and D. Mukamel, Phys. A **389**, 4389 (2010).
[3] Y. Levin, R. Pakter, F. B. Rizzato, T. N. Teles, and F. P. C. Benetti, Phys. Rep. **535**, 1 (2014).
[4] A. Campa, T. Dauxois, D. Fanelli, and S. Ruffo, *Physics of Long-Range Interacting Systems* (Oxford University Press, Oxford, UK, 2014).
[5] J. Sopik, C. Sire, and P. H. Chavanis, Phys. Rev. E **72**, 026105 (2005).
[6] D. R. Nicholson, *Introduction to Plasma Physics* (Krieger Publishing, Malabar, FL, 1992).
[7] L. D. Landau and E. M. Lifshitz, *Electrodynamics of Continuous Media* (Pergamon, London, 1960).
[8] P. H. Chavanis, in *Dynamics and Thermodynamics of Systems with Long-range Interactions*, Lecture Notes in Physics Vol. 602, edited by T. Dauxois, S. Ruffo, E. Arimondo, and M. Wilkens (Springer-Verlag, Berlin, 2002).
[9] T. Padmanabhan, Phys. Rep. **188**, 285 (1990).
[10] D. Lynden-Bell and R. Wood, Mon. Not. R. Astron. Soc. **138**, 495 (1968).

[11] W. Thirring, Z. Phys. **235**, 339 (1970).
[12] M. K. H. Kiessling and J. L. Lebowitz, Lett. Math. Phys. **42**, 43 (1997).
[13] J. Barré, D. Mukamel, and S. Ruffo, Phys. Rev. Lett. **87**, 030601 (2001).
[14] I. Ispolatov and E. G. D. Cohen, Phys. A **295**, 475 (2001).
[15] J. Barré and B. Gonçalves, Phys. A **386**, 212 (2007).
[16] D. Mukamel, S. Ruffo, and N. Schreiber, Phys. Rev. Lett. **95**, 240604 (2005).
[17] A. Venaille and F. Bouchet, Phys. Rev. Lett. **102**, 104501 (2009).
[18] A. Venaille and F. Bouchet, J. Stat. Phys. **143**, 346 (2011).
[19] T. N. Teles, D. Fanelli, and Stefano Ruffo, Phys. Rev. E **89**, 050101(R) (2014).
[20] F. Bouchet and J. Barré, J. Stat. Phys. **118**, 1073 (2005).
[21] F. Bouchet, T. Dauxois, D. Mukamel, and S. Ruffo, Phys. Rev. E **77**, 011125 (2008).
[22] M. Antoni and S. Ruffo, Phys. Rev. E **52**, 2361 (1995).
[23] Y. Y. Yamaguchi, J. Barré, F. Bouchet, T. Dauxois, and S. Ruffo, Phys. A **337**, 36 (2004).
[24] A. Campa, A. Giansanti, and G. Morelli, Phys. Rev. E **76**, 041117 (2007).
[25] M. Joyce and T. Worrakitpoonpon, J. Stat. Mech.: Theory Exp. (2010) P10012.
[26] D. H. Lee and G. Grinstein, Phys. Rev. Lett. **55**, 541 (1985).
[27] T. N. Teles, Fernanda P. da C. Benetti, R. Pakter, and Y. Levin, Phys. Rev. Lett. **109**, 230601 (2012).
[28] M. Kac, G. E. Uhlenbeck, and P. C. Hemmer, J. Math. Phys. **4**, 216 (1963).
[29] K. Qi, M. H. Qin, X. T. Jia, and J.-M. Liu, J. Magn. Magn. Mater. **340**, 127 (2013).
[30] D. B. Carpenter and J. T. Chalker, J. Phys.: Condens. Matter **1**, 4907 (1989)
[31] J.-H. Park, S. Onoda, N. Nagaosa, and J. H. Han, Phys. Rev. Lett. **101**, 167202 (2008).
[32] M. Antoni, S. Ruffo, and A. Torcini, Phys. Rev. E **66**, 025103(R) (2002).
[33] M. Komarov and A. Pikovsky, Phys. Rev. Lett. **111**, 204101 (2013); Phys. D **289**, 18 (2014); V. Vlasov, M. Komarov, and A. Pikovsky, arXiv:1411.3204.
[34] S. Gupta, A. Campa, and S. Ruffo, Phys. Rev. E **89**, 022123 (2014).
[35] S. Gupta, A. Campa, and S. Ruffo, J. Stat. Mech.: Theory Exp. (2014) R08001.

Chapter 6

Gravitation

Galaxies, globular clusters and other self-gravitating systems are the quintessential LRI systems. Many of the instigating characteristics of LRI systems were first observed by astrophysicists, such as negative specific heat [10], out-of-equilibrium stationary states and long relaxation times [79]. The study of self-gravitating systems in three dimensions, however, has serious setbacks. The gravitational potential $\phi(r) \sim 1/r$ is unbounded: bodies of mass can gain enough energy to escape confinement and become separated by infinitely large distances. At close distances, the potential $1/r$ diverges, requiring the introduction of a cut-off parameter to bound the potential from below.

These two complications can be circumvented by using initial distributions close to the virial condition. For these distributions, particle evaporation is avoided because the distribution does not undergo strong oscillations. Also, if the initial distribution is spherically symmetric, symmetry breaking does not occur near the virial condition [111]. Particles subject to spherically symmetric potentials conserve angular momentum, thus avoiding the divergence and collapse when $r \to 0$.

6.1 Nonequilibrium stationary states of 3d self-gravitating systems

In the work presented in this chapter, we generalized the integrable model developed for the HMF model for a three-dimensional self-gravitating system. Being more complex than the HMF model, it is natural to presume that the IM for the self-gravitating system will also have new complications. Considering only spherically symmetric distributions, both the energy ϵ and the angular momentum ℓ are conserved. Therefore, the construction of the IM should take into account not only the conservation of the energy distribution function $f(\epsilon)$, as is the case for the HMF IM, but the conservation of the distribution in energy and angular momentum $f(\epsilon,\ell)$. Also, the functional form of the external potential of the HMF IM is already known, $H\cos\theta$, so that it is only necessary to determine the value H. For the gravitational case, however, the dependency of the external potential $\psi(r)$ depends on the

stationary distribution of the IM. The potential must be calculated for each value of r self-consistently. In the publication that follows, we show how this is done. We compare the IM results with molecular dynamics and obtain good results for different initial distributions. For the WB distribution, we show that the IM is a better description of the marginal distributions than LB statistics, as is the case for the HMF model. On the other hand, systems with very unstable initial distributions, for example, with extreme density variations, are not well described by the IM. These cases are similar to the results for the HMF model in which we saw that, as we increase the number of density levels in the initial distributions, the IM predictions start to deviate from the molecular dynamics results, even for virialised initial conditions.

These results were published in our paper "Nonequilibrium Stationary States of 3D Self-Gravitating Systems", *Physical Review Letters*, volume 113, pages 100602 (2014). The Letter is presented in the following pages.

Nonequilibrium Stationary States of 3D Self-Gravitating Systems

Fernanda P. C. Benetti, Ana C. Ribeiro-Teixeira, Renato Pakter, and Yan Levin
Instituto de Física, Universidade Federal do Rio Grande do Sul, Caixa Postal 15051, CEP 91501-970, Porto Alegre, Rio Grande do Sul, Brazil

(Received 21 May 2014; revised manuscript received 15 July 2014; published 4 September 2014)

Three-dimensional self-gravitating systems do not evolve to thermodynamic equilibrium but become trapped in nonequilibrium quasistationary states. In this Letter, we present a theory which allows us to *a priori* predict the particle distribution in a final quasistationary state to which a self-gravitating system will evolve from an initial condition which is isotropic in particle velocities and satisfies a virial constraint $2K = -U$, where K is the total kinetic energy, and U is the potential energy of the system.

DOI: 10.1103/PhysRevLett.113.100602 PACS numbers: 05.20.-y, 05.45.-a, 05.70.Ln

Unlike systems with short-range forces which relax to thermodynamic equilibrium starting from an arbitrary initial condition, systems with long-range interactions become trapped in nonequilibrium quasistationary states (QSS), the lifetime of which diverges with the number of particles [1–9]. For interaction potentials unbounded from above, the QSS have been observed to have a characteristic core-halo structure [10]. The extent of the halo is determined by the parametric resonances which arise from the collective density oscillations during the relaxation process [11]. The dynamics of 3D self-gravitating systems, however, is significantly more complex due to the existence of unbound states [12,13]. Indeed, Newton's gravitational potential is bounded from above so that the parametric resonances may actually transfer enough energy to allow some particles to completely escape from the gravitational cluster [13,14]. This makes the study of 3D self-gravitating systems particularly challenging [15,16]. Recently, however, it was shown that if the initial particle distribution function is isotropic in velocity and satisfies the so-called virial condition (VC), density oscillations and parametric resonances will be suppressed [17–20]. The relaxation to equilibrium will then proceed adiabatically. In the thermodynamic limit, each particle of the gravitational cluster will evolve under the action of a quasistatic mean-field potential, and the phase mixing of particle trajectories will lead to a nonequilibrium QSS. In this Letter, we will show that it is possible to *a priori* predict the density and the velocity distribution functions within the QSS to which a 3D gravitational system will evolve if the initial distribution is isotropic in particle velocities and satisfies the VC.

The virial theorem requires that a stationary gravitational system must have $2K = -U$, where K is the total kinetic energy and U is the potential energy. This, however, does not mean that an arbitrary initial distribution which satisfies the VC will remain stationary. To be stationary, a distribution function must be a time-independent solution of the collisionless Boltzmann (Vlasov) equation [21–23]. From Jeans's theorem, this will only be the case if the distribution depends on the phase space coordinates solely through the integrals of motion [24]. Recently, however, it was shown that if the initial particle distribution $f_0(\mathbf{r}, \mathbf{p})$ is spherically symmetric and isotropic in velocity, $f_0(\mathbf{r}, \mathbf{p}) = f_0(r, p)$, and satisfies the VC, strong density oscillations will be suppressed, and the relaxation to QSS will be intrinsically different than for initial distributions which do not satisfy the VC [10,25]. In principle, a spherically symmetric distribution does not need to be a function of the modulus of momentum. A spherical symmetry is compatible with the distribution being a function of both radial and angular momentum independently. The assumption of isotropicity is included to prevent the radial orbit instability (ROI) which leads to spontaneous symmetry breaking of the distribution function. ROI can occur when kinetic energy of the system is dominated by the radial velocity component [26,27]. On the other hand, for isotropic velocity distributions, symmetry breaking occurs only when the initial distribution deviates strongly from the VC [28]. For initial particle distributions isotropic in velocity and satisfying the VC, relaxation to equilibrium is a consequence of phase mixing of particle trajectories [29], while for nonvirial initial conditions, relaxation results from the excitation of parametric resonances [11] and a nonlinear Landau damping [10,30].

Consider a spherically symmetric—in both positions and velocities—initial phase space particle distribution. We will work in the thermodynamic limit $N \to \infty$, $m \to 0$, while $mN = M$, where N is the total number of particles, m is the mass of each particle, and M is the total mass of the gravitational system. At $t = 0$, the particles are distributed in accordance with the initial distribution $f_0(r, p)$ inside an infinite 3D configuration space. We would like to predict the distribution function for the system when it relaxes to a QSS. It is easy to see that in the thermodynamic limit, the positional correlations between the particles vanish and all the dynamics is controlled by the mean-field potential [23]. Furthermore, if the initial distribution is such that the VC is satisfied, the mean-field potential should vary adiabatically,

and the energy of each particle should change little. Since the mean-field potential is a nonlinear function of position, the particles on the energy shell $[\mathcal{E}, \mathcal{E}+d\mathcal{E}]$ with slightly distinct one-particle energies $\mathcal{E}$ will have incommensurate orbital frequencies. This means that after a transient period, the phase mixing will result in a uniform particle distribution over the energy shell. The particle distribution in the final QSS can then be obtained by a coarse graining of the initial distribution over the phase space available to the particle dynamics, taking into account the conservation of the angular momentum of each particle, given the spherical symmetry of the mean-field potential.

Consider an arbitrary initial particle distribution $f_0(r,p)$ that satisfies the VC. For $t>0$, the particles will evolve under the action of an external adiabatically varying potential $\varphi(r,t)$, which will eventually converge to some $\psi(r)$. Our approach will be to construct a coarse-grained distribution for particles evolving directly under the action of the static potential $\psi(r)$, which will then be calculated self-consistently [31–33]. Clearly, such an approximation will only work if the variation of $\varphi(r,t)$ is adiabatic and no resonances are excited. This is precisely the case for the initial distributions which are isotropic in velocity and satisfy the VC [29].

Since $\psi(r)$ is static and spherically symmetric, the energy and the angular momentum of each particle will be preserved. The nonlinearity of $\psi(r)$ will lead to phase mixing of particle trajectories with the same energy and angular momentum. The number of particles with energy between $[\mathcal{E}, \mathcal{E}+d\mathcal{E}]$ and the square of the angular momentum between $[\ell^2, \ell^2+d\ell^2]$ is $n(\mathcal{E},\ell^2)d\mathcal{E}d\ell^2$ and is conserved throughout dynamics. In the QSS, these particles will spread over the phase space volume $g(\mathcal{E},\ell^2)d\mathcal{E}d\ell^2$, so that the coarse-grained distribution function for the QSS will be

$$f(\mathcal{E},\ell^2)=\frac{n(\mathcal{E},\ell^2)}{g(\mathcal{E},\ell^2)}. \tag{1}$$

The self-consistent potential $\psi(r)$ must satisfy the Poisson equation,

$$\frac{1}{r^2}\frac{d}{dr}\left(r^2\frac{d\psi}{dr}\right)=4\pi G m\rho(r), \tag{2}$$

where

$$\rho(\mathbf{r})=\int d^3p f[\mathcal{E}(\mathbf{r},\mathbf{p}),\ell^2(\mathbf{r},\mathbf{p})] \tag{3}$$

is the asymptotic particle density. This gives us a closed set of equations which can be used to calculate the distribution function in the QSS. To simplify the notation, we will scale all the distances to an arbitrary length scale L_0, time to $\sqrt{L_0^3/GM}$, the potential to GM/L_0, and the energy to GM^2/L_0.

Because of the conservation of the angular momentum of each particle, it is convenient to work with the canonical positions $(r,\ \theta,\ \phi)$ and conjugate momenta $(p_r,\ p_\theta,\ p_\phi)$. Note that in terms of these variables, the invariant phase space measure is $d^3xd^3p=drd\theta d\phi dp_r dp_\theta dp_\phi$. The particle energy and square modulus of the angular momentum are

$$\epsilon(r,\theta,p_r,p_\theta,p_\phi)=\frac{1}{2}\left(p_r^2+\frac{p_\theta^2}{r^2}+\frac{p_\phi^2}{r^2\sin^2\theta}\right)+\psi(r), \tag{4}$$

$$l^2(\theta,p_\theta,p_\phi)=p_\theta^2+\frac{p_\phi^2}{\sin^2\theta}, \tag{5}$$

respectively. The density of states $g(\mathcal{E},\ell^2)$ is

$$g(\mathcal{E},\ell^2)=\int dp_r dp_\theta dp_\phi\int drd\theta d\phi\delta[\ell^2-l^2(\theta,p_\theta,p_\phi)]\times\delta[\mathcal{E}-\epsilon(r,\theta,p_r,p_\theta,p_\phi)], \tag{6}$$

and the particle phase space density $n(\mathcal{E},\ell^2)$ is

$$n(\mathcal{E},\ell^2)=\int dp_r dp_\theta dp_\phi\int drd\theta d\phi\delta[\ell^2-l^2(\theta,p_\theta,p_\phi)]\times\delta[\mathcal{E}-\epsilon(r,\theta,p_r,p_\theta,p_\phi)]\times f_0\left(r,\sqrt{p_r^2+\frac{p_\theta^2}{r^2}+\frac{p_\phi^2}{r^2\sin^2\theta}}\right). \tag{7}$$

Integration over all the variables in Eqs. (6) and (7), other than dr, can be performed with the help of a Dirac delta function identity

$$\delta[f(x)]=\frac{\sum_i\delta(x-x_i)}{|f'(x_i)|}, \tag{8}$$

where x_i is the ith root of $f(x)$. Carrying out the integration, we obtain the coarse-grained distribution function for the QSS,

$$f(\mathcal{E},\ell^2)=\frac{\int drf_0[r,\sqrt{2(\mathcal{E}-\psi(r))}]\frac{\Theta[\mathcal{E}-\frac{\ell^2}{2r^2}-\psi(r)]}{\sqrt{\mathcal{E}-\frac{\ell^2}{2r^2}-\psi(r)}}}{\int dr\frac{\Theta[\mathcal{E}-\frac{\ell^2}{2r^2}-\psi(r)]}{\sqrt{\mathcal{E}-\frac{\ell^2}{2r^2}-\psi(r)}}}, \tag{9}$$

where Θ is the Heaviside step function. The coarse-grained distribution function depends on position and momentum only through the conserved quantities $\mathcal{E}$ and ℓ^2; therefore, it is automatically a stationary solution of the Vlasov equation.

The Poisson equation can be rewritten as

$$r^2\frac{d^2\psi}{dr^2}+2r\frac{d\psi}{dr}=N(r), \tag{10}$$

where $N(r)=4\pi r^2\rho(r)$, or

$$N(r)=\int dp_r dp_\theta dp_\phi \int d\theta d\phi f(\mathcal{E},\ell^2). \tag{11}$$

Multiplying Eq. (11) by the identity

$$\int d(\ell^2)\delta\left(\ell^2-p_\theta^2-\frac{p_\phi^2}{\sin^2\theta}\right)=1, \tag{12}$$

and changing the order of integration, we can write

$$N(r)=\int d(\ell^2)dp_r dp_\theta dp_\phi \int d\theta d\phi \delta\left(\ell^2-p_\theta^2-\frac{p_\phi^2}{\sin^2\theta}\right) \times f\left(\frac{p_r^2}{2}+\frac{p_\theta^2}{2r^2}+\frac{p_\phi^2}{2r^2\sin^2\theta}+\psi(r),p_\theta^2+\frac{p_\phi^2}{\sin^2\theta}\right). \tag{13}$$

The integration over the variables p_θ, p_ϕ, θ, and ϕ can now be performed explicitly with the help of Eq. (8). Finally, changing the integration variable from p_r to $\mathcal{E}$, Eq. (13) simplifies to

$$N(r)=8\pi^2\int_0^\infty d(\ell^2)\int_{\mathcal{E}_0}^\infty d\mathcal{E} f(\mathcal{E},\ell^2)\frac{\Theta[\mathcal{E}-\frac{\ell^2}{2r^2}-\psi(r)]}{\sqrt{2(\mathcal{E}-\frac{\ell^2}{2r^2}-\psi(r))}}, \tag{14}$$

where the lower limit of integration is $\mathcal{E}_0=(\ell^2/2r^2)+\psi(r)$ and $f(\mathcal{E},\ell^2)$ is given by Eq. (9). Substituting Eq. (14) into Eq. (10), we find an integrodifferential equation for the gravitational potential $\psi(r)$ in the QSS. Equation (10) can be solved numerically using the Picard iteration. Once the gravitational potential is known, the coarse-grained distribution function can be easily calculated by performing the integration in Eq. (9).

We next validated the proposed theory by comparing the marginal position and velocity distribution functions $N(r)$ and $N(p)$ to explicit molecular dynamics (MD) simulations of a 3D self-gravitating system of N particles. The simulations were performed using a version of the particle-in-cell (PIC) algorithm, in which each particle interacts with a mean-field potential produced by all other particles [10]. In the absence of ROI, these simulations produce identical particle distributions in QSS as calculated using traditional binary interaction methods but are 3 orders of magnitude faster. This allows us to easily reach the QSS [34]. The density distribution $N(r)$ is given by Eq. (14). To obtain the momentum distribution, we first calculate the distribution

$$N(p_r)=\int dr dp_\theta dp_\phi \int d\theta d\phi f(\mathcal{E},\ell^2), \tag{15}$$

where $\mathcal{E}=p_r^2/2+(\ell^2/2r^2)+\psi(r)$ and $\ell^2=p_\theta^2+(p_\phi^2/\sin^2\theta)$. The change of variable from p_r to the modulus of momentum p can be performed with the help of Eq. (12) and the identity

$$\int dp^2\delta\left(p^2-p_r^2-\frac{\ell^2}{r^2}\right)=1, \tag{16}$$

yielding

$$N(p)=8\pi^2 p\int_0^\infty d(\ell^2)\int_0^\infty dr f(\mathcal{E},\ell^2)\frac{\Theta[p^2-\frac{\ell^2}{r^2}]}{\sqrt{p^2-\frac{\ell^2}{r^2}}}, \tag{17}$$

where $\mathcal{E}=p^2/2+\psi(r)$.

We first consider a water-bag initial distribution,

$$f_0(r,p)=\eta\Theta(r_m^2-r^2)\Theta(p_m^2-p^2), \tag{18}$$

where $\eta=9/(16\pi^2 r_m^3 p_m^3)$ is the normalization constant. We will measure all the lengths in units of r_m, which is equivalent to setting $r_m=1$. The VC requires that $2K=-U$, where

$$K=\frac{1}{2}\int d^3r d^3p f_0(r,p)p^2 \tag{19}$$

is the kinetic energy and

$$U=\frac{1}{2}\int d^3r d^3p f_0(r,p)\psi_0(r) \tag{20}$$

is the potential energy of the system. The potential $\psi_0(r)$ for the initial water-bag distribution is

$$\psi_0(r)=\begin{cases}\frac{r^2-3}{2} & \text{if } r<1\\ -\frac{1}{r} & \text{if } r\geq 1.\end{cases} \tag{21}$$

Using Eqs. (18) and (21) to calculate K and U, the VC reduces to $p_m=1$. In Fig. 1, we plot the joint distribution function $f(\mathcal{E},\ell^2)$ for the QSS.

The marginal distribution functions can be calculated using Eqs. (14) and (17) together with Eq. (9). Figure 2 shows the position and velocity distributions $N(r)$ and $N(p)$ predicted by the integrable model. The symbols are the results of MD simulations. An excellent agreement between the theory and the simulations can be seen.

One particularly nice feature of the present theory is that it can be easily used to predict the final QSS for any initial distribution as long as it satisfies the VC. We next study a parabolic initial distribution given by

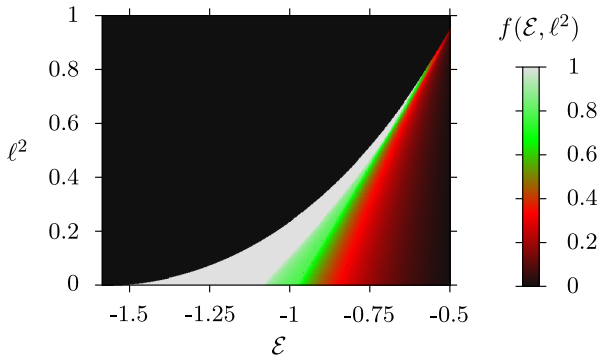

FIG. 1 (color online). Distribution function in energy and angular momentum for the QSS for an initial water-bag distribution, Eq. (18), satisfying the VC.

$$f_0(r,p) = \eta(1-r^2)\Theta(1-r^2)\Theta(p_m^2 - p^2), \qquad (22)$$

with $\eta = 45/(32\pi^2 p_m^3)$. The VC for this distribution is $p_m = 5/\sqrt{21}$. The marginal distributions predicted by the theory are compared with simulations in Fig. 3. Once again, the agreement is very good. For strongly inhomogeneous initial distributions, the VC is not enough to completely prevent the temporal dynamics of the mean-field potential. That is, even if we restrict one moment of the distribution function, other moments might still have sufficiently strong dynamics to excite parametric resonances. Indeed, we find that for very strongly inhomogeneous initial distributions, there is some discrepancy between the theory and the simulations. Nevertheless, even in these extreme cases, the theory remains quite accurate [34].

We have presented a theory that is able to predict the particle distribution in the final QSS to which a 3D self-gravitating system will relax from an initial condition. The theory can be used for initial distributions which are isotropic in particle velocity and satisfy the VC. It is interesting to compare and contrast our approach with the theory of violent relaxation developed by Lynden-Bell (LB). The statistical mechanics of LB is based on the

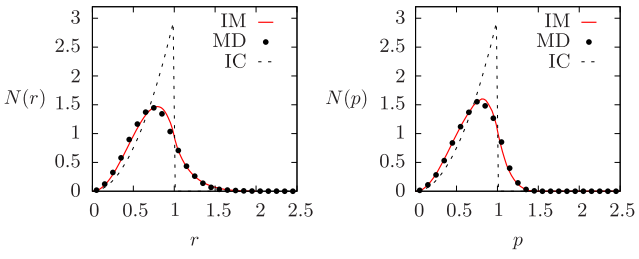

FIG. 2 (color online). Theoretically predicted density (left) and momentum (right) distributions (solid lines) for the QSS for the initial water-bag distribution. The symbols (black dots) are the results of MD simulations. The initial $t = 0$ density and momentum distributions are plotted with dashed lines—an initial water-bag distribution is given by Eq. (18).

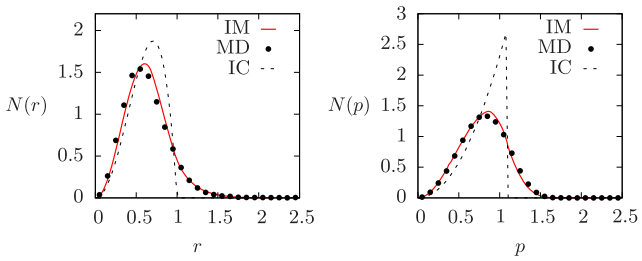

FIG. 3 (color online). Solid lines are the theoretically predicted density (left) and momentum (right) distributions for the QSS for initial distribution (dashed lines) given by Eq. (22). The symbols (black dots) are the results of MD simulations.

assumption of ergodicity and perfect mixing of the density levels of the initial distribution function over the phase space [36]. This is contrary to the approach presented in this Letter, which shows that dynamics of 3D self-gravitating systems with initial distribution satisfying the virial condition is closer to integrable than ergodic.

Curiously for various systems, in which the particles are either self-bound—like 1D and 2D gravity—or are bounded by an external potential or by the topology—such as magnetically confined plasmas or spin systems—the LB approach was found to work best for the initial water-bag distributions that satisfied the VC [10,20]. For distributions away from the VC, QSS were found to have a characteristic core-halo structure very different from the predictions of LB theory [17–19,37,38]. It was recently observed, however, that for more complex inhomogeneous or multilevel distributions, LB theory failed even when the initial distribution function satisfied the VC [29,39]. The failure of LB theory can now be attributed to the almost complete absence of ergodicity and mixing when the initial distribution satisfies the VC. The evolution of the mean-field potential of such systems is almost adiabatic, and the dynamics is closer to integrable than to ergodic [29]. The relaxation to QSS is the result of phase mixing of particles on the same energy shells and not a consequence of

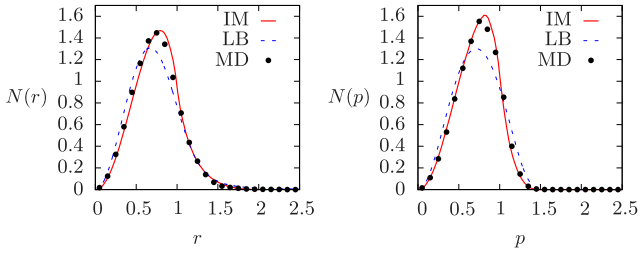

FIG. 4 (color online). Comparison between the density, left panel, and momentum, right panel, distributions calculated using LB statistics and the present theory. Initial distribution is the water-bag in momentum and position, Eq. (18), satisfying the VC. Solid curves are the results of the present theory, dashed curves are the predictions of the LB theory, and the solid circles are the results of MD simulations.

ergodicity over the full energy surface. Indeed, for 3D gravitational systems, LB theory fails to accurately account for either velocity or density distributions, as can be seen in Fig. 4, even for the initial virial water-bag distribution, Eq. (18). Furthermore, LB theory is very difficult to extend to more complicated initial conditions than a one-level water-bag distribution, while the present approach can, in principle, be used for any arbitrary distribution as long as it satisfies the VC. The goal of the future work will be to extend the theory presented in this Letter to initial distributions which do not satisfy the VC. Parametric resonances and particle evaporation, however, make this a very difficult task.

This work was partially supported by the CNPq, FAPERGS, CAPES, INCT-FCx, and by the US-AFOSR under Grant No. FA9550-12-1-0438.

[1] S. Chandrasekhar, Astrophys. J. **93**, 285 (1941).
[2] T. Konishi and K. Kaneko, J. Phys. A **25**, 6283 (1992).
[3] V. Latora, A. Rapisarda, and S. Ruffo, Phys. Rev. Lett. **80**, 692 (1998).
[4] V. Latora, A. Rapisarda, and S. Ruffo, Physica (Amsterdam) **280A**, 81 (2000).
[5] Y. Y. Yamaguchi, J. Barré, F. Bouchet, T. Dauxois, and S. Ruffo, Physica (Amsterdam) **337A**, 36 (2004).
[6] K. Jain, F. Bouchet, and D. Mukamel, J. Stat. Mech.: Theory Exp. (**2007**) P11008.
[7] A. Antoniazzi, D. Fanelli, J. Barré, P.-H. Chavanis, T. Dauxois, and S. Ruffo, Phys. Rev. E **75**, 011112 (2007).
[8] A. Gabrielli, M. Joyce, and B. Marcos, Phys. Rev. Lett. **105**, 210602 (2010).
[9] P.-H. Chavanis, Astron. Astrophys. **556**, A93 (2013).
[10] Y. Levin, R. Pakter, F. B. Rizzato, T. N. Teles, and F. P. C. Benetti, Phys. Rep. **535**, 1 (2014).
[11] R. L. Gluckstern, Phys. Rev. Lett. **73**, 1247 (1994).
[12] T. Padmanabhan, Phys. Rep. **188**, 285 (1990).
[13] Y. Levin, R. Pakter, and F. B. Rizzato, Phys. Rev. E **78**, 021130 (2008).
[14] M. Joyce, B. Marcos, and F. Sylos Labini, Mon. Not. R. Astron. Soc. **397**, 775 (2009).
[15] P. Chavanis and F. Bouchet, Astron. Astrophys. **430**, 771 (2005).
[16] M. Champion, A. Alastuey, T. Dauxois, and S. Ruffo, J. Phys. A **47**, 225001 (2014).
[17] T. N. Teles, Y. Levin, R. Pakter, and F. B. Rizzato, J. Stat. Mech. (2010) P05007.
[18] T. Teles, Y. Levin, and R. Pakter, Mon. Not. R. Astron. Soc. **417**, L21 (2011).
[19] M. Joyce and T. Worrakitpoonpon, Phys. Rev. E **84**, 011139 (2011).
[20] F. P. C. Benetti, T. N. Teles, R. Pakter, and Y. Levin, Phys. Rev. Lett. **108**, 140601 (2012).
[21] W. Braun and K. Hepp, Commun. Math. Phys. **56**, 101 (1977).
[22] A. Campa, T. Dauxois, and S. Ruffo, Phys. Rep. **480**, 57 (2009).
[23] T. M. Rocha Filho, M. A. Amato, A. E. Santana, A. Figueiredo, and J. R. Steiner, Phys. Rev. E **89**, 032116 (2014).
[24] J. Binney and S. Tremaine, *Galactic Dynamics*, 2nd ed. (Princeton University Press, Princeton, NJ, 2008).
[25] Y. Y. Yamaguchi, Phys. Rev. E **78**, 041114 (2008).
[26] L. A. Aguilar and D. Merritt, Astrophys. J. **354**, 33 (1990).
[27] E. I. Barnes, P. A. Lanzel, and L. L. R. Williams, Astrophys. J. **704**, 372 (2009).
[28] R. Pakter, B. Marcos, and Y. Levin, Phys. Rev. Lett. **111**, 230603 (2013).
[29] A. C. Ribeiro-Teixeira, F. P. C. Benetti, R. Pakter, and Y. Levin, Phys. Rev. E **89**, 022130 (2014).
[30] C. Villani, Phys. Plasmas **21**, 030901 (2014).
[31] X. Leoncini, T. L. Van Den Berg, and D. Fanelli, Europhys. Lett. **86**, 20002 (2009).
[32] P. de Buyl, D. Mukamel, and S. Ruffo, Phil. Trans. R. Soc. A **369**, 439 (2011).
[33] P. de Buyl, D. Mukamel, and S. Ruffo, Phys. Rev. E **84**, 061151 (2011).
[34] See the Supplemental Material at http://link.aps.org/supplemental/10.1103/PhysRevLett.113.100602, which includes Ref. [35], for a comparison of simulation methods—mean-field molecular dynamics (used in the present Letter) and explicit molecular dynamics with binary interactions—as well as results of the theory presented in this Letter applied to strongly inhomogeneous initial conditions.
[35] H. Nguyen, *GPU Gems 3* (Addison-Wesley Professional, Reading, MA, 2007), Chap. 31.
[36] D. Lynden-Bell, Mon. Not. R. Astron. Soc. **136**, 101 (1967).
[37] R. Pakter and Y. Levin, Phys. Rev. Lett. **106**, 200603 (2011).
[38] A. Figueiredo, T. M. Rocha Filho, M. A. Amato, Z. T. Oliveira, Jr., and R. Matsushita, Phys. Rev. E **89**, 022106 (2014).
[39] R. Pakter and Y. Levin, J. Stat. Phys. **150**, 531 (2013).

Chapter 7

Review of Statistical Mechanics of Systems with Long-Range Interactions

This last chapter of the research content contains a review of the work our research group has done in the field of systems with long-range interactions up to 2013. Previously to this thesis project, T. N. Teles, F. Rizzato, R. Pakter and Y. Levin had worked on describing the QSS of systems as diverse as non-neutral plasmas and self-gravitating systems in several dimensions, using the core-halo distribution described in section 2.3.1. Combined with our later work with the HMF and GHMF models, this resulted in our review, summarized below.

7.1 Nonequilibrium statistical mechanics of systems with long-range interactions

This review agglomerates the work on LRI systems done by our research group until 2013. It contains a thorough introduction to the fundamental concepts of LRI systems, such as collisionless dynamics and nonequilibrium quasistationary states. Several chapters are dedicated to self-gravitating systems in one, two and three dimensions, and to magnetically confined ion beams.

My contribution to this work was in the chapters of the HMF and GHMF models. These chapters exposed more thoroughly the work we had done in references [57] and [104] (presented in sections 4.1 and 5.1 of this thesis, respectively) as well as reviews of the equilibrium properties of the HMF model. We show that the magnetization of the HMF model evolves from a paramagnetic QSS to its ferromagnetic equilibrium value with a timescale that scales as $N^{1.7}$. The expected exponent should be 2 [112]. A possible explanation for this divergence is that the initial distribution of our simulations was ferromagnetic; therefore the homogeneous arguments that indicate the exponent 2 are not completely satisfied.

Besides the equilibrium properties, we also tentatively apply the core-halo distribution described in subsection 2.3.1 to the QSS of the HMF and GHMF models. Since these models are periodical, there is an added difficulty to using the core-halo theory: particles located

in orbits above the separatrix (the orbit which separates rotating and librating orbits) have effectively "escaped" from confinement. The test particle method described in subsection 2.3.1 relies on the envelope equation, which determines the oscillating potential for their dynamics. The envelope becomes ill-defined, however, when it reaches the periodical limit; that is, when $\theta_e > \pi$. Therefore, the halo energy determined by the maximum energy of the test particles is also ill-defined.

Nevertheless, we show that structurally the core-halo distribution works very well if we measure the halo energy from the actual molecular dynamics results instead of the test-particle method[1]. The only setback is the lack of a way to determine the halo energy without resorting to full molecular dynamics.

This review, "Nonequilibrium statistical mechanics of systems with long-range interactions", was published in *Physics Reports*, volume 535, pages $1 - 60$ (2014).

[1] It also works if the energy is low enough so that the envelope does not reach the periodical limit $\theta_e = \pi$.

Physics Reports 535 (2014) 1–60

Contents lists available at ScienceDirect

Physics Reports

journal homepage: www.elsevier.com/locate/physrep

Nonequilibrium statistical mechanics of systems with long-range interactions

Yan Levin *, Renato Pakter, Felipe B. Rizzato, Tarcísio N. Teles [1], Fernanda P.C. Benetti

Instituto de Física, Universidade Federal do Rio Grande do Sul, Caixa Postal 15051, CEP 91501-970, Porto Alegre, RS, Brazil

ARTICLE INFO

Article history:
Accepted 3 October 2013
Available online 24 October 2013
editor: H. Orland

Keywords:
Long-range interactions
Vlasov equation
Collisionless relaxation
Quasi-stationary states
Nonequilibrium statistical mechanics

ABSTRACT

Systems with long-range (LR) forces, for which the interaction potential decays with the interparticle distance with an exponent smaller than the dimensionality of the embedding space, remain an outstanding challenge to statistical physics. The internal energy of such systems lacks extensivity and additivity. Although the extensivity can be restored by scaling the interaction potential with the number of particles, the non-additivity still remains. Lack of additivity leads to inequivalence of statistical ensembles. Before relaxing to thermodynamic equilibrium, isolated systems with LR forces become trapped in out-of-equilibrium quasi-stationary states (qSSs), the lifetime of which diverges with the number of particles. Therefore, in the thermodynamic limit LR systems will not relax to equilibrium. The qSSs are attained through the process of collisionless relaxation. Density oscillations lead to particle–wave interactions and excitation of parametric resonances. The resonant particles escape from the main cluster to form a tenuous halo. Simultaneously, this cools down the core of the distribution and dampens out the oscillations. When all the oscillations die out the ergodicity is broken and a qSS is born. In this report, we will review a theory which allows us to quantitatively predict the particle distribution in the qSS. The theory is applied to various LR interacting systems, ranging from plasmas to self-gravitating clusters and kinetic spin models.

Contents

* Corresponding author. Tel.: +55 5133086446.
E-mail addresses: levin@if.ufrgs.br (Y. Levin), pakter@if.ufrgs.br (R. Pakter), rizzato@if.ufrgs.br (F.B. Rizzato), tarcisio.teles@fi.infn.it (T.N. Teles), fbenetti@if.ufrgs.br (F.P.C. Benetti).
[1] Present address: Istituto Nazionale Di Fisica Nucleare, Viale delle Idee 1, Zona Osmanoro, 50019 - Sesto Fiorentino, Italy.

0370-1573/$ – see front matter © 2013 Elsevier B.V. All rights reserved.
http://dx.doi.org/10.1016/j.physrep.2013.10.001

1. Introduction

A long time ago Einstein expressed his belief that thermodynamics is "the only physical theory of universal content concerning which I am convinced that, within the framework of applicability of its basic concepts, it will never be overthrown" [1]. One can, however, wonder about the extent of the "applicability" to which Einstein was referring. For example, can thermodynamics in any form be applied to study non-neutral plasmas or galaxies in which "particles" interact by long-range (LR) forces?

The difficulty of studying systems with LR interactions was already well appreciated by Gibbs, who noted the inapplicability of statistical mechanics when interparticle potentials decay with exponents smaller than the dimensionality of the embedding space [2,3]. For such systems energy is not extensive and traditional thermodynamics fails. One way to correct the lack of extensivity is to scale the interaction energy with the inverse of the number of particles. This is the so-called Kac prescription designed to restore extensivity to the free energy [4–6]. The problem, however, remains — although the energy is now extensive, it is still non-additive. On the other hand, it is a fundamental postulate of thermodynamics that entropy and energy must be additive over the subsystems — that is, the interfacial contributions should be negligibly small. For systems with short-range forces this condition is clearly satisfied — in the thermodynamic limit the interfacial energy is much smaller than the energy of the bulk. This, however, is not true for systems with LR forces for which the interfacial region cannot be clearly defined [7] — every particle interacts with every other particle of the system, so that no clear separation into bulk and interface exists.

One can still hope that although the additivity of energy breaks down, it might still be possible to use equilibrium statistical mechanics to describe stationary states of systems with LR interactions. Very quickly, however, one runs into difficulties. For example, depending on the ensemble used, one finds that a system can remain either in one phase or undergo a phase transition [8]. One also finds that in the microcanonical ensemble such systems can have negative specific heat [9–14], contrary to the laws of usual thermodynamics.

There is, however, an even more profound problem with applying classical statistical mechanics to systems with LR forces. The underlying assumption of Boltzmann–Gibbs (BG) statistics is the existence of ergodicity and mixing [15]. For a closed system of particles (in a microcanonical ensemble) the initial distribution should uniformly spread over the available phase space, so that in equilibrium all microstates corresponding to a given thermodynamic macrostate should be equally probable. Although there is no general proof of ergodicity and mixing, in practice it has been found to apply to most nonintegrable systems with short-range forces. There is, however, no indication that ergodicity and mixing exist for systems with LR interactions [7,16–19]. In fact, one should expect precisely the opposite. Kac renormalization of the interaction potential kills off the correlations between particles. Within the kinetic theory, it is precisely these correlations (collisions) that drive a system to thermodynamic equilibrium. In the absence of correlations, the dynamical evolution of the one-particle distribution function $f(\mathbf{r}, \mathbf{p}, t)$ is governed by the collisionless Boltzmann (Vlasov) equation [20,21]. Starting from an arbitrary initial condition, a solution of this equation does not evolve to a stationary state — the spatiotemporal evolution continues *ad infinitum* on smaller and smaller length scales. It is only in a coarse-grained sense that we can say that the system has reached an "equilibrium" — a finite resolution imposed on us by an experiment or a computer simulation will not allow us to see the full fine-grained evolution of the distribution function. The coarse-grained stationary state will, in general, be very different from the normal thermodynamic equilibrium. Unlike the state of thermodynamic equilibrium, it will explicitly depend on the initial distribution of particle positions and velocities [22]. In particular, the velocity distribution in the stationary state (SS) will not have the characteristic Maxwell–Boltzmann form [23–25]. Indeed, observations and simulations of both gravitational clusters [26–40] and confined non-neutral plasmas [23,41–52], indicate the presence of such nonequilibrium stationary states.

It is, therefore, clear that in the thermodynamic limit, traditional methods of equilibrium statistical mechanics cannot be applied to systems with LR forces. A new theory is needed. The goal of the present Report is to show how such theory can be constructed. Using the properties of Vlasov dynamics and the theory of parametric resonances, we will derive coarse-grained distribution functions for the nonequilibrium stationary states of systems with LR interactions, without explicitly solving the collisionless Boltzmann equation. Comparing the theory with the explicit N-body simulations, we will show that it is able to quantitatively predict both position and velocity distribution functions of self-gravitating clusters [38,39,53], magnetically confined plasmas [23,24], and of kinetic spin models [25,54,55], without any adjustable parameters. We will focus on a statistical theory of nonequilibrium quasi-stationary states; only briefly shall we address the thermodynamic equilibrium, which has already been thoroughly covered by Campa et al. in Ref. [7].

The Report is organized as follows: in Section 1 we begin with an introduction to the principal properties of systems with LR interactions, followed by a review of the Vlasov dynamics. Sections 2–4 present results for self-gravitating clusters in one, two, and three dimensions, respectively. In Section 5 we address the nonequilibrium properties of magnetically confined plasmas, and in Sections 6 and 7 we discuss two different kinetic spin models. Section 8 concludes the Report, reviewing the theories and the results obtained so far and outlining the perspectives for future research.

2. Systems with long range forces

Among the physical systems, a significant fraction involves those whose particles interact by long-range potentials of the form $\psi(r) \sim 1/r^{\alpha}$, where $\alpha < d$ and d is the dimensionality of the embedding space. Examples of such systems include galaxies and globular clusters [56–64], two-dimensional and geophysical flows and vortex models [18,65–70], quantum spin models [71], dipolar excitons [72], cold atom models [73], colloids at interfaces [74–77] as well as magnetically confined plasmas [23,78–80]. In order to predict the behavior of systems with short-range forces we can rely on thermodynamics and statistical mechanics both of which, however, fail for systems with LR interactions.

Thermodynamics requires extensivity and additivity [81], neither of which is valid for LR systems [7]. A system of N particles confined inside a volume V is said to be extensive if, when the number of particles and the volume are scaled by λ, the internal energy $U(\lambda N, \lambda V)$ of the system scales as $\lambda U(N, V)$. It is easy to see that systems with short-range forces are extensive. If the interaction potential is short-range, each particle will interact only with the particles which are within the range γ of the interaction potential. Suppose that a system is homogeneous, the number of particles within the distance γ of a given particle will then be proportional to $N\gamma^d/V$ and the internal energy must have the form of $U(N, V) = Nf(N/V)$, where $f(x)$ is a function that depends on the microscopic interactions between the particles. This form of internal energy is clearly extensive. In fact, it is not necessary for the interaction potential to be strictly short-range – bounded by γ – algebraically decaying potentials will lead to extensive thermodynamics as long as they decay sufficiently rapidly, i.e. if $\alpha > d$ [82]. We shall call all such systems "finite range".

Extensivity is important for the existence of a nontrivial thermodynamic limit and the equivalence of different statistical ensembles. A thermodynamic system in contact with a thermal reservoir at temperature T – canonical ensemble – must be at the minimum of its Helmholtz free energy $F(N, V) = U(N, V) - TS(N, V)$, where $S(N, V)$ is the entropy. The celebrated Boltzmann formula $S = k_B \ln W$ relates the thermodynamics with dynamics by associating W, the number of microstates available to the system through its dynamics, to the concept of entropy of classical thermodynamics. The phase space volume of a confined Hamiltonian system, which is proportional to W, grows exponentially with the number of particles so that $S \sim N$, irrespective of the range of interactions. Therefore, both the internal energy and entropy of a finite range system scale linearly with the number of particles in the system, allowing for a nontrivial thermodynamic equilibrium.

LR systems, however, are intrinsically different. The infinite range of the interaction potential results in an internal energy that scales superlinearly with the number of particles in the system, $U \sim N^2$. Therefore if such a system is put in contact with a thermal bath, for large N the Helmholtz free energy will be dominated by the internal energy. The equilibrium state will then correspond to the minimum of the internal energy U. The entropy will be irrelevant, unless the temperature of the reservoir is unrealistically large and scales with the number of particles in the system, $T \sim N$.

In practice, most LR systems are isolated from the environment. This is the case for galaxies and magnetically confined plasmas. Gravity in three dimensions is particularly challenging because of the evaporation of particles [26,83,84]; however, one and two dimensional gravitational systems and magnetically confined plasmas can be studied straightforwardly using molecular dynamics simulations (MD). Unlike systems with short-range forces – which must be confined to a box in order to have a nontrivial thermodynamics – one and two dimensional gravitational systems are self-confining and can exist in an infinite volume, $V \to \infty$. Once again, however, one runs into a difficulty with the long-range nature of the interaction potential. The superextensive interaction energy leads to strong forces and velocities which rapidly exceed that of the speed of light. To avoid this problem and to obtain a well defined thermodynamic limit it is necessary to rescale the gravitational coupling constant by a factor $1/N$. This is the so-called Kac prescription [4]. For a gravitational system of N particles in an infinite volume, the Kac prescription is equivalent to the requirement that the mass of each particle $m \to 0$, while mN remains finite, $mN = M$. One can show that this leads to a well defined thermodynamic limit as $N \to \infty$.

Although the rescaled gravity and plasmas are extensive, they remain nonadditive. For a d-dimensional system of particles interacting by a finite-range potential, the interfacial energy scales with the number of particles as $N^{\frac{d-1}{d}}$, while the bulk energy grows as N. Thus, the total energy of a finite-range system in the thermodynamic limit is equivalent to the sum of the energies of its macroscopic subsystems. This is not true for LR systems. As the interaction range grows, the concept of interface loses its meaning. One can no longer consider a total system as a sum of smaller subsystems, since the LR nature of the potential leads to a nontrivial interaction between all the subsystems. The lack of additivity can result in a negative specific heat for an isolated LR system [7,9,10,12]. On the other hand, if a LR system is in contact with a thermal bath, its specific heat must be positive. Contrary to what happens with finite-range systems the predictions of microcanonical and canonical ensembles may, therefore, be inequivalent for systems with LR interactions [85–88]. Similarly, the canonical and the grand-canonical ensembles may also become inequivalent [89]. Besides inequivalence of ensembles, it has also been debated that negative specific heat may result in yet another abnormality: the violation of the zeroth law of thermodynamics [90–93].

Another difficulty with the statistical treatment of LR systems is the lack of ergodicity. The ergodic hypothesis allows us to replace the time averages by the ensemble averages [94]. Consider a $2dN$ dimensional phase space of N interacting particles. Each point $\mathbf{X}$ in this phase space represents a possible configuration (microstate) of the system. For a given thermodynamic macrostate there is a huge number of possible microstates. This allows us to define a statistical ensemble of microstates with a probability density $\rho(\mathbf{X}, t)$. The dynamics of $\rho(\mathbf{X}, t)$ is governed by the Liouville equation. For equilibrium statistical mechanics to work, the initial probability density should uniformly spread over the energy surface — producing a, so-called, mixing flow [15].

The fundamental problem of ergodic theory is to understand under what conditions a nonstationary phase space density will converge to a stationary one [95,96]. Note that for a time reversible system one cannot have a "fine-grained" equilibrium, a thermodynamic equilibrium exists only in a coarse-grained sense. On a fine-grained scale, the dynamical evolution of the probability density will never stop, so that if at some point during the dynamical evolution the velocities of all the particles are reversed, the system will diverge from the equilibrium. Although ergodicity and mixing have been verified for many different systems with finite-range forces, both seem to fail for systems with LR interactions [16,17,19,97].

The relaxation to a stationary state (SS) of systems with LR interactions is fundamentally different from the relaxation to equilibrium of systems with short-range forces. For the latter, the relaxation is collisional and the reduced probability densities are governed by the BBGKY (Born, Bogoliubov, Green, Kirkwood, Yvon) hierarchy of equations [98]. At the leading order of this hierarchy is the Boltzmann equation $Df/Dt = (\partial f/\partial t)_{\rm col}$, where $Df/Dt \equiv \partial f/\partial t + (\mathbf{p}/m) \cdot \nabla_{\rm r} f + \mathbf{F} \cdot \nabla_p f$ is the convective derivative of $f(\mathbf{r}, \mathbf{p}, t)$ and $\mathbf{F} = \dot{\mathbf{p}}$. This equation describes the evolution of the one-particle distribution function $f(\mathbf{r}, \mathbf{p}, t)$ [99]. The right hand side of the Boltzmann equation is the collision term that drives the system toward thermodynamic equilibrium [99]. The distribution functions in thermodynamic equilibrium do not depend on the initial condition, but only on the global conserved quantities, and are described by the Boltzmann–Gibbs statistical mechanics [100].

The situation is very different for systems with LR forces. In the thermodynamic limit $N \to \infty$ the dynamics of these systems is completely dominated by the mean-field and the collisions (correlations) are negligible. To see why this is so, let us consider, for example, a one dimensional gravitational system of particles of mass m, interacting by $\varphi(x) = Gm^2|x|$, where G is the gravitational constant. As was discussed above, to have a well defined thermodynamic limit we need to require that $m \to 0$, while the total mass of the system remains fixed, $mN = M$. Although the interaction between any two particles is vanishingly small, the infinite range of the potential results in a finite total force acting on each particle. To quantify the discreteness (correlations) effects [101] we can define a plasma parameter – corresponding to the ratio of the characteristic two-body interaction energy and the average kinetic energy – $\Gamma \equiv 2Gm^2a/m\langle v^2\rangle$, where $\langle v^2\rangle$ is the average particle velocity and a is a characteristic separation between the particles. Γ measures the degree to which the dynamics of a system is dominated by the correlations — if $\Gamma > 1$ the correlations (collisions) are important and if $\Gamma < 1$ the dynamics is

governed purely by the mean-field. Starting from an initial particle distribution, a one dimensional gravitational cluster will relax to a stationary state, with a characteristic velocity $\langle v^2 \rangle \sim O(1)$. It will be shown in the following sections that the extent of the mass distribution is controlled by the parametric resonances, so that starting from an initial particle distribution with a compact support, the final distribution will be restricted to a finite "volume" or radius r_h, so that $a \sim r_h/N$. We then come to the conclusion that $\Gamma \sim 1/N^2$, in the thermodynamic limit the correlations vanish and the dynamics of a LR system is determined purely by the mean-field.

The argument above suggests that for LR systems the (collisional) right-hand side of the Boltzmann equation should vanish and the one-particle distribution function should satisfy the collisionless Boltzmann equation $Df/Dt = 0$. This equation is also known as the Vlasov equation [20]. While the stationary solution to the Boltzmann equation is the Maxwell–Boltzmann distribution, the Vlasov equation has an infinite number of stationary states, depending on the initial particle distribution. The one-particle distribution function evolves on ever-decreasing length scales. Eventually, the dynamical scale becomes so small that the evolution of $f(\mathbf{r}, \mathbf{p}, t)$ can no longer be observed at any resolution available to us. It is only in this coarse-grained sense that a LR system achieves a stationary state (SS).

For a finite number of particles, the correlations – although very small – remain finite. The cumulative effect of weak correlations will drive a LR system from a quasi-stationary state (qSS) toward the true thermodynamic equilibrium. The relaxation time $t_\times$, however, is very slow, diverging with the number of particles as N^γ [53,102,103]. The value of the exponent γ depends on each system [39], but is usually $\gamma \geq 1$. We expect that $t_\times \sim 1/\Gamma$, so that for 1D gravity $t_\times \sim N^2$. For 2D gravitational clusters the interaction potential is logarithmic, so that the crossover time should scale as $t_\times \sim N/\ln N$. In the following sections we will see if these simple estimates of the relaxation time agree with the results of N-body simulations.

Although interesting theoretically, the strong divergence of $t_\times$ precludes the equilibrium state from ever being reached by most physically relevant systems, such as galaxies and plasmas. To achieve equilibrium these systems would require a span of time longer than the age of the universe [61,64,104].

3. Vlasov dynamics

In the thermodynamic limit $N \to \infty$, the correlations between the particles of a LR system vanish and the dynamics of the one-particle distribution function $f(\mathbf{q}, \mathbf{p}, t)$ is governed exactly [20] by the Vlasov equation,

$$\left(\frac{\partial}{\partial t} + \mathbf{p} \cdot \frac{\partial}{\partial \mathbf{q}} - \frac{\partial \psi}{\partial \mathbf{q}} \cdot \frac{\partial}{\partial \mathbf{p}} \right) f(\mathbf{q}, \mathbf{p}, t) = 0. \tag{1}$$

The one-particle distribution function evolves in the phase space as the density of an incompressible fluid — its local value remains constant along the flow. The $\psi(\mathbf{q})$ represents the potential felt by a "fluid element" located at $(\mathbf{q}, \mathbf{p})$. It can be shown that the Vlasov dynamics has an infinite number of conserved quantities called Casimir invariants [105,106]. Any local functional of the distribution function is a Casimir invariant,

$$C[f] = \int g(f) d\mathbf{q} d\mathbf{p}. \tag{2}$$

In particular, the fine-grained Boltzmann entropy

$$S(f) = -\int f(\mathbf{q}, \mathbf{p}, t) \ln f(\mathbf{q}, \mathbf{p}, t) d\mathbf{q} d\mathbf{p} \tag{3}$$

is a Casimir invariant and is conserved by the Vlasov flow. The entropy can increase only in a coarse-grained sense [107]. To see this let us define a coarse-grained distribution function

$$\bar{f}(\mathbf{q}, \mathbf{p}, t) = \frac{1}{(\Delta p \Delta q)^d} \int_{\Delta p, \Delta q} f(\mathbf{q}', \mathbf{p}', t) d\mathbf{q}' d\mathbf{p}'. \tag{4}$$

Consider the evolution of the coarse-grained entropy

$$\Delta \bar{S} = \bar{S}(t_1) - S(t_0) = \int \left[s(\bar{f}, t_1) - s(f, t_0) \right] d\mathbf{q} d\mathbf{p}, \tag{5}$$

where we have defined the Boltzmann entropy density $s(f, t) = -f(\mathbf{q}, \mathbf{p}, t) \ln f(\mathbf{q}, \mathbf{p}, t)$. We have also supposed that at $t = t_0$ the exact particle distribution is known. Since the fine-grained entropy is conserved, we can rewrite Eq. (5) as

$$\Delta \bar{S} = \int \left[s(\bar{f}, t_1) - s(f, t_1) \right] d\mathbf{q} d\mathbf{p}. \tag{6}$$

To perform the coarse-graining, we divide the macrocells of volume $(\Delta p \Delta q)^d$ into K microcells, with the local value of the distribution function inside the microcell i given by f_i. Now, consider the variation of the coarse-grained entropy inside the

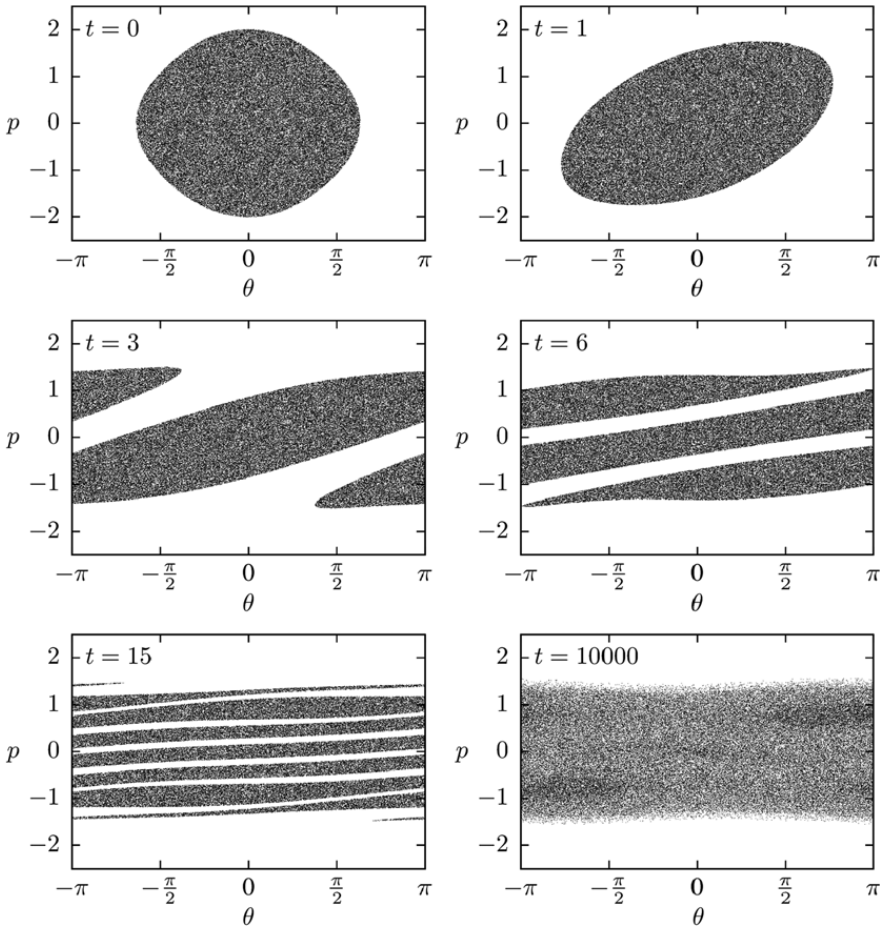

Fig. 1. Evolution of particle distribution in the phase space of the Hamiltonian mean field (HMF) model.

macrocell j,

$$\Delta\bar{S}_j = (\Delta p \Delta q)^d \sum_i^K \left[s\left(\frac{\sum_l^K f_l}{K} \right) - s(f_i) \right] = (\Delta p \Delta q)^d \left[Ks\left(\frac{\sum_i^K f_i}{K} \right) - \sum_i^K s(f_i) \right]. \tag{7}$$

Since the entropy density $s(x)$ is a concave function it must satisfy Jensen's inequality

$$\frac{1}{K}\sum_i^K s(f_i) \leq s\left(\frac{\sum_i^K f_i}{K} \right), \tag{8}$$

from which we conclude that the coarse-grained entropy of the system should increase with time, $\Delta\bar{S} \geq 0$. The Boltzmann entropy will be maximum in equilibrium; this, however, does not mean that the equilibrium can always be reached. As we shall see, in the thermodynamic limit, systems with LR interactions can become trapped in a non-ergodic stationary state.

If the initial fine-grained distribution function $f_0(\mathbf{q}, \mathbf{p})$ is divided into p levels of phase space density η_j, Vlasov dynamics will preserve the hypervolume of each level, $C(\eta_j) = \int \delta[f(\mathbf{q}, \mathbf{p}, t) - \eta_j] d\mathbf{q} d\mathbf{p}$. In this review, we will concentrate on one-level (waterbag) initial distributions of the form

$$f_0(\mathbf{q}, \mathbf{p}) = \eta \Theta(q_m - |\mathbf{q}|)\Theta(p_m - |\mathbf{p}|), \tag{9}$$

where $\Theta(x)$ is the Heaviside step function, q_m and p_m represent the maximum values for the generalized coordinates and momentum, and η is the phase space density of the initial particle distribution. Starting from this initial condition, the fine-grained distribution function $f(\mathbf{q}, \mathbf{p}, t)$ will evolve in phase space through the process of filamentation, developing structure on smaller and smaller length scales, see Fig. 1. Eventually, the length scale of the dynamical evolution will become so small, that to an observer it will appear that the dynamics has ceased. At this stage, we may say that the coarse-grained

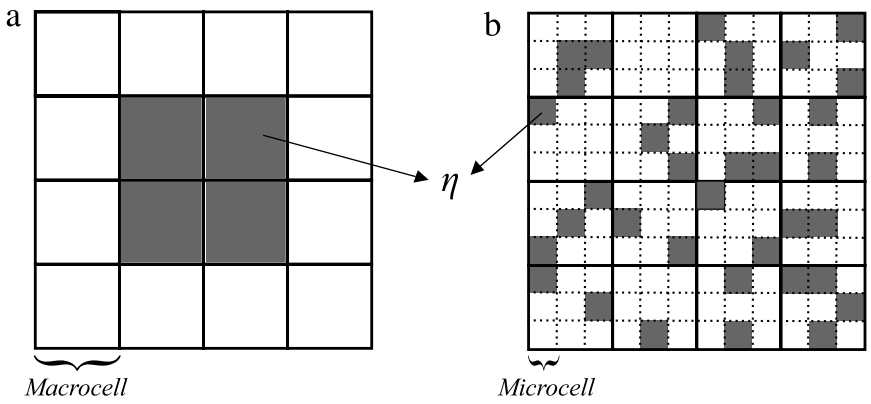

Fig. 2. Schematic of phase space evolution described by the Vlasov dynamics: (a) initial and (b) final stationary state for a distribution with initial phase space density η. In this example, $\nu = 9$.

distribution, $\bar{f}$, has achieved a stationary state, even though the fine-grained distribution f is still evolving. For a practical purpose of describing the results of molecular dynamics simulations – which, of course, have finite precision – we only need to have the knowledge of $\bar{f}(\mathbf{q}, \mathbf{p})$.

3.1. Lynden-Bell statistics

In a seminal work, Lynden-Bell (LB) proposed a statistical approach for calculating $\bar{f}(\mathbf{q}, \mathbf{p})$ for the final stationary state [108]. LB theory is similar in its construction to the usual Boltzmann statistics, but instead of working with the particles, Lynden-Bell studied the distribution of the phase space density levels, η. It is important to keep in mind that, similar to the usual equilibrium statistical mechanics, the LB approach requires the existence of ergodicity and mixing [7,104].

The phase space is divided into P macrocells which are in turn subdivided into ν microcells of volume h^d. As the dynamics progresses, the distribution function spreads over the phase space, occupying more macrocells than it did initially. This process is illustrated in Fig. 2. The volume fraction occupied by the level η inside the macrocell i is

$$\rho(\mathbf{q}, \mathbf{p}) = \frac{n_i}{\nu}, \tag{10}$$

where n_i is the number of microcells inside a macrocell i occupied by the level η. The volume fraction is related to the distribution function by $\rho(\mathbf{q}, \mathbf{p}) = \bar{f}(\mathbf{q}, \mathbf{p})/\eta$. Due to the incompressibility of Vlasov dynamics, each microcell can be occupied by at most one level η, so that the density must satisfy

$$\rho(\mathbf{q}, \mathbf{p}) \leq 1. \tag{11}$$

LB supposed that in a stationary state the dynamics of the density levels is ergodic — η's have an equal probability of occupying any of the microcells. He then applied the usual Boltzmann counting to calculate the most probable distribution of the density level over the phase space.

The total number of occupied microcells,

$$N = \sum_i n_i \tag{12}$$

remains constant throughout the dynamics. The number of ways in which these N occupied microcells can be divided among the P macrocells is given by

$$\frac{N!}{\prod_i^P n_i!}. \tag{13}$$

Now consider a macrocell. The number of ways in which n_i of its ν microcells can be occupied by a density level is

$$\frac{\nu!}{(\nu - n_i)!}. \tag{14}$$

Note that the density levels are treated as distinguishable. Multiplying expressions (14) and (13) we obtain the total number of possible microstates,

$$W(n_i) = \frac{N!}{\prod_i^P n_i!} \prod_i \frac{\nu!}{(\nu - n_i)!}. \tag{15}$$

The coarse-grained entropy of the system is defined as $S_{lb} \equiv -k_B \ln W(n_i)$ where k_B is the Boltzmann constant. In the limit in which the variations of $\rho(\mathbf{q}, \mathbf{p})$ between the macrocells are infinitesimal, the entropy can be written as

$$S_{lb} = -k_B \int \frac{d\mathbf{q}d\mathbf{p}}{h^d} \{\rho(\mathbf{q}, \mathbf{p}) \ln[\rho(\mathbf{q}, \mathbf{p})] + [1 - \rho(\mathbf{q}, \mathbf{p})] \ln[1 - \rho(\mathbf{q}, \mathbf{p})]\}. \tag{16}$$

Similar to the usual thermodynamic equilibrium, LB proposed that the SS of a LR system corresponds to the most probable distribution of the density levels among the macrocells. To find this distribution, we must maximize the LB entropy under the constraints of energy

$$\int \left(\frac{p^2}{2m} + \frac{\psi(\mathbf{q})}{2}\right) \bar{f}(\mathbf{q}, \mathbf{p}) d\mathbf{q}d\mathbf{p} = \mathcal{E}_0 \tag{17}$$

and particle

$$\int \bar{f}(\mathbf{q}, \mathbf{p}) d\mathbf{q}d\mathbf{p} = 1, \tag{18}$$

conservation. In the above equations $\mathcal{E}_0$ is the average particle energy in the initial distribution and $\psi(\mathbf{q})$ is the potential at position $\mathbf{q}$ in the stationary state. Maximizing the entropy Eq. (16), under the constraints given by Eqs. (17) and (18), we find the coarse-grained distribution function $\bar{f}(\mathbf{q}, \mathbf{p}) = \eta\rho(\mathbf{q}, \mathbf{p})$ for the SS,

$$f_{lb}(\mathbf{q}, \mathbf{p}) = \bar{f}(\mathbf{q}, \mathbf{p}) = \frac{\eta}{1 + e^{\beta[\epsilon(\mathbf{q},\mathbf{p}) - \mu]}} \tag{19}$$

where $\epsilon(\mathbf{q}, \mathbf{p}) = \frac{p^2}{2m} + \psi(\mathbf{q})$ is the one-particle energy. The Lagrange multipliers β and μ are the inverse temperature and the chemical potential of the stationary state. The expression (19) is similar to the distribution function of fermions in an equilibrium system.

Besides Lynden-Bell's theory, other statistical approaches have also been proposed to study qSSs which arise in the process of collisionless relaxation. Example include, statistics based on particles instead of the distribution function [109] and an information-theoretical approach [106,110]. Just like LB theory these approaches require existence of ergodicity and good mixing [111,112] which, in general, are not valid for systems with LR forces. In this Report, we will only focus on LB theory. In the following sections we will see how well it compares with the simulations.

4. Gravitation in one dimension

Due in part to complications of 3D gravitational systems, which will be addressed later on, many studies of self-gravitating systems have focused on one and two dimensions [30,34,113–122]. The reduced dimensionality makes the study of these systems much simpler. The fact that the gravitational potential in one and two dimensions is unbounded from above prevents particle evaporation which makes theoretical and simulation work on 3D systems very difficult. In spite of their greater simplicity, 1D and 2D gravitational systems share many characteristics of 3D gravity. For example, the global structure of disk-like galaxies, found using 3D numerical simulation, are also reproduced by 2D simulations [83]. One-dimensional self-gravitating systems have also been used to study the stellar dynamics of galaxy clusters and of cosmological models [28,31,58,59,122–131].

A 1D self-gravitating system consists of N sheets of mass density m uniformly distributed in the y–z plane, free to move along the x axis. The dynamics of the sheets is the same as the dynamics of point particles of mass m interacting by a linear potential. The particles are free to cross one another. The thermodynamic limit, $\lim_{N\to\infty} mN = M =$ constant, is equivalent to the Kac prescription necessary to guarantee the extensivity of the energy.

The Poisson equation for this system is

$$\nabla^2\psi(x, t) = 4\pi G\rho(x, t) \tag{20}$$

where G is the gravitational constant and $\rho(x, t)$ is the mass density. In order to simplify the expressions, we will work with dimensionless variables. We rescale the mass, length, velocity, potential, mass density, and energy[2] by M, L_0 (an arbitrary length scale), $V_0 = \sqrt{2\pi GML_0}$, $\psi_0 = 2\pi GML_0$, $\rho_0 = M/L_0$, and $E_0 = MV_0^2 = 2\pi GM^2L_0$, respectively. This is equivalent to considering $G = M = 1$ and to defining a dynamical time scale

$$\tau_D = (2\pi G\rho_0)^{-1/2}. \tag{21}$$

[2] A system's energy takes into account the total work necessary to bring a particle from infinity (or from a position where the potential is zero) to a position $\mathbf{q}$, i.e. $\int[\psi(\mathbf{q}) - \psi(\infty)]d\mathbf{q}$. For 3D self-gravitating systems the potential at infinity is zero, and for plasmas it is zero at the conducting wall. However, it is important to note that for 1D and 2D self-gravitating systems, the potential diverges at infinity. Since this divergent term appears in both the initial and the final state, the problem is avoided by using a renormalized energy, see Ref. [39] for more details.

Thus, the Poisson equation becomes

$$\nabla^2\psi(x,t) = 2\rho(x,t). \tag{22}$$

For a particle (sheet) of (reduced) mass density located at x', the density is $\rho(x,x') = \delta(x-x')$, and the long-range potential is given by the Green's function,

$$G(x,x') = |x-x'|. \tag{23}$$

A particularly interesting aspect of one-dimensional gravity is that the interaction potential does not have any singularities, which simplifies significantly molecular dynamics (MD) simulations, allowing us to explore in great detail the relaxation of this model to the qSS.

4.1. Molecular dynamics

The reduced Hamiltonian for a system of N particles interacting by a one-dimensional gravitational potential is

$$\mathcal{H}(x,v) = \sum_{i=1}^{N}\frac{v_i^2}{2} + \frac{1}{2N}\sum_{i,j}^{N}|x_i - x_j|. \tag{24}$$

This Hamiltonian, along with Hamilton's equations of motion, completely determines the dynamics of the system. The acceleration of a particle at position x, due to its interaction with the other $N-1$ particles, is given by

$$\ddot{x} = -\frac{1}{N}\sum_{i=1}^{N}\frac{x-x_i}{|x-x_i|}, \tag{25}$$

which may be expressed as

$$\ddot{x} = \frac{N_>(x) - N_<(x)}{N}, \tag{26}$$

where $N_>(x)$ and $N_<(x)$ represent the number of particles to the right and to the left of x, respectively. To simulate the system according to Eq. (26) requires time that scales with N^2. However, the simulation may be simplified by using a vector containing the indices of each particle, and reordering it according to each particle's position at each new calculation. The expression in Eq. (26) then may be written as

$$\ddot{x} = \frac{(N-i)-(i-1)}{N} = \frac{N-2i+1}{N}, \tag{27}$$

where i is the index of the particle at position x. This simplification involves no approximation; the advantage is purely computational, for the simulations become more efficient regarding the computational time [132]—the typical time required to order a vector of size N varies at most with $N\ln N$ [133]. Using this method, the trajectories may be obtained exactly, that is, at machine precision [132]. However, for the exact procedure, the trajectories must be calculated at each collision, and the number of collisions grows as N^2. Therefore, in our simulations, we used a fourth-order symplectic integrator, reordering the index vector at each time step and maintaining the relative error in energy at 10^{-5}.

We simulate numerically the evolution of a system of particles that are initially distributed uniformly with positions x_i where $x_i \in [-x_m, x_m]$ and velocities $v_i \in [-v_m, v_m]$, so that the initial distribution function is given by

$$f_0(x,v) = \eta\Theta(x_m - |x|)\Theta(v_m - |v|) \tag{28}$$

where $\eta = (4x_m v_m)^{-1}$. In order to calculate the initial energy, we must find the potential that is the solution of the Poisson equation (22) at $t = 0$,

$$\frac{d^2}{dx^2}\psi(x) = \begin{cases}\dfrac{1}{x_m} & \text{for } |x| \le x_m\\ 0 & \text{for } |x| \ge x_m\end{cases} \tag{29}$$

with boundary conditions $\lim_{|x|\to\infty}\psi(x) = |x|$ and $\psi'(0) = 0$. The solution is given by

$$\psi(x) = \begin{cases}\dfrac{x^2}{2x_m} + \dfrac{x_m}{2} & \text{for } |x| \le x_m\\ |x| & \text{for } |x| \ge x_m.\end{cases} \tag{30}$$

Using the definition of the mean energy, Eq. (17), the initial energy of the system is found to be

$$\mathcal{E}_0 = \frac{v_m^2}{6} + \frac{1}{3} \tag{31}$$

where without loss of generality we have set $x_m = 1$.

4.2. Equilibrium

If the system relaxes to equilibrium the gravitational potential must satisfy the Poisson equation

$$\nabla^2\psi(x) = 2n(x) \tag{32}$$

where $n(x)$ is the equilibrium density distribution. Using the Maxwell–Boltzmann distribution, $f_{mb}(x, v) = Ce^{-\beta(v^2/2+w(x))}$, the equilibrium density distribution is given by

$$n(x) = \int f_{mb}(x, v)\, dv = \sqrt{\frac{2\pi}{\beta}} Ce^{-\beta\omega(x)}, \tag{33}$$

where β is the Lagrange multiplier used to conserve total energy, C is the normalization constant and $\omega(x)$ is the potential of mean force [101]. As $N \to \infty$, interparticle correlations vanish and $\omega(x) \sim \psi(x)$. Substituting Eq. (33) into Eq. (32), we obtain the Poisson–Boltzmann equation in its dimensionless form

$$\nabla^2\psi_{eq}(x) = \sqrt{\frac{8\pi}{\beta}} Ce^{-\beta\psi_{eq}(x)}. \tag{34}$$

Solving this equation using the boundary conditions $\lim_{|x|\to\infty} \psi_{eq}(x) = |x|$ and $\psi'_{eq}(0) = 0$, the potential is found to be [124]

$$\psi_{eq}(x) = -\frac{1}{\beta} \ln\left[\frac{1}{4}\mathrm{sech}^2\left(\frac{\beta x}{2}\right)\right], \tag{35}$$

and the distribution function is given by

$$f_{eq}(x, v) = \sqrt{\frac{\beta^3}{32\pi}} e^{-\frac{\beta v^2}{2}} \mathrm{sech}^2\left[\frac{\beta x}{2}\right]. \tag{36}$$

The value of β is determined by the conservation of energy, Eq. (17) with $\bar{f}(x, v) = f_{eq}(x, v)$, yielding

$$\beta = \frac{3}{2\mathcal{E}}. \tag{37}$$

The equilibrium density and velocity distributions are given by

$$n(x) = \frac{\beta}{4}\mathrm{sech}^2\left(\frac{\beta x}{2}\right) \tag{38}$$

and

$$n(v) = \sqrt{\frac{\beta}{2\pi}} e^{-\beta v^2/2}. \tag{39}$$

In Fig. 3 we compare the equilibrium distributions, Eqs. (38) and (39), with the results of MD simulations. As can be seen, the predictions of equilibrium statistical mechanics are very different from those of MD simulations. This clearly shows that the ergodicity required by the Boltzmann–Gibbs statistical mechanics is violated.

In the next section we will compare the predictions of Lynden-Bell statistics with the results of MD simulations.

4.3. Lynden-Bell theory for one-dimensional gravity

The application of Lynden-Bell statistics to one-dimensional gravitational systems has spanned various decades, with divergent results. While early studies have suggested some correspondence between numerical simulations and the predictions of LB statistics, especially for low-energies, they have also shown the occurrence of high-energy tails in the distribution, which LB statistics could not describe [29,134–137]. More recent works demonstrated that although for some very specific initial conditions LB theory agrees well with MD simulations, in general it fails to describe the qSS [112,127,138,139]. In this section we will examine the predictions of LB statistics and compare them with the results of MD simulations for various initial conditions.

In order to determine $f_{lb}(x, v)$, Eq. (19), for a one-dimensional gravitational system, we need to calculate the gravitational potential $\psi_{lb}(x)$. To do this we must solve the Poisson equation (Eq. (22)) with $f(x, v) = f_{lb}(x, v)$ and the one-particle energy given by $\epsilon(x, v) = v^2/2 + \psi_{lb}(x)$. Integrating the LB distribution over momentum, we obtain the Poisson equation

$$\frac{d^2\psi_{lb}(x)}{dx^2} = -\sqrt{\frac{8\pi}{\beta}}\eta\, \mathrm{Li}_{1/2}\left[-e^{-\beta(\psi_{lb}(x)-\mu)}\right], \tag{40}$$

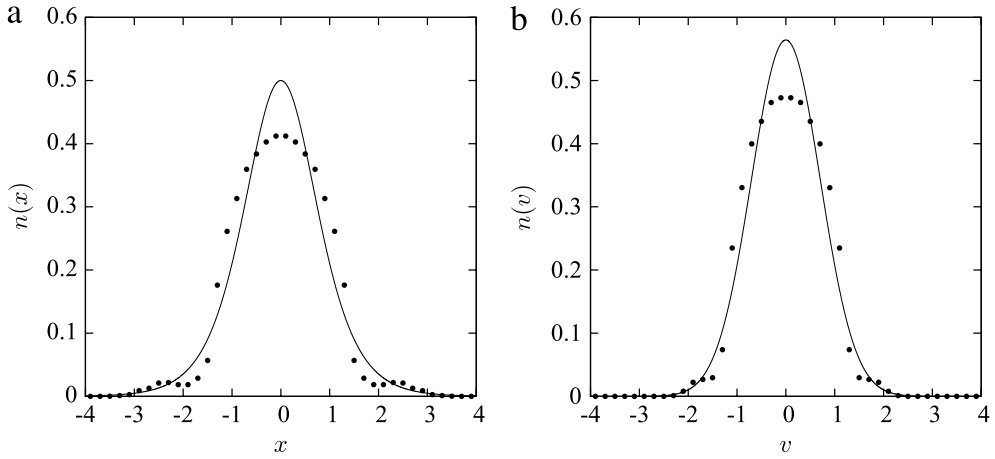

Fig. 3. Distributions in (a) position and (b) velocity for a 1D gravitational system with $\mathcal{E}_0 = 0.75$, obtained using MD simulations with $N = 2 \times 10^4$ (points), averaged over times $t = 1000\tau_D$ to $t = 1100\tau_D$, compared with the equilibrium distributions (lines), given by Eqs. (38) and (39). Repeating the MD simulation for the same initial energy, but different initial conditions, and taking the average value of the resulting distributions, error bars are smaller than the symbol size.

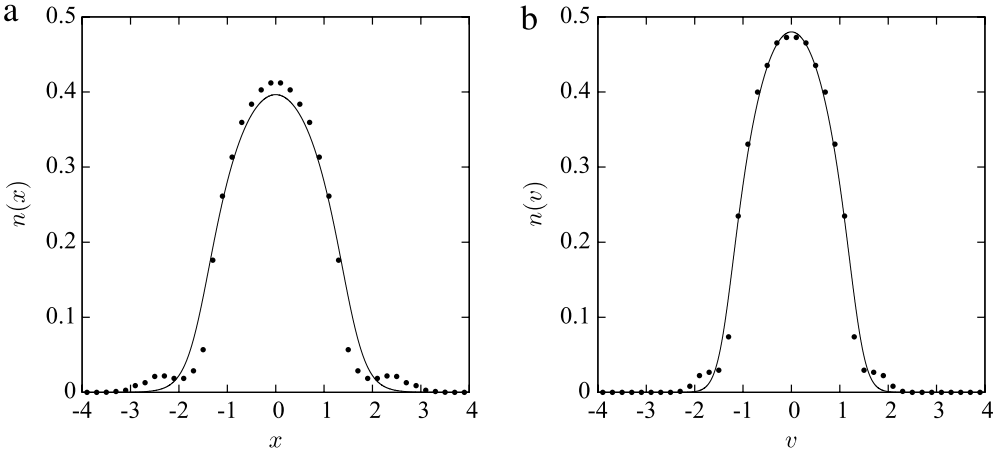

Fig. 4. Distributions in (a) position and (b) velocity for a 1D gravitational system with $\mathcal{E}_0 = 0.75$, obtained using MD simulations with $N = 2 \times 10^4$ (points), averaged over $t = 1000\tau_D$ and $t = 1100\tau_D$, compared with the LB distributions (lines), $n(x) = \int f_{lb}(x, v)dv$ and $n(v) = \int f_{lb}(x, v)dx$ with $f_{lb}(x, v)$ given by Eq. (19). Error bars are smaller than the symbol size.

with boundary conditions $\lim_{|x|\to\infty} \psi_{lb}(x) = |x|$ and $\psi'_{lb}(0) = 0$, where $\mathrm{Li}_n(x)$ is the polylogarithm function of order n [140]. The solution to this equation is obtained numerically. We see that the predictions of LB statistics are in general quite different from the results of MD simulations, as exemplified in Fig. 4, which compares the position and the velocity distributions $n(x) = \int f_{lb}(x, v)dv$ and $n(v) = \int f_{lb}(x, v)dx$ with the results of MD simulations.

The problem, common to both BG and LB statistics, is that in the thermodynamic limit, systems with LR forces are intrinsically non-ergodic, invalidating the basic assumptions that underlie both theories. For systems with a finite number of particles, however, ergodicity is restored on a sufficiently long time scale. Such systems will eventually relax to the BG equilibrium (if it exists, and the BG entropy has a maximum), after being trapped in a qSS for a time proportional to the number of particles in the system.

The Kac scaling required by the LR nature of the interaction potential destroys the correlations (collisions) between the particles [101]. Therefore, in the thermodynamic limit, LR systems are intrinsically collisionless — particles move under the action of the mean-field potential produced by all the other particles. In general, the mean-field potential has a complex dynamics, characterized by quasi-periodic oscillations [125]. It is possible, therefore, for some particles to enter in resonance with the oscillations and gain large amounts of energy at the expense of the collective motion [46,141,142]. This process is known as Landau damping [143]. The Landau damping diminishes the amplitude of the oscillations and leads to the formation of a tenuous halo of highly energetic particles which surround the high density core [144]. After all the oscillations have died out, a SS state is established. The phase space distribution of particles in the SS has a characteristic core–halo structure, very different from the predictions of either BG or LB statistics. Once the stationary state is established, there is no longer a mechanism through which highly energetic particles of the halo can equilibrate with the particles of the core, and the ergodicity is broken.

4.4. The virial condition

If the system is in a stationary state, it must satisfy the virial theorem. Consider a system with a Hamiltonian given by

$$\mathcal{H} = \sum_i \frac{\mathbf{p}_i^2}{2m_i} + \frac{1}{2}\sum_{i,j} V(\mathbf{r}_i - \mathbf{r}_j) + \frac{\kappa}{2}\sum_{i=1}^{N} |\mathbf{r}_i|^\gamma \tag{41}$$

where $(\mathbf{r}_i, \mathbf{p}_i)$ are respectively the coordinates of position and momentum of the ith particle, $V(\mathbf{r}_i - \mathbf{r}_j)$ is the interaction potential and $(\kappa/2)\sum_{i=1}^{N}(\mathbf{r}_i)^\gamma$ is a generic confining potential. The virial function I is defined as

$$I = \left\langle \sum_i \mathbf{r}_i \cdot \mathbf{p}_i \right\rangle, \tag{42}$$

where $\langle x \rangle$ represents a time average. Differentiating the virial function with respect to time and using Hamilton's equations [145], we find

$$\frac{d}{dt} I = \left\langle \sum_i \frac{\mathbf{p}_i^2}{m_i} \right\rangle - \left\langle \sum_i \mathbf{r}_i \cdot \frac{\partial}{\partial \mathbf{r}_i} \left(\tilde{V} + \frac{\kappa}{2} \sum_j |\mathbf{r}_j|^\gamma \right) \right\rangle, \tag{43}$$

where

$$\tilde{V} = \frac{1}{2}\sum_{j,k} V(\mathbf{r}_j - \mathbf{r}_k). \tag{44}$$

If $\tilde{V}$ is a homogeneous function of order p, that is, $\tilde{V}(\mathbf{r}) = \lambda^{-p}\tilde{V}(\lambda\mathbf{r})$, then by Euler's theorem,

$$p\tilde{V} = \sum_i \mathbf{r}_i \cdot \frac{\partial}{\partial \mathbf{r}_i}\tilde{V}.$$

For a stationary state, $dI/dt = 0$, which determines the virial condition

$$2K - pU - \frac{\gamma\kappa}{2} r_m^\gamma = 0 \tag{45}$$

where $K = \frac{1}{N}\langle \sum_i^N \mathbf{p}_i^2/2m_i \rangle$ is the average kinetic energy per particle in a SS, $U = \frac{1}{N}\langle \tilde{V} \rangle$ is the average potential energy per particle in a SS, and $r_m^\gamma = \frac{1}{N}\langle \sum_i^N |\mathbf{r}_i|^\gamma \rangle$. In the case of two-dimensional gravity,[3] which will be discussed in Section 5, the interaction potential is logarithmic, $V = 2Gm^2 \ln(|\mathbf{r}_i - \mathbf{r}_j|)$, and is not a homogeneous function. However, writing the logarithm as $\ln x = \lim_{p\to 0}\left(\frac{x^p}{p} - \frac{1}{p}\right)$, after some manipulation (see [39]), we find

$$GM^2 \frac{(N-1)}{N} = \sum_i \mathbf{r}_i \cdot \frac{\partial}{\partial \mathbf{r}_i}\tilde{V}. \tag{46}$$

Using Eq. (46) in Eq. (43), the virial condition for a 2D gravitational system is found to be

$$\langle v^2 \rangle = GM\frac{N-1}{N} \tag{47}$$

where we have set $\kappa = 0$ in Eq. (41).

In 1D the gravitational potential is a homogeneous function of order $p = 1$, so that the virial condition reduces to

$$2K = U. \tag{48}$$

If at $t = 0$ the initial distribution function is not a stationary solution of the Vlasov equation, the system will undergo oscillations. When the relaxation is completed and a qSS is established, Eq. (48) must be satisfied. However, even if the initial distribution function does not satisfy the stationary Vlasov equation – as is the case for the waterbag distributions considered above – we can significantly diminish the amplitude of oscillations during the relaxation process if the initial distribution is forced to satisfy the virial condition, Eq. (48). For such distributions, even though the initial state is not stationary, it is not "too far" from a qSS. To quantify this, we define the virial number for 1D gravity as $\mathcal{R} = 2K/U$. When $\mathcal{R} = 1$, the virial condition is satisfied and the oscillations should be suppressed; on the other hand, if $\mathcal{R} \neq 1$, the system will experience strong density oscillations due to the imbalance between the kinetic and the potential energies. We expect that the process of relaxation to the qSS should be quite different for these two cases. Indeed, we find that when $\mathcal{R}_0 = 1$, where $\mathcal{R}_0$ is the virial number at time $t = 0$, the resulting qSS has a compact structure, which is reasonably well captured by LB theory, see Fig. 5. On the other hand when $\mathcal{R}_0 \neq 1$, the system separates into a central core surrounded by a halo of highly energetic particles. To understand the mechanism of the core–halo formation, we need to explore the parametric resonances which appear as a result of the density oscillations.

[3] The specific case of two-dimensional gravity is addressed in Ref. [146], which presents a study of the virial theorem in the general case of d dimensions and includes terms for friction and noise.

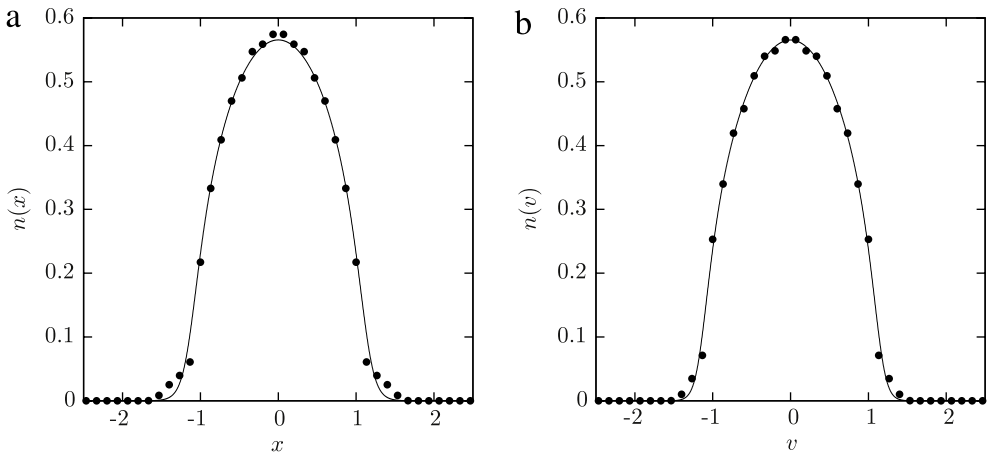

Fig. 5. Distributions in (a) position and (b) velocity of a system that initially was in a waterbag distribution with $\mathcal{R}_0 = 1$. The solid line represents the predictions of LB theory, Eq. (19), while the points are results of MD simulation with $N = 2 \times 10^4$, averaged over $t = 1000\tau_D$ to $t = 1100\tau_D$. For this case, LB theory provides a fairly accurate approximation for the qSS distribution, despite a small deviation in the distribution tails. Error bars in the distributions are comparable to the symbol size.

4.5. The envelope equation

To explore the density oscillations, we define the envelope $x_e(t)$ to be the extent of the system, $x_e(t) \equiv \sqrt{3\langle x^2(t)\rangle}$. Note that at $t = 0$, the envelope $x_e(t)$ coincides with the boundary of the initial waterbag distribution, $x_e(0) = 1$. Differentiating $x_e(t)$ twice with respect to time, we have

$$\ddot{x}_e(t) = \frac{3\langle x(t)\ddot{x}(t)\rangle}{x_e(t)} + \frac{3\langle \dot{x}^2(t)\rangle}{x_e(t)} - \frac{9\langle x(t)\dot{x}(t)\rangle^2}{x_e^3(t)}. \tag{49}$$

To simplify the first term, we suppose that the mass density oscillations are smooth, so that the particle distribution remains uniform. Under these conditions, the oscillating gravitational potential $\psi_e(x, t)$ maintains the functional form given by Eq. (30), but with $x_m \to x_e(t)$,

$$\psi_e(x, t) = \begin{cases} \dfrac{x^2}{2x_e(t)} + \dfrac{x_e(t)}{2} & \text{for } |x| \le x_e(t) \\ |x| & \text{for } |x| \ge x_e(t). \end{cases} \tag{50}$$

Similarly, the distribution function will be approximated by a waterbag

$$f_e(x, v, t) = \eta_e \Theta(x_e(t) - |x|)\Theta(v_m - |v|) \tag{51}$$

with $\eta_e = [4x_e(t)v_m]^{-1}$. The average $\langle x\ddot{x}\rangle$ can then be expressed as

$$\begin{aligned} \langle x\ddot{x}\rangle &= -\left\langle x\frac{d}{dx}\psi_e(x, t)\right\rangle \\ &= -\int x\frac{d}{dx}\psi_e(x, t)f_e(x, v, t)\,dx\,dv \\ &= -\frac{1}{2x_e(t)}\int_{-x_e(t)}^{x_e(t)} \frac{x^2}{x_e(t)}\,dx, \end{aligned} \tag{52}$$

resulting in

$$\langle x\ddot{x}\rangle = -\frac{x_e(t)}{3}. \tag{53}$$

The second and the third terms of Eq. (49) are

$$\langle \dot{x}^2\rangle = \frac{1}{2v_m}\int_{-v_m}^{v_m} v^2\,dv = \frac{v_m^2}{3} \tag{54}$$

and

$$\langle x\dot{x}\rangle = \frac{1}{4x_e(t)v_m}\int_{-x_e(t)}^{x_e(t)} x\,dx \int_{-v_m}^{v_m} v\,dv = 0, \tag{55}$$

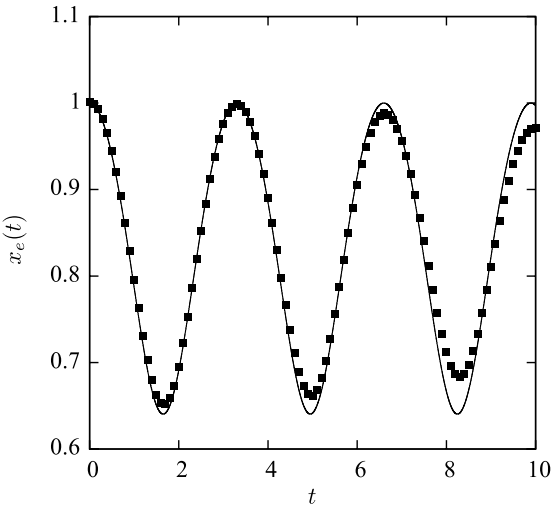

Fig. 6. Oscillations of the envelope $x_e(t)$ determined by Eq. (56) (solid line) compared to results of MD simulation (squares). The virial number is $\mathcal{R}_0 = 0.5$.

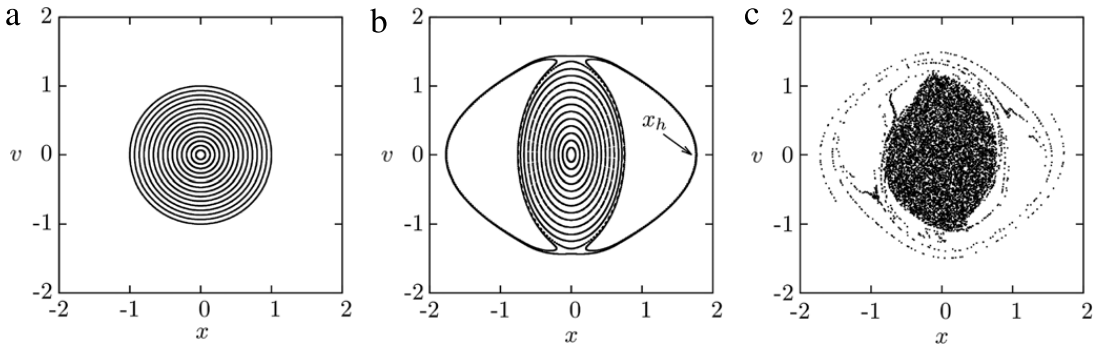

Fig. 7. Poincaré sections of test particle dynamics (see Eq. (58)) for $\mathcal{R}_0 \approx 1$ (a) and $\mathcal{R}_0 = 0.5$ (b). In (a) the dynamics is integrable while in (b), two resonance islands are formed. Panel (c) shows the phase space obtained using MD simulation of a 1D self-gravitating system with $\mathcal{R}_0 = 0.5$ at $t = 7$. The test particle dynamics enables us to determine the maximum energy ϵ_h that a particle in the full N-body simulation can achieve. In the case of 1D gravitation, $\epsilon_h = |x_h|$, where x_h, indicated in panel (b), is the maximum position reached by a test particle.

considering that at $t = 0$ there is no correlation between position and velocity. The envelope equation reduces to

$$\ddot{x}_e(t) = \frac{\mathcal{R}_0}{x_e(t)} - 1, \tag{56}$$

where $\mathcal{R}_0 = 2K(t = 0)/U(t = 0) = v_m^2$ and the initial conditions are $x_e(0) = 1$ and $\dot{x}_e(t) = 0$. If $\mathcal{R}_0 = 1$, then $\ddot{x}_e(t) = 0$, and the system does not develop oscillations. Fig. 6 compares the oscillations of the envelope predicted by Eq. (56) with the results of MD simulation, showing a reasonable agreement for short times.

4.6. The test particle model

To understand the mechanism of halo formation, we first study the dynamics of noninteracting test particles initially located at positions $x_i^0 \in [-1, 1]$ with velocities $v_i^0 \in [-v_m, v_m]$, where $v_m = \sqrt{\mathcal{R}_0}$. Each particle moves in a gravitational potential produced by the oscillating mass density

$$\rho(t) = \frac{1}{2x_e(t)}\Theta(x_e(t) - |x|) \tag{57}$$

where $x_e(t)$ is governed by the envelope equation, Eq. (56). The trajectory of a test particle is then determined by the equation of motion

$$\ddot{x}_i(t) = \begin{cases} -\dfrac{x_i(t)}{x_e(t)} & \text{for } |x_i(t)| \le x_e(t) \\ -\operatorname{sgn}[x_i(t) - x_e(t)] & \text{for } |x_i(t)| \ge x_e(t) \end{cases} \tag{58}$$

where sgn is the sign function [147].

In Fig. 7 we show the Poincaré sections for test particle dynamics. When $\mathcal{R}_0 = 1$, the trajectories of the test particles correspond to harmonic oscillators and the dynamics is completely regular; on the other hand, when $\mathcal{R}_0 \neq 1$, we see the

appearance of resonance islands. At short times a very similar structure of the phase space is also found in the complete MD simulation, as shown in panel (c) of the same figure. The formation of resonance islands is the result of the particle(density)-wave interactions [148–150]. The parametric resonances allow some particles to move into the regions of the phase space which are highly improbable from the perspective of BG or LB statistics. Once the oscillations die out, these particles are trapped, becoming a part of a halo.

4.7. The core–halo distribution

From the Jeans theorem, a steady-state solution of the Vlasov equation depends on the phase space coordinates only through the integrals of motion of the mean-field potential. Conversely, any function of the integrals of motion is a steady-state solution of the Vlasov equation [64]. In all the cases treated in this Report, the only integral of motion is the one-particle energy. Thus, a Maxwell–Boltzmann distribution is only one of the infinite number of solutions of the Vlasov equation. In particular an arbitrary initial distribution will not converge to the Maxwell–Boltzmann distribution, as is the case for systems with finite-range forces.

Unlike gravitation in three dimensions, in 1D particles cannot escape to infinity. The test particle dynamics shows, however, that the resonant particles may gain a lot of energy from collective oscillations and form a tenuous high-energy halo that surrounds the central core region. Since the Hamiltonian dynamics is conservative, the gain of energy of resonant particles must result in the loss of energy (cooling down) of the core particles. In principle, the halo formation will continue until the oscillations of the core have completely died down. Once the SS state is established, the core particles should be in the "ground state". The incompressibility constraint imposed by the Vlasov dynamics, however, does not allow the core particles to collapse to the minimum of the potential energy. Rather, these particles will arrange in such a way as to occupy all of the low energy states up to the allowed maximum phase space density η,

$$\bar{f}_{core}(x, v) = \eta\Theta(\epsilon_F - \epsilon(x, v)), \tag{59}$$

where ϵ_F is the "Fermi energy" of the core.

The maximum energy that a halo particle can gain corresponds to the resonant orbit. As the oscillations die down, the resonances shift toward the smaller energies, resulting in a quasi-homogeneous population of the phase space between ϵ_F and the maximum halo energy, ϵ_h. We will, therefore, suppose that in a qSS the halo particles are distributed according to

$$\bar{f}_{halo}(x, v) = \chi\Theta(\epsilon(x, v) - \epsilon_F)\Theta(\epsilon_h - \epsilon(x, v)), \tag{60}$$

where χ is the phase space density of the halo particles and the maximum halo energy, ϵ_h, can be calculated using the test particle dynamics and is given by $\epsilon_h = |x_h|$, see Fig. 7. The complete core–halo distribution is then

$$\bar{f}_{ch}(x, v) = \eta\Theta(\epsilon_F - \epsilon(x, v)) + \chi\Theta(\epsilon(x, v) - \epsilon_F)\Theta(\epsilon_h - \epsilon(x, v)). \tag{61}$$

From now on, for simplicity we will write f_{ch} instead of $\bar{f}_{ch}$. After determining ϵ_h using the test particle dynamics, two unknowns remain, ϵ_F and χ, which are obtained using the conservation of the total energy and the number of particles in the system. Integrating the core–halo distribution function over velocities and substituting the resulting particle density into the Poisson equation, the gravitational potential is found to satisfy

$$\frac{d^2}{dx^2}\psi_{ch}(x) = 2\sqrt{2}\begin{cases}(\eta - \chi)\sqrt{\epsilon_F - \psi_{ch}(x)} + \chi\sqrt{\epsilon_h - \psi_{ch}(x)} & \text{for } \psi_{ch}(x) \le \epsilon_F,\\ \chi\sqrt{\epsilon_h - \psi_{ch}(x)} & \text{for } \epsilon_F \le \psi_{ch}(x) \le \epsilon_h,\\ 0 & \text{for } \psi_{ch}(x) \ge \epsilon_h,\end{cases} \tag{62}$$

with the boundary conditions given by $\lim_{|x|\to\infty}\psi_{ch}(x) = |x|$ and $\psi'_{ch}(0) = 0$. The parameters χ and ϵ_F are determined self-consistently from the numerical solution of Eq. (62) and the conservation of the total energy and the number of particles (Eqs. (17) and (18)) in the system. Once the potential is known we can easily calculate the distributions $n(x) = \int f_{ch}(x, v)\,dv$ and $n(v) = \int f_{ch}(x, v)\,dx$, see Fig. 8.

4.8. Thermodynamic equilibrium

For finite N, correlations are not completely negligible and eventually they will drive the system to thermodynamic equilibrium. The equilibrium state should be described by the MB distribution Eq. (36), discussed in Section 4.2. Therefore if the number of particles in the system is not too large and the simulation is run for a sufficiently long time the thermodynamic equilibrium should be observed. Fig. 9 shows the results of MD simulation for $t = 3 \times 10^6\tau_D$. We see that after this time the system indeed relaxes to the thermodynamic equilibrium with the particle distribution given by Eq. (36).

The approach to equilibrium can be observed using a crossover parameter, $\zeta(t)$, which measures how well the system's density profile is described by the core–halo distribution $f_{ch}(x, v)$, Eq. (61) at each instant. We define

$$\zeta(t) = \frac{1}{N^2}\int [N(x, t) - N_{ch}(x)]^2 dx \tag{63}$$

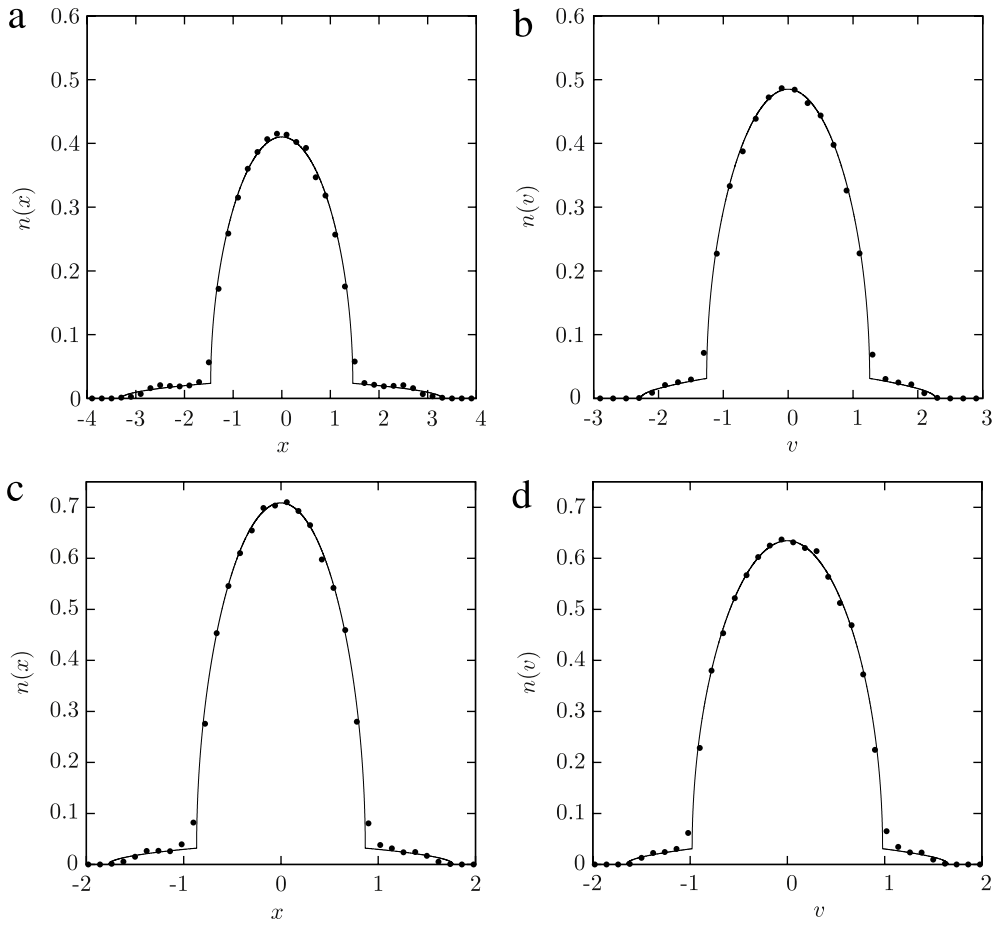

Fig. 8. Distributions inside qSS in (a) position and (b) velocity, for a system with $\mathcal{R}_0 = 2.5$, and distributions in (c) position and (d) velocity for a system with $\mathcal{R}_0 = 0.5$. Points show the results of MD simulations with $N = 2 \times 10^4$ averaged over $t = 1000\tau_D$ to $t = 1100\tau_D$, and the solid lines correspond to the marginal distributions predicted by the core–halo theory. Error bars in the distributions are comparable to the symbol size.

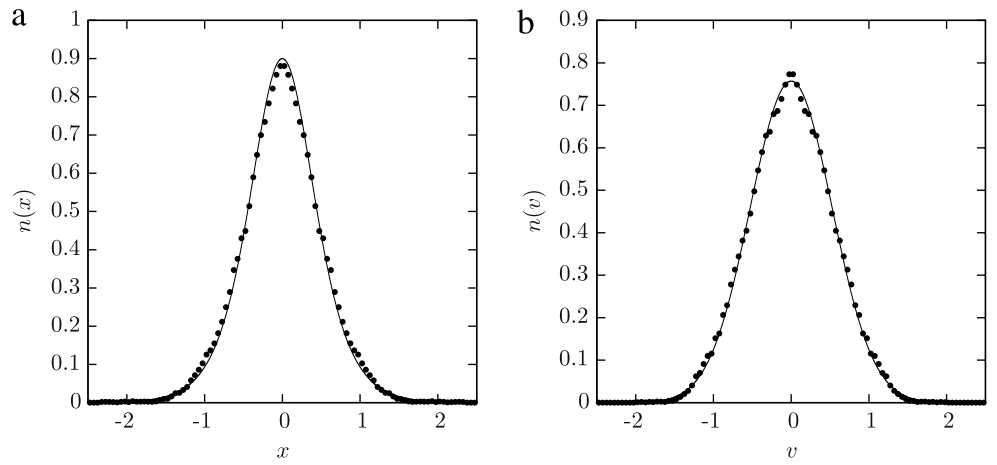

Fig. 9. Equilibrium distributions: (a) position and (b) velocity, for a system with $\mathcal{R}_0 = 2.5$ at time $t = 3 \times 10^6 \tau_D$, obtained using MD simulation with $N = 1000$ (points). Solid lines are the predictions of BG statistics, Eqs. (38) and (39).

where $N(x, t)$ is the number of particles located between x and $x + dx$ at time t and $N_{ch}(x) = N \int f_{ch}(x, v)dv$. The smaller the value of $\zeta(t)$, the better the agreement between the system's marginal distribution in position and the predicted distribution of the core–halo theory. When the system starts to cross over to equilibrium, $\zeta(t)$ begins to deviate from its minimum, growing until it reaches the equilibrium value, given by $\zeta_{eq} = \frac{1}{N^2} \int [N_{mb}(x) - N_{ch}(x)]^2 dx$ where $N_{mb}(x) = Nn(x)$ with $n(x)$ given by Eq. (38). In Fig. 10, we show the evolution of $\zeta(t)$ for different values of N. After relaxing to the qSS, $\zeta(t)$ rises and approaches the equilibrium value. Rescaling time with $\tau_\times = \tau_D N^\gamma$, with $\gamma = 1.8$, all the curves collapse onto one universal curve. This value of γ is approximate — to find a precise value of γ, a very large number of particles must be used in MD simulations. Nevertheless, the observed value of γ agrees quite well with the exponent $\gamma = 2$ predicted by the theoretical

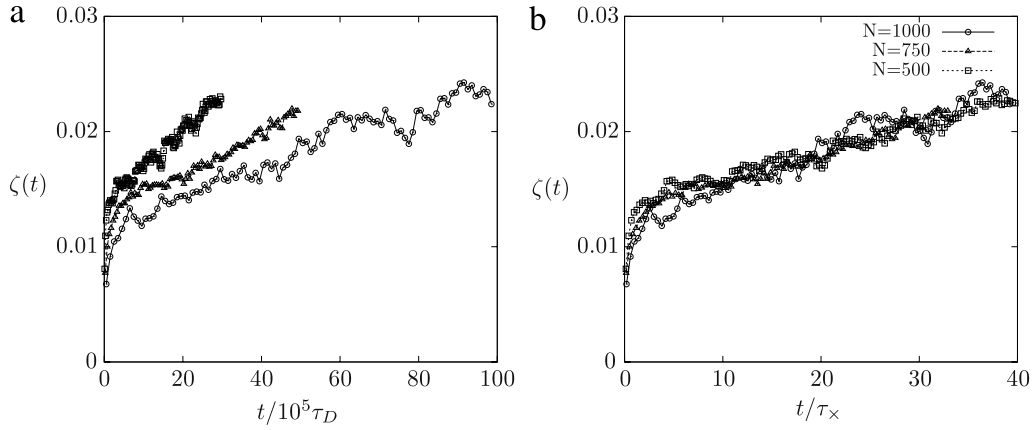

Fig. 10. Relaxation to equilibrium, shown by the crossover parameter $\zeta(t)$, Eq. (63), with time rescaled by $10^5\tau_D$ in (a) and by $\tau_\times = \tau_D N^{1.8}$ in (b). In this case, the equilibrium value ζ_{eq} is approximately 0.032. The virial number is $R_0 = 0.5$.

argument of Section 2. While our simulations find $\gamma = 1.8$, other previous simulations with smaller number of particles find $\gamma = 1$ [115], $\gamma = 2$ [151] and greater [31,32,152].

5. Gravitation in two dimensions

We next consider self-gravitating systems in two dimensions. Such systems and their dynamics have been applied to study topics ranging from the spiral structure of disk-like galaxies [113,114,153] to the large-scale structure of the universe [154]. They have also been analyzed in the context of equilibrium thermodynamics [155,156].

The system consists of N particles of mass m in a two-dimensional space. The total mass of the system is $M = mN$. It is convenient to define dimensionless variables by rescaling length, velocity, potential, and energy with respect to L_0 (an arbitrary length scale), $V_0 = \sqrt{2GM}$, $\psi_0 = 2GM$ and $E_0 = MV_0^2 = 2GM^2$, respectively, where G is the gravitational constant. This process is equivalent to setting $M = G = 1$ and to defining the dynamical time

$$\tau_D = \frac{L_0}{\sqrt{2GM}}. \tag{64}$$

In three-dimensional space, the system corresponds to rods of mass density m [155].

Considering only systems with azimuthal symmetry, the corresponding gravitational potential ψ satisfies the dimensionless Poisson equation,

$$\nabla^2\psi(r,t) = 2\pi\rho(r,t), \tag{65}$$

where $\rho(r,t)$ is the mass density of a self-gravitating system which is obtained from the one particle distribution function, $\rho(r,t) = \int f(r,\mathbf{v};t)\,d^2v$. For an isolated particle the density is

$$\rho(\mathbf{r},\mathbf{r}') = \delta(|\mathbf{r}-\mathbf{r}'|), \tag{66}$$

so that the Green's function solution to Eq. (65) is

$$G(\mathbf{r},\mathbf{r}') = \ln|\mathbf{r}-\mathbf{r}'|. \tag{67}$$

The Hamiltonian for a N particle gravitational system is then

$$\mathcal{H} = \sum_{i=1}^{N}\frac{p_i^2}{2m} + \frac{m^2}{2}\sum_{i,j=1}^{N}\ln|\mathbf{r}_i-\mathbf{r}_j|. \tag{68}$$

5.1. Molecular dynamics

We will study 2D gravitational systems in the thermodynamic limit. In this limit, if the initial distribution is azimuthally symmetric, the mean-field potential will also retain this symmetry, so that the angular momentum, $p_\theta = mr^2\dot\theta$, of each particle is conserved. This allows us to use an effective Hamiltonian description based on Gauss's law. A particle at position r_i is subject to an interaction potential produced by all the particles with $r \le r_i$, leading to an effective Hamiltonian

$$\mathcal{H}_{eff}(r_i,\theta_i,p_{r_i},p_{\theta_i}) = \sum_{i=1}^{N}\left(\frac{p_{r_i}^2}{2m} + \frac{p_{\theta_i}^2}{2mr_i^2}\right) + \sum_{i=1}^{N} m_{eff}(r_i)m\ln r_i, \tag{69}$$

where

$$m_{eff}(r_i) = m\sum_{j=1}^{N}\Theta(r_i - r_j), \tag{70}$$

is the mass of all the particles with the radial coordinates $r < r_i$. The equation of motion for r_i is then

$$\ddot{r_i} = \frac{v_{\theta_i}^2}{r_i^3} - \frac{m_{eff}(r_i)}{r_i}, \tag{71}$$

where $v_{\theta_i} = p_\theta/m$ is determined by the initial distribution. The advantage of the effective Hamiltonian is that the simulation time of the system's dynamics depends exclusively on the time of sorting a vector composed of N elements, similar to 1D gravity.

At the start of the simulation the N point particles are distributed uniformly inside a circle of radius r_m. They are also assigned velocities from a uniform distribution with the maximum value v_m. This corresponds to a one-level initial distribution of the form

$$f_0(r, v) = \eta\Theta(r_m - r)\Theta(v_m - v) \tag{72}$$

where $\eta = (\pi^2 r_m^2 v_m^2)^{-1}$ is the normalization constant.

Since in the thermodynamic limit the mean-field potential is purely radial, the angular momentum of each particle will remain constant throughout the simulation. The radial dynamics of each particle is then determined by the Eq. (71), while the $\theta_i(t)$ dynamics is controlled by the angular momentum conservation $v_{\theta_i}(t) = v_{\theta_i}(0)$. The magnitude of the velocity of the particle i is $v_i = \sqrt{v_{r_i}^2 + (r_i\dot{\theta}_i)^2}$.

The potential ψ associated with the initial distribution satisfies the Poisson equation,

$$\frac{d^2\psi(r)}{dr^2} + \frac{1}{r}\frac{d\psi(r)}{dr} = \begin{cases} \dfrac{2}{r_m^2} & \text{for } r \le r_m \\ 0 & \text{for } r > r_m \end{cases} \tag{73}$$

with the boundary conditions given by $\lim_{r\to\infty}\psi(r) = \ln(r)$ and $\psi'(0) = 0$. The solution to this equation is

$$\psi(r) = \begin{cases} \dfrac{r^2 - r_m^2}{2r_m^2} + \ln(r_m) & \text{for } r \le r_m \\ \ln(r) & \text{for } r > r_m. \end{cases} \tag{74}$$

Using this potential, Eq. (74), and the initial distribution function, Eq. (72), in the expression for conservation of energy, Eq. (17), the initial energy of the system is calculated to be

$$\mathcal{E}_0 = \frac{v_m^2}{4} - \frac{1}{8}, \tag{75}$$

where without loss of generality we have set $r_m = 1$.

We now consider two cases: one in which the initial distribution obeys the virial condition ($\mathcal{R}_0 = 1$) and one in which it does not ($\mathcal{R}_0 \neq 1$). In Section 4.4, we have shown that the virial condition for a two-dimensional gravitational system requires that $\langle v^2\rangle = GM(N-1)/N$. In the thermodynamic limit, using the rescaled variables, the virial condition reduces to

$$\langle v^2\rangle = \frac{1}{2}. \tag{76}$$

We then define the virial number for a 2D gravitational system to be

$$\mathcal{R} = 2\langle v^2\rangle. \tag{77}$$

5.2. Lynden-Bell theory for a 2D self-gravitating system

In analogy with 1D gravity, if the initial distribution of a 2D self-gravitating system obeys the virial condition, we expect that the parametric resonances will not be excited and the qSS should be well described by the Lynden-Bell statistics. The mean-field potential should then satisfy the Poisson equation with the mass density given by the momentum integral of Eq. (19),

$$\frac{d^2\psi_{lb}(r)}{dr^2} + \frac{1}{r}\frac{d\psi_{lb}(r)}{dr} = \frac{4\pi^2\eta}{\beta}\ln[1 + e^{-\beta(\psi_{lb}(r)-\mu)}]. \tag{78}$$

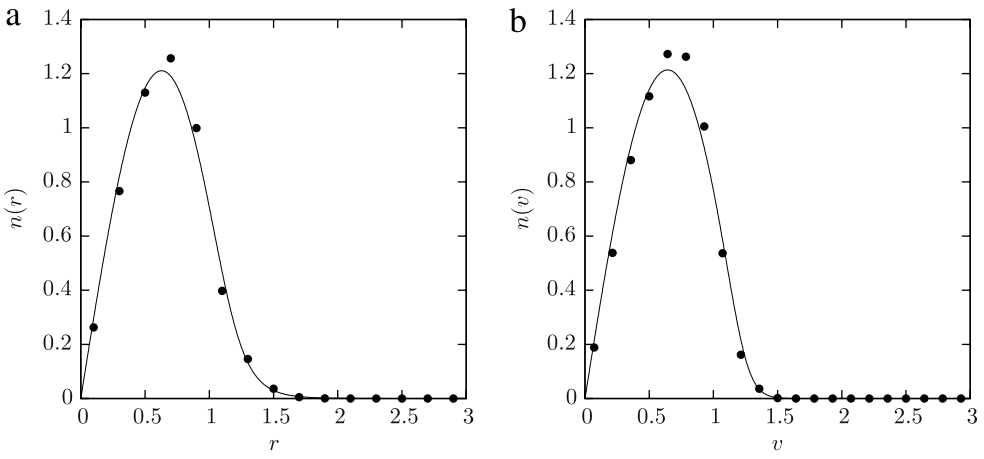

Fig. 11. Particle distributions in (a) position and (b) velocity of a 2D gravitational system that initially satisfied the virial condition. The solid lines represent the prediction of LB statistics, $n(r) = N(r)/N$ and $n(v) = N(v)/N$, with $N(r)$ and $N(v)$ given by Eqs. (79) and (80). Points are results of MD simulation for $N = 10{,}000$ particles, averaged over times $t = 1000$ to $t = 1100$. Error bars in the distributions are comparable to the symbol size.

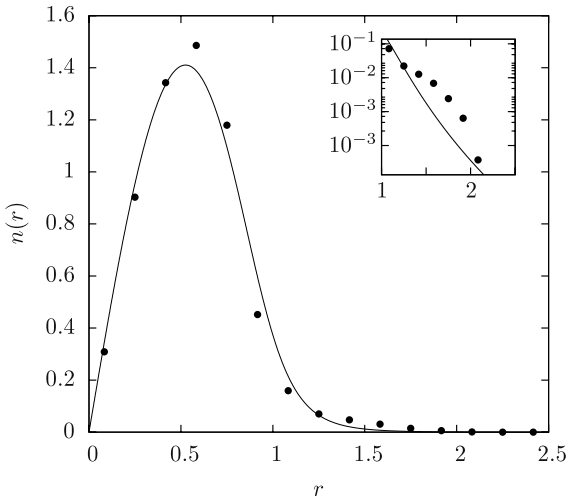

Fig. 12. Distribution in position for a 2D self-gravitating system with $\mathcal{R}_0 = 0.694$. The solid line represents the prediction of LB theory, $n(r) = N(r)/N$ with $N(r)$ given by Eq. (79), while the symbols are the results of MD simulation with $N = 10{,}000$ particles, averaged over times $t = 2000$ to $t = 2100$. Error bars in the distributions are comparable to the symbol size.

The boundary conditions for this equation are $\lim_{r\to\infty} \psi_{lb}(r) = \ln(r)$ and $\psi'_{lb}(0) = 0$. The parameters β and μ are determined self-consistently by the conservation of energy and norm of the distribution function, Eqs. (17) and (18). Once $\psi_{lb}(r)$, β, and μ are calculated, we can compare the theoretical predictions with the results of the MD simulations. To do this we calculate the marginal distributions: the number of particles located between $[r, r + dr]$,

$$N(r) = 2\pi N r \int d^2\mathrm{v} f_{lb}(\mathbf{r}, \mathbf{v}) = \frac{4Nr}{\beta v_m^2} \ln[1 + e^{-\beta(\psi_{lb}(r)-\mu)}]\,; \tag{79}$$

and the number of particles with velocities between $[v, v + dv]$,

$$N(v) = 2\pi N v \int d^2\mathrm{r} f_{lb}(\mathbf{r}, \mathbf{v}). \tag{80}$$

Comparing the theory and the simulation, we see a reasonably good agreement between the LB statistics and the results of MD simulations, Fig. 11. However, if the initial distribution does not satisfy the virial condition, LB theory starts to deviate from the results of MD simulations. A tail in the marginal distribution functions emerges, showing the formation of a core–halo structure, see Fig. 12.

5.3. The envelope equation

The appearance of the core–halo structure is a consequence of the parametric resonances which arise from the density oscillations. To study these oscillations we define the envelope of the particle distribution as $r_e(t) = \sqrt{2\langle \mathbf{r} \cdot \mathbf{r} \rangle}$. Note that

with this definition $r_e(0) = r_m$. Differentiating $r_e(t)$ twice with respect to time, we find

$$\ddot{r}_e(t) = \frac{2\langle \mathbf{r}\cdot\ddot{\mathbf{r}}\rangle}{r_e(t)} + \frac{2\langle \dot{\mathbf{r}}\cdot\dot{\mathbf{r}}\rangle}{r_e(t)} - \frac{4\langle \mathbf{r}\cdot\dot{\mathbf{r}}\rangle^2}{{r_e}^3(t)}, \tag{81}$$

which can be rewritten as

$$\ddot{r}_e(t) = \frac{2\langle \mathbf{r}\cdot\ddot{\mathbf{r}}\rangle}{r_e(t)} + \frac{\varepsilon^2(t)}{r_e^3(t)} \tag{82}$$

where

$$\varepsilon^2(t) \equiv 4\left(\langle \mathbf{r}\cdot\mathbf{r}\rangle\langle \dot{\mathbf{r}}\cdot\dot{\mathbf{r}}\rangle - \langle \mathbf{r}\cdot\dot{\mathbf{r}}\rangle^2\right) \tag{83}$$

is known as the "emittance". The emittance is an important parameter in the physics of charged particle beams, and is related to the area occupied by the particles in the phase space [79]. Unlike the one-dimensional case, in two dimensions the term $\langle \mathbf{r}\cdot\ddot{\mathbf{r}}\rangle$ can be simplified using the Poisson equation (65),

$$\begin{aligned}
\langle \mathbf{r}\cdot\ddot{\mathbf{r}}\rangle &= \int \mathbf{r}\cdot\ddot{\mathbf{r}}\, f_e(\mathbf{r},\mathbf{v},t) d^2r d^2\mathrm{v} \\
&= \frac{1}{2\pi}\int \mathbf{r}\cdot\ddot{\mathbf{r}}\,\nabla^2\psi_e d^2r \\
&= -\int r^2\frac{\partial\psi}{\partial r}\nabla^2\psi_e dr \\
&= -\int r\frac{\partial\psi_e}{\partial r}\frac{\partial}{\partial r}\left(r\frac{\partial\psi_e}{\partial r}\right)dr \\
&= -\frac{1}{2}\int_0^{r_e(t)} dr\frac{\partial}{\partial r}\left[\left(r\frac{\partial\psi_e}{\partial r}\right)^2\right].
\end{aligned} \tag{84}$$

The gradient of the potential at r_e is $1/r_e$, and we obtain

$$\langle \mathbf{r}\cdot\ddot{\mathbf{r}}\rangle = -1/2. \tag{85}$$

We are interested to study the behavior of a 2D self-gravitating system when its initial distribution does not deviate significantly from the virial condition. In this case, we expect that the emittance will remain close to its initial value, $\varepsilon^2(0) = v_m^2 = \mathcal{R}_0$, so that the envelope equation reduces to

$$\ddot{r}_e(t) = \frac{\mathcal{R}_0}{r_e^3(t)} - \frac{1}{r_e(t)}. \tag{86}$$

As expected, if $r_e(0) = 1$ and $\mathcal{R}_0 = 1$, $\ddot{r}_e = 0$, so that the envelope does not develop oscillations.

Comparing the temporal evolution of $r_e(t)$ with the data from MD simulations, we see that there is a reasonably good agreement between the two, especially for short times (Fig. 13).

5.4. The test particle model

We now study the behavior of test particles subject to a gravitational potential $\psi_e(t)$ produced by an oscillating uniform mass distribution,

$$\rho(t) = \frac{1}{\pi r_e^2(t)}\Theta(r_e(t) - r). \tag{87}$$

Solving the Poisson equation we find

$$\psi_e(r,t) = \begin{cases} \dfrac{r^2 - r_e(t)^2}{2r_e(t)^2} + \ln(r_e(t)) & \text{for } r \le r_e(t) \\ \ln(r) & \text{for } r \ge r_e(t). \end{cases} \tag{88}$$

This means that the dynamics of a test particle i which at $t = 0$ was at $r_i(0)$ and had an angular momentum p_{θ_i} will be governed by the equation of motion

$$\ddot{r}_i(t) - \frac{{v_{\theta_i}}^2}{{r_i}^3(t)} = \begin{cases} -\dfrac{r_i(t)}{r_e^2(t)} & \text{for } r_i(t) \le r_e(t) \\ -\dfrac{1}{r_i(t)} & \text{for } r_i(t) \ge r_e(t) \end{cases} \tag{89}$$

where $r_e(t)$ is the solution of Eq. (86).

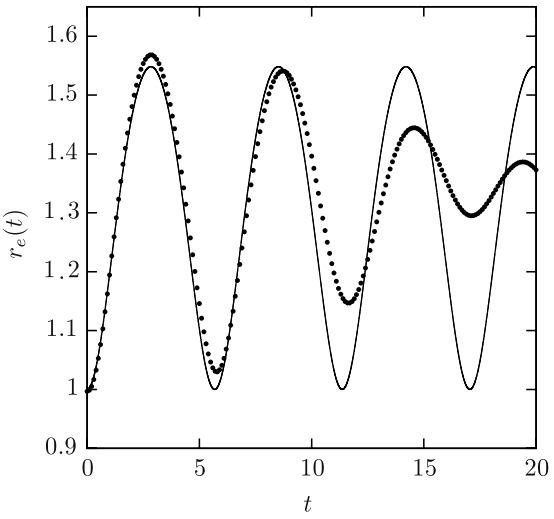

Fig. 13. Evolution of the envelope r_e according to Eq. (86) (solid line) compared to MD simulation (points) for a 2D self-gravitating system with $\mathcal{R}_0 = 1.5$. A reasonably good agreement is seen for short times.

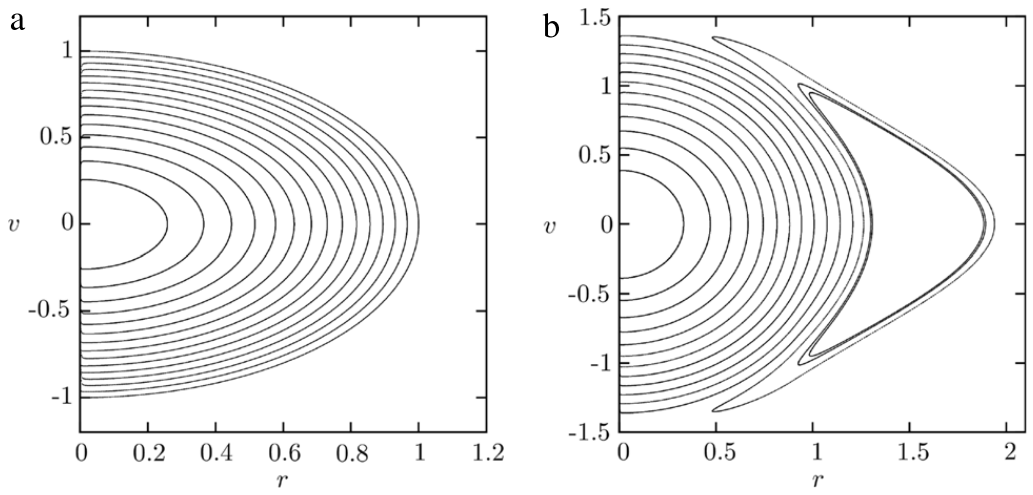

Fig. 14. Poincaré sections for a 2D self-gravitating system with (a) $\mathcal{R}_0 \approx 1$ and (b) $\mathcal{R}_0 = 0.9$. While in (a) the dynamics is completely regular in (b) we see the formation of a resonance island. We have considered $v_{\theta_i} = 0$ so that only the radial velocity appears in the Poincaré sections.

We integrate the equations of motion (89) for 15 test particles, uniformly distributed at $t = 0$, $r_i(0) \in [0, 1]$ and $v_i(0) \in [0, v_m]$, with $v_m = \sqrt{\mathcal{R}_0}$. The Poincaré section is constructed by plotting the position and velocity of each test particle when the envelope $r_e(t)$ is at its minimum value, see Fig. 14.

In Fig. 15 we compare the phase space structure of the test particle dynamics to a snapshot of the phase space obtained using MD simulation, after the qSS has been established. We see that the test particle dynamics allows us to calculate the maximum energy that a particle of a self-gravitating system can gain from the density oscillations.

5.5. The core–halo distribution

The particles which enter in resonance with the core density oscillations escape from the central region producing a tenuous halo. The halo formation progressively dampens the oscillations, bringing the resonances closer and closer to the core. When the qSS is established, we expect that the particle distribution will, once again, correspond to the core–halo distribution, given by

$$f_{ch}(r, v) = \eta\Theta(\epsilon_F - \epsilon(r, v)) + \chi\Theta(\epsilon(r, v) - \epsilon_F)\Theta(\epsilon_h - \epsilon(r, v)), \tag{90}$$

where ϵ_F and χ are calculated using conservation of energy and norm and ϵ_h is determined by the test particle dynamics, see Fig. 15. Integrating the core–halo distribution over v, we obtain the particle density in the qSS state. Substituting this

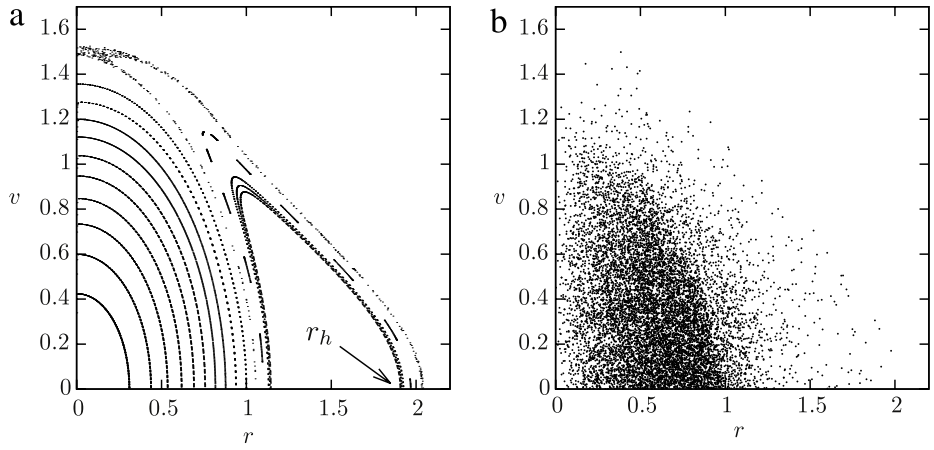

Fig. 15. Poincaré section of test particles (a) moving in an effective potential given by Eq. (88) and the phase space of MD simulation at $t = 2000$ with $N = 20{,}000$ (b). The virial number is $\mathcal{R}_0 = 0.694$. Comparing the two phase spaces, we see that the test particle dynamics allows us to accurately determine the maximum energy ϵ_h that a particle of a 2D self-gravitating system can gain from the density oscillations. In this particular case, $\epsilon_h = \ln(r_h)$, where r_h is the maximum position reached by a test particle, as indicated in the panel (a).

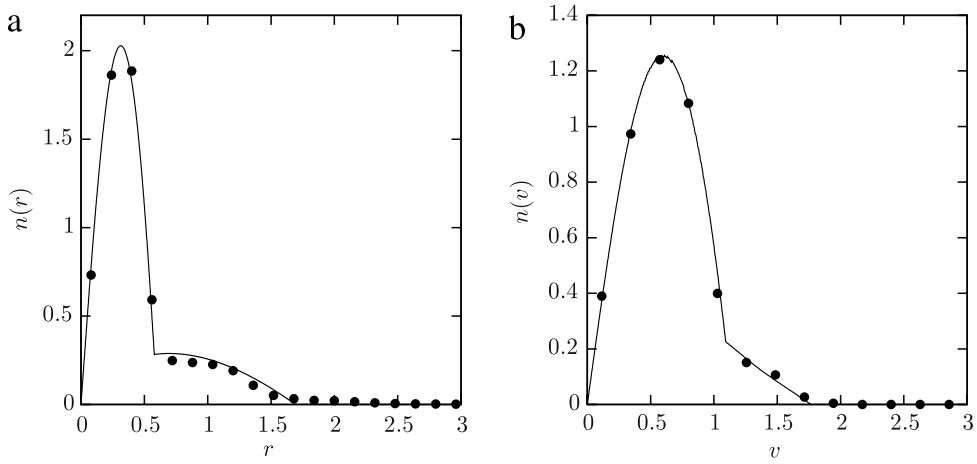

Fig. 16. Distributions in (a) position and (b) velocity for a 2D self-gravitating system with $\mathcal{R}_0 = 0.25$. The solid line corresponds to the prediction of the core–halo distribution function, Eq. (90), and points are results of MD simulation with $N = 10{,}000$ particles averaged over times $t = 2000$ to $t = 2100$. Error bars in the distributions are comparable to the symbol size.

into Poisson equation (65), we obtain the equation for the gravitational potential of a 2D cluster

$$\nabla^2\psi_{ch}(r) = 4\pi^2 \begin{cases} \eta(\epsilon_F - \psi_{ch}(r)) + \chi(\epsilon_h - \epsilon_F) & \text{for } \psi_{ch}(r) < \epsilon_F, \\ \chi(\epsilon_h - \psi_{ch}(r)) & \text{for } \epsilon_F \le \psi_{ch}(r) \le \epsilon_h, \\ 0 & \text{for } \psi_{ch}(r) > \epsilon_h, \end{cases} \tag{91}$$

with boundary conditions $\lim_{r\to\infty} \psi_{ch}(r) = \ln(r)$ and $\psi'_{ch}(0) = 0$. The system of equations (91) can be solved analytically, see Ref. [39]. Comparing the marginal distributions predicted by the core–halo theory to the results of MD simulations (Fig. 16), an excellent agreement between the two is observed.

5.6. Relaxation time

Finally, it is interesting to explore how much time $\tau_\times(N)$ a finite system of N particles remains in the qSS before relaxing to the true thermodynamic equilibrium. To this end, we use the crossover parameter $\zeta(t)$, defined as

$$\zeta(t) = \frac{1}{N^2}\int_0^\infty [N(r,t) - N_{ch}(r)]^2 dr \tag{92}$$

where $N(r,t)$ is the number of particles located inside shells between r and $r+dr$ at time t and $N_{ch}(r) = 2\pi N r \int f_{ch}(\mathbf{r},\mathbf{v})\, d^2\mathrm{v}$, where $f_{ch}(\mathbf{r},\mathbf{v})$ is the core–halo distribution, Eq. (90). Fig. 17 shows the value of $\zeta(t)$ for systems with different numbers of particles. The panel Fig. 17b shows that if the time is rescaled by $\tau_\times = N^\gamma \tau_D$, where $\gamma = 1.35$ and τ_D is the dynamical time defined by Eq. (64), all the curves fall on a universal curve, indicating the divergence of the crossover time in the thermodynamic limit. Thus, in the limit $N \to \infty$ a self-gravitating system will remain forever trapped in a nonequilibrium

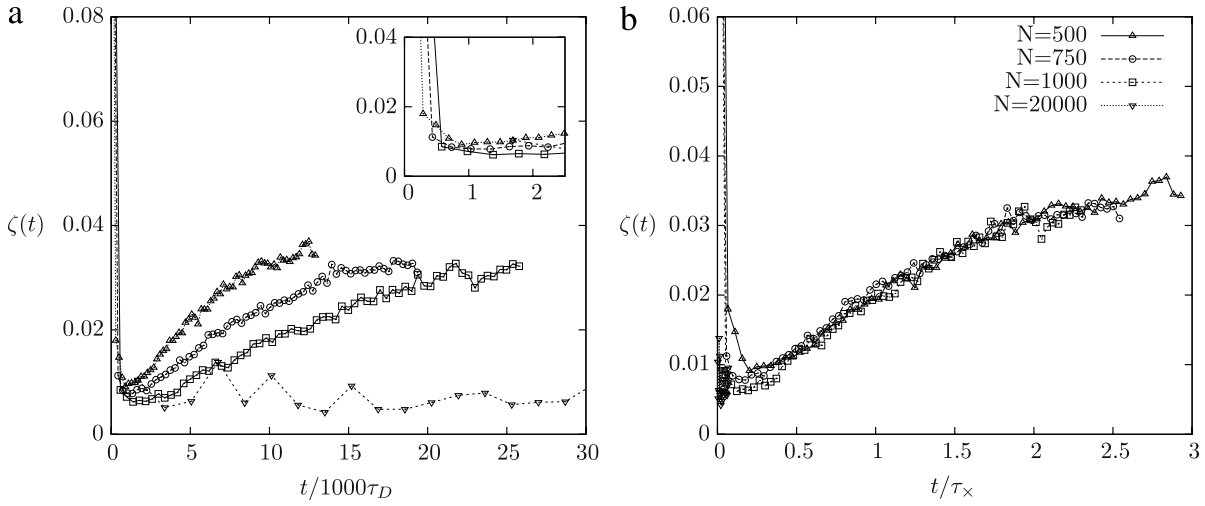

Fig. 17. (a) $\zeta(t)$ for different numbers of particles in the 2D self-gravitating system. In the inset, we show the fast (N independent) relaxation to the core–halo qSS after a time $t \approx 2000\tau_D$. The system remains in the qSS for a time interval that scales with the number of particles. When the time is rescaled by $\tau_\times(N)$ all the data in (a) fall on a universal curve (b).

stationary state. Recent simulations performed with discrete particles instead of the concentric shells used in this Report have lead to exponent $\gamma \approx 1$ [157], which is in good agreement with the scaling argument presented in Section 2, $t_\times N/\ln N$.

5.7. Thermodynamic equilibrium

For a finite number of particles, after a time $\tau_\times(N)$, we expect the system to relax to thermodynamic equilibrium, with

$$f_{mb}(\mathbf{r},\mathbf{v}) = Ce^{-\beta\left(\frac{v^2}{2}+\psi_{eq}(r)\right)}, \tag{93}$$

where C is the normalization constant. To see that this is the case, we calculate the gravitational potential and the marginal distributions and compare them to the results of MD simulations. The gravitational potential in equilibrium ψ_{eq} will satisfy the Poisson–Boltzmann equation

$$\nabla^2\psi_{eq}(r) = \frac{d^2\psi_{eq}(r)}{dr^2} + \frac{1}{r}\frac{d\psi_{eq}}{dr} = \frac{4\pi^2 C}{\beta}e^{-\beta\psi_{eq}(r)}, \tag{94}$$

where $\beta = 1/T$ is the Lagrange multiplier used to enforce the conservation of the total energy. The solution of this equation is given in Ref. [39],

$$\psi_{eq}(r) = \frac{1}{2}\ln\left(e^{2(2\mathcal{E}-1)} + r^2\right). \tag{95}$$

Curiously, an isolated 2D gravitational system can only exist at one temperature, $T = 1/4$, independent of the initial energy. If such a system is put in contact with a thermal bath, it will either gain energy from the bath and grow without bound or lose energy and shrink, depending if the temperature of the bath is greater or smaller than $T = 1/4$, respectively.

Fig. 18 compares the marginal distributions obtained using the MD simulations with the predictions of equilibrium statistical mechanics. The number density of particles located between $[r, r + dr]$ is

$$N(r) = 2\pi Nr\int d^2v\, f_{mb}(\mathbf{r},\mathbf{v}) = \frac{2Ne^{2(2\mathcal{E}-1)}r}{(e^{2(2\mathcal{E}-1)}+r^2)^2}, \tag{96}$$

and the number density of particles with velocities between $[v, v + dv]$ is

$$N(v) = 2\pi Nv\int d^2r\, f_{mb}(\mathbf{r},\mathbf{v}) = 4Nve^{-2v^2}. \tag{97}$$

The figure shows a good agreement between the results of MD simulations and BG statistics. However, to reach thermodynamic equilibrium, it was necessary to run a simulation with $N = 10{,}000$ particles for $t = 10^6$ dynamical times. Up to this time, the system remained trapped in a qSS state with the particles distributed in accordance with the core–halo distribution function $f_{ch}(r, v)$, Eq. (90).

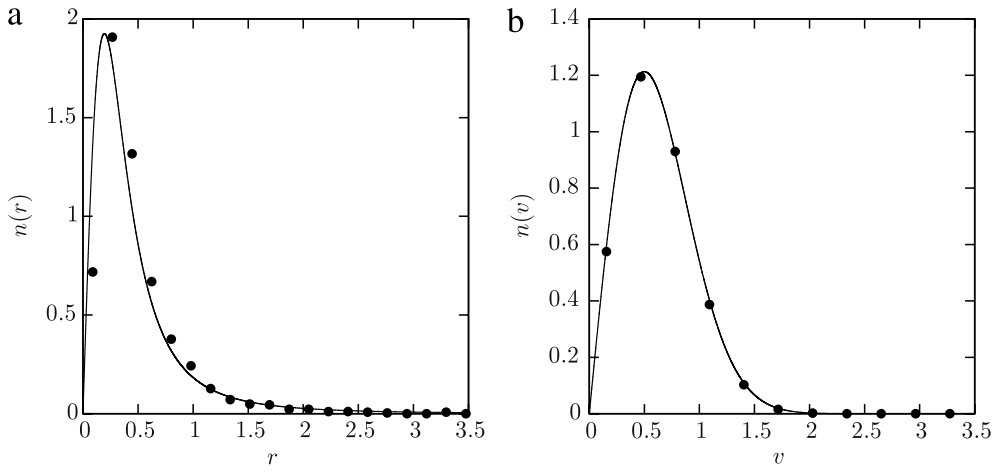

Fig. 18. Equilibrium distributions: (a) position and (b) velocity of a 2D self-gravitating system with $\mathcal{E}_0 = -0.0434$. The solid line corresponds to the equilibrium distributions, Eqs. (96) and (97), and the points are results of MD simulations with $N = 10{,}000$ particles at $t = 10^6$.

6. Gravitation in three dimensions

The relaxation of 3D self-gravitating systems is extremely difficult to study. There are two basic problems arising from the fact that Newton's gravitational potential has no lower bound, but is bounded from above. The consequence of the upper bound is that some particles of a self-gravitating system can gain enough kinetic energy to escape the gravitational field of the cluster. In principle, there is no limit to the particle evaporation since the energy can be constantly supplied by the two-body collisions [38,61,105] and the gravitational collapse. As a consequence, the Poisson–Boltzmann equation for a 3D open system has no solutions. Based on cosmological simulations, however, it has been observed that 3D systems do relax to qSSs [158–160]. There have been a number of phenomenological models proposed to describe the observed density profiles in such qSS: "de Vaucouleurs", "Sérsic" and "NFW" models [161–168]. These, phenomenological density distributions, however, lack the theoretical foundation.

The fact that the Poisson–Boltzmann equation does not have a solution indicates that open 3D self-gravitating systems are intrinsically unstable in the *infinite time limit*. This instability is a consequence of the binary collisions which lead to a flux of evaporating particles. On shorter time scales, however, it is possible for a system to relax to a collisionless qSS. Again, however, the situation in 3D is much more complex than in one and two dimensions [30,34,113–118,120–122]. Significant evaporation of particles can happen even on very short time scales, leading to a halo that extends all the way to infinity. At the moment, there is no theory that can account for the particle distribution inside a 3D halo. The theory of parametric resonances, which was so successful for treating 1D and 2D gravity, cannot be applied in 3D since, in general, there are no bounded resonant orbits.

Although the particle distribution in a qSS cannot be predicted *a priori*, we expect that it will have a core–halo structure. Evaporation should progressively cool down the core region. Statistically only a completely degenerate core can remain stable in an infinite space — at finite temperature the entropy gain will always favor particle evaporation. Furthermore, since the collisionless relaxation is controlled by the Vlasov equation, the phase space density in the core cannot exceed that of the initial waterbag distribution. We, therefore, expect that the core will be described by a fully degenerate Fermi–Dirac distribution [38] with the "spin" degeneracy equal to the phase space density of the initial waterbag distribution. The difficulty, however, is that without knowing the full particle distribution in the halo, we cannot calculate the self-consistent gravitational potential and close all the equations of the theory.

For a 3D gravitational system of total mass M, the gravitational potential in the qSS must satisfy the Poisson equation,

$$\nabla^2\psi(r) = 4\pi GM \int f(\mathbf{r},\mathbf{v})d^3\mathrm{v}, \tag{98}$$

where $f(\mathbf{r},\mathbf{v})$ is the one particle distribution function. If the potential $\psi(r)$ has a radial symmetry, the particles can be represented as spherical shells of mass $m = M/N$. This approach greatly facilitates the numerical simulations, and becomes exact in the thermodynamic limit.

It is convenient to measure all the distances in an arbitrary length unit r_0, the time in units of dynamical time,

$$\tau_D = \sqrt{\frac{r_0^3}{GM}}, \tag{99}$$

and the gravitational potential in units of $\psi_0 = GM/r_0$. The Poisson equation (98) then reduces to

$$\nabla^2\psi(r,t) = 4\pi \int f(\mathbf{r},\mathbf{v},t)d^3\mathrm{v}. \tag{100}$$

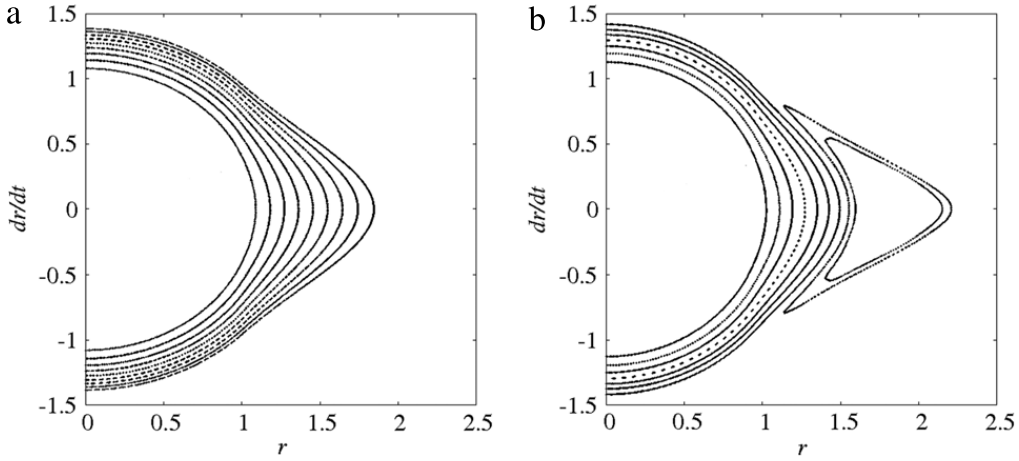

Fig. 19. Poincaré sections of a 3D gravitational system, for (a) $\mathcal{R}_0 \approx 1$ and (b) $\mathcal{R}_0 = 0.97$. In (a) the orbits are completely integrable, whereas in (b), we see a resonance island.

For a particle located at $\mathbf{r}'$, $\rho(\mathbf{r}) = \delta(|\mathbf{r}-\mathbf{r}'|)$, the Green's function of the Poisson equation is the usual Newton's gravitational potential

$$G(|\mathbf{r}-\mathbf{r}'|) = 1/|\mathbf{r}-\mathbf{r}'|. \tag{101}$$

This potential diverges at small distances and is bounded from above. We saw already that in 1D and 2D some particles enter in resonance with the density oscillations and gain a lot of energy. The situation in 3D is even more complex — the potential is bounded from above so that the resonant particles can gain enough energy to completely escape from the gravitational field of the cluster.

6.1. Test particle dynamics

To get a better idea of the relaxation process which leads to the core–halo formation, we study the dynamics of test particles moving under the action of an oscillating gravitational potential. Once again we consider particles which at $t = 0$ were distributed uniformly in the phase space inside a sphere of radius $0 < r \leq r_m$ and $0 < v \leq v_m$. We define the "envelope radius" as $r_e(t) = \sqrt{\frac{5\langle r^2\rangle}{3}}$, which at $t = 0$ satisfies $r_e(t) = r_m$. We will work in dimensionless units and set $r_0 = r_m$. Differentiating twice with respect to time and performing manipulations similar to those for 1D and 2D gravitational systems, we obtain a differential equation that governs the envelope dynamics,

$$\ddot{r}_e + \frac{1}{r_e^2} - \frac{\mathcal{R}_0}{r_e^3} = 0, \tag{102}$$

where

$$\mathcal{R}_0 = -\frac{2K_0}{V_0} \tag{103}$$

is the virial number, and K_0 and V_0 are the kinetic and the potential energy of the initial distribution.

We consider the dynamics of 10 test particles, initially distributed uniformly with positions $r_i \in [0, 1]$ and velocities $v_i \in [0, v_m]$,

$$\ddot{r}_i(t) - \frac{l_i^2}{{r_i}^3(t)} = \begin{cases} -\dfrac{r_i(t)}{r_e^3(t)} & \text{for } r_i(t) \leq r_e(t) \\ -\dfrac{1}{r_i^2(t)} & \text{for } r_i(t) \geq r_e(t), \end{cases} \tag{104}$$

where $l_i = |\mathbf{r}_i(0) \times \mathbf{v}_i(0)|$ and $r_e(t)$ evolves according to Eq. (102). Fig. 19 shows the Poincaré sections for two systems with $\mathcal{R}_0 \approx 1$ and $\mathcal{R}_0 = 0.97$. For $\mathcal{R}_0 \approx 1$, the orbits remain integrable, while even a small deviation from the virial condition results in the appearance of a resonance island. For slightly larger or smaller $\mathcal{R}_0$ the resonant orbit becomes unbounded.

6.2. Lynden-Bell theory for a 3D self-gravitating system

It is interesting to consider the predictions of the LB theory for a 3D self-gravitating system. In this case the one-particle distribution function becomes

$$f_{lb}(\mathbf{r}, \mathbf{v}) = \frac{\eta}{e^{\beta[\epsilon(\mathbf{r},\mathbf{v})-\mu]} + 1}, \tag{105}$$

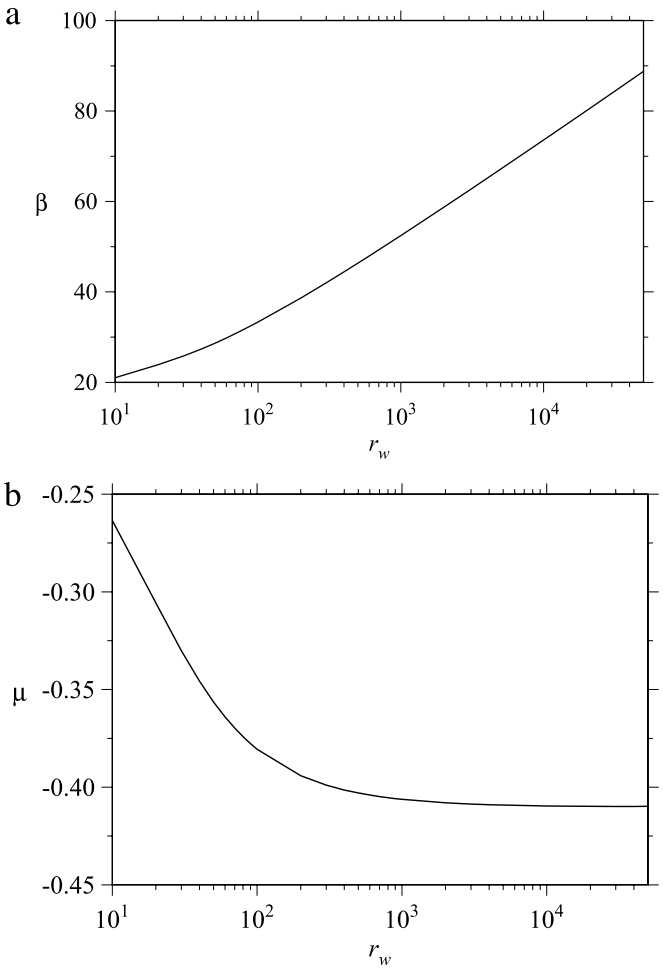

Fig. 20. (a) β and (b) μ as a function of r_w, for a 3D self-gravitating system. While the inverse temperature parameter β diverges in (a), the chemical potential μ in (b) asymptotically goes to a finite value $\mu \approx -0.41$, as r_w increases. The virial number is $\mathcal{R}_0 = 1.7$.

where $\eta = 9/16\pi^2 v_m^3$ and $\epsilon(r, v) = v^2/2 + \psi(r)$. Integrating over the velocities we obtain the density distribution corresponding the LB stationary state. Substituting this into the Poisson equation allows us to write a self-consistent equation for the gravitational potential

$$\frac{1}{r^2}\frac{\partial}{\partial r} r^2 \frac{\partial \psi}{\partial r} = -16\pi^2 \eta \sqrt{\frac{\pi}{2\beta^3}}\ \mathrm{Li}_{3/2}(-e^{\beta[\mu-\psi(r)]}), \tag{106}$$

where $\mathrm{Li}_n(x)$ is the nth polylogarithm function of x. This equation has to be solved numerically and the two Lagrange multiplier β and μ must be calculated to preserve the number of particles and the energy of the system. The solution of Eq. (106) is complicated by the open boundary conditions. In practice, we will solve this equation by enclosing the system in a spherical box of radius r_w and then take the limit $r_w \to \infty$. As expected, when $r_w \to \infty$, the LB distribution separates into a completely degenerate core and a very tenuous halo which extends all the way to r_w. However, the particle distribution in the halo is very different from the ones found in MD simulations, see Fig. 21, so that LB theory fails to correctly describe a 3D self-gravitating system.

6.3. Systems with $\mathcal{R}_0 = 1$

If the initial particle distribution satisfies the virial condition $\mathcal{R}_0 = 1$, the macroscopic oscillations will be suppressed and the parametric resonances will not be excited, see Fig. 19. For such initial distributions, we saw that LB theory worked reasonably well for 1D and 2D gravitational systems. For 3D systems, however, LB theory fails even when $\mathcal{R}_0 = 1$. As $r_w \to \infty$, the solution of Eq. (106) requires that $\beta \to \infty$ (see Fig. 20) and the distribution function approaches the degenerate limit $f_{core}(\mathbf{r}, \mathbf{v}) = \eta_1\, \Theta(\mu - \epsilon)$ (plus halo particles at infinity). Thus, for an open system, LB theory will always predict a fully degenerate core [169]. This conclusion, however, is valid only in the asymptotic $t \to \infty$ limit. In this limit, even small oscillations of the envelope will lead to particle evaporation and result in formation of a cold core. In practice, however, for $\mathcal{R}_0 = 1$ the rate of evaporation is very low, so that the degenerate limit will not be reached in the time of simulation. To treat this "short" time limit, we can introduce an effective cutoff (a wall) at r_w. The precise value of the

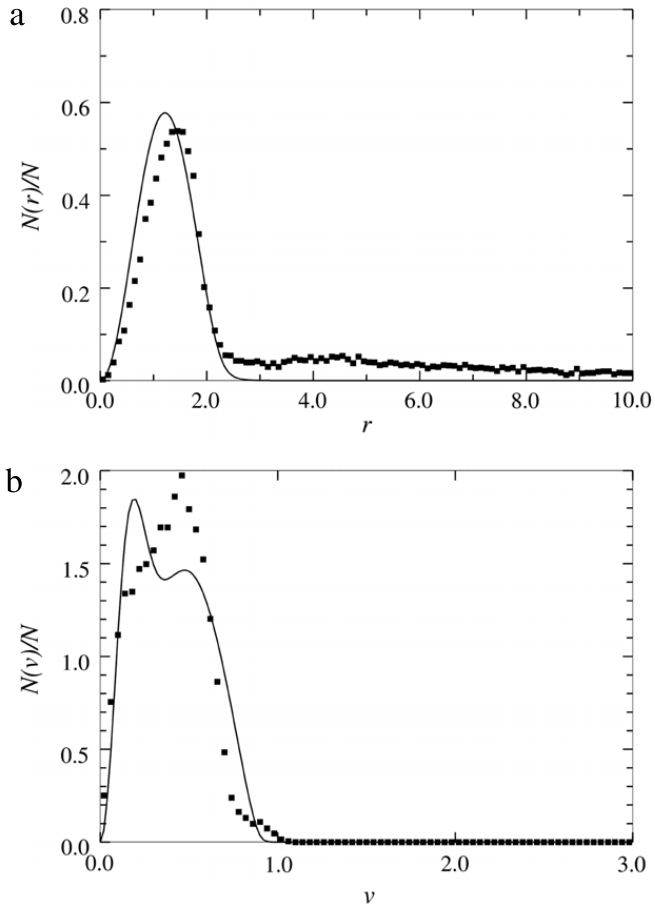

Fig. 21. The (a) mass and (b) velocity distributions of a 3D self-gravitating system in the qSS obtained by MD simulation (symbols) and the LB prediction (solid line). The wall radius is placed at $r_w = 10^4$ and the virial number is $\mathcal{R}_0 = 1.7$.

cutoff is unimportant, as long as it is not too large $5 \leq r_w \leq 100$. The wall will prevent the particle evaporation and a complete cooling of the core region. Indeed, the cutoff-LB distribution (cLB) is found to describe reasonably the qSS state for $\mathcal{R}_0 = 1$ [38], see Fig. 22.

7. Non-neutral plasmas

In this chapter we will analyze qSSs of magnetically confined non-neutral plasmas. The non-neutrality condition is crucial for the plasma to be a long-ranged interacting system — for neutral two component plasmas, Debye screening leads to an effective short-range interaction potential [79,170,171]. The equilibrium state of neutral plasmas and electrolytes, therefore, can be studied using the usual Boltzmann–Gibbs statistical mechanics [101].

Many different applications, such as heavy ion fusion, high-energy physics, communications, materials processing, and cancer therapy, depend on the physics of transport of intense charged-particle beams. The goal is to avoid the heavy particle losses produced by the parametric resonances [47,172], which can lead to halo formation that is detrimental to the beam quality, and can result in damage to the accelerator walls. A theory which can quantitatively predict this effect is, therefore, highly desirable for a better understanding of the physics of beam transport [50,144,173–175].

In general, the dynamics of the beams is influenced by multiple effects, including the mismatched envelope (rms radius of the beam) [50–52,144,176], movement outside the axis of symmetry [177–182], nonuniformities in the beam distribution [149,183–185], and the image forces due to the surrounding conducting walls [186–188]. Of all these, the study of parametric resonances resulting from the transverse beam oscillations has attracted the most attention. Envelope mismatch is believed to be the main cause of the halo formation in space-charge dominated beams [189]. In this section we will show that the mismatch of the beam envelope is closely related to the virial condition – similarly to the one found for self-gravitating systems – and that the final qSS is, once again, described by the core–halo distribution function.

7.1. The model

Our system consists of a beam of charged point particles, confined by an external magnetic field $\mathbf{B}^{ext}(\mathbf{r}) = B_0\hat{z}$, propagating along the axial $\hat{z}$ direction, with velocity V_b. The beam has a characteristic radius r_b and is surrounded by a

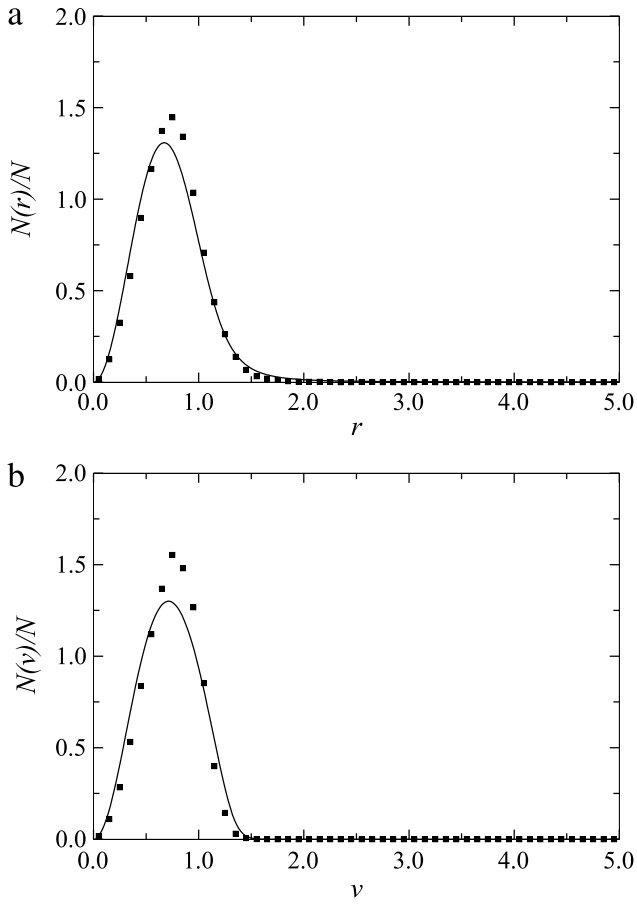

Fig. 22. The mass (a) and velocity (b) distributions in the qSS of a 3D self-gravitating system obtained by MD simulation with $N = 2 \times 10^4$ (symbols) and the distributions obtained using LB theory with a cutoff at $r_w = 10$ (solid line), for an initially virialized waterbag distribution, $\mathcal{R}_0 = 1$.

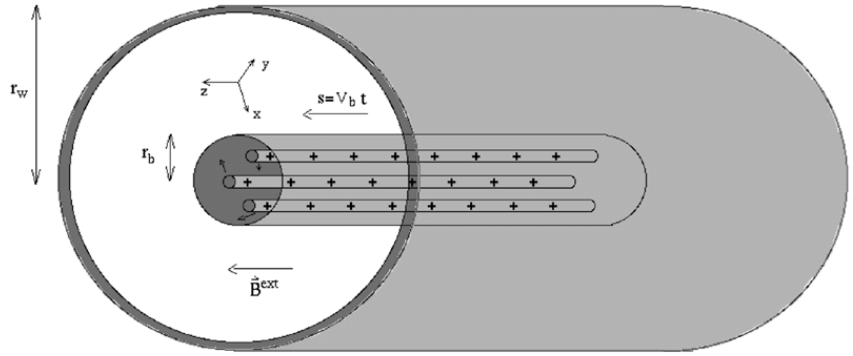

Fig. 23. Charged particle beam of characteristic radius r_b propagating along the longitudinal direction $\hat{z}$ with constant velocity V_b. The particles are confined by a magnetic field $\mathbf{B}^{ext} = B_0\hat{z}$, and the beam is isolated from the external environment by a conducting cylindrical wall located at r_w.

conductive cylindrical wall of radius r_w.[4] We assume that the beam has axial symmetry and that the motion along the $\hat{z}$ direction is uniform. Consequently, we consider that the relevant dynamics takes place only in the transverse plane "$\perp$".[5] Under these conditions, the time t can be replaced by the longitudinal coordinate s, by means of a canonical transformation of the original Hamiltonian, where $s = V_b t$ and $V_b = \beta_b c$, c being the speed of light in vacuum, as illustrated in Fig. 23.

The charge of the beam particle is $Z_i e$, where Z_i is the valence and e is the electron charge. Furthermore, assuming that the transverse velocity of the beam particles is much lower than the longitudinal velocity, the dynamics along the transverse plane may be considered non-relativistic. This set of conditions, known as the paraxial approximation, is sufficient to study narrow and intense charged-particle beams [79].

[4] A conducting grounded wall requires that the electric potential at the wall vanishes $\phi^s(r_w) = 0$.

[5] We approximate $\nabla^2 \approx \nabla_\perp^2$ since the variation of the potential along the longitudinal direction is negligible compared to the variations in the transverse plane. Therefore, in this section, ∇ will be understood to represent $\nabla_\perp$.

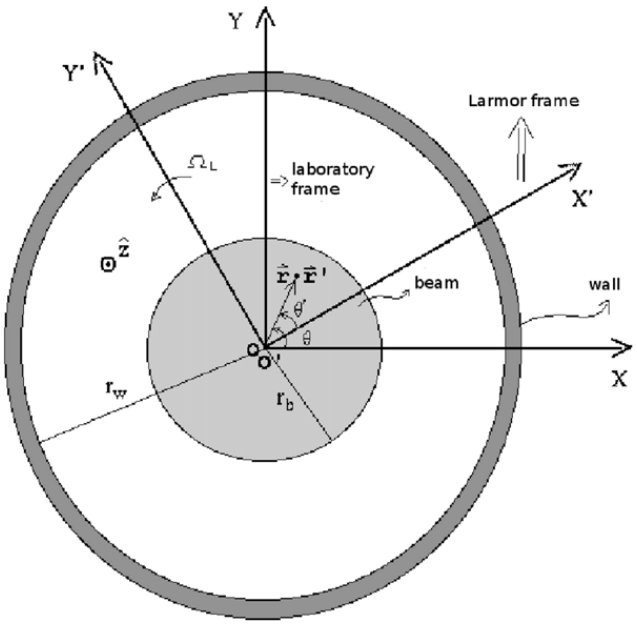

Fig. 24. Change of reference frames: "O" represents the laboratory frame and "O'" the Larmor frame.

The electric $\mathbf{E}^s$ and magnetic $\mathbf{B}^s$ fields satisfy Maxwell's equations [79] and the electric potential the Poisson equation,

$$\nabla^2\phi^s = \frac{1}{r}\frac{\partial}{\partial r}\left(r\frac{\partial}{\partial r}\right)\phi^s(r,s) = -4\pi Z_i e n_b \tag{107}$$

with boundary conditions $\phi(r_w) = 0$ and $\phi'(0) = 0$, where n_b is the number density of the particles. The electric potential is always zero outside the conductive wall, located at r_w. The vector potential, $\hat{z}A_z^s(r,s)$, produced by the current of charges $Z_i e n_b V_{zb}$ – the longitudinal velocity of the beam, $V_{zb}(r,s)$, is approximated by V_b – satisfies

$$\nabla^2 A_z^s(r,s) = -4\pi Z_i e n_b \beta_b. \tag{108}$$

Comparing Eqs. (107) and (108), we see that the electric and vector potentials are related by

$$A_z^s = \beta_b \phi^s. \tag{109}$$

Thus, solving the Poisson equation (107), we find the electromagnetic field acting on each particle,

$$\mathbf{E}^s = -\nabla\phi^s(r,s), \tag{110}$$

$$\mathbf{B} = \mathbf{B}^{ext} + \beta_b \nabla\phi^s(r,s) \times \hat{z}. \tag{111}$$

As a matter of convenience, [47,79], we study the system in the Larmor frame which rotates in relation to the laboratory with a constant angular frequency $\Omega_L = -Z_i eB_0/2\gamma_b mc$, where $\gamma_b = (1-\beta_b^2)^{-1/2}$ and m is the mass of a particle, see Fig. 24. We define the dimensionless potential as

$$\psi^b(r,s) = \left(Z_i e/\gamma_b^3 m\beta_b^2 c^2\right)\phi^s(r,s). \tag{112}$$

In the Larmor frame, the focusing due to the magnetic field $\mathbf{B}^{ext}$, results in a radial confining force. The change to the Larmor frame is accomplished by a change of coordinates $(r,\theta) \to (r',\theta')$, where

$$\begin{aligned} r' &= r, \\ \theta' &= \theta - \Omega_L s, \end{aligned} \tag{113}$$

as shown in Fig. 24. The evolution of the distribution function $f(\mathbf{r},\mathbf{v},s)$ in the Larmor frame satisfies the Poisson–Vlasov systems of equations [79],

$$\frac{\partial f}{\partial s} + \mathbf{v}\cdot\nabla f + \left[-\kappa_z^2\mathbf{r} - \nabla\psi^b(r)\right]\cdot\nabla_{\mathbf{v}} f = 0, \tag{114}$$

$$\nabla^2\psi^b(r) = -2\pi K n(\mathbf{r},s), \tag{115}$$

where $n(\mathbf{r},s) = \int f\, d\mathbf{v}$ is the density profile of the beam, $\kappa_z = |\Omega_L|/\beta_b c$ is the focusing field parameter, and $K = 2Z_i^2 e^2 N_b/\gamma_b^3\beta_b^2 mc^2$ is the perveance which measures the intensity of the beam. The number of particles per unit axial length

is N_b, $\mathbf{r}$ is the position vector in the transverse plane, and $\mathbf{v} \equiv d\mathbf{r}/ds$ is the dimensionless transverse "velocity". The problem then reduces to studying the dynamics of 2D pseudo-particles of charge $q = \sqrt{\frac{K}{N_b}}$ confined by an external parabolic potential $U = \kappa_z r^2/2$. The interaction potential between the particles is $\mu_b(\mathbf{r}, \mathbf{r}') = q^2 G_b(\mathbf{r}, \mathbf{r}')$ where $G_b(\mathbf{r}, \mathbf{r}')$ is the Green's function of the two-dimensional Poisson equation. For conducting boundary conditions at r_w, the Green's function can be calculated using Kelvin's inversion theorem [147,190]. The Hamiltonian for the effective 2D system is then

$$\mathcal{H}^b(r_i, \theta_i, v_{r_i}, v_{\theta_i}) = \sum_{i=1}^{N_b} \left(\frac{v_{r_i}^2}{2} + \frac{v_{\theta_i}^2}{2r_i^2} \right) - \frac{q^2}{2} \sum_{i,j=1}^{N_b} G_b(\mathbf{r}_i, \mathbf{r}_j) + \frac{\kappa_z^2 r_i^2}{2}. \tag{116}$$

Starting from an arbitrary initial distribution, the system of particles can now be simulated to obtain the final qSS.

If the system has azimuthal symmetry, the simulations can be simplified further. In the thermodynamic limit the Vlasov mean-field description becomes exact, so that each particle moves under the action of the mean electromagnetic potential produced by all the other particles. To approach the mean-field limit with a finite number of particles we can uniformly smear the charge of each particle over a circle or radius r_i corresponding to its position. This is the same approximation that was used to efficiently simulate 2D and 3D gravitational systems. Using Gauss's law, the equation of motion for the radial coordinate of a particle i becomes

$$\ddot{r}_{eff}(r_i) = \frac{v_{\theta_i}^2}{r_i^3} + \frac{K}{N_b} \frac{n_{eff}(r_i)}{r_i} - \kappa_z^2 r_i, \tag{117}$$

$$n_{eff}(r_i) = \sum_{j=1}^{N_b} \Theta(r_i - r_j), \tag{118}$$

where n_{eff} is the number of particles with $r < r_i$ and $v_{\theta_i} = r_i^2 \dot{\theta}_i$. Since the force acting on each particle is radially symmetric, v_{θ_i} is a conserved quantity determined from the initial condition, $v_{\theta_i}(t) = v_{\theta_i}(0)$. The effective Hamiltonian in the mean-field limit can then be written as

$$\mathcal{H}^b_{eff}(r_i, \theta_i, v_{r_i}, v_{\theta_i}) = \sum_{i=1}^{N_b} \left(\frac{v_{r_i}^2}{2} + \frac{v_{\theta_i}^2}{2r_i^2} - \frac{K}{N_b} n_{eff}(r_i) \ln\left(\frac{r_i}{r_w}\right) + \frac{\kappa_z^2 r_i^2}{2} \right). \tag{119}$$

7.2. The envelope equation

We define the beam envelope as $r_b \equiv \left[2\langle r^2 \rangle\right]^{1/2}$. Differentiating twice with respect to s gives us the beam envelope equation,

$$\ddot{r}_b + \kappa_z^2 r_b - \frac{K}{r_b} - \frac{\varepsilon^2(t)}{r_b^3} = 0, \tag{120}$$

where $\varepsilon(t)$ is the emittance, Eq. (83). This equation is exact; however, the dynamics of $\varepsilon(t)$ is unknown. For short times we will set it equal to the initial emittance $\varepsilon(t) = \varepsilon(0) \equiv \varepsilon_0$.

The beam envelope will not oscillate if $\ddot{r}_b = 0$. This defines the matched beam radius,

$$r_b^* = \left\{ \frac{K}{2\kappa_z^2} + \left[\frac{K^2}{4\kappa_z^4} + \frac{\varepsilon_0^2}{\kappa_z^2} \right]^{1/2} \right\}^{1/2}, \tag{121}$$

which is equivalent to the virial condition, Eq. (45).

If the initial beam is launched with the radius $r_b = r_b^*$, it will not develop significant oscillations and will not suffer emittance growth. However, in practice it is virtually impossible to launch a beam precisely at this radius. We, therefore, define the virial parameter as

$$\mu(t) \equiv r_b(t)/r_b^*, \tag{122}$$

which measures how far the initial beam deviates from the virial condition.

7.3. Initial conditions

At $t = 0$ the N_b particles are distributed uniformly in phase space with $r_i \in [0, r_m]$ and velocities $v_i \in [0, v_m]$,

$$f_0(r_m, v_m) = \eta \Theta(r_m - r) \Theta(v_m - v). \tag{123}$$

It is convenient to measure all length in units $\sqrt{\varepsilon_0/\kappa_z}$ and "time" (longitudinal length) s in units of $1/\kappa_z$. The transverse velocities will then be measured in units $\sqrt{\varepsilon_0\kappa_z}$. In these dimensionless units the matched beam radius becomes

$$r_b^* = \left\{ \frac{K^*}{2} + \left[\frac{K^{*2}}{4} + 1 \right]^{1/2} \right\}^{1/2}, \tag{124}$$

where $K^* = K/\varepsilon_0\kappa_z$. Unlike for self-gravitating systems, for which only the virial number determined the dynamical evolution, in the case of beams we have two dimensionless parameters, K^* and $\mu_0 = \mu(0)$.

In the reduced units, $\varepsilon_0 = 1$ and

$$v_m = 1/r_m, \tag{125}$$

where $r_m = r_b(0)$ and the emittance growth is ε_{qSS}.

The potential ψ^b_{wb} associated with the initial distribution given by Eq. (123) can be obtained by solving the Poisson equation (115),

$$\frac{d^2\psi^b_{wb}(r)}{dr^2} + \frac{1}{r}\frac{d\psi^b_{wb}(r)}{dr} = \begin{cases} -2K^*/r_m^2 & \text{for } r \le r_m, \\ 0 & \text{for } r_m < r \le r_w, \end{cases} \tag{126}$$

with the boundary conditions $\psi^b_{wb}(r_w) = 0$ and $\psi'^b_{wb}(0) = 0$. The solution is

$$\psi^b_{wb}(r) = \begin{cases} -K^*\left[\dfrac{(r^2 - r_m^2)}{2r_m^2} + \ln(r_m/r_w) \right] & \text{for } r \le r_m, \\ -K^* \ln(r/r_w) & \text{for } r_m \le r \le r_w. \end{cases} \tag{127}$$

For the initial waterbag distribution (123), the initial energy of the system is

$$\mathcal{E}_0(K^*, r_w; \mu_0) = \frac{v_m^2}{4} + \frac{r_m^2}{4} + \frac{K^*}{8} - \frac{K^*}{2}\ln\left(\frac{r_m}{r_w}\right), \tag{128}$$

with r_m and v_m defined by Eqs. (122) and (125), respectively.[6]

7.4. Lynden-Bell theory for a charged particle beam

We will first analyze the situation in which the beam envelope at $t = 0$ is matched, i.e. satisfies the virial condition $\mu_0 = 1$. From our experience with self-gravitating systems, we expect that in this case LB statistics should work reasonably well. The electromagnetic potential should then satisfy the Poisson equation (115), with the charge density obtained by integrating the distribution function, Eq. (19), over velocities,

$$\frac{d^2\psi^b_{lb}(r)}{dr^2} + \frac{1}{r}\frac{d\psi^b_{lb}(r)}{dr} = -\frac{4\pi^2 K^*}{\beta}\ln\left[1 + e^{-\beta\left(\psi^b_{lb}(r) + \frac{r^2}{2} - \alpha\right)}\right]. \tag{129}$$

The Lagrange multipliers α and β are determined using energy and norm conservation. The solution to this equation is obtained numerically and the resulting marginal distributions

$$N(r) = 2\pi N_b r \int d^2\mathrm{v} f_{lb}(\mathbf{r}, \mathbf{v}) \tag{130}$$

and

$$N(v) = 2\pi N_b v \int d^2\mathrm{r} f_{lb}(\mathbf{r}, \mathbf{v}) \tag{131}$$

are compared with the results of MD simulations in Fig. 25, showing a very good agreement.

[6] If the initial distribution is nonuniform, the functional dependence between v_m and r_m will change.

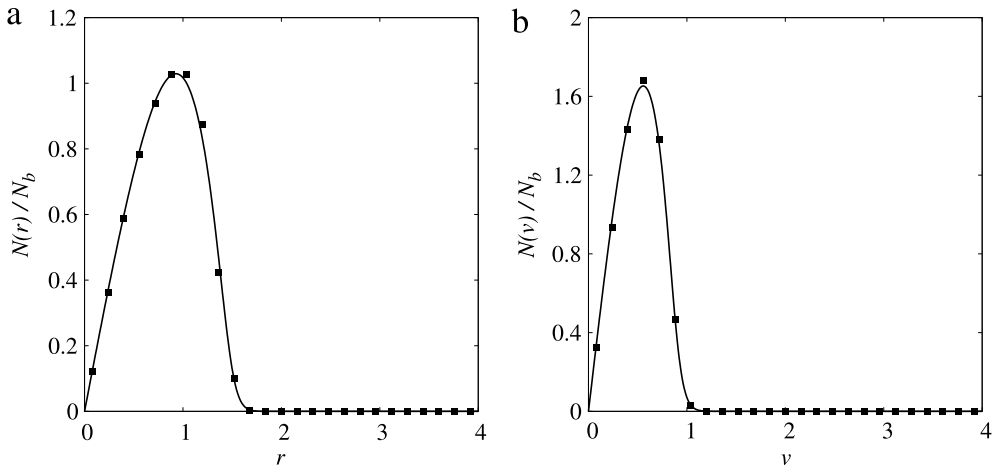

Fig. 25. Number density of particles in (a) position and (b) velocity for a system initially in a waterbag distribution with $\mu_0 = 1$, where $K^* = 1$ and $r_w = 4$. The solid line corresponds to the distribution obtained using LB theory, Eq. (19), and the points are results of MD simulation with $N_b = 50{,}000$ particles, averaged over 100 dynamical times after the system reached a qSS. Error bars in the distributions are comparable to the symbol size.

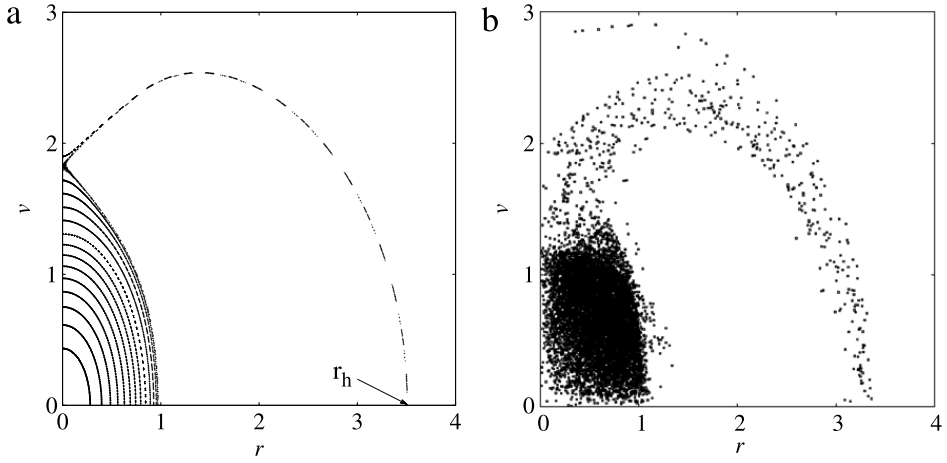

Fig. 26. Poincaré section of the test particles (a) and phase space of the N-body MD simulation (b) using the Hamiltonian (119) at $t = 200$, for an initial distribution with $\mu_0 = 1.5$ and $K^* = 1$. The test particle dynamics allows us to determine the maximum position r_h reached and, consequently, the maximum energy ϵ_h that a particle may attain, $\epsilon_h = \frac{r_h^2}{2} - \ln \frac{r_h}{r_w}$.

7.5. The test particle model

In practice, it is very difficult to launch a perfectly matched beam. In most case $\mu_0 \neq 1$ and parametric resonances will be excited. To study these, we once again appeal to the model of non-interacting test particles moving in an oscillating potential $\psi_e(r_b(t))$. We consider 15 test particles initially distributed uniformly with positions $r_i \in [0, r_m]$ and velocities $v_i \in [0, v_m]$. The equation of motion for the particle i is

$$\ddot{r}_i(t) - \frac{{v_{\theta_i}}^2}{{r_i}^3(t)} + r_i(t) = \begin{cases} K^* \dfrac{r_i(t)}{r_b^2(t)} & \text{for } r_i(t) \leq r_b(t) \\ K^* \dfrac{1}{r_i(t)} & \text{for } r_i(t) \geq r_b(t), \end{cases} \tag{132}$$

where $r_b(t)$ evolves according to (120) with $\varepsilon(t) = \varepsilon_0$.

Comparing the result of the test particle dynamics with the full N-body MD simulation, shown in Fig. 26, we see that the reduced test-particle model predicts accurately the location of the resonant orbit. This allows us to calculate the maximum energy ϵ_h that a particle can gain from the parametric resonance, $\epsilon_h = \frac{r_h^2}{2} - \ln \frac{r_h}{r_w}$, where r_h is the maximum distance from the origin reached by a test particle of the initial distribution, see Fig. 26(a). Phenomenologically it has been found [50] that for beams with large space charge K^*, r_h is simply related to the virial parameter and the matched envelope radius, $r_h = 2r_b^*(1 + \ln(\mu_0))$.

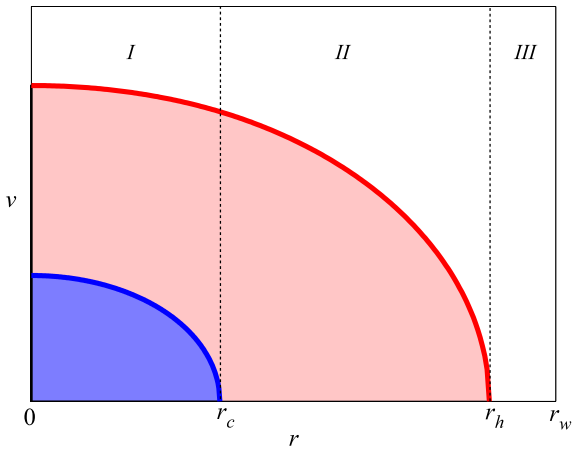

Fig. 27. Regions of phase space used in the solution of Eq. (115).

7.6. The core–halo distribution

For mismatched beams ($\mu_0 \neq 1$), we expect that the qSS distribution function will, once again, be of the core–halo type,

$$f_{ch}(\mathbf{r},\mathbf{v}) = \frac{1}{\pi^2}\left[\Theta(\epsilon_F - \epsilon(\mathbf{r},\mathbf{v})) + \chi\Theta(\epsilon_h - \epsilon(\mathbf{r},\mathbf{v}))\Theta(\epsilon(\mathbf{r},\mathbf{v}) - \epsilon_F)\right]. \tag{133}$$

It is convenient to divide phase space into three regions, *I*, *II*, and *III* (Fig. 27), corresponding respectively to $r < r_c$, $r_c < r < r_h$, and $r_h < r < r_w$, where r_c is the core radius. The particle density

$$n(r) = \int f_{ch}(\mathbf{r},\mathbf{v})d^2\mathrm{v} \tag{134}$$

in the three regions can be written as

$$n_I(r) = \frac{2}{\pi}\left[\epsilon_F + \chi(\epsilon_h - \epsilon_F) - V_I(r)\right], \tag{135}$$

$$n_{II}(r) = \frac{2\chi}{\pi}\left[\epsilon_h - V_{II}(r)\right], \tag{136}$$

and $n_{III}(r) = 0$, where $V_i(r) \equiv \psi_{chi}(r) + r^2/2$, $i = I, II, III$ is the total potential that takes into account the effects of the interaction between particles as well as the contribution of the external field. The parameter r_c is determined by the condition $V(r_c) = \epsilon_F$. The maximum halo extent r_h is calculated using test particle dynamics, see Fig. 26(a). Both $\psi_{chi}(r)$ and $V_i(r)$ and their first derivatives must be continuous at $r = r_c$ and $r = r_h$. These conditions, together with the Poisson equation (115), provide a closed set of equations for the potential in different regions. The equations can be solved analytically, allowing us to calculate the distribution function in the qSS [191]. A good agreement between theory and MD simulation is shown in Fig. 28.

The theory also allows us to predict the emittance growth, a quantity which is of primary importance for beam physics. Comparing the predictions of the present theory with the results of MD simulations, an excellent agreement between the two is observed, Fig. 29. The theory is also in excellent agreement with the experimental measurements [50].

The fraction of particles that escape from the core region to form a high energy halo can be obtained by integrating the distribution function between the energies ϵ_F and ϵ_h, $\mathcal{F}_h = (\chi/\pi^2)\int \Theta(\epsilon_h - \epsilon)\Theta(\epsilon - \epsilon_F)d^2r d^2\mathrm{v}$ (Fig. 30). We find

$$\mathcal{F}_h = 1 - 2Ar_c^2 I_2(\alpha_c r_c), \tag{137}$$

where $I_n(z)$ is the modified Bessel function of the first kind of order n.

7.7. Relaxation time

Since plasmas contain astronomical numbers of charged particles, relaxation to Boltzmann–Gibbs thermodynamic equilibrium will not happen on laboratory time scale. From the purely theoretical stand point, however, it is interesting to study what would happen if the number of particles can be reduced. This can be easily achieved on computer, if not in practice. We thus define a crossover parameter

$$\zeta(t) = \frac{1}{N^2}\int_0^\infty [N(v,t) - N_{lb}(v)]^2 dv \tag{138}$$

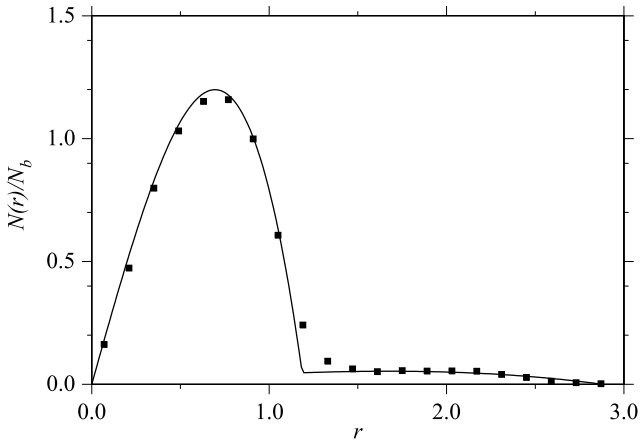

Fig. 28. Particle distribution for a mismatched beam, with $\mu_0 = 1.5$ and $K^* = 1$. Points are results of MD simulation with $N = 5 \times 10^4$, averaged over 100 dynamical times in the qSS, and the line shows the prediction obtained using the core–halo distribution, Eq. (134). Error bars in the distributions are comparable to the symbol size.

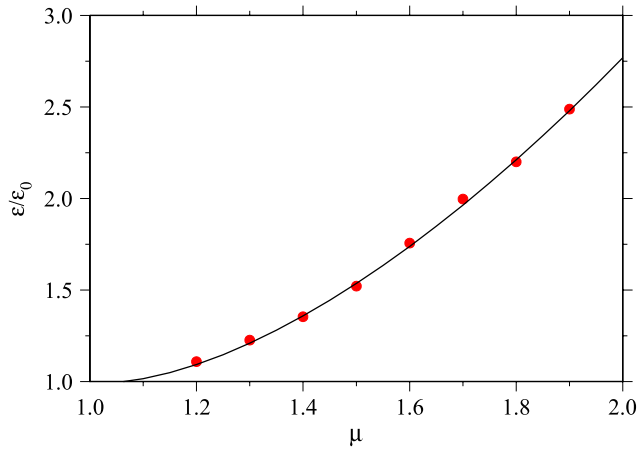

Fig. 29. Emittance growth, $\varepsilon/\varepsilon_0$, as a function of the initial virial parameter μ_0 predicted by the core–halo theory (solid line) and compared with the MD simulations (points) for $K^* = 1$.

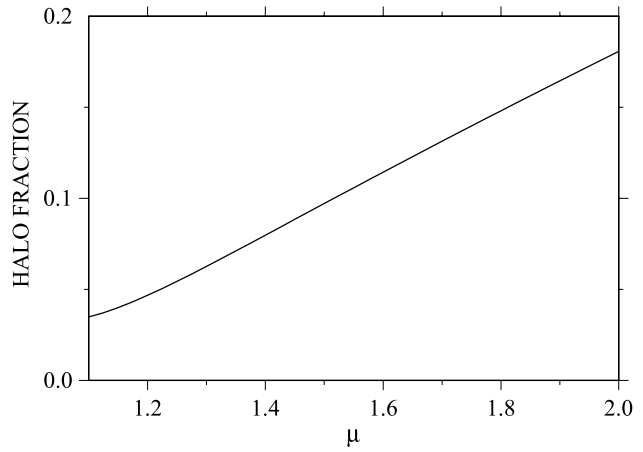

Fig. 30. Fraction of particles occupying the halo, Eq. (137), as a function of the initial mismatch μ_0, for $K^* = 1$.

where $N(v, t)$ is the number of particles with velocity in the interval $[v, v + dv]$ at simulation time t, and $N_{lb}(v)$ is given by Eq. (131). The LB distribution is used in the definition of $\zeta(t)$ because we consider cases when the virial condition is initially satisfied. The value of $\zeta(t)$ should tend toward its asymptotic value, ζ_{eq}, as the system approaches thermodynamic equilibrium. This value is given by

$$\zeta_{eq} = \frac{1}{N^2} \int_0^\infty [N_{eq}(v) - N_{lb}(v)]^2 dv, \tag{139}$$

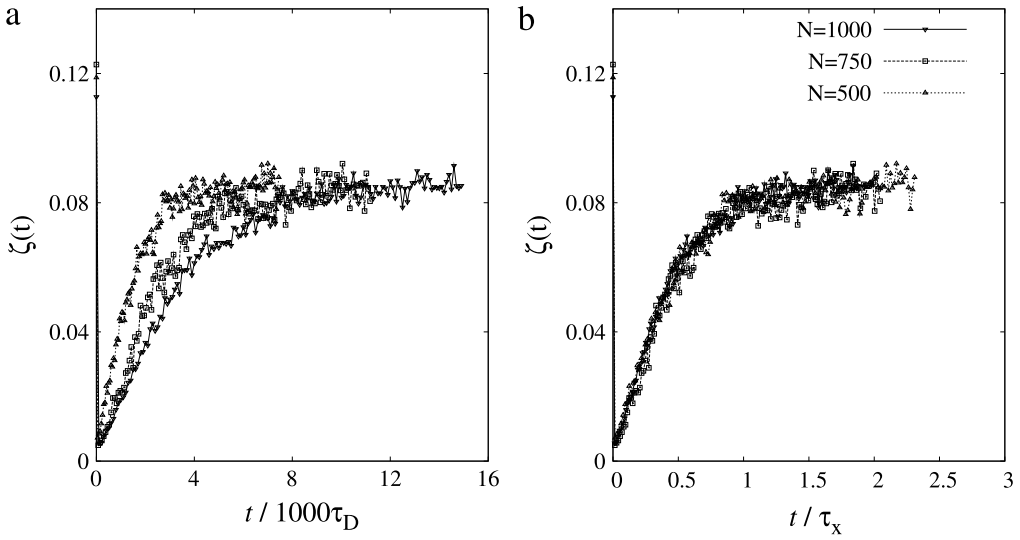

Fig. 31. (a) $\zeta(t)$ for different numbers of particles in the system. When the dynamical time τ_D is rescaled by $\tau_\times$, all points in (a) converge to a universal curve (b). In this case, the asymptotic value of ζ is $\zeta_{eq} \approx 0.08$. The simulations were performed with explicit particles with initial distribution satisfying the virial condition, $\mu_0 = K^* = 1$.

where $N_{eq}(v) = 2\pi N v \int f_{mb}(\mathbf{r}, v)\, d\mathbf{r}$ and $f_{mb}(\mathbf{r}, v)$ is the equilibrium distribution function. The dynamic time scale is set to $\tau_D = \kappa_z$. If the simulation time is scaled with $\tau_\times = N^\gamma \tau_D$, where $\gamma = 1.3$, all curves fall on the same universal curve. This shows that in thermodynamic limit the crossover time diverges as $N^{1.3}\tau_D$ (Fig. 31). The result is very similar to the one found in self-gravitating systems. Recently a theoretical model based on the Chandrasekhar collisional mechanism has been proposed to account for such large crossover time. The theory predicts that the most important factor in determining the exponent γ is the system dimensionality [192,193].

7.8. Thermodynamic equilibrium

After the crossover time $\tau_\times(N)$, during which the plasma remains trapped in an out of equilibrium qSS, it should relax to the thermodynamic equilibrium in which the particle density and velocity distributions should be given by the usual Boltzmann–Gibbs statistical mechanics

$$n(\mathbf{r}) = Ce^{-\beta\left[\omega(\mathbf{r})+\frac{r^2}{2}\right]} \tag{140}$$

and

$$n(\mathbf{v}) = \frac{\beta}{2\pi} e^{-\frac{\beta|\mathbf{v}|^2}{2}}, \tag{141}$$

where C is the normalization constant, $\beta = 1/T$ is the Lagrange multiplier for conservation of energy, and $\omega(\mathbf{r})$ is the potential of mean force [101]. For large number of particles, the correlations become unimportant and $\omega(\mathbf{r}) \approx \psi(\mathbf{r})$. The potential ψ_{eq} must then satisfy the Poisson–Boltzmann equation,

$$\frac{d^2\psi_{eq}(r)}{dr^2} + \frac{1}{r}\frac{d\psi_{eq}(r)}{dr} = -\frac{4\pi^2 K^* C}{\beta} e^{-\beta\left[\psi_{eq}(r)+\frac{r^2}{2}\right]} \tag{142}$$

with the boundary conditions $\psi_{eq}(r_w) = 0$ and $\psi'_{eq}(0) = 0$. The solution to this equation can be obtained numerically. In Fig. 32 we compare the predictions of the Boltzmann–Gibbs statistical mechanics with the results of MD simulations. The computer runs were performed with not too many particles to allow the system to relax to equilibrium within reasonable CPU time. Fig. 32 shows the marginal distributions $N(r) = 2\pi r n(r)$, and $N(v) = 2\pi v n(v)$ with $n(r)$ and $n(v)$ given by Eqs. (140) and (141). As expected, after a sufficiently long time the system relaxes to the thermodynamic equilibrium.

8. The Hamiltonian mean field model

The gravitational and plasma systems studied up to now are of great practical importance. From the perspective of statistical mechanics, however, they have a serious drawback — they do not exhibit a phase transition. In the last two sections of this review we will consider two systems with long-range forces which do show a spontaneous symmetry breaking. In particular, we are interested to explore how the phase transitions between the qSSs differ from the usual equilibrium phase transitions.

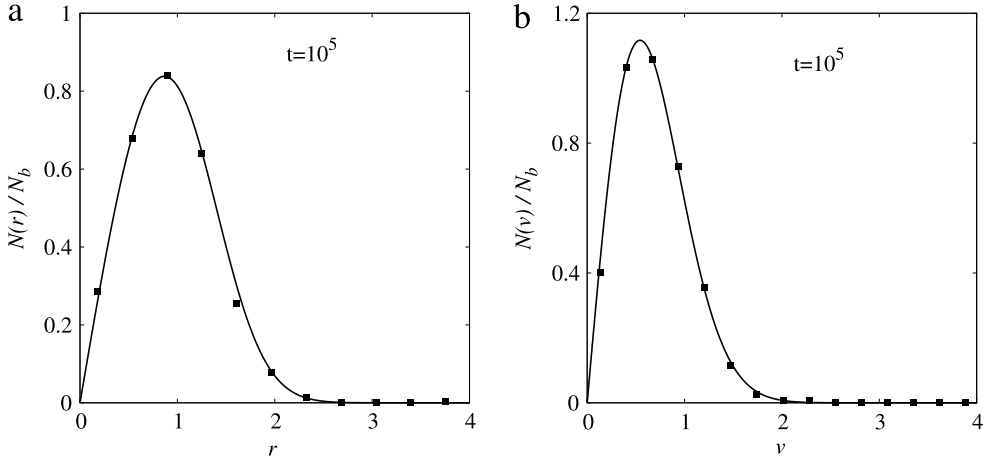

Fig. 32. Distribution in (a) position and (b) velocity for a system with $\mathcal{E}_0 = 1.597$. The solid line represents the equilibrium results $N(r)$ and $N(v)$, obtained using the Maxwell–Boltzmann distribution, and the points are the results of molecular dynamics simulations with $N = 1000$ particles. A fourth-order symplectic integrator with constant step size of $dt = 10^{-2}$ was used for the molecular dynamics [194].

The first system that we will study is the Hamiltonian Mean Field (HMF) model. The HMF is a mean-field version of the *XY*-model, in which all spins interact with each other [195,196]. It has become a paradigm of a system with long-range interaction [197–200], and is especially interesting due to its phase transition. For one-dimensional systems with short-range forces the Mermin–Wagner theorem prohibits spontaneous symmetry breaking in 1D [201]. The phase transition in the HMF is only possible because of the infinite range interaction between the spins [202,203]. The HMF model can also be considered a simplified representation of a one-dimensional self-gravitating [204] or Coulomb system [205] on a ring, and has some similarity with the Colson–Bonifacio model of a single-pass free electron laser [206–209].

8.1. The model

The HMF model can be interpreted in terms of interacting spins or as particles confined to move on a circle of radius one. The particle interpretation is more convenient for studying the dynamics of this model, so we will adopt it for most of our discussion. The dynamics of N particles of the HMF is governed by the Hamiltonian [196]

$$\mathcal{H} = \sum_{i=1}^{N} \frac{p_i^2}{2} + \frac{\gamma}{2N} \sum_{i,j=1}^{N} \left[1 - \cos(\theta_i - \theta_j)\right], \tag{143}$$

where θ_i is the coordinate and p_i the conjugate momentum of the ith particle, and γ is a parameter that controls the intensity of the interaction. The sign of γ determines the type of coupling between the particles: if $\gamma > 0$, the interaction is attractive and the coupling is ferromagnetic; if $\gamma < 0$, the interaction is repulsive and the coupling is antiferromagnetic.

The Hamiltonian (143) is a simplification of a one-dimensional gravitational or a Coulomb system with periodic boundary conditions and a neutralizing background. For example, consider a system formed by N particles distributed along a ring of unit radius, i.e. with position $\theta \in [-\pi\,,\ \pi]$. The Poisson equation is

$$\nabla^2 \psi(\theta) = \xi \sum_{i=1}^{N} \left[\delta(\theta - \theta_i) - \frac{1}{2\pi}\right] \tag{144}$$

where ξ depends on the system under consideration, and $\psi(-\pi) = \psi(\pi)$, $\psi'(-\pi) = \psi'(\pi) = 0$ if $\theta_i = 0,\ \forall i$. In the gravitational case $\xi = 4\pi G m$, where G is the gravitational constant, $m = M/N$ is the particle mass and M the total mass. For the Coulomb case, $\xi = -q/\varepsilon_0$, where $q = Q/N$ is the charge density, Q the total charge and ε_0 the vacuum permittivity. The term $1/2\pi$ represents the uniform neutralizing background which is necessary both for Coulomb and gravitational systems with periodic boundary conditions.

Expressing the Dirac delta in its Fourier representation, $\delta(\theta - \theta_i) = \sum_n \exp[\,\mathrm{i}\, n(\theta - \theta_i)]/2\pi$ and integrating the Poisson equation, the potential produced by N particles is found to be

$$\psi(\theta) = \xi \sum_{i=1}^{N} \sum_{n=1}^{\infty} \left[\frac{1 - \cos(n(\theta - \theta_i))}{\pi n^2}\right]. \tag{145}$$

The potential is normalized so that $\psi(0) = 0$ when $\theta_i = 0,\ \forall i$. Truncating the series at $n = 1$ and taking $\gamma/N = \xi/\pi$, we recover the potential of the HMF model.

We will consider the ferromagnetic HMF model. Rescaling time, we can set $\gamma = 1$. The Hamiltonian (143) can then be written as

$$\mathcal{H} = \sum_{i=1}^{N} \frac{p_i^2}{2} + \frac{1}{2N} \sum_{i,j=1}^{N} (1 - \cos\theta_i \cos\theta_j - \sin\theta_i \sin\theta_j), \tag{146}$$

or

$$\mathcal{H} = \sum_{i=1}^{N} \frac{p_i^2}{2} + \frac{1}{2} - \frac{1}{2N} \left(\sum_{i=1}^{N} \cos\theta_i \right)^2 - \frac{1}{2N} \left(\sum_{i=1}^{N} \sin\theta_i \right)^2. \tag{147}$$

The order parameter of the system is the magnetization per particle, $\mathbf{M} = (M_x, M_y)$, which measures how "bunched" is the particle distribution. If $M = 0$ the particles are uniformly distributed over the ring. The components of the magnetization are

$$M_x = \langle \cos\theta \rangle = \frac{1}{N} \sum_{i=1}^{N} \cos\theta_i \tag{148}$$

and

$$M_y = \langle \sin\theta \rangle = \frac{1}{N} \sum_{i=1}^{N} \sin\theta_i. \tag{149}$$

The energy per particle, $\mathcal{E} = \mathcal{H}/N$, can be written as

$$\mathcal{E} = \frac{\langle p^2 \rangle}{2} + \frac{1 - M_x^2 - M_y^2}{2}, \tag{150}$$

and the one particle energy is

$$\epsilon(\theta_i, p_i) = \frac{p_i^2}{2} + 1 - M_x \cos(\theta_i) - M_y \sin(\theta_i). \tag{151}$$

If the initial distribution is symmetric in θ, then $M_y = 0$, and in the thermodynamic limit, it will remain so throughout the evolution [25]. For now we will only consider symmetric distributions and set $M_y(t) = 0$.

8.2. Thermodynamic equilibrium

Classical statistical mechanics provides a prediction for the thermodynamic equilibrium of the HMF model [196]. In this subsection, we shall briefly describe the results in the microcanonical ensemble. A more extensive treatment of the equilibrium state of the HMF model can be found in Ref. [7].

The microcanonical ensemble is defined by the surface of constant energy E in the $2Nd$-dimensional configuration space, d being the number of degrees of freedom of each particle ($d = 1$ for the HMF),

$$\Omega(E, N) = \int_{-\pi}^{\pi} d\boldsymbol{\theta} \int_{-\infty}^{\infty} d\mathbf{p}\ \delta(H(\mathbf{p}, \boldsymbol{\theta}) - E), \tag{152}$$

where $\boldsymbol{\theta}$ and $\mathbf{p}$ are N-dimensional vectors representing the positions and velocities of all N particles that compose the system: $\boldsymbol{\theta} = (\theta_1, \theta_2, \ldots, \theta_N)$ and $\mathbf{p} = (p_1, p_2, \ldots, p_N)$. Thus, we also write $d\boldsymbol{\theta} = \prod_{i=1}^{N} d\theta_i$ and $d\mathbf{p} = \prod_{i=1}^{N} dp_i$.

The Boltzmann entropy per particle is $s = \frac{1}{N} \ln \Omega$ which is calculated to be [7,210]

$$s(\mathcal{E}) = \frac{1}{2}(\ln 4\pi + 1) + \sup_{M} \left[\frac{1}{2} \ln \left(\mathcal{E} - \frac{1 - M^2}{2} \right) - \frac{M^2}{2\mathcal{E} - 1 + M^2} + \ln I_0 \left(\frac{M}{2\mathcal{E} - 1 + M^2} \right) \right] \tag{153}$$

where $I_n(z) = \int d\theta \cos n\theta \exp(z \cos\theta)$ is the modified Bessel function of the first kind. The curve $s(\mathcal{E})$ is shown on Fig. 33. The equilibrium magnetization is obtained by solving the equation

$$\frac{I_1 \left(\frac{M}{2\mathcal{E} - 1 + M^2} \right)}{I_0 \left(\frac{M}{2\mathcal{E} - 1 + M^2} \right)} = M, \tag{154}$$

and is plotted as a function of $\mathcal{E}$ in Fig. 34. Finally, Fig. 35 shows the inverse temperature $\beta = 1/T$ as a function of $\mathcal{E}$. These figures indicate a second-order phase transition between ferromagnetic and paramagnetic states at $\mathcal{E}_c = 0.75$.

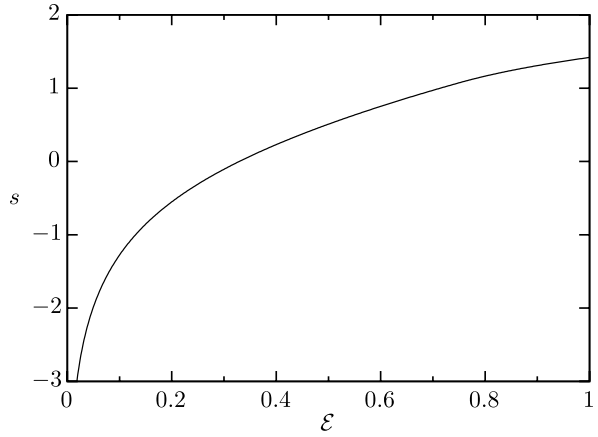

Fig. 33. Microcanonical entropy as a function of the mean energy for the HMF model.

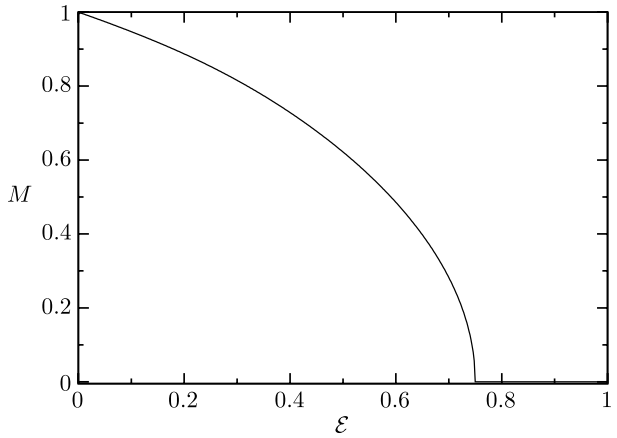

Fig. 34. Equilibrium magnetization as a function of the mean energy ε for the HMF.

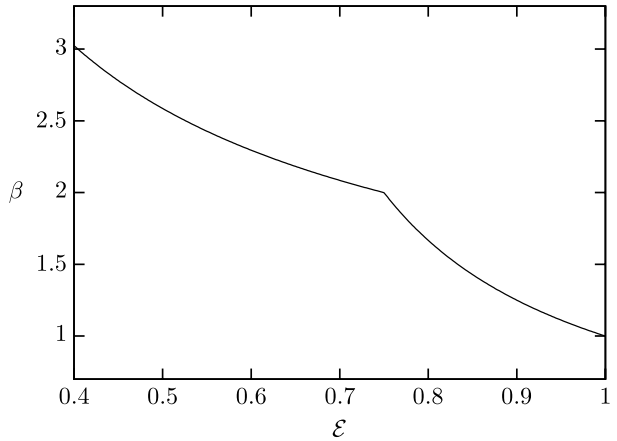

Fig. 35. The inverse temperature $\beta = 1/(2\varepsilon - 1 + M^2)$ as a function of the mean energy ε for the HMF. The sharp corner at $\varepsilon = 0.75$ indicates a second-order phase transition.

8.3. Nonequilibrium quasi-stationary states

The results shown in Section 8.2 are valid if the HMF is able to relax to thermodynamic equilibrium. However, as we have seen throughout this report, in thermodynamic limit systems with long-range interactions do not reach the equilibrium, but become trapped in a qSS, the lifetime of which diverges with the number of particles [102]. Thus, in practice the equilibrium state will never be achieved by the HMF model with a large enough number of particles. To explore the properties of the qSS and the possible phase transitions between the different nonequilibrium states, we use MD simulations. In this report we focus on simulations with initial distributions of the one-level waterbag type — Eq. (155); for results of studies of the qSSs of the HMF model using other types of initial distributions, see for example Refs. [211–213].

At $t = 0$ the particles are distributed in accordance with the one-level waterbag distribution,

$$f_0(\theta, p) = \eta\Theta(\theta_m - |\theta|)\Theta(p_m - |p|), \tag{155}$$

where $\Theta(x)$ is the Heaviside step function. The constants η (density), θ_m (maximum value of θ) and p_m (maximum value of p) are determined by the normalization of the distribution, initial magnetization (M_0) and mean energy ($\mathcal{E}$), respectively,

$$1 = \int_{-\pi}^{\pi} d\theta \int_{-\infty}^{\infty} dp\, f_0(\theta, p), \tag{156}$$

$$M_0 = \int_{-\pi}^{\pi} d\theta \int_{-\infty}^{\infty} dp\, f_0(\theta, p) \cos\theta, \tag{157}$$

and

$$\mathcal{E} = \int_{-\pi}^{\pi} d\theta \int_{-\infty}^{\infty} dp\, f_0(\theta, p) \frac{p^2}{2} + \frac{1 - M_0^2}{2}. \tag{158}$$

These lead to

$$\eta = \frac{1}{4\theta_m\, p_m}, \tag{159}$$

$$M_0 = \frac{\sin\theta_m}{\theta_m}, \tag{160}$$

and

$$p_m = \sqrt{3\,(2\mathcal{E} - 1 + M_0^2)}. \tag{161}$$

To simulate a system composed of N particles, we use two vectors of dimension $N/2$, where the ith component of the first vector represents the angle θ_i of the ith particle, and similarly the ith component of the second vector is the momentum p_i of the respective particle. As the initial condition, each θ_i and p_i take a random value between $[-\theta_m, \theta_m]$ and $[-p_m, p_m]$, respectively. For each of these particles, we consider that there exists a particle in a symmetrical position in phase space: $\theta_{i+N/2} = -\theta_i$ and $p_{i+N/2} = -p_i$, which ensures that $M_y(t) = 0\,\forall\, t$ and increases the simulation speed — since the dynamics is symmetric, we only need to integrate the motion of half of the particles.

The trajectory of each particle is governed by the equation of motion $\ddot{\theta}_i = \dot{p}_i = -\partial H/\partial\theta_i$, or

$$\begin{aligned}\ddot{\theta}_i &= -\frac{1}{N}\sin\theta_i \sum_{j=1}^{N}\cos\theta_j + \frac{1}{N}\cos\theta_i \sum_{j=1}^{N}\sin\theta_j \\ &= -M_x\sin\theta_i + M_y\cos\theta_i \\ &= -M\sin\theta_i.\end{aligned} \tag{162}$$

The numerical integration is implemented using a fourth-order symplectic integrator [214], available online from E. Hairer [215]. To control the numerical precision, the error in conservation of energy per particle $\mathcal{E}$, given by Eq. (150), was kept at approximately 10^{-8}.

Fig. 36 shows examples of two initial phase space distributions, panels (a) and (c), and the respective distributions after a qSS have been achieved, panels (b) and (d). The simulations were performed with $N = 2 \times 10^5$ particles. The initial magnetization was the same in both simulations, $M_0 = 0.8$ — both initial waterbags had the same θ_m. The p_m's for the two distributions were different corresponding to energies (a) $\mathcal{E} = 0.7$ and (c) $\mathcal{E} = 0.45$. The two initial conditions lead to different phases: the higher energy configuration leads to a paramagnetic (homogeneous) distribution, panel (b), while the system with lower energy remains magnetized, panel (d).

The final qSS state depends both on the initial magnetization M_0 and energy $\mathcal{E}$. This is very different from the state of thermodynamic equilibrium which depends only on $\mathcal{E}$. The evolution of M for two systems with the same energy $\mathcal{E} = 0.62$ and different values of M_0 is shown in Fig. 37. A system with an initial magnetization $M_0 = 0.2$ quickly relaxes to a paramagnetic state in which its magnetization oscillates around $M = 0$. On the other hand, a system with $M_0 = 0.8$ remains magnetized. In both cases, the magnetization $M(t)$ oscillates around its quasi-stationary value M_s, given by the temporal average of $M(t)$ [211]. However, while the oscillations inside the ferromagnetic state are clearly damped, the amplitude of oscillations in the paramagnetic state remains finite. The difference between the two states is that inside the ferromagnetic phase the particles experience a finite mean-field potential produced by $M(t)$ while in the paramagnetic phase the average potential is zero. This means that inside the ferromagnetic state some particles can enter in resonance with the oscillations of the potential and gain energy from the collective motion. This, in turn, will result in Landau damping of the magnetization and the relaxation to qSS. In the paramagnetic phase, $M(t)$ oscillates around zero, so there is no resonant mechanism to dampen the oscillations.

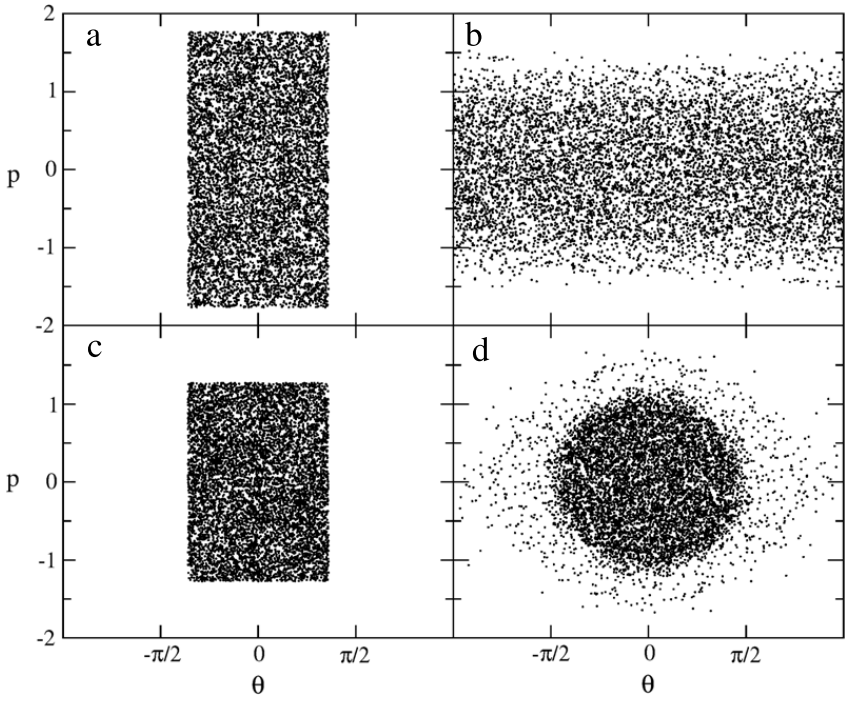

Fig. 36. Phase space of molecular dynamics with $N = 2 \times 10^5$. The left column shows the initial distributions with (a) $\mathcal{E} = 0.7$ and (c) $\mathcal{E} = 0.45$. The initial magnetization is the same for both cases, $M_0 = 0.8$. The right column shows the two final qSS to which the system relaxes: (b) paramagnetic and (d) ferromagnetic. The simulation time is $t = 5000$.

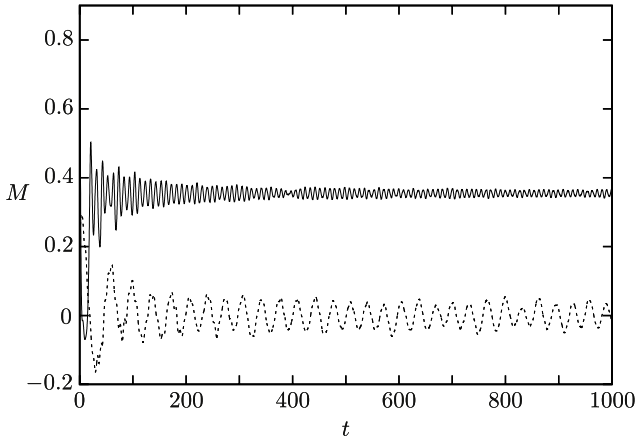

Fig. 37. Magnetization as a function of time obtained using MD simulation with $N = 10^6$ particles. For the same energy $\mathcal{E} = 0.62$, different initial magnetizations result in distinct qSS: for $M_0 = 0.8$ ferromagnetic (solid line) and for $M_0 = 0.2$ paramagnetic (dashed line).

The location of the phase transition can be determined by performing simulations for different initial conditions, varying $\mathcal{E}$ for a fixed initial magnetization and calculating M_s. The resulting nonequilibrium phase diagram for the HMF model is shown in Fig. 38. The results are fairly similar to the nonequilibrium phase diagram found using the Lynden-Bell entropy [216], yet has some differences, primarily as to the order of the phase transition in some regions, as will be seen further on in this chapter, and in the location of the transition for higher initial magnetizations.

It is interesting to compare the nonequilibrium phase diagram with the one found for the equilibrium of the HMF model. In equilibrium, the critical energy $\mathcal{E}_e = 0.75$ separates the paramagnetic ($\mathcal{E} > \mathcal{E}_e$) from the ferromagnetic phase ($\mathcal{E} < \mathcal{E}_e$) and is independent of the initial magnetization, as is shown by the dashed–dotted line of zero slope in the phase diagram, Fig. 38. On the other hand, the transition between the nonequilibrium ferromagnetic and paramagnetic phases occurs at different values of $\mathcal{E}$, depending on the initial magnetization. This transition is represented by a solid line. The shaded region is the forbidden zone — since the minimum kinetic energy is zero, M_0 determines the minimum allowed energy per particle $\mathcal{E}_{\min} = (1 - M_0^2)/2$. The diagram also shows a region in which the nonequilibrium order–disorder transition is not well defined: the wide, shaded line around the critical line for $M_0 > 0.6$, approximately. For these values of M_0, there are regions where the average energy $\mathcal{E}$ is above the critical line, yet in which the system remains magnetized. Similar regions, or reentrances, have also been observed in studies of the HMF model using numerical resolution of the Vlasov

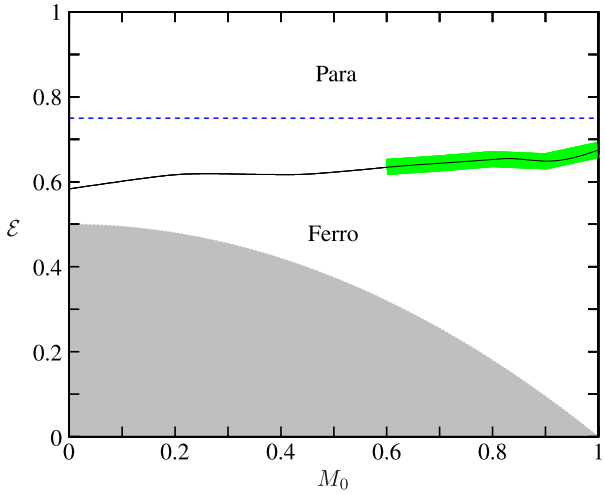

Fig. 38. Phase diagram of the HMF model. The solid line shows the nonequilibrium transition, obtained using MD simulations. Around this line, for $M_0 > 0.6$, approximately, the green line shows a region in which the transition is not very well defined, where "reentrances", small ferromagnetic regions exist above the critical line, inside the paramagnetic region. The equilibrium transition, at $\mathcal{E} = 0.75$, is represented by the blue dash-dotted line. The gray area represents forbidden initial conditions, delimited by the minimum energy necessary for a given M_0. (For interpretation of the references to colour in this figure legend, the reader is referred to the web version of this article.)

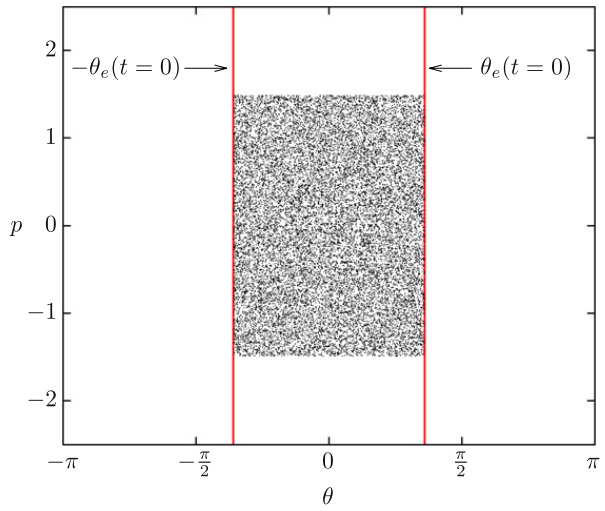

Fig. 39. Example of the envelope θ_e at $t = 0$ (red lines) in comparison with an initial waterbag distribution of particles (dots). (For interpretation of the references to colour in this figure legend, the reader is referred to the web version of this article.)

equation [217] and Lynden-Bell statistics [218]. Finally, while the equilibrium phase transition between the ferromagnetic and paramagnetic phases is of second order [7], the nonequilibrium phase transition is of first order.

In our studies of self-gravitating systems and plasmas, we saw the importance of the virial theorem to determine when strong collective oscillations will occur. However, since the potential of the HMF is not a homogeneous function of the separation between the particles, we cannot directly apply the results of Section 4.4 to determine the virial condition. To discover under what conditions the magnetization of the HMF model will remain constant, so that the parametric resonances will not be excited, we need to derive a Generalized Virial Condition (GVC). To do this we define the envelope of the particle distribution of the HMF as [19]

$$\theta_e(t) = \sqrt{3\langle\theta^2(t)\rangle}. \tag{163}$$

Note that at $t = 0$, the envelope coincides with the maximum θ of the initial waterbag distribution, θ_m, see Fig. 39. Differentiating Eq. (163) twice with respect to time, we find

$$\ddot{\theta}_e(t) = \frac{3\langle\dot{\theta}^2(t)\rangle}{\theta_e(t)} + \frac{3\langle\theta\ddot{\theta}(t)\rangle}{\theta_e(t)} - \frac{9\langle\theta(t)\dot{\theta}(t)\rangle^2}{\theta_e^3(t)}. \tag{164}$$

As the result of the conservation of energy, see Eq. (150), in the first term, the mean square velocity $\langle\dot{\theta}^2(t)\rangle$ is $2\mathcal{E} - 1 + M^2(t)$. To calculate the other averages, we assume the marginal distribution in θ remains uniform in the interval $[-\theta_e(t), \theta_e(t)]$

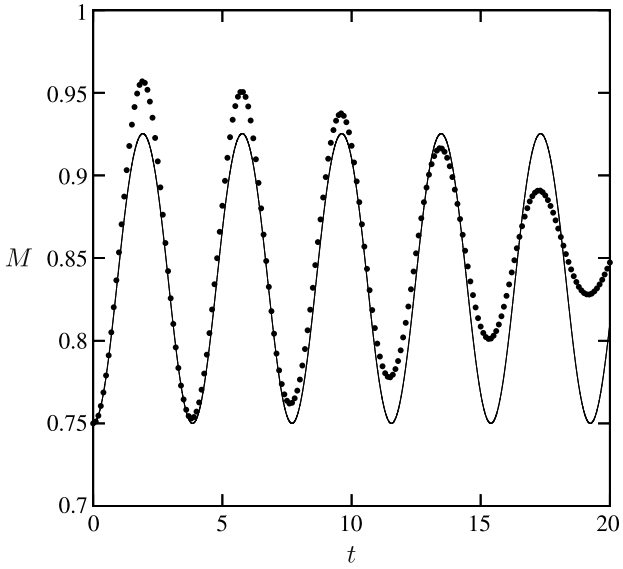

Fig. 40. Comparison of the magnetization $M(t) = \sum_i \cos\theta_i/N$ of molecular dynamics (dots) and of the envelope magnetization $M_e(t) = \sin\theta_e(t)/\theta_e(t)$ (line). The initial condition is ($M_0 = 0.75$, $\mathcal{E} = 0.25$), off the generalized virial curve.

and zero outside. Using this approximation, the second term of Eq. (164) reduces to

$$\begin{aligned}\langle\theta\ddot{\theta}(t)\rangle &= \frac{-M(t)}{2\theta_e(t)}\int_{-\theta_e(t)}^{\theta_e(t)}\theta\sin\theta d\theta\\ &= \frac{M(t)}{2\theta_e(t)}\left[\theta\cos\theta-\sin\theta\right]_{-\theta_e(t)}^{\theta_e(t)}\\ &= \frac{M(t)}{2\theta_e(t)}\left[2\theta_e(t)\cos\theta_e(t)-2\sin\theta_e(t)\right]\\ &= M(t)\cos\theta_e - M(t)\frac{\sin\theta_e(t)}{\theta_e(t)}.\end{aligned}$$

The last term of Eq. (164) may be neglected by disregarding the correlations between θ and p. The resulting envelope equation is

$$\ddot{\theta}_e(t) = \frac{3}{\theta_e}\left(2\mathcal{E} + M_e(t)\cos\theta_e - 1\right), \tag{165}$$

where we have used

$$\begin{aligned}M_e(t) &= \frac{1}{2\theta_e(t)}\int_{-\theta_e(t)}^{\theta_e(t)}\cos\theta d\theta\\ &= \frac{\sin\theta_e(t)}{\theta_e(t)}.\end{aligned} \tag{166}$$

Fig. 40 compares the evolution of magnetization $M_e(t)$, predicted by the Eqs. (165) and (166), with the magnetization obtained using the full N-body MD simulation. We see an excellent agreement between the theory and simulation, especially at short times. For longer times, the amplitude of the magnetization observed in the simulations is damped, while in the envelope oscillations it is not. This occurs because the envelope equation is conservative, while in the simulation the parametric resonances transfer the energy from the collective oscillations to the individual particles.

The GVC corresponds to the initial condition for which the envelope does not oscillate, so that $M_e(t) = M_0$. This happens when [19],

$$2\mathcal{E} + M_0\cos\theta_m - 1 = 0, \tag{167}$$

so that $\ddot{\theta}_e(t) = 0$. Eq. (167) defines the GVC condition which is plotted by the dashed line in the nonequilibrium phase diagram of Fig. 41.

To test the GVC we perform MD simulations starting with initial waterbag distributions which lie directly on top of the GVC curve (167). We then plot with triangles in Fig. 41 the final magnetization to which the system relaxes (note that for both the initial and the final state the energy is the same). We see that the final stationary magnetizations M_s are almost exactly the same as the initial magnetizations M_0. Furthermore, for systems with initial conditions *off* the GVC curve, the magnetization

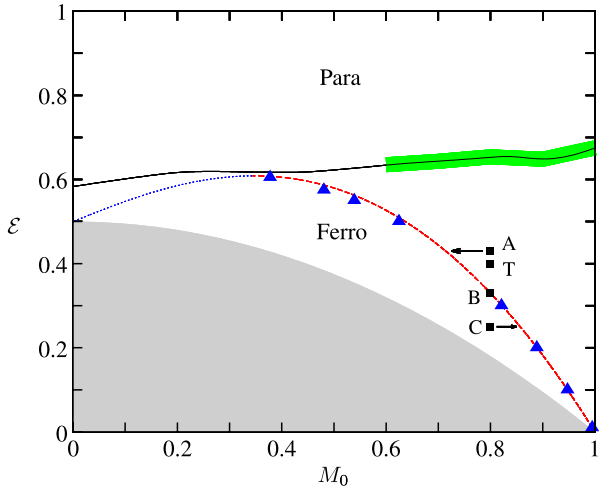

Fig. 41. Phase diagram of the HMF model, exhibiting the generalized virial condition (red dashed line). Triangles represent the stationary magnetization M_s, determined using MD simulations, of systems with initial conditions on the generalized virial condition. Points *A*, *B* and *C* show the initial state of the systems corresponding to Fig. 42, and *T* and *B* to Fig. 43. The arrows next to *A* and *C* indicate that the stationary magnetization corresponding to these initial conditions is close to the magnetization of the GVC curve for the same energy $\mathcal{E}$. The continuation of the GVC curve, the blue dotted line for $M_0 < 0.343$, shows an unstable region. The lower gray area represents inaccessible initial conditions. The black solid line shows the phase transition, and the thick green line represents the region of reentrances, where some small ferromagnetic regions exist above the critical line.

quickly changes and begins to oscillate around the stationary value corresponding to M_s on the GVC curve with the same $\mathcal{E}$. For example, points *A* and *C* of Fig. 41 each represent initial conditions *off* the GVC. Let us call the coordinates of these points $(M_0^A, \mathcal{E}^A)$ and $(M_0^C, \mathcal{E}^C)$, respectively. The stationary values obtained using the MD simulations correspond to $(M_s^A, \mathcal{E}^A)$ and $(M_s^C, \mathcal{E}^C)$. The arrows next to points *A* and *C* indicate the values of M_s^A and M_s^C on the GVC curve to which the system relaxes. This result is quite surprising, since the distribution functions for the initial and the final state are very different for systems that do not satisfy the GVC [19]. It is not clear at this moment why the approximate GVC derived using the waterbag distribution works so well to predict the final magnetizations for systems which initially are very far from their qSS.

Eq. (167) has an unstable branch, represented by the blue dotted line in Fig. 41. If the initial conditions place the system exactly on this branch, the magnetization will remain the same, however, any perturbation will make the system evolve from the line of unstable fixed points toward the line of stable ones, represented by the red dashed curve.

8.4. Lynden-Bell theory for the HMF model

The LB theory has been extensively applied to the HMF model, in some cases showing reasonable agreement with the results of MD simulations [54,55,219,220]. From the examples of gravity and plasma, however, we expect that LB theory should only work when the initial distribution satisfies the GVC. For non-virial initial conditions, resonances should drive the HMF into a qSS with a core–halo particle distribution [19,25].

The LB distribution for the HMF model is given by [55]

$$\bar{f}_{lb}(\theta, p) = \eta \frac{e^{-\beta(p^2/2 - M[\bar{f}_{lb}]\cos\theta - \mu)}}{1 + e^{-\beta(p^2/2 - M[\bar{f}_{lb}]\cos\theta - \mu)}}, \tag{168}$$

where $M(\bar{f}_{lb}) = \int \bar{f}_{lb} \cos\theta dp d\theta$. The phase space density η is determined by the initial distribution (159), while β and μ are the Lagrange multipliers used to preserve the norm and the energy. Solving the system of equations

$$\mathcal{E} = \frac{\eta}{2} \int p^2 \left[1 + \exp(\beta p^2/2 - \beta M(\bar{f}) \cos\theta - \beta\mu)\right]^{-1} dp d\theta + \frac{1 - M(\bar{f})^2}{2}, \tag{169}$$

$$1 = \eta \int \left[1 + \exp(\beta p^2/2 - \beta M(\bar{f}) \cos\theta - \beta\mu)\right]^{-1} dp d\theta \tag{170}$$

and

$$M = \eta \int \cos\theta \left[1 + \exp(\beta p^2/2 - \beta M(\bar{f}) \cos\theta - \beta\mu)\right]^{-1} dp d\theta \tag{171}$$

we can calculate β, μ and M and obtain the particle distribution predicted by LB for the qSS.

In Fig. 42, we show the marginal distributions, in angle and momentum, obtained using MD simulations, and compare them with the predictions of LB theory. Three different initial conditions are shown in Fig. 41: panels *A* and *C* correspond to non-virial initial conditions, while panel *B* shows the initial condition that lies on the GVC. For the non-virial initial

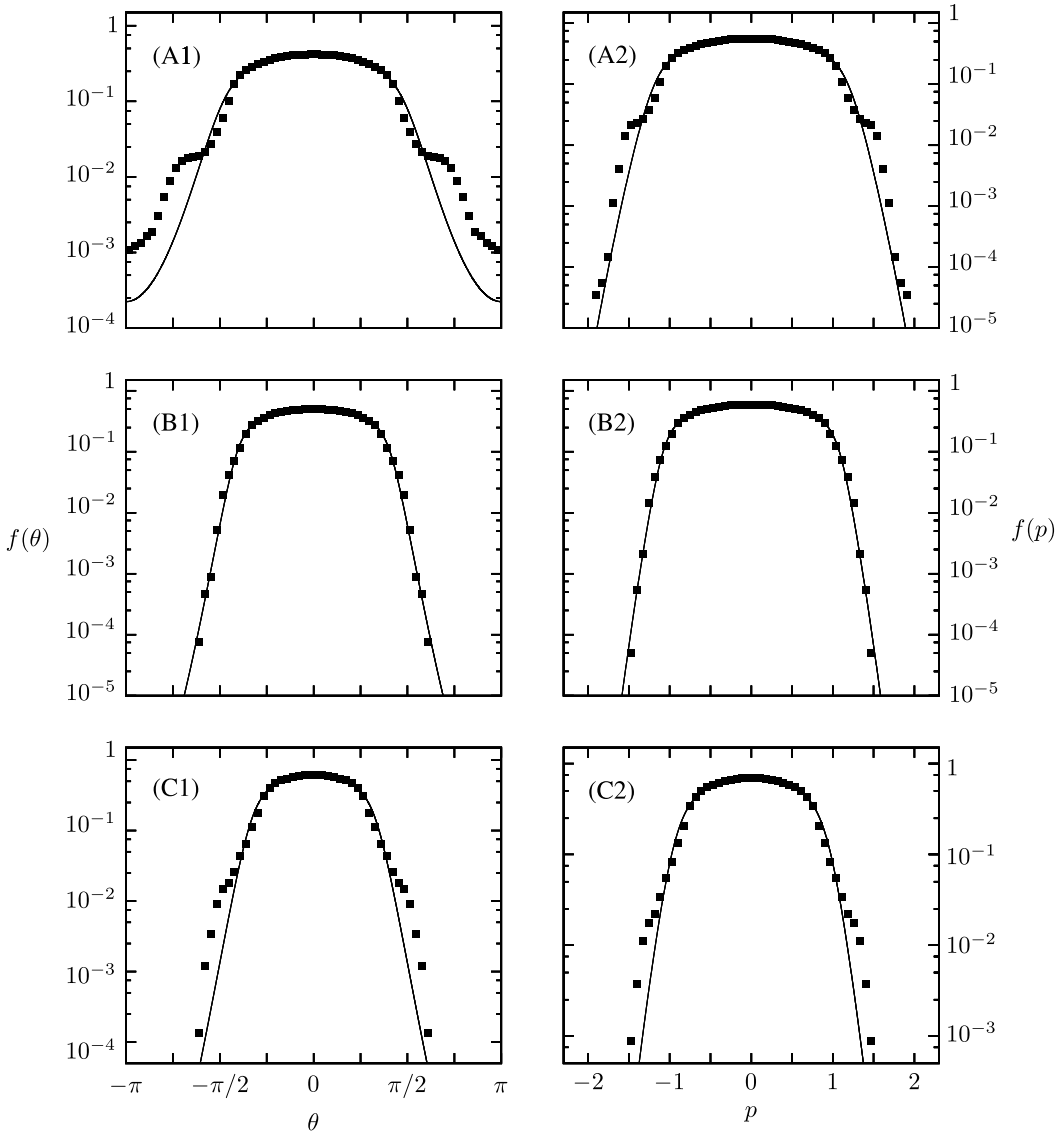

Fig. 42. Distributions in angle (left column) and momentum (right column) of the stationary states calculated using molecular dynamics (squares) and LB theory (lines) for three different initial conditions — top row (point *A* of Fig. 41): $M_0 = 0.8$, $\mathcal{E} = 0.43$ (off the generalized virial curve); middle row (point *B* of Fig. 41): $M_0 = 0.8$, $\mathcal{E} = 0.3297$ (on the generalized virial curve); bottom row (point *C* of Fig. 41): $M_0 = 0.8$, $\mathcal{E} = 0.25$ (off the GVC). In the MD simulations were used $N = 10^5$ and the corresponding distributions were averaged between times $t = 15{,}000$ and $t = 17{,}000$. Error bars in the distributions are smaller than the symbol size.

conditions, the distribution functions show a significant deviation from the LB theory. On the other hand, the initial distribution that satisfies the GVC is found to relax to the qSS which is well described by LB theory, panel *B* of Fig. 41.

8.5. The test particle model

The discrepancies between the results of MD simulations and the LB theory, for initial distributions which do not satisfy the GVC, are a consequence of the parametric resonances which transfer the energy from the collective motion to the individual particles [19]. To study these resonances we, once again, appeal to the test particle model. The test particles obey the equation of motion (162), with the magnetization determined by the envelope equation, $M_e(t)$. Fig. 43 shows the Poincaré sections of test particle dynamics – the phase space of the test particles plotted when $M_e(t)$ is at its minimum – compared with the phase space of the HMF, obtained using MD simulation. Two cases are shown: top panels correspond to the initial conditions that obey the GVC (point *B* of Fig. 41), while the bottom panels correspond to the initial conditions slightly off the GVC (point *T* of Fig. 41). For the initial distribution satisfying the GVC, the test particle dynamics is regular and no halo is formed. On the other hand, for the non-virial initial distributions (off the GVC), we see resonances which lead to the halo formation in the HMF.

The mechanism of core–halo formation in the HMF is the same as was discussed for gravitational and plasma systems. The parametric resonances transfer the energy from the collective motion to the individual particles. This, in turn, dampens

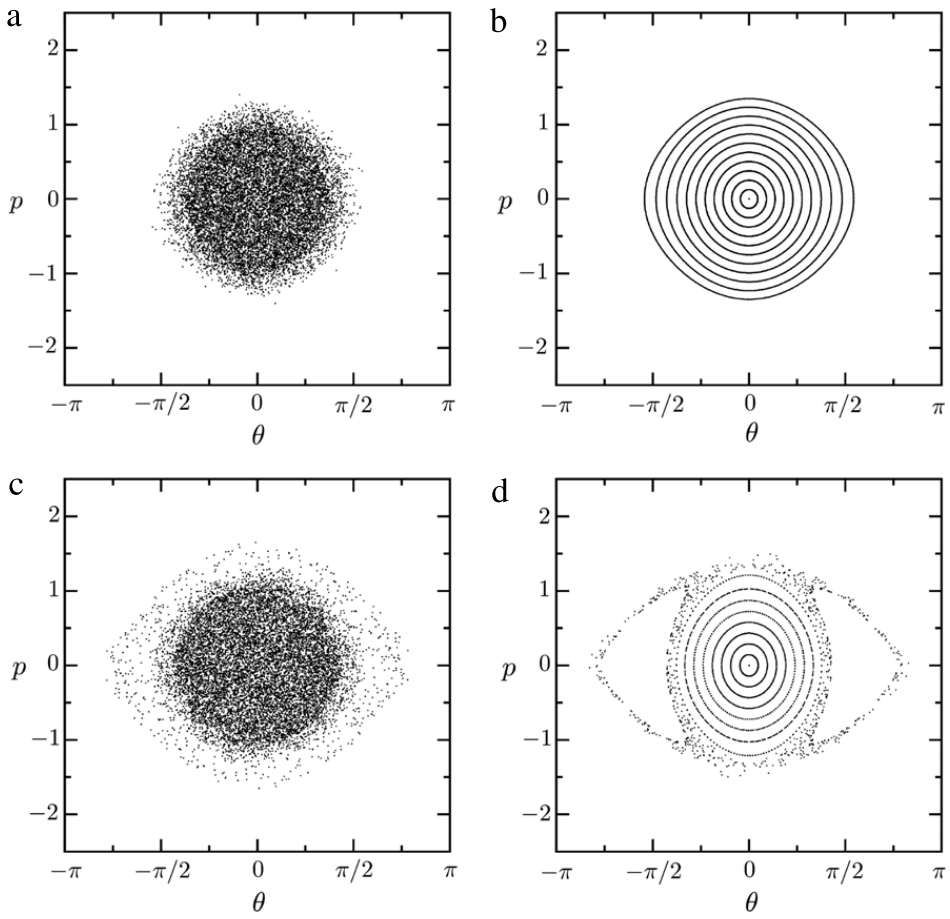

Fig. 43. Right column: Poincaré sections of test particle dynamics. Left column: phase space of molecular dynamics of $N = 10^5$ particles. Top row: initial conditions on the generalized virial curve ($M_0 = 0.8$, $\mathcal{E} = 0.3297$) – point B of Fig. 41. Bottom row: initial conditions off the generalized virial curve ($M_0 = 0.8$, $\mathcal{E} = 0.4$) – point T of Fig. 41.

the collective oscillations, forcing the core particles into low energy orbits. Once the oscillations die out completely, the dynamics of all the particles becomes integrable, and the ergodicity is irreversibly broken. The high energy particles become trapped inside a halo, while the low energy particles form a degenerate core. The LB theory, which relies on the assumptions of ergodicity and efficient mixing [104], is not able to describe such qSSs [19].

8.6. The core–halo distribution

The core–halo distribution for the HMF model is [25]

$$\bar{f}_{ch}(\theta, p) = \eta\Theta(\epsilon_F - \epsilon(\theta, p)) + \chi\Theta(\epsilon(\theta, p) - \epsilon_F)\Theta(\epsilon_h - \epsilon(\theta, p)), \tag{172}$$

with the one-particle energy given by $\epsilon(\theta, p) = \frac{p^2}{2} + 1 - M\cos(\theta)$. To calculate this distribution we need to determine ϵ_h, ϵ_F, M_s and χ. The parameters ϵ_F and χ are calculated using the conservation of energy and norm, respectively,

$$\mathcal{E} = \frac{1}{2}\int p^2 f_{ch}(\theta, p)dpd\theta + \frac{1}{2}(1 - M_s^2), \tag{173}$$

$$1 = \int f_{ch}(\theta, p)dpd\theta, \tag{174}$$

and M_s is given by

$$M_s = \int \cos\theta f_{ch}(\theta, p)d\theta dp. \tag{175}$$

To calculate ϵ_h for gravitational systems and plasmas we have used the test particle dynamics to locate precisely the resonant orbit. However, there is an inherent difficulty in using this approach for the HMF model. The interaction potential for HMF particles is bounded from above. Depending on the initial conditions, some particles can gain enough energy to completely escape the confining potential, and start moving in rotating orbits. This makes it difficult to pinpoint the highest

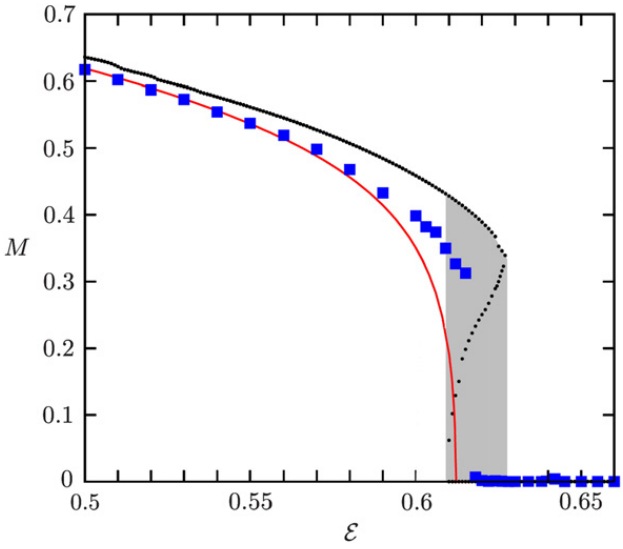

Fig. 44. qSS magnetization according to the core–halo theory (black dots), LB theory (red line), and as determined by MD simulations with $N = 2 \times 10^6$ particles (blue squares), averaged over 200 dynamical times in the qSS. For the core–halo theory, ϵ_h was determined by test particle dynamics. The shaded region shows where the first order transition predicted by the core–halo theory will occur. Error bars of the MD simulation results are comparable to the symbol size.

possible energy of the resonant particle. In this sense, the HMF model is similar to 3d self-gravitating systems, for which particles can escape the gravitational potential of the cluster. Another difficulty with the test particle dynamics is that while the system is spatially periodic, the envelope equation (165) is not. The oscillations of the envelope may be so large that the envelope surpasses $\theta_e = \pi$, in which case an artificial periodicity must be introduced into the test particle dynamics. In spite of these difficulties, we can still attempt to use the core–halo distribution with the approximate values of ϵ_h to locate the order–disorder transition in this model. Fig. 44 shows the qSS magnetization M_s as determined by the core–halo theory and the test particle dynamics for various values of $\mathcal{E}$ at fixed initial magnetization $M_0 = 0.4$. The core–halo theory predicts a first order phase transition between the paramagnetic and ferromagnetic phases. In the same figure we also plot the prediction of LB theory. Although the distribution functions of LB theory deviate significantly from the results of MD simulations, far from the transition point the theory accounts quite accurately for the values of M_s. LB theory, however, incorrectly predicts that the phase transition between the qSSs for $M_0 = 0.4$ is of second order [216], while the simulations find it to be of first order, Fig. 44. Numerical resolution of the Vlasov equation, which may be used to study the dynamics of the HMF model [221], also shows only first-order transitions in the HMF [217].

At the moment, we lack a general method to calculate the halo energy ϵ_h for arbitrary values of M_0 and $\mathcal{E}$. The envelope equation and the test particles dynamics allow us to make accurate predictions of ϵ_h for distributions close to the GVC. To predict the final particle distributions in the qSS which are far from the GVC, we can use a short MD simulation of the full HMF model with not too many particles. Since the formation of resonances is a fast process, the ϵ_h can be defined as the highest energy achieved by any particle after a few oscillations of $M(t)$. Fig. 45 shows that this procedure leads to an excellent description of the final qSS.

8.7. Relaxation to equilibrium

For finite N, the lifespan of the qSS is finite, and eventually a crossover to thermodynamic equilibrium occurs [222]. In equilibrium the particle distribution has the usual Maxwell–Boltzmann form, with the magnetization given by the solution of Eq. (154) [7]. The relaxation to equilibrium is shown in Fig. 46, which demonstrates the evolution of M for different values of N. The initial condition ($M_0 = 0.4$ and $\mathcal{E} = 0.65$) is such that the qSS is paramagnetic, while the equilibrium state is ferromagnetic. For this energy, the equilibrium magnetization is $M_{eq} = 0.397$, represented by the black dotted line in Fig. 46. As the figure shows, the fewer particles in the system, the faster the magnetization relaxes to the equilibrium value. Rescaling time with N^γ, with $\gamma \approx 1.7$, all the curves collapse onto one universal curve. The lifespan of the qSS therefore scales with $\tau_\times \sim N^\gamma$. The exponent $\gamma \approx 1.7$ is the same as the value found in other studies of the HMF model [102]. However, recent large-scale MD simulations show that for large N, the exponent γ crosses over to $\gamma = 2$. This is consistent with the arguments based on the Balescu–Lenard equation, which suggest that the crossover time from a paramagnetic (homogeneous) qSS to a ferromagnetic equilibrium state should scale as N^2 [223–225].

9. The generalized Hamiltonian mean field model

From the perspective of statistical mechanics, the HMF model is significantly richer than self-gravitating or plasma systems. Unlike these systems, the HMF possesses a genuine nonequilibrium phase transition between qSSs. The structure

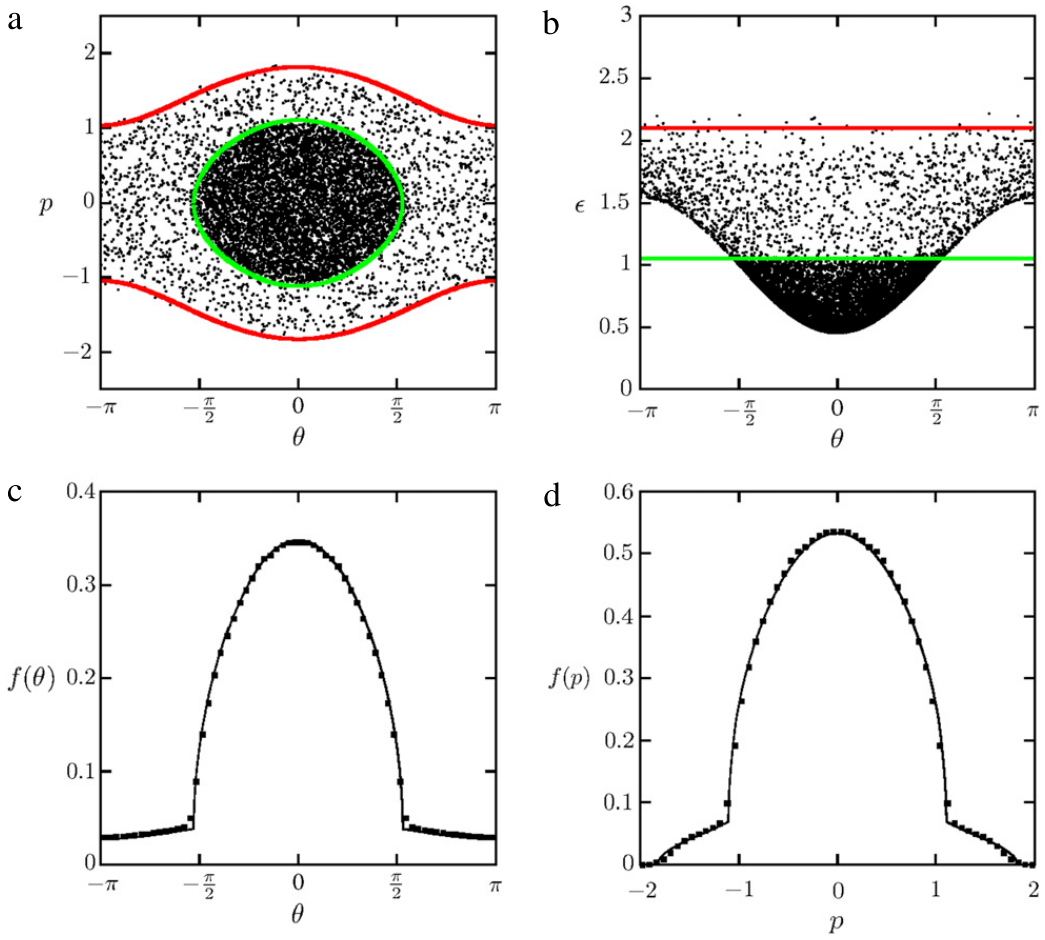

Fig. 45. Comparison of MD simulation with $N = 8 \times 10^5$ particles and predictions of the core–halo theory for ($M_0 = 0.8$, $\mathcal{E} = 0.55$). Panel (a) shows the phase space at $t = 10{,}000$ (black dots) and the curves $\epsilon(\theta, p) = \epsilon_h$ (red line) and $\epsilon(\theta, p) = \epsilon_F$ (green line). Panel (b) shows the one-particle energy $\epsilon(\theta, p)$ (black dots) and the energies ϵ_h (red line) and ϵ_F (green line). Panels (c) and (d) show the distributions in θ and p, respectively, of molecular dynamics (squares) and core–halo theory (lines). The halo energy ϵ_h was determined using a short MD simulation with $N = 1000$. The distributions of MD simulations are averaged over 100 dynamical times in the qSS, and error bars are comparable to symbol size. (For interpretation of the references to colour in this figure legend, the reader is referred to the web version of this article.)

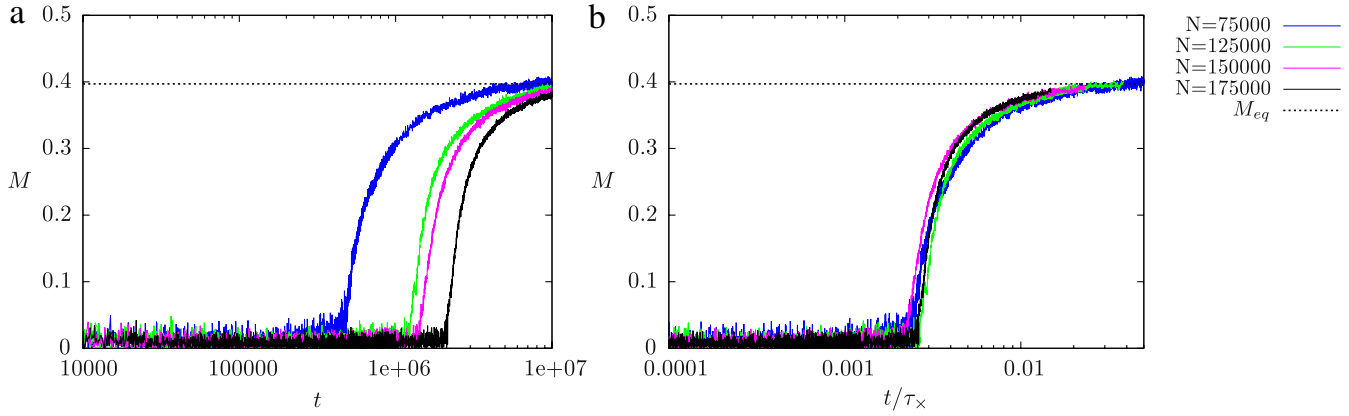

Fig. 46. Magnetization as a function of time for different values of N: $N = 75 \times 10^3$ (blue), $N = 125 \times 10^3$ (green), $N = 150 \times 10^3$ (magenta) and $N = 175 \times 10^3$ (black). The results are from MD simulations with initial magnetization $M_0 = 0.4$, and mean energy $\mathcal{E} = 0.65$. For this energy, the equilibrium state is ferromagnetic, while the qSS is paramagnetic. The black dotted line represents the equilibrium magnetization, $M_{eq} = 0.397$, corresponding to this energy. (For interpretation of the references to colour in this figure legend, the reader is referred to the web version of this article.)

of the phase diagram of the HMF, however, is still relatively simple, since only paramagnetic and ferromagnetic phases exist. To explore further the differences between equilibrium and nonequilibrium phase transitions, we introduce a Generalized Hamiltonian Mean Field (GHMF) model. In addition to paramagnetic and ferromagnetic phases, this model also has a nematic

phase. In this section we will compare the equilibrium and nonequilibrium phase diagrams of the GHMF and show that in the new qSS nematic phase, particles are once again distributed in accordance with the core–halo distribution.

9.1. The model

The Hamiltonian of the GHMF model is given by

$$H = \sum_{i=1}^{N} \frac{p_i^2}{2} + \frac{1}{2N} \sum_{i,j=1}^{N} \left[1 - \Delta \cos(\theta_i - \theta_j) - (1 - \Delta) \cos(q\theta_i - q\theta_j)\right], \tag{176}$$

where $q \in \mathbb{N}$ and $\Delta \in [0, 1]$ [226]. This model is a long-range version of the models studied in Refs. [227,228]. Considering the particles as a collection of spins, the generalized nematic coupling $\cos(q\theta_i - q\theta_j)$ favors either alignment or misalignment of spins. For example, for $q = 2$, it favors either parallel or antiparallel spins. From the perspective of the particle dynamics, either homogeneous or bunched states are possible, with the number of bunches controlled by the parameter q.

The order parameters for the GHMF model are the generalized magnetizations

$$M_1 = \frac{1}{N} \sum_{i=1}^{N} \cos\theta \tag{177}$$

and

$$M_q = \frac{1}{N} \sum_{i=1}^{N} \cos(q\theta). \tag{178}$$

Note that the full definition of the magnetizations should include $\langle \sin\theta \rangle$ and $\langle \sin q\theta \rangle$, analogous to the HMF model; however, we neglect these terms because only initial distributions symmetric in θ will be considered.

The GHMF Hamiltonian (176) can be rewritten as

$$H = \sum_{i=1}^{N} \frac{p_i^2}{2} + \frac{1}{2} - \frac{1}{2N} \Delta \left(\sum_{i=1}^{N} \cos\theta_i \right)^2 - \frac{1}{2N} (1 - \Delta) \left(\sum_{i=1}^{N} \cos(q\theta_i) \right)^2.$$

The average energy per particle is

$$\mathcal{E} = \frac{\langle p^2 \rangle}{2} + \frac{1 - \Delta M_1^2 - (1 - \Delta) M_q^2}{2} \tag{179}$$

and the one-particle energy is

$$\epsilon(\theta, p) = \frac{p^2}{2} + 1 - \Delta M_1 \cos\theta - (1 - \Delta) M_q \cos(q\theta). \tag{180}$$

9.2. Thermodynamic equilibrium

The procedure for obtaining the equilibrium values of M_1 and M_q is the same as used for the HMF model. Here we present only the final results; more details can be found in the Ref. [226]. The microcanonical entropy is given by

$$s(\mathcal{E}) = \frac{1}{2} \ln 2\pi + \frac{1}{2} + \sup_{M_1, M_q} \left[\frac{1}{2} \ln\left(2\mathcal{E} - 1 + \Delta M_1^2 + (1 - \Delta) M_q^2\right) - M_1 a(M_1, M_q) \right.$$
$$\left. - M_q\, b(M_1, M_q) + \ln\left(\int d\theta \exp[a(M_1, M_q) \cos\theta + b(M_1, M_q) \cos q\theta] \right) \right]. \tag{181}$$

The equilibrium magnetizations correspond to the maximum of the entropy (181) and must satisfy the coupled equations

$$M_1 = \frac{\int d\theta \cos\theta \exp\left[a \cos\theta + b \cos q\theta\right]}{\int d\theta \exp\left[a \cos\theta + b \cos q\theta\right]} \tag{182}$$

and

$$M_q = \frac{\int d\theta \cos q\theta \exp\left[a \cos\theta + b \cos q\theta\right]}{\int d\theta \exp\left[a \cos\theta + b \cos q\theta\right]}, \tag{183}$$

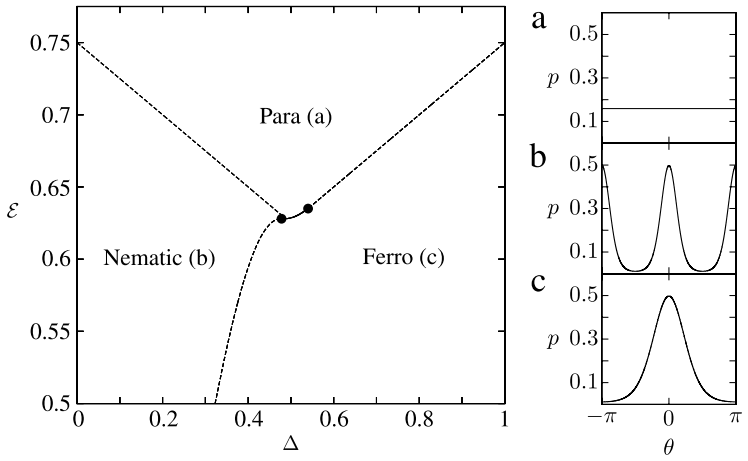

Fig. 47. Equilibrium phase diagram (microcanonical ensemble) for $q = 2$. The transitions are second order (dashed lines), with the exception of a small region in the center, between two tricritical points (solid circles), in which the transition is first order (solid line). On the right, the three panels show the equilibrium (MB) angular distributions $f(\theta)$ for each phase: paramagnetic (a), nematic (b), and ferromagnetic (c).

where

$$a(M_1, M_q) = \frac{\Delta M_1}{2\mathcal{E} - 1 + \Delta M_1^2 + (1-\Delta)M_q^2}, \tag{184}$$

$$b(M_1, M_q) = \frac{(1-\Delta)M_q}{2\mathcal{E} - 1 + \Delta M_1^2 + (1-\Delta)M_q^2}. \tag{185}$$

The roots of Eqs. (182)–(185) determine the equilibrium magnetizations for a given $\mathcal{E}$, q and Δ. Fig. 47 shows the phase diagram for $q = 2$ [226]. Most transitions are of second order (dashed lines), except for a small region near $\Delta = 0.5$, where the transition is of first order (solid line). The equilibrium distribution functions $f(\theta)$ for the three phases are illustrated in the right-hand panels of Fig. 47:

(a) the paramagnetic phase ($M_1 = M_2 = 0$),
(b) the nematic phase ($|M_2| > |M_1| \geq 0$) and
(c) the ferromagnetic phase ($|M_1| > 0$, $|M_2| \geq 0$).

The generalized magnetizations M_1 (solid line) and M_2 (dotted line) as a function of energy, for four values of Δ, are shown in Fig. 48: panels (a), (b) and (c) show second order transitions (nematic–paramagnetic, ferromagnetic–paramagnetic, and ferromagnetic–nematic, respectively), and panel (d) shows a first order ferromagnetic–paramagnetic transition. In the latter case, the critical energy is the energy for which the entropies of the ferromagnetic and paramagnetic phases are equal.

9.3. Nonequilibrium quasi-stationary states

Unlike the equilibrium states of the GHMF, which only depends on the initial energy, the qSSs depend explicitly on the initial particle distribution. In this Report we will explore how the ordered ferromagnetic and nematic phases arise from the initially homogeneous particle distribution of the waterbag form,

$$f_0(\theta, p) = \frac{1}{4\pi p_m}\Theta(\pi - |\theta|)\Theta(p_m - |p|). \tag{186}$$

In MD simulations, N particles are distributed so that $(-\pi, -p_m) \leq (\theta_i, p_i) \leq (\pi, p_m)$, where (θ_i, p_i) is the position and momentum of the ith particle. The average energy per particle is $\mathcal{E} = p_m^2/6$. The equation of motion for the ith particle is given by

$$\ddot{\theta}_i = -\frac{\partial H}{\partial \theta_i} = -\Delta M_1(t)\sin\theta_i - 2(1-\Delta)M_2(t)\sin(2\theta_i). \tag{187}$$

In simulations we observe that the system quickly relaxes into a qSS in which $M_1(t)$ and $M_2(t)$ oscillate slightly around their average values (M_1 and M_2), which depend on $\mathcal{E}$ and Δ. Phase transitions are located by performing a series of simulations varying Δ, for a given value of $\mathcal{E}$, and calculating the average value of $M_1(t)$ and $M_2(t)$ over a time interval inside a qSS. The transitions are found to be of first order.

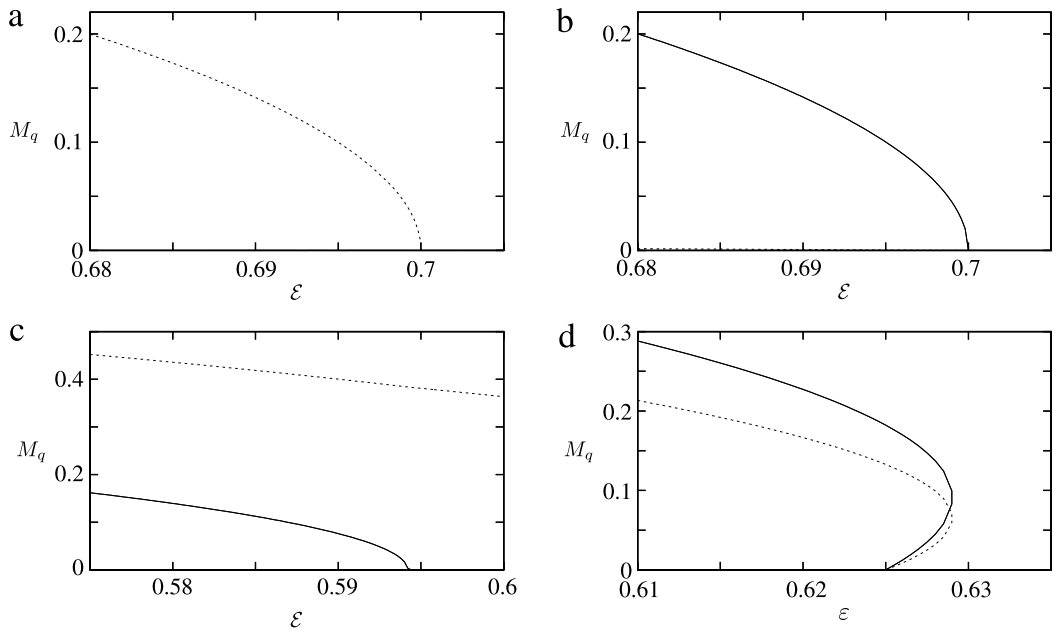

Fig. 48. Equilibrium solutions of M_1 (solid line) and M_2 (dotted line) as a function of the mean energy $\mathcal{E}$, exhibiting the (a) nematic–paramagnetic, (b) ferromagnetic–paramagnetic, (c) ferromagnetic–nematic, and (d) ferromagnetic–paramagnetic phase transitions, at $\Delta = 0.2$, 0.8, 0.4 and 0.5, respectively. The transitions shown in (a), (b) and (c) are second order, and the transition in (d) is first order.

9.4. Stability of the homogeneous state

The distribution given by Eq. (186) is a stationary solution of the Vlasov equation. Therefore, a transition between a homogeneous state and a non-homogeneous state, either ferromagnetic or nematic, can occur only as a result of a dynamical instability. Therefore, by studying the stability of the homogeneous solution, we should be able to gain an insight into the structure of the phase diagram of the GHMF model. A similar approach has also been used to study the HMF model in an external magnetic field [229] and was shown to agree with the predictions of the linear response theory [230].

To explore the stability of the distribution function Eq. (186), we perturb the upper momentum limit, p_m, as

$$p_m(t) = p_0 + \sum_{k=1}^{\infty} A_k(t)\cos(k\theta). \tag{188}$$

We define the generalized magnetizations M_n as

$$\begin{aligned} M_n(t) &= \eta \int_{-\infty}^{\infty} dp \int_{-\pi}^{\pi} d\theta \cos(n\theta)\Theta(p_m(t) - |p|)\Theta(\pi - |\theta|) \\ &= 2\eta \int_{-\pi}^{\pi} d\theta p_m(t)\cos(n\theta) \\ &= 2\eta \int_{-\pi}^{\pi} d\theta p_0 \cos(n\theta) + 2\eta \sum_{k=1}^{\infty} \int_{-\pi}^{\pi} d\theta A_k(t)\cos(k\theta)\cos(n\theta) \\ &= 2\pi\eta A_n(t) \\ &= \frac{A_n(t)}{2p_0}, \end{aligned} \tag{189}$$

where $\eta = 1/4\pi p_0$. Differentiating the term $\langle\cos(n\theta)\rangle$ twice with respect to time, we find the equation of motion

$$\ddot{M}_n(t) = -n\langle F(\theta)\sin(n\theta)\rangle - n^2\langle p^2\cos(n\theta)\rangle. \tag{190}$$

The average values are calculated using the distribution function $f(\theta, p, t) = \eta\,\Theta(p_m(t) - |p|)\Theta(\pi - |\theta|)$. Thus, the integral above involves an infinite series of cosines. For our analysis, we consider the series up to $k = 4$, which will prove to be sufficient to locate and determine the order of the phase transitions. Performing the averages, we obtain a system of differential equations for the generalized magnetizations,

$$\ddot{M}_1 + \left(\frac{12\mathcal{E} - 6 - \Delta}{2}\right) M_1 = f_1(M_1, M_2, M_3, M_4) \tag{191}$$

$$\ddot{M}_2 + 2\,(12\mathcal{E} + \Delta - 7)\,M_2 = f_2(M_1, M_2, M_3, M_4) \tag{192}$$

$$\ddot{M}_3 + 27(2\mathcal{E} - 1)\,M_3 = f_3(M_1, M_2, M_3, M_4) \tag{193}$$

$$\ddot{M}_4 + 48(2\mathcal{E} - 1)\,M_4 = f_4(M_1, M_2, M_3, M_4), \tag{194}$$

where

$$f_1 = M_1 M_2 \left(1 - \frac{3\Delta}{2}\right) + (\Delta - 1)M_2 M_3 - 3(2\mathcal{E} - 1)\{M_1^3 + M_1^2 M_3 + M_3[M_2(2 + M_2) + 2(1 + M_2)M_4] + 2M_1[M_2 + M_2^2 + M_3^2 + M_2 M_4 + M_4^2]\}, \tag{195}$$

$$f_2 = \Delta(M_1^2 - M_1 M_3 + 2M_2 M_4) - 2M_2 M_4 - 12(2\mathcal{E} - 1)[M_2^3 + M_3^2 M_4 + 2M_1 M_3(1 + M_2 + M_4) + M_1^2(1 + 2M_2 + M_4) + 2M_2(M_3^2 + M_4 + {M_4}^2)], \tag{196}$$

$$f_3 = \frac{3M_1}{2}[(2 - \Delta)M_2 - \Delta M_4] - 9(2\mathcal{E} - 1)\{M_1^3 + 6M_1^2 M_3 + 3M_1[M_2(2 + M_2) + 2(1 + M_2)M_4] + 3M_3[M_3^2 + 2(M_2^2 + M_2 M_4 + M_4^2)]\} \tag{197}$$

and

$$f_4 = 2\Delta M_1 M_3 - 4(\Delta - 1)M_2^2 - 48(2\mathcal{E} - 1)[2M_1(1 + M_2)M_3 + M_2(M_2 + M_3^2) + 2(M_2^2 + M_3^2)M_4 + M_4^3 + M_1^2(M_2 + 2M_4)]. \tag{198}$$

Eqs. (191)–(194) have been written so as to separate linear terms on the left hand side and the nonlinear terms on the right hand side of the equality. To calculate the paramagnetic–ferromagnetic and paramagnetic–nematic phase boundaries, we analyze the linear stability of $M_1(t)$ and $M_2(t)$. Neglecting the nonlinear terms (195)–(198), Eqs. (191) and (192) take the form $\ddot{M}_{1,2} = -\kappa_{1,2} M_{1,2}$, whose solutions are $\exp(\pm i\sqrt{\kappa_{1,2}}t)$. Thus, the magnetizations will remain stable only if $\kappa_{1,2} \geq 0$. If $\kappa_{1,2} < 0$, the exponents will become real and any infinitesimal fluctuation will experience an exponential growth, destabilizing the paramagnetic phase. The phase boundary that separates the paramagnetic phase from the ferromagnetic and nematic phases is, therefore, determined by the conditions $\kappa_1 = 0$ and $\kappa_2 = 0$, respectively. According to the Eqs. (191) and (192), $\kappa_1 = (12\mathcal{E} - 6 - \Delta)/2$ and $\kappa_2 = 2(12\mathcal{E} + \Delta - 7) = 0$ and we find the phase boundaries to be

$$\mathcal{E}_c^{pf}(\Delta) = \frac{6 + \Delta}{12} \tag{199}$$

and

$$\mathcal{E}_c^{pn}(\Delta) = \frac{7 - \Delta}{12}, \tag{200}$$

where $\mathcal{E}_c^{pf}$ and $\mathcal{E}_c^{pn}$ are the boundaries for the paramagnetic–ferromagnetic and paramagnetic–nematic transitions, respectively.

To determine the order of the phase transitions, we study the fixed points of the system of equations (191)–(194), including the nonlinear terms (195)–(198). Although the equations are conservative, we expect that in the full GHMF, the Landau damping will provide dissipation which will drive the system toward the qSS. The dissipation can be included by adding terms proportional to $\dot{M}_n$ into Eqs. (191)–(194). This will make the system relax to the stable fixed points of Eqs. (191)–(194), which will then correspond to the generalized magnetizations in the final qSS. We find that once the paramagnetic–nematic boundary is crossed, the value of M_2 jumps discontinuously from zero to approximately 0.459, while M_1 remains zero. The jump in M_2 is very close to the value observed in MD simulation, 0.450, independent of Δ. For the paramagnetic–ferromagnetic transition, the two magnetizations jump from zero to finite values which depend on Δ. In this case the theory is again consistent with the simulations predicting that when crossing the phase transition boundary, M_2 is always negative, while M_1 may be positive or negative.

The ferromagnetic–nematic phase boundary should be determined by the two growth rates ($\sqrt{\kappa_{1,2}}$) of $M_1(t)$ and $M_2(t)$. If M_1 grows faster than M_2, the system will reach the ferromagnetic fixed point prior to reaching the nematic one, and vice versa. Therefore, we expect that the ferromagnetic–nematic phase boundary should be close to the curve $\kappa_1 = \kappa_2$,

$$\mathcal{E}_c^{nf} = (22 - 5\Delta)/36. \tag{201}$$

Fig. 49 show the nonequilibrium phase diagram for the GHMF model for an initially homogeneous particle distribution. The theoretically calculated phase boundaries obtained using Eqs. (199)–(201) are shown as the solid lines. The results of MD simulations are shown as symbols. The paramagnetic–nematic and the paramagnetic–ferromagnetic phase boundaries predicted by the theory are in perfect agreement with the results of MD simulations. For the ferromagnetic–nematic transition the simulations find an instability region in which either phase can occur with equal probability, Fig. 50. The theoretically predicted phase boundary for the ferromagnetic–nematic transition Eq. (201) passes through the instability region.

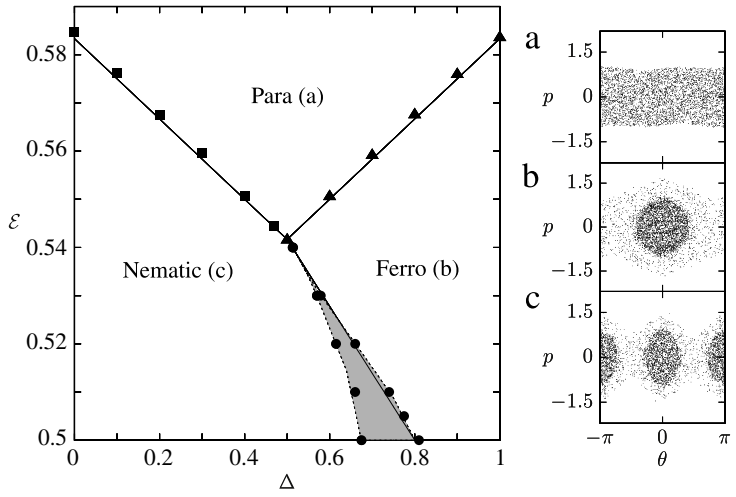

Fig. 49. The nonequilibrium phase diagram of the GHMF model ($q = 2$). Lines are the phase transitions predicted by the linear stability analysis. Squares and triangles are the results of MD simulations and represent the paramagnetic–nematic and the paramagnetic–ferromagnetic phase boundaries, respectively. Solid circles show the limits of the nematic–ferromagnetic transition region. Error bars are smaller than the size of the symbols. The gray area, between the circles, is an unstable region where MD simulations find both nematic and ferromagnetic phases, with almost equal probability, see Fig. 50. The right hand panels show examples of the phase space distributions obtained using the MD simulations for each of the three phases: (a) paramagnetic, (b) ferromagnetic, and (c) nematic.

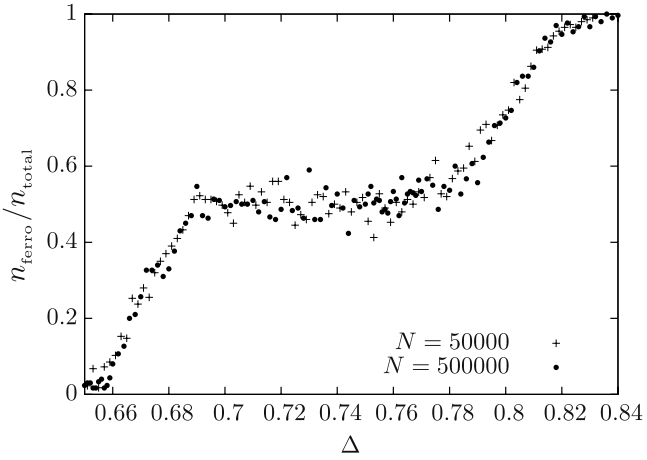

Fig. 50. The probability of finding a ferromagnetic phase, within the instability region of Fig. 49, at energy $\mathcal{E} = 0.5$ for various values of Δ. To calculate the probability for $N = 50{,}000$, we have used $n_{total} = 100$ different initial conditions drawn from the same waterbag distribution, Eq. (186), and observed how many of these (n_{ferro}) evolved into a ferromagnetic phase. For $N = 500{,}000$, we have used $n_{total} = 300$ different initial conditions for each value of Δ.

9.5. The core–halo distribution

The particle distributions in the ferromagnetic and nematic phases are, once again, of the core–halo form, Eq. (172), with the one-particle energy given by Eq. (180). In Fig. 51 we plot a snapshot of the phase space of the GHMF and the energy of each particle once the system has relaxed into a nematic qSS. In both panels of Fig. 51 a core–halo structure can be clearly seen. In the nematic phase it actually appears that there are two cores. This happens because $M_1 = 0$ and the one-particle energy has two minimums at $\theta = 0$ and $\theta = \pi$. Both cores, however, appear in the core–halo distribution function, given by

$$f_{ch}(\theta, p) = \eta\Theta(\epsilon_F - \epsilon(\theta, p)) + \chi\Theta(\epsilon_h - \epsilon(\theta, p))\Theta(\epsilon(\theta, p) - \epsilon_F), \tag{202}$$

where η and χ are the phase space densities of the core and halo, respectively; ϵ_F and ϵ_h are the maximum energies of the core and halo, respectively; and the one-particle energy $\epsilon(\theta, p)$ is given by Eq. (180).

In Fig. 52 we plot the marginal distributions calculated using the core–halo theory,

$$N(\theta) = \int f_{ch}(\theta, p)\, dp \tag{203}$$

and

$$N(p) = \int f_{ch}(\theta, p)\, d\theta \tag{204}$$

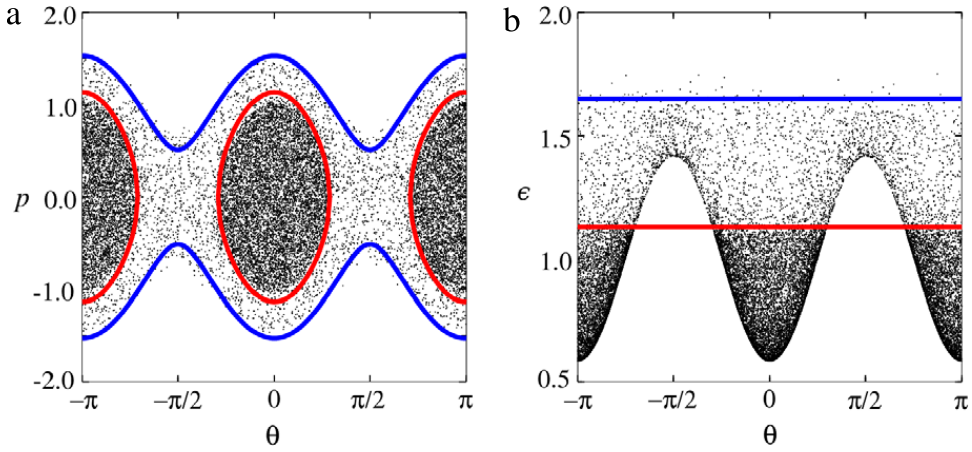

Fig. 51. (a) Phase space particle distribution and (b) one-particle energy obtained using MD simulation for GHMF with $\Delta = 0.2$ and $N = 10^5$ particles. In panel (a) the blue line shows the orbit corresponding to energy ϵ_h and the red line to the orbit with energy ϵ_F. In panel (b) the same color lines show the halo and Fermi energies. The initial distribution was homogeneous (paramagnetic) waterbag of energy $\mathcal{E} = 0.55$. (For interpretation of the references to colour in this figure legend, the reader is referred to the web version of this article.)

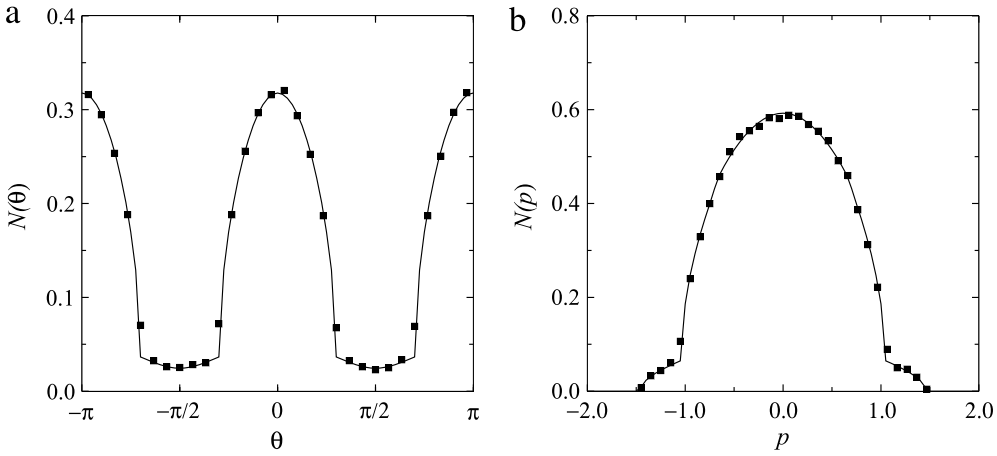

Fig. 52. Marginal distributions $N(\theta)$, Eq. (203), and $N(p)$, Eq. (204), for a nematic qSS of the GHMF model. All the parameters are the same as in Fig. 51.

with $f_{ch}(\theta, p)$ given by Eq. (202), and compare them with the results of MD simulations. The halo energy ϵ_h (blue line in Fig. 51(b)) was obtained using a short simulation with $N = 1000$ particles, which ran for only 10 dynamical times. The Fermi energy ϵ_F and the halo phase space density χ were calculated using the conservation of energy and of norm. The predicted value for the Fermi energy ϵ_F is the red line in Fig. 51(b). In panel (a) of the same figure we show the orbit of a particle with energy equal to ϵ_F (red line). This orbit perfectly encloses the core. In the same panel, the blue line represents an orbit of a particle with energy ϵ_h.

As with other long-range systems, eventually the GHMF will relax to thermodynamic equilibrium described by the Boltzmann–Gibbs statistical mechanics. The resultant phase diagram will then change to the one shown in Fig. 47. In the thermodynamic limit $N \to \infty$, this relaxation, however, will never occur and the system will remain trapped forever in one of the qSSs.

10. Conclusions and perspectives

In this Review we have explored statistical mechanics of systems with long-range interactions. A number of different examples have been considered, ranging from plasmas and self-gravitating systems to the kinetic spin models. In the thermodynamic limit, these systems do not relax to the Boltzmann–Gibbs equilibrium, but become trapped in the qSSs, the life time of which diverges with the number of particles N. If N is small, after staying in the qSS for a time of approximately $\tau_\times \sim N^\gamma$, where γ is usually larger or equal to one, a system relaxes to the thermodynamic equilibrium described by the usual Boltzmann–Gibbs statistical mechanics. This is what has been observed for all the models studied so far — after a time $\tau_\times$, they all (with the exception of 3D gravity, which always remains out of equilibrium) relaxed to thermodynamic equilibrium. In this respect, speculations that long-ranged systems should be described by the non-extensive Tsallis statistics are unfounded [231].

In the case of plasmas and elliptical galaxies, the number of "particles" is so large that the state of thermodynamic equilibrium cannot be reached within the life time of the universe. Furthermore, for 3D gravity, we saw that there is an

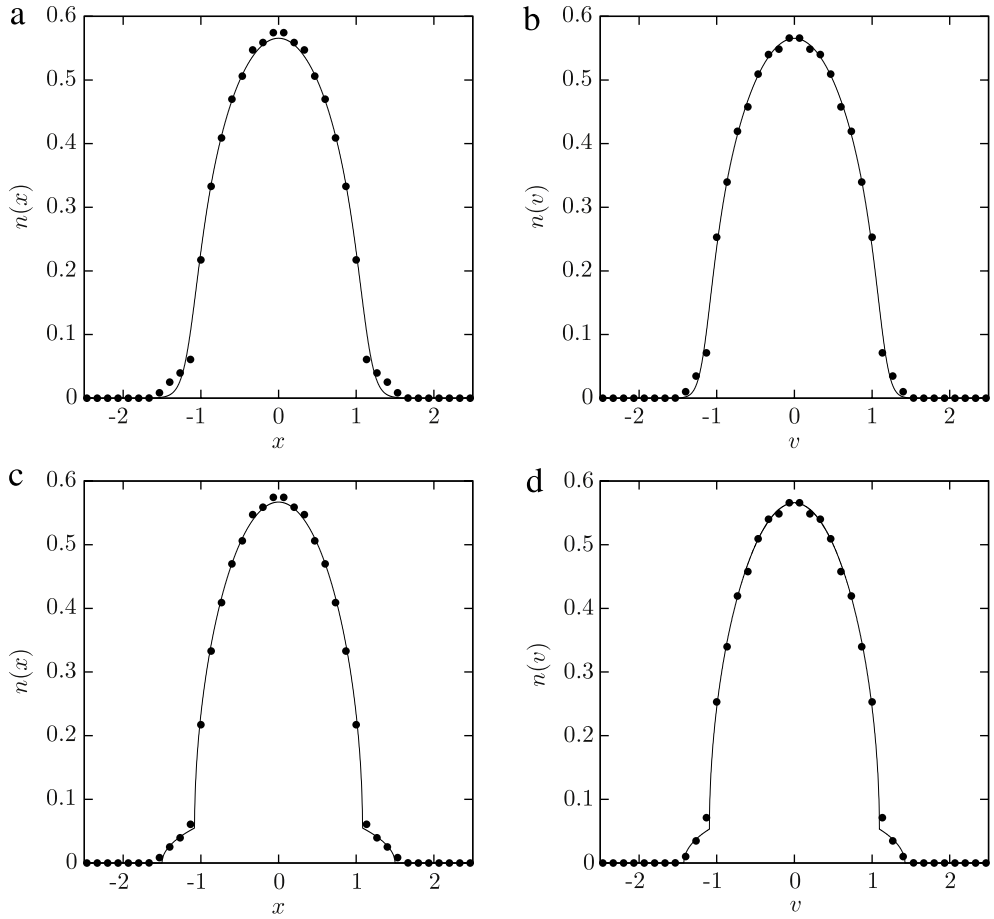

Fig. 53. Comparison of theoretical (lines) and N-body MD simulation (dots) results for the 1D self-gravitating system that initially satisfies the virial condition ($\mathcal{R}_0 = 1$). In panels (a) and (b), the theoretical distribution corresponds to LB theory, and in panels (c) and (d) corresponding to core–halo theory.

additional problem related to the bounded (from above) nature of Newton's gravitational potential and the resulting flux of evaporating particles. For 1D and 2D gravitational systems, on the other hand, there is no problem with particle evaporation. After a short time, these systems relax to qSSs which have a characteristic core–halo structure. The distribution function that describes qSSs of self-gravitating systems is the same as the one that describes the qSS of magnetically confined plasmas and of spin systems. The ubiquity of core–halo distributions, observed in so many different contexts, suggests that there is a significant degree of universality to the process of collisionless relaxation. The core–halo distribution appears to be a universal attractor – in a coarse-grained sense – analogous to the Maxwell–Boltzmann distribution for systems with short-range forces.

A qSS reached by a long-range interacting system depends explicitly on the initial particle distribution. In this Report we have considered only the initial conditions of the waterbag form. In the future, it will be important to extend the theory to more complex initial conditions. Preliminary work in this direction indicates that multilevel distributions lead to significantly more complex qSSs, with very interesting topological structure which, nevertheless, preserves some of the core–halo characteristics [212]. Curiously, for such initial distributions, the LB theory fails to describe the qSSs, even when initial conditions satisfy the virial theorem. This indicates that for multilevel distributions mixing is even poorer than it is for one level waterbags. Furthermore, even for one-level waterbag distributions satisfying the virial condition, there are small deviations between the results of simulations and the LB theory, and some halo formation may be observed. This suggests that the core–halo distribution may also be relevant for predicting the qSS of initially virialized waterbag distributions. Since for $\mathcal{R}_0 = 1$ the parametric resonances are not excited, the halo energy in this case should be the same as the energy of the most energetic particle of the initial distribution. In Fig. 53 we compare the predictions of the core–halo and the LB theories with the results of MD simulations for 1D self-gravitating system with $\mathcal{R}_0 = 1$. It appears that even in this case the core–halo theory agrees better with the results of simulations than does the LB approach. This suggests that mixing and ergodicity are not perfect even for initially virialized distributions. This, however, should be tested for other models discussed in this Review.

A trapping of a system in a qSS is a consequence of the ergodicity breaking. The process of Landau damping decreases the amplitude of collective oscillations which are responsible for the energy transfer between the particles. For long-range systems, there are no collisions (correlations) between the particles, and the only mechanism of energy transfer is the

wave–particle interaction. Therefore, once the oscillations have completely died out, each particles will move in a static mean-field potential and the ergodicity of the system will be broken. All the systems that have been considered so far had either spherical (in 3D) or polar (in 2D) symmetry. The equations of motion for a particle inside such potentials are integrable. This, in general, is not true for asymmetric potentials for which particle trajectories can become chaotic. It should be of great interest to explore if the chaotic dynamics in the qSS can lead to a faster relaxation to the Boltzmann–Gibbs equilibrium and a shorter lifetime of a qSS.

There are a number of outstanding open question which remain to be addressed. Can the core–halo theory developed above be extended to study 3D self-gravitating systems? For such systems the halo will extend all the way to infinity. At the moment we do not have an understanding of the structure of such halos. Furthermore, both 2D and 3D gravitational systems are susceptible to symmetry breaking instabilities [232]. The simulation methods used in the present work, which primarily relied on the Gauss's law, do not allow us to study such instabilities. The theoretical understanding of the symmetry breaking mechanism that leads to asymmetric QSS is still lacking and it is not clear how to extend the core–halo theory to describe the asymmetric stationary states. Finally, in the future it will be important to move beyond the waterbag initial distributions. As discussed above, multilevel initial distributions appear to exhibit ergodicity breaking and poor mixing even when they are virialized. This makes the study of such initial conditions very challenging [212]. Nevertheless, it has been observed that even such complex initial distributions also relax to core–halo QSS, with the particle distribution in the core well fitted by polytropic distributions [213].

In spite of their ubiquity, long-range interacting systems are still poorly understood. They are the unexplored frontier of statistical physics. We hope that the present Report helps to attract the attention of the statistical mechanics community to this fascinating field.

Acknowledgments

Y.L. would like to thank Michael Fisher, without whose insistence and encouragement this review would not have been written. We acknowledge the computational support of the Center of Computational Physics CFCIF (IF/UFRGS). This work was partially supported by the CNPq, FAPERGS, INCT-FCx, and by the US-AFOSR under the grant FA9550-12-1-0438.

References

[1] M.J. Klein, Thermodynamics in Einstein's thought, Science 157 (3788) (1967) 509. http://dx.doi.org/10.1126/science.157.3788.509.
[2] M.E. Fisher, The free energy of a macroscopic system, Archive for Rational Mechanics and Analysis 17 (5) (1964) 377.
[3] D. Ruelle, Superstable interactions in classical statistical mechanics, Communications in Mathematical Physics 18 (2) (1970) 127.
[4] M. Kac, On the partition function of a one-dimensional gas, Physics of Fluids 2 (1) (1959) 8–12. URL http://link.aip.org/link/?PFLDAS/2/8/1.
[5] M. Kac, G.E. Uhlenbeck, P.C. Hemmer, On the van der Waals theory of the vapor–liquid equilibrium. I. Discussion of a one-dimensional model, Journal of Mathematical Physics 4 (2) (1963) 216. http://dx.doi.org/10.1063/1.1703946.
[6] G.A. Baker, Ising model with a long-range interaction in the presence of residual short-range interactions, Physical Review 130 (4) (1963) 1406. http://dx.doi.org/10.1103/PhysRev.130.1406.
[7] A. Campa, T. Dauxois, S. Ruffo, Statistical mechanics and dynamics of solvable models with long-range interactions, Physics Reports 480 (3–6) (2009) 57–159. http://dx.doi.org/10.1016/j.physrep.2009.07.001.
[8] J. Barré, D. Mukamel, S. Ruffo, Inequivalence of ensembles in a system with long-range interactions, Physical Review Letters 87 (3) (2001) 30601. http://dx.doi.org/10.1103/PhysRevLett.87.030601.
[9] W. Thirring, Systems with negative specific heat, Zeitschrift für Physik 235 (4) (1970) 339.
[10] D. Lynden-Bell, R.M. Lynden-Bell, On the negative specific heat paradox, Monthly Notices of the Royal Astronomical Society 181 (1977) 405.
[11] A. El-Zant, Approach to equilibrium in N-body gravitational systems, Physical Review E 58 (4) (1998) 4152. http://dx.doi.org/10.1103/PhysRevE.58.4152.
[12] D. Lynden-Bell, Negative specific heat in astronomy, physics and chemistry, Physica A: Statistical Mechanics and its Applications 263 (1999) 293. http://dx.doi.org/10.1016/S0378-4371(98)00518-4.
[13] M. Kiessling, T. Neukirch, Negative specific heat of a magnetically self-confined plasma torus, Proceedings of the National Academy of Sciences of the United States of America 100 (4) (2003) 1510. URL http://www.pnas.org/content/100/4/1510.short.
[14] W. Thirring, H. Narnhofer, H. Posch, Negative specific heat, the thermodynamic limit, and ergodicity, Physical Review Letters 91 (13) (2003) 130601. http://dx.doi.org/10.1103/PhysRevLett.91.130601.
[15] L. Reichl, A Modern Course in Statistical Physics, second ed., Wiley-Interscience, 1998.
[16] T. Tsuchiya, T. Konishi, N. Gouda, Quasiequilibria in one-dimensional self-gravitating many-body systems, Physical Review E 50 (4) (1994) 2607. http://dx.doi.org/10.1103/PhysRevE.50.2607.
[17] F. Borgonovi, G.L. Celardo, M. Maianti, E. Pedersoli, Broken ergodicity in classically chaotic spin systems, Journal of Statistical Physics 116 (5–6) (2004) 1435. http://dx.doi.org/10.1023/B:JOSS.0000041745.62340.00.
[18] P. Chen, M. Cross, Mixing and thermal equilibrium in the dynamical relaxation of a vortex ring, Physical Review Letters 77 (20) (1996) 4174–4177. http://dx.doi.org/10.1103/PhysRevLett.77.4174.
[19] F.P.da C. Benetti, T.N. Teles, R. Pakter, Y. Levin, Ergodicity breaking and parametric resonances in systems with long-range interactions, Physical Review Letters 108 (2012) 140601. http://dx.doi.org/10.1103/PhysRevLett.108.140601.
[20] W. Braun, K. Hepp, The Vlasov dynamics and its fluctuations in the 1/N limit of interacting classical particles, Communications in Mathematical Physics 56 (2) (1977) 101–113. http://dx.doi.org/10.1007/BF01611497.
[21] A. Gabrielli, M. Joyce, Gravitational force in an infinite one-dimensional Poisson distribution, Physical Review E 81 (2) (2010) 1–9. http://dx.doi.org/10.1103/PhysRevE.81.021102.
[22] M. Luwel, G. Severne, P. Rousseeuw, Numerical study of the relaxation of one-dimensional gravitational systems, Astrophysics and Space Science 100 (1–2) (1984) 261. http://dx.doi.org/10.1007/BF00651601.
[23] Y. Levin, R. Pakter, T. Teles, Collisionless relaxation in non-neutral plasmas, Physical Review Letters 100 (4) (2008) 040604. http://dx.doi.org/10.1103/PhysRevLett.100.040604.
[24] T.N. Teles, R. Pakter, Y. Levin, Relaxation and emittance growth of a thermal charged-particle beam, Applied Physics Letters 95 (17) (2009) 173501. http://dx.doi.org/10.1063/1.3254245.

[25] R. Pakter, Y. Levin, Core-halo distribution in the Hamiltonian mean-field model, Physical Review Letters 106 (2011) 200603. http://dx.doi.org/10.1103/PhysRevLett.106.200603.
[26] M. Hénon, L'évolution initiale d'un amas sphérique, Annales d'Astrophysique 27 (1964) 83. URL http://adsabs.harvard.edu/full/1964AnAp...27...83H.
[27] A.M. Salzberg, Exact statistical thermodynamics of gravitational interactions in one and two dimensions, Journal of Mathematical Physics 6 (1) (1965) 158. http://dx.doi.org/10.1063/1.1704254.
[28] M. Lecar, A one-dimensional self-gravitating stellar gas, in: G.I. Kontopoulos (Ed.), The Theory of Orbits in the Solar System and in Stellar Systems. Proceedings from Symposium No. 25 held in Thessaloniki, 1964, International Astronomical Union, Academic Press, 1966, p. 46. URL http://adsabs.harvard.edu/full/1966IAUS...25...46L.
[29] F. Hohl, J.W. Campbell, Statistical mechanics of a collisionless self-gravitating system, The Astronomical Journal 73 (7) (1968) 611. URL http://adsabs.harvard.edu/full/1968AJ.....73..611H.
[30] R.H. Miller, Numerical experiments in collisionless systems, Astrophysics and Space Science 14 (1) (1971) 73. http://dx.doi.org/10.1007/BF00649196.
[31] H. Wright, B. Miller, W. Stein, The relaxation time of a one-dimensional self-gravitating system, Astrophysics and Space Science 84 (2) (1982) 421. http://dx.doi.org/10.1007/BF00651321.
[32] M. Luwel, G. Severne, Collisionless mixing in 1-dimensional gravitational systems initially in a stationary waterbag configuration, Astronomy & Astrophysics 152 (1985) 305.
[33] R. Carlberg, The phase space density in elliptical galaxies, The Astrophysical Journal 310 (1986) 593–596. http://dx.doi.org/10.1086/164711.
[34] C.J. Reidl Jr., B.N. Miller, Gravity in one dimension: selective relaxation? The Astrophysical Journal 318 (1987) 248. http://dx.doi.org/10.1086/165364.
[35] K.R. Yawn, B.N. Miller, Incomplete relaxation in a two-mass one-dimensional self-gravitating system, Physical Review E 68 (5) (2003) 1–17. http://dx.doi.org/10.1103/PhysRevE.68.056120.
[36] R. De Simone, X. Wu, S. Tremaine, The stellar velocity distribution in the solar neighbourhood, Monthly Notices of the Royal Astronomical Society 350 (1) (2004) 627. http://dx.doi.org/10.1111/j.1365-2966.2004.07675.x.
[37] P. Klinko, B.N. Miller, Dynamical study of a first order gravitational phase transition, Physics Letters A 333 (2004) 187.
[38] Y. Levin, R. Pakter, F. Rizzato, Collisionless relaxation in gravitational systems: from violent relaxation to gravothermal collapse, Physical Review E 78 (2) (2008) 021130. http://dx.doi.org/10.1103/PhysRevE.78.021130.
[39] T.N. Teles, Y. Levin, R. Pakter, F.B. Rizzato, Statistical mechanics of unbound two-dimensional self-gravitating systems, Journal of Statistical Mechanics: Theory and Experiment 2010 (05) (2010) P05007. http://dx.doi.org/10.1088/1742-5468/2010/05/P05007.
[40] M.A. Jalali, S. Tremaine, Density waves in debris discs and galactic nuclei, Monthly Notices of the Royal Astronomical Society 421 (3) (2012) 2368. http://dx.doi.org/10.1111/j.1365-2966.2012.20469.x.
[41] A. Lenard, Exact statistical mechanics of a one-dimensional system with Coulomb forces, Journal of Mathematical Physics 2 (5) (1961) 682. http://dx.doi.org/10.1063/1.1703757. URL http://link.aip.org/link/doi/10.1063/1.1703757.
[42] S.F. Edwards, A. Lenard, Exact statistical mechanics of a one-dimensional system with Coulomb forces. II. The method of functional integration, Journal of Mathematical Physics 3 (4) (1962) 778. http://dx.doi.org/10.1063/1.1724281.
[43] O. Eldridge, M. Feix, Numerical experiments with a plasma model, Physics of Fluids 6 (3) (1963) 398. URL http://link.aip.org/link/?PFLDAS/6/398/1.
[44] M.J. Stephen, Oscillations of a plasma in a magnetic field, Physical Review 129 (3) (1963) 997–1004. URL http://prola.aps.org/abstract/PR/v129/i3/p997_1.
[45] S. Rand, Collision damping of electron plasma waves, Physics of Fluids 8 (1) (1965) 143. URL http://link.aip.org/link/?PFLDAS/8/143/1.
[46] B.B. Kadomtsev, O.P. Pogutse, Collisionles relaxation in systems with Coulomb interactions, Physical Review Letters 25 (1970) 1155. http://dx.doi.org/10.1103/PhysRevLett.25.1155.
[47] M. Reiser, Free energy and emittance growth in nonstationary charged particle beams, Journal of Applied Physics 70 (4) (1991) 1919. http://dx.doi.org/10.1063/1.349474.
[48] X.-P. Huang, C.F. Driscoll, Relaxation of 2D turbulence to a metaequilibrium near the minimum enstrophy state, Physical Review Letters 72 (14) (1994) 2187. http://dx.doi.org/10.1103/PhysRevLett.72.2187.
[49] S.M. Lund, J.J. Barnard, J.M. Miller, On the relaxation of semi-Gaussian and K-V beams to thermal equilibrium, in: Proceedings of the 1995 Particle Accelerator Conference, Vol. 5, 1995, p. 3278. http://dx.doi.org/10.1109/PAC1995.505854.
[50] C. Allen, K. Chan, P. Colestock, K. Crandall, R. Garnett, J. Gilpatrick, W. Lysenko, J. Qiang, J. Schneider, M. Schulze, R. Sheffield, H. Smith, T. Wangler, Beam-halo measurements in high-current proton beams, Physical Review Letters 89 (21) (2002) 214802. http://dx.doi.org/10.1103/PhysRevLett.89.214802.
[51] H. Okamoto, M. Ikegami, Simulation study of halo formation in breathing round beams, Physical Review E 55 (4) (1997) 4694. http://dx.doi.org/10.1103/PhysRevE.55.4694.
[52] T.P. Wangler, K.R. Crandall, R. Ryne, T.S. Wang, Particle-core model for transverse dynamics of beam halo, Physical Review Special Topics – Accelerators and Beams 1 (8) (1998) 84201. http://dx.doi.org/10.1103/PhysRevSTAB.1.084201.
[53] T. Teles, Y. Levin, R. Pakter, Statistical mechanics of 1D self-gravitating systems: the core-halo distribution, Monthly Notices of the Royal Astronomical Society 417 (2011) L21–L25. http://dx.doi.org/10.1111/j.1745-3933.2011.01112.x.
[54] J. Barré, F. Bouchet, T. Dauxois, S. Ruffo, Out-of-equilibrium states as statistical equilibria of an effective dynamics in a system with long-range interactions, Physical Review Letters 89 (2002) 110601. http://dx.doi.org/10.1103/PhysRevLett.89.110601.
[55] A. Antoniazzi, F. Califano, D. Fanelli, S. Ruffo, Exploring the thermodynamic limit of Hamiltonian models: convergence to the Vlasov equation, Physical Review Letters 98 (15) (2007) 150602. http://dx.doi.org/10.1103/PhysRevLett.98.150602.
[56] J. Kapteyn, First attempt at a theory of the arrangement and motion of the sidereal system, Astrophysical Journal 55 (1922) 302. URL http://articles.adsabs.harvard.edu/full/1922ApJ....55..302K.
[57] J. Jeans, The motions of stars in a Kapteyn universe, Monthly Notices of the Royal Astronomical Society 82 (1922) 122–132. URL http://adsabs.harvard.edu/full/1922MNRAS..82..122J.
[58] F.H. Oort, The force exerted by stellar system in the direction perpendicular to the galactic plane and some related problems, Bulletin Of The Astronomical Institutes of the Netherlands 6 (17) (1932) 238.
[59] G. Camm, Self-gravitating star systems, Monthly Notices of the Royal Astronomical Society 110 (1950) 305. URL http://adsabs.harvard.edu/full/1950MNRAS.110..305C.
[60] K. Ogorodnikov, Statistical mechanics of the simplest types of galaxies, Soviet Astronomy 1 (1957) 748. URL http://adsabs.harvard.edu/full/1957SvA.....1..748O.
[61] T. Padmanabhan, Statistical mechanics of gravitating systems, Physics Reports 188 (5) (1990) 285–362. http://dx.doi.org/10.1016/0370-1573(90)90051-3.
[62] S. Tremaine, J.P. Ostriker, Relaxation in stellar systems, and the shape and rotation of the inner dark halo, Monthly Notices of the Royal Astronomical Society 306 (3) (1999) 662. http://dx.doi.org/10.1046/j.1365-8711.1999.02558.x.
[63] S. Tremaine, The geometry of phase mixing, Monthly Notices of the Royal Astronomical Society 307 (4) (1999) 877. http://dx.doi.org/10.1046/j.1365-8711.1999.02690.x.
[64] J. Binney, S. Tremaine, Galactic Dynamics, second ed., Princeton University Press, 2009.
[65] P.H. Chavanis, J. Sommeria, R. Robert, Statistical mechanics of two-dimensional vortices and collisionless stellar systems, The Astrophysical Journal 471 (1) (1996) 385. http://dx.doi.org/10.1086/177977.
[66] P.-H. Chavanis, Quasilinear theory of the 2D Euler equation, Physical Review Letters 84 (24) (2000) 5512–5515. http://dx.doi.org/10.1103/PhysRevLett.84.5512.
[67] T. Andersen, C. Lim, Negative specific heat in a quasi-2D generalized vorticity model, Physical Review Letters 99 (16) (2007) 165001. http://dx.doi.org/10.1103/PhysRevLett.99.165001.

[68] F. Bouchet, J. Barré, A. Venaille, A. Campa, A. Giansanti, G. Morigi, F.S. Labini, Equilibrium and out of equilibrium phase transitions in systems with long range interactions and in 2D flows, AIP Conference Proceedings (2008) 117–152. http://dx.doi.org/10.1063/1.2839113.
[69] A. Venaille, F. Bouchet, Statistical ensemble inequivalence and bicritical points for two-dimensional flows and geophysical flows, Physical Review Letters 102 (2009) 104501. http://dx.doi.org/10.1103/PhysRevLett.102.104501.
[70] F. Bouchet, A. Venaille, Statistical mechanics of two-dimensional and geophysical flows, Physics Reports 515 (2012) 227. http://dx.doi.org/10.1016/j.physrep.2012.02.001.
[71] M. Kastner, Diverging equilibration times in long-range quantum spin models, Physical Review Letters 106 (13) (2011) 1–4. http://dx.doi.org/10.1103/PhysRevLett.106.130601.
[72] O.L. Berman, R.Y. Kezerashvili, G.V. Kolmakov, Y.E. Lozovik, Turbulence in a Bose–Einstein condensate of dipolar excitons in coupled quantum wells, Physical Review B: Condensed Matter and Materials Physics 86 (4) (2012) 045108. http://dx.doi.org/10.1103/PhysRevB.86.045108.
[73] S. Slama, G. Krenz, S. Bux, C. Zimmermann, P.W. Courteille, Collective atomic recoil lasing and superradiant Rayleigh scattering in a high-Q ring cavity, in: A. Campa, A. Giansanti, G. Morigi, F.S. Labini (Eds.), Dynamics and Thermodynamics of Systems with Long-range Interaction: Theory and Experiments, in: Mathematical and Statistical Physics, vol. CP 970, American Institute of Physics, 2008, p. 319. http://dx.doi.org/10.1063/1.2839129.
[74] M. Oettel, S. Dietrich, Colloidal interactions at fluid interfaces, Langmuir 24 (2008) 1425. http://dx.doi.org/10.1021/la702794d.
[75] A. Domínguez, M. Oettel, S. Dietrich, Dynamics of colloidal particles with capillary interactions, Physical Review E 82 (2010) 011402. http://dx.doi.org/10.1103/PhysRevE.82.011402.
[76] J. Bleibel, S. Dietrich, A. Domínguez, M. Oettel, Shock Waves in Capillary Collapse of Colloids: A Model System for Two-Dimensional Screened Newtonian Gravity, Physical Review Letters 107 (2011) 128302. http://dx.doi.org/10.1103/PhysRevLett.107.128302.
[77] J. Bleibel, A. Domínguez, M. Oettel, S. Dietrich, Collective dynamics of colloids at fluid interfaces, European Physical Journal E: Soft Matter 34 (2011) 125. http://dx.doi.org/10.1140/epje/i2011-11125-5.
[78] C. Chen, R.C. Davidson, Nonlinear properties of the Kapchinskij–Vladimirskij equilibrium and envelope equation for an intense charged-particle beam in a periodic focusing field, Physical Review E 49 (6) (1994) 5679. http://dx.doi.org/10.1103/PhysRevE.49.5679.
[79] R.C. Davidson, H. Qin, Physics of Intense Charged Particle Beams in High Energy Accelerators, first ed., World Scientific, 2001.
[80] I.D. Kaganovich, R.C. Davidson, M.a. Dorf, E.a. Startsev, a.B. Sefkow, E.P. Lee, A. Friedman, Physics of neutralization of intense high-energy ion beam pulses by electrons, Physics of Plasmas 17 (5) (2010) 056703. http://dx.doi.org/10.1063/1.3335766.
[81] H.B. Callen, Thermodynamics and an Introduction to Thermostatics, second ed., John Wiley & Sons, 1985.
[82] M.E. Fisher, D. Ruelle, The stability of many-particle systems, Journal of Mathematical Physics 7 (1966) 260. http://dx.doi.org/10.1063/1.1704928.
[83] F. Hohl, Three-dimensional galaxy simulations, The Astronomical Journal 83 (7) (1978) 768–778. URL http://adsabs.harvard.edu/full/1978AJ.....83..768H.
[84] K.R. Yawn, B.N. Miller, Equipartition and mass segregation in a one-dimensional self-gravitating system, Physical Review Letters 79 (19) (1997) 3561. http://dx.doi.org/10.1103/PhysRevLett.79.3561.
[85] P. Hertel, W. Thirring, A soluble model for a system with negative specific heat, Annals of Physics 63 (2) (1971) 520. http://dx.doi.org/10.1016/0003-4916(71)90025-X.
[86] F. Bouchet, J. Barré, Classification of phase transitions and ensemble inequivalence, in systems with long range interactions, Journal of Statistical Physics 118 (516) (2005) 1073. http://dx.doi.org/10.1007/s10955-004-2059-0.
[87] P.H. Chavanis, Phase transitions in self-gravitating systems, International Journal of Modern Physics B 20 (22) (2006) 3113. http://dx.doi.org/10.1142/S0217979206035400.
[88] T.M.R. Filho, M.A. Amato, A. Figueiredo, A novel approach to the determination of equilibrium properties of classical Hamiltonian systems with long-range interactions, Journal of Physics A: Mathematical and Theoretical 42 (16) (2009) 165001. http://dx.doi.org/10.1088/1751-8113/42/16/165001.
[89] O. Cohen, D. Mukamel, Ensemble inequivalence: Landau theory and the ABC model, Journal of Statistical Mechanics: Theory and Experiment 2012 (2012) P12017. http://dx.doi.org/10.1088/1742-5468/2012/12/P12017.
[90] A. Ramírez-Hernández, H. Larralde, F. Leyvraz, Violation of the zeroth law of thermodynamics in systems with negative specific heat, Physical Review Letters 100 (12) (2008) 120601. http://dx.doi.org/10.1103/PhysRevLett.100.120601.
[91] A. Ramírez-Hernández, H. Larralde, F. Leyvraz, Systems with negative specific heat in thermal contact: violation of the zeroth law, Physical Review E 78 (6) (2008) 1–8. http://dx.doi.org/10.1103/PhysRevE.78.061133.
[92] K. Michaelian, I. Santamaría-Holek, A. Pérez-Madrid, Comment on violation of the zeroth law of thermodynamics in systems with negative specific heat, Physical Review Letters 102 (13) (2009) 138901. http://dx.doi.org/10.1103/PhysRevLett.102.138901.
[93] A. Ramírez-Hernández, H. Larralde, F. Leyvraz, Ramírez-Hernández, Larralde, and Leyvraz reply, Physical Review Letters 102 (13) (2009) 138902. http://dx.doi.org/10.1103/PhysRevLett.102.138902.
[94] O. Penrose, Foundations of statistical mechanics, Reports on Progress in Physics 42 (12) (1979) 1937–2007. URL http://iopscience.iop.org/0034-4885/42/12/002/pdf/0034-4885_42_12_002.pdf.
[95] J.L. Lebowitz, O. Penrose, Modern ergodic theory, Physics Today 26 (2) (1973) 155–175. URL http://ergodic.ugr.es/FisicaEstadistica/copialibros/libros/LeboPenPT1973.pdf.
[96] J.L. Lebowitz, Microscopic origins of irreversible macroscopic behavior, Physica A: Statistical Mechanics and its Applications 263 (1–4) (1999) 516–527. http://dx.doi.org/10.1016/S0378-4371(98)00514-7. URL http://linkinghub.elsevier.com/retrieve/pii/S0378437198005147.
[97] D. Mukamel, S. Ruffo, N. Schreiber, Breaking of ergodicity and long relaxation times in systems with long-range interactions, Physical Review Letters 95 (2005) 240604. http://dx.doi.org/10.1103/PhysRevLett.95.240604.
[98] R. Balescu, Statistical Dynamics: Matter Out of Equilibrium, World Scientific, 1997.
[99] K. Huang, Statistical Mechanics, second ed., John Wiley & Sons, 1987.
[100] J.W. Gibbs, Collected Works, Longmans, Green and Co., 1928.
[101] Y. Levin, Electrostatic correlations: from plasma to biology, Reports on Progress in Physics 65 (11) (2002) 1577. http://dx.doi.org/10.1088/0034-4885/65/11/201.
[102] Y. Yamaguchi, J. Barré, F. Bouchet, T. Dauxois, S. Ruffo, Stability criteria of the Vlasov equation and quasi-stationary states of the HMF model, Physica A: Statistical and Theoretical Physics 337 (1–2) (2004) 36–66. http://dx.doi.org/10.1016/j.physa.2004.01.041.
[103] K. Jain, F. Bouchet, D. Mukamel, Relaxation times of unstable states in systems with long range interactions, Journal of Statistical Mechanics: Theory and Experiment 2007 (11) (2007) P11008. http://dx.doi.org/10.1088/1742-5468/2007/11/P11008.
[104] M.-a. Sakagami, N. Gouda, On the collective relaxation in self-gravitating stellar systems, Monthly Notices of the Royal Astronomical Society 249 (1991) 241. URL http://adsabs.harvard.edu/full/1991MNRAS.249..241S.
[105] P. Chavanis, F. Bouchet, On the coarse-grained evolution of collisionless stellar systems, Astronomy and Astrophysics 430 (3) (2005) 771–778. http://dx.doi.org/10.1051/0004-6361:20041462.
[106] T.M.R. Filho, A. Figueiredo, M. Amato, Entropy of classical systems with long-range interactions, Physical Review Letters 95 (19) (2005) 190601. http://dx.doi.org/10.1103/PhysRevLett.95.190601.
[107] S. Tremaine, M. Hénon, D. Lynden-Bell, H-functions and mixing in violent relaxation, Monthly Notices of the Royal Astronomical Society 219 (1986) 285. URL http://adsabs.harvard.edu/full/1986MNRAS.219..285T.
[108] D. Lynden-Bell, Statistical mechanics of violent relaxation in stellar systems, Monthly Notices of the Royal Astronomical Society 136 (1967) 101–121. URL http://adsabs.harvard.edu/full/1967MNRAS.136..101L.
[109] F.H. Shu, On the statistical mechanics of violent relaxation, Astrophysical Journal 225 (1978) 83. http://dx.doi.org/10.1086/156470.
[110] T.K. Nakamura, Statistical mechanics of a collisionless system based on the maximum entropy principle, The Astrophysical Journal 531 (2) (2000) 739. http://dx.doi.org/10.1086/308484.

[111] I. Arad, D. Lynden-Bell, Inconsistency in theories of violent relaxation, Monthly Notices of the Royal Astronomical Society 361 (2) (2005) 385–395. http://dx.doi.org/10.1111/j.1365-2966.2005.09133.x.
[112] D. Bindoni, L. Secco, Violent relaxation in phase–space, New Astronomy Reviews 52 (1) (2008) 1–18. http://dx.doi.org/10.1016/j.newar.2007.11.001.
[113] R.H. Miller, K.H. Prendergast, Stellar dynamics in a discrete phase space, Astrophysical Journal 151 (1968) 699. URL http://adsabs.harvard.edu/full/1968ApJ...151..699M.
[114] R.H. Miller, K.H. Prendergast, W.J. Quirk, Numerical experiments on spiral structure, Astrophysical Journal 161 (1970) 903. URL http://adsabs.harvard.edu/abs/1970ApJ...161..903M.
[115] G. Severne, M. Luwel, P. Rousseeuw, Equipartition and mass segregation in 1-dimensional gravitational systems, Astronomy and Astrophysics 138 (2) (1984) 365.
[116] H.L. Wright, B.N. Miller, Gravity in one dimension: a dynamical and statistical study, Physical Review A 29 (3) (1984) 1411. http://dx.doi.org/10.1103/PhysRevA.29.1411.
[117] G. Severne, M. Luwel, Violent relaxation and mixing in non-uniform one-dimensional gravitational systems, Astrophysics and Space Science 122 (2) (1986) 299. http://dx.doi.org/10.1007/BF00650198.
[118] T. Yano, N. Gouda, Evolution of the power spectrum and self-similarity in the expanding one-dimensional universe, The Astrophysical Journal Supplement Series 118 (2) (1998) 267. http://dx.doi.org/10.1086/313142.
[119] V.P. Youngkins, B.N. Miller, Gravitational phase transitions in a one-dimensional spherical system, Physical Review E 62 (2000) 4583. http://dx.doi.org/10.1103/PhysRevE.62.4583.
[120] B.N. Miller, J.L. Rouet, Influence of expansion on hierarchical structure, Physical Review E 65 (5) (2002) 056121. http://dx.doi.org/10.1103/PhysRevE.65.056121.
[121] P. Valageas, Relaxation of a one-dimensional gravitational system, Physical Review E 74 (1) (2006) 1. http://dx.doi.org/10.1103/PhysRevE.74.016606.
[122] M. Joyce, F. Sicard, Non-linear gravitational clustering of cold matter in an expanding universe: indications from 1D toy models, Monthly Notices of the Royal Astronomical Society 413 (2) (2011) 1439. http://dx.doi.org/10.1111/j.1365-2966.2011.18225.x.
[123] F. Hohl, M.R. Feix, Numerical experiments with a one-dimensional model for a self-gravitating star system, Astrophysical Journal 147 (1967) 1164.
[124] G.B. Rybicki, Exact statistical mechanics of a one-dimensional self-gravitating system, Astrophysics and Space Science 14 (1) (1971) 56–72. http://dx.doi.org/10.1007/BF00649195.
[125] S.D. Mathur, Existence of oscillation modes in collisionless gravitating systems, Monthly Notices of the Royal Astronomical Society 243 (1990) 529–536. URL http://adsabs.harvard.edu/full/1990MNRAS.243..529M.
[126] M. Joyce, T. Worrakitpoonpon, Relaxation to thermal equilibrium in the self-gravitating sheet model, Journal of Statistical Mechanics: Theory and Experiment 2010 (10) (2010) P10012. http://dx.doi.org/10.1088/1742-5468/2010/10/P10012.
[127] M. Joyce, T. Worrakitpoonpon, Quasi-stationary states in the self-gravitating sheet model, Physical Review E 84 (1) (2011) 011139. http://dx.doi.org/10.1103/PhysRevE.84.011139.
[128] B.N. Miller, J.-L. Rouet, Development of fractal geometry in a one-dimensional gravitational system, Comptes Rendus Physique 7 (3–4) (2006) 383–390. http://dx.doi.org/10.1016/j.crhy.2006.02.005.
[129] B. Miller, J.-L. Rouet, E. Le Guirriec, Fractal geometry in an expanding, one-dimensional, Newtonian universe, Physical Review E 76 (3) (2007) 1–14. http://dx.doi.org/10.1103/PhysRevE.76.036705.
[130] B.N. Miller, J.-L. Rouet, Cosmology in one dimension: fractal geometry, power spectra and correlation, Journal of Statistical Mechanics: Theory and Experiment 2010 (12) (2010) P12028. http://dx.doi.org/10.1088/1742-5468/2010/12/P12028.
[131] A.E. Schulz, W. Dehnen, G. Jungman, S. Tremaine, Gravitational collapse in one dimension, Monthly Notices of the Royal Astronomical Society 431 (1) (2013) 49. http://dx.doi.org/10.1093/mnras/stt073.
[132] A. Noullez, D. Fanelli, E. Aurell, A heap-based algorithm for the study of one-dimensional particle systems, Journal of Computational Physics 186 (2) (2003) 697. http://dx.doi.org/10.1016/S0021-9991(03)00048-2.
[133] W.H. Press, S.A. Teukolsky, W.T. Vetterling, B.P. Flannery, Fortran Numerical Recipes, Vol. 1, second ed., Cambridge University Press, 1992.
[134] S. Cuperman, S. Goldstein, M. Lecar, Numerical experimental check of Lynden-Bell statistics-II. The core-halo structure and the role of the violent relaxation, Monthly Notices of the Royal Astronomical Society 146 (1969) 161–169.
[135] S. Goldstein, S. Cuperman, M. Lecar, Numerical experimental check of Lynden-Bell statistics for a collisionless one-dimensional stellar system, Monthly Notices of the Royal Astronomical Society 143 (1969) 209.
[136] M. Lecar, L. Cohen, Numerical experiments on Lynden-Bell's statistics, Astrophysics and Space Science 13 (2) (1971) 397. http://dx.doi.org/10.1007/BF00649169.
[137] S.J. Aarseth, M. Lecar, Computer simulations of stellar systems, Annual Review of Astronomy and Astrophysics 13 (1975) 1. URL http://adsabs.harvard.edu/full/1975ARA%26A..13....1A.
[138] P. Mineau, M. Feix, J. Rouet, Numerical simulations of violent relaxation and formation of phase space holes in gravitational systems, Astronomy and Astrophysics 228 (2) (1990) 344.
[139] Y.Y. Yamaguchi, One-dimensional self-gravitating sheet model and Lynden-Bell statistics, Physical Review E 78 (4) (2008) 1. http://dx.doi.org/10.1103/PhysRevE.78.041114.
[140] D.G. Duffy, Green's functions with applications, in: Studies in Advanced Mathematics, CRC Press, 2001.
[141] C.-S. Wu, Landau damping and resonant energy absorption, Physical Review 127 (5) (1962) 1419. http://dx.doi.org/10.1103/PhysRev.127.1419.
[142] D. Sagan, On the physics of Landau damping, American Journal of Physics 62 (5) (1994) 450. http://dx.doi.org/10.1119/1.17547.
[143] L.D. Landau, On the vibrations of the electronic plasma, Journal of Physics (USSR) (2013).
[144] R. Gluckstern, Analytic model for halo formation in high current ion linacs, Physical Review Letters 73 (9) (1994) 1247–1250. http://dx.doi.org/10.1103/PhysRevLett.73.1247.
[145] H. Goldstein, C.P. Poole, J.L. Safko, Classical Mechanics, third ed., Addison Wesley, 2001.
[146] P.-H. Chavanis, C. Sire, Virial theorem and dynamical evolution of self-gravitating Brownian particles in an unbounded domain: II. Inertial models, Physical Review E: Statistical, Nonlinear, and Soft Matter Physics 73 (6) (2006) 066104. http://dx.doi.org/10.1103/PhysRevE.73.066104.
[147] G.B. Arfken, H.J. Weber, F. Harris, Mathematical Methods for Physicists, fifth ed., Academic Press, 2001.
[148] W. Simeoni, F.B. Rizzato, R. Pakter, Nonlinear coupling between breathing and quadrupole-like oscillations in the transport of mismatched beams in continuous magnetic focusing fields, Physics of Plasmas 13 (6) (2006) 063104. http://dx.doi.org/10.1063/1.2208293.
[149] F.B. Rizzato, R. Pakter, Y. Levin, Wave breaking and particle jets in intense inhomogeneous charged beams, Physics of Plasmas 14 (11) (2007) 110701. http://dx.doi.org/10.1063/1.2802072.
[150] F.B. Rizzato, R. Pakter, Y. Levin, Driven one-component plasmas, Physical Review E: Statistical, Nonlinear, and Soft Matter Physics 80 (2009) 021109. http://dx.doi.org/10.1103/PhysRevE.80.021109.
[151] F. Hohl, D.T. Broaddus, Thermalization effects in a one-dimensional self-gravitating system, Physics Letters A 25 (10) (1967) 713. http://dx.doi.org/10.1016/0375-9601(67)90956-5.
[152] T. Tsuchiya, N. Gouda, T. Konishi, Relaxation processes in one-dimensional self-gravitating many-body systems, Physical Review E 53 (3) (1996) 2210–2216. URL http://pre.aps.org/abstract/PRE/v53/i3/p2210_1.
[153] F. Hohl, Numerical experiments with a disk of stars, Astrophysical Journal 168 (1971) 343. http://dx.doi.org/10.1086/151091.
[154] A. Doroshkevich, E. Kotok, I. Novikov, A. Poliudov, S. Shandarin, Y.S. Sigov, Two-dimensional simulation of the gravitational system dynamics and formation of the large-scale structure of the universe, Monthly Notices of the Royal Astronomical Society 192 (1980) 321.
[155] J. Aly, Thermodynamics of a two-dimensional self-gravitating system, Physical Review E 49 (5) (1994) 3771. http://dx.doi.org/10.1103/PhysRevE.49.3771.

[156] J.-J. Aly, J. Perez, Thermodynamics of a two-dimensional unbounded self-gravitating system, Physical Review E 60 (5) (1999) 5185. http://dx.doi.org/10.1103/PhysRevE.60.5185.
[157] B. Marcos, Collisional relaxation of two-dimensional gravitational systems, Physical Review E 88 (2013) 032112. http://dx.doi.org/10.1103/PhysRevE.88.032112.
[158] J. Binney, Discreteness effects in cosmological N-body simulations, Monthly Notices of the Royal Astronomical Society 350 (3) (2004) 939. http://dx.doi.org/10.1111/j.1365-2966.2004.07699.x.
[159] R.N. Henriksen, Isolated and non-isolated dark matter haloes and the Navarro, Frenk and White profile, Monthly Notices of the Royal Astronomical Society 366 (2) (2006) 697. http://dx.doi.org/10.1111/j.1365-2966.2005.09915.x.
[160] C.J. Saxton, Galaxy stability within a self-interacting dark matter halo, Monthly Notices of the Royal Astronomical Society 430 (3) (2013) 1578. http://dx.doi.org/10.1093/mnras/sts689.
[161] G. de Vaucouleurs, Recherches sur les Nébuleuses extragalactiques, Annales d'Astrophysique 11 (1948) 247.
[162] J.L. Sérsic, Influence of the atmospheric and instrumental dispersion on the brightness distribution in a galaxy, Boletin de la Asociacion Argentina de Astronomia La Plata Argentina 6 (1963) 41.
[163] J. Hjorth, J. Madsen, Small deviations from the $R^{1/4}$ law, the fundamental plane, and phase densities of elliptical galaxies, Astrophysical Journal 445 (1995) 55. http://dx.doi.org/10.1086/175672.
[164] J.F. Navarro, C.S. Frenk, S.D.M. White, The structure of cold dark matter halos, The Astrophysical Journal 462 (1996) 563. http://dx.doi.org/10.1086/177173.
[165] J.F. Navarro, C.S. Frenk, S.D. White, A Universal density profile from hierarchical clustering, The Astrophysical Journal 490 (2) (1997) 493. http://dx.doi.org/10.1086/304888.
[166] L.L.R. Williams, J. Hjorth, Statistical mechanics of collisionless orbits. II. Structure of halos, Astrophysical Journal 722 (1) (2010) 856. http://dx.doi.org/10.1088/0004-637X/722/1/856.
[167] L.L.R. Williams, J. Hjorth, R. Wojtak, Statistical mechanics of collisionless orbits. III. Comparison with N-body simulations, The Astrophysical Journal 725 (1) (2010) 282. http://dx.doi.org/10.1088/0004-637X/725/1/282.
[168] J. Hjorth, L. Williams, Statistical mechanics of collisionless orbits. I. Origin of central cusps in dark-matter halos, The Astrophysical Journal 722 (2010) 851. http://dx.doi.org/10.1088/0004-637X/722/1/851.
[169] P.-H. Chavanis, J. Sommeria, Degenerate equilibrium states of collisionless stellar systems, Monthly Notices of the Royal Astronomical Society 296 (3) (1998) 569. http://dx.doi.org/10.1046/j.1365-8711.1998.01414.x.
[170] D. DuBois, V. Gilinsky, M. Kivelson, Collision damping of plasma oscillations, Physical Review Letters 8 (11) (1962) 419–421. http://dx.doi.org/10.1103/PhysRevLett.8.419.
[171] R. Balescu, Equilibrium and nonequilibrium statistical mechanics, NASA STI/Recon Technical Report A 76 (1975) 32809.
[172] R.P. Nunes, R. Pakter, F.B. Rizzato, Simplified self-consistent model for emittance growth in charged beams with mismatched envelopes, Physics of Plasmas 14 (2) (2007) 023104. http://dx.doi.org/10.1063/1.2472294.
[173] S. Banna, L. Schächter, Analytic method for evaluation of the field of a charge traversing a geometric discontinuity, Applied Physics Letters 80 (2002) 2842. http://dx.doi.org/10.1063/1.1472477.
[174] Y. Chekh, A. Goncharov, I. Protsenko, I.G. Brown, Effect of the electrostatic plasma lens on the emittance of a high-current heavy ion beam, Applied Physics Letters 86 (2005) 041502. http://dx.doi.org/10.1063/1.1855428.
[175] P. Muggli, B. Blue, C. Clayton, F. Decker, M. Hogan, C. Huang, C. Joshi, T. Katsouleas, W. Lu, W. Mori, C. O'Connell, R. Siemann, D. Walz, M. Zhou, Halo formation and emittance growth of positron beams in plasmas, Physical Review Letters 101 (5) (2008) 1–4. http://dx.doi.org/10.1103/PhysRevLett.101.055001.
[176] C. Chen, R. Pakter, Mechanisms and control of beam halo formation in intense microwave sources and accelerators, Physics of Plasmas 7 (5) (2000) 2203. http://dx.doi.org/10.1063/1.874042.
[177] M. Hess, C. Chen, Confinement criterion for a highly bunched beam, Physics of Plasmas 7 (12) (2000) 5206. http://dx.doi.org/10.1063/1.1319639.
[178] J.S. Moraes, R. Pakter, F.B. Rizzato, Equilibrium and stability of off-axis periodically focused particle beams, Physical Review Letters 93 (24) (2004) 244801. http://dx.doi.org/10.1103/PhysRevLett.93.244801.
[179] J.S. Moraes, R. Pakter, F.B. Rizzato, Centroid motion in periodically focused beams, Physics of Plasmas 12 (2) (2005) 023104. http://dx.doi.org/10.1063/1.1848546.
[180] M. Hess, Off-axis space-charge limit for a bunched electron beam in a coaxial conducting structure, IEEE Transactions on Plasma Science 36 (3) (2008) 729. http://dx.doi.org/10.1109/TPS.2008.917163.
[181] L.C. Martins, F.B. Rizzato, R. Pakter, Off-axis stability of intense continuous relativistic beams, Journal of Applied Physics 106 (4) (2009) 043305. http://dx.doi.org/10.1063/1.3204972.
[182] P.S. Babu, A. Goswami, V.S. Pandit, A Vlasov equilibrium for space charge dominated beam in a misaligned solenoidal channel, Physics of Plasmas 19 (8) (2012) 080702. http://dx.doi.org/10.1063/1.4747694.
[183] S. Bernal, R.A. Kishek, M. Reiser, I. Haber, Observations and simulations of transverse density waves in a collimated space-charge dominated electron beam, Physical Review Letters 82 (20) (1999) 4002. http://dx.doi.org/10.1103/PhysRevLett.82.4002.
[184] S.G. Anderson, J.B. Rosenzweig, Nonequilibrium transverse motion and emittance growth in ultrarelativistic space-charge dominated beams, Physical Review Special Topics - Accelerators and Beams 3 (2000) 094201. http://dx.doi.org/10.1103/PhysRevSTAB.3.094201.
[185] S.M. Lund, D.P. Grote, R.C. Davidson, Simulations of beam emittance growth from the collective relaxation of space-charge nonuniformities, Nuclear Instruments & Methods in Physics Research, Section A: Accelerators, Spectrometers, Detectors, and Associated Equipment 544 (1–2) (2005) 472. http://dx.doi.org/10.1016/j.nima.2005.01.280.
[186] B.L. Qian, J. Zhou, C. Chen, Image-charge effects on the envelope dynamics of an unbunched intense charged-particle beam, Physical Review Special Topics - Accelerators and Beams 6 (1) (2003) 014201. http://dx.doi.org/10.1103/PhysRevSTAB.6.014201.
[187] J. Zhou, B.L. Qian, C. Chen, Chaotic particle motion and beam halo formation induced by image-charge effects in a small-aperture alternating-gradient focusing system, Physics of Plasmas 10 (11) (2003) 4203. http://dx.doi.org/10.1063/1.1622388.
[188] R. Pakter, Y. Levin, F.B. Rizzato, Image effects on the transport of intense nonaxisymmetric charged beams, Applied Physics Letters 91 (25) (2007) 251503. http://dx.doi.org/10.1063/1.2827580.
[189] J.S. O'Connell, T.P. Wangler, R.S. Mills, K.R. Crandall, Beam halo formation from space-charge dominated beams in uniform focusing channels, in: Proceedings of the 1993 Particle Accelerator Conference, Vol. 5, 1993, p. 3657. http://dx.doi.org/10.1109/PAC.1993.309749.
[190] J.D. Jackson, Classical Electrodynamics, third ed., Wiley, 1998.
[191] T. Teles, R. Pakter, Y. Levin, Emittance growth and halo formation in the relaxation of mismatched beams, Physical Review Special Topics - Accelerators and Beams 13 (11) (2010) 1–8. http://dx.doi.org/10.1103/PhysRevSTAB.13.114202.
[192] A. Gabrielli, M. Joyce, B. Marcos, Quasistationary states and the range of pair interactions, Physical Review Letters 105 (21) (2010) 1–4. http://dx.doi.org/10.1103/PhysRevLett.105.210602.
[193] A. Gabrielli, M. Joyce, B. Marcos, F. Sicard, A dynamical classification of the range of pair interactions, Journal of Statistical Physics 141 (6) (2010) 970–989. http://dx.doi.org/10.1007/s10955-010-0090-x.
[194] E. Hairer, C. Lubich, G. Wanner, Geometric Numerical Integration: Structure-Preserving Algorithms for Ordinary Differential Equations, second ed., Springer, 2006.
[195] T. Konishi, K. Kaneko, Clustered motion in symplectic coupled map systems, Journal of Physics A: Mathematical and General 25 (23) (1992) 6283. http://dx.doi.org/10.1088/0305-4470/25/23/023.
[196] M. Antoni, S. Ruffo, Clustering and relaxation in Hamiltonian long-range dynamics, Physical Review E 52 (3) (1995) 2361–2374. http://dx.doi.org/10.1103/PhysRevE.52.2361.

[197] V. Latora, A. Rapisarda, S. Ruffo, Superdiffusion and out-of-equilibrium chaotic dynamics with many degrees of freedoms, Physical Review Letters 83 (11) (1999) 2104. http://dx.doi.org/10.1103/PhysRevLett.83.2104.
[198] A. Pluchino, V. Latora, A. Rapisarda, Glassy phase in the Hamiltonian mean-field model, Physical Review E 69 (2004) 056113. http://dx.doi.org/10.1103/PhysRevE.69.056113.
[199] A. Antoniazzi, D. Fanelli, J. Barré, P.-H. Chavanis, T. Dauxois, S. Ruffo, Maximum entropy principle explains the quasistationary states in systems with long-range interactions: the example of the Hamiltonian mean-field model, Physical Review E 75 (2007) 011112. http://dx.doi.org/10.1103/PhysRevE.75/011112.
[200] R. Bachelard, C. Chandre, D. Fanelli, X. Leoncini, S. Ruffo, Abundance of regular orbits and nonequilibrium phase transitions in the thermodynamic limit for long-range systems, Physical Review Letters 101 (26) (2008) 260601–260603. http://dx.doi.org/10.1103/PhysRevLett.101.260603.
[201] N.D. Mermin, H. Wagner, Absence of ferromagnetic or antiferromagnetism in one- or two-dimensional isotropic Heisenberg models, Physical Review Letters 17 (22) (1966) 1133. http://dx.doi.org/10.1103/PhysRevLett.17.1133.
[202] F. Tamarit, C. Anteneodo, Rotators with long-range interactions: connection with the mean-field approximation, Physical Review Letters 84 (2) (2000) 208. http://dx.doi.org/10.1103/PhysRevLett.84.208.
[203] S. De Nigris, X. Leoncini, Emergence of a non-trivial fluctuating phase in the XY-rotors model on regular networks, EPL (Europhysics Letters) 101 (1) (2013) 10002. http://dx.doi.org/10.1209/0295-5075/101/10002.
[204] P. Valageas, Thermodynamics and dynamics of a 1-D gravitational system, Astronomy & Astrophysics 450 (2) (2006) 445. http://dx.doi.org/10.1051/0004-6361:20054472.
[205] J. Dawson, One-dimensional plasma model, Physics of Fluids 5 (4) (1962) 445.
[206] W.B. Colson, Theory of a free electron laser, Physics Letters A 59 (3) (1976) 187. http://dx.doi.org/10.1016/0375-9601(76)90561-2.
[207] R. Bonifacio, C. Pellegrini, L.M. Narducci, Collective instabilities and high-gain regimei in a free electron laser, Optics Communications 50 (6) (1984) 373. http://dx.doi.org/10.1016/0030-4018(84)90105-6.
[208] J. Barré, F. Bouchet, T. Dauxois, S. Ruffo, Large deviation techniques applied to systems with long-range interactions, Journal of Statistical Physics 119 (3) (2005) 677–713. http://dx.doi.org/10.1007/s10955-005-3768-8.
[209] A. Antoniazzi, Y. Elskens, D. Fanelli, S. Ruffo, Statistical mechanics and Vlasov equation allow for a simplified Hamiltonian description of single-pass free electron laser saturated dynamics, The European Physical Journal B 50 (4) (2006) 603–611. http://dx.doi.org/10.1140/epjb/e2006-00175-0.
[210] J. Barré, F. Bouchet, T. Dauxois, S. Ruffo, Birth and long-time stabilization of out-of-equilibrium coherent structures, European Physical Journal B: Condensed Matter Physics 29 (4) (2002) 577. http://dx.doi.org/10.1140/epjb/e2002-00342-3.
[211] H. Morita, K. Kaneko, Collective oscillation in a Hamiltonian system, Physical Review Letters 96 (2006) 050602. http://dx.doi.org/10.1103/PhysRevLett.96.050602.
[212] R. Pakter, Y. Levin, Topology of collisionless relaxation, Physical Review Letters 110 (14) (2013) 140601. http://dx.doi.org/10.1103/PhysRevLett.110.140601.
[213] A. Campa, P.-H. Chavanis, Caloric curves fitted by polytropic distributions in the HMF model, The European Physical Journal B 86 (2013) 170. http://dx.doi.org/10.1140/epjb/e2013-30947-0.
[214] H. Yoshida, Construction of higher order symplectic integrators, Physics Letters A 150 (5–7) (1990) 262. http://dx.doi.org/10.1016/0375-9601(90)90092-3.
[215] E. Hairer, Fortran and Matlab Codes, Website, 2004, URL http://www.unige.ch/~hairer/software.html.
[216] A. Antoniazzi, D. Fanelli, S. Ruffo, Y.Y. Yamaguchi, Nonequilibrium tricritical point in a system with long-range interactions, Physical Review Letters 99 (4) (2007) 2–5. http://dx.doi.org/10.1103/PhysRevLett.99.040601.
[217] T.M.R. Filho, M.A. Amato, A. Figueiredo, Nonequilibrium phase transitions and violent relaxation in the Hamiltonian mean-field model, Physical Review E 85 (6) (2012) 062103. http://dx.doi.org/10.1103/PhysRevE.85.062103.
[218] F. Staniscia, P. Chavanis, G. De Ninno, D. Fanelli, Out-of-equilibrium phase re-entrance(s) in long-range interacting systems, Physical Review E 80 (2) (2009) 1. http://dx.doi.org/10.1103/PhysRevE.80.021138.
[219] P.-H. Chavanis, Lynden-Bell and Tsallis distributions for the HMF model, European Physical Journal B: Condensed Matter Physics 53 (2006) 487. http://dx.doi.org/10.1140/epjb/e2006-00405-5.
[220] M. Assllani, D. Fanelli, A. Turchi, T. Carletti, X. Leoncini, Statistical theory of quasistationary states beyond the single water-bag case study, Physical Review E 85 (2) (2012) 021148. http://dx.doi.org/10.1103/PhysRevE.85.021148.
[221] T.M.R. Filho, Solving the Vlasov equation for one-dimensional models with long range interactions on a GPU, Computer Physics Communications 184 (1) (2013) 34. http://dx.doi.org/10.1016/j.cpc.2012.08.005.
[222] F. Bouchet, S. Gupta, D. Mukamel, Thermodynamics and dynamics of systems with long-range interactions, Physica A: Statistical Mechanics and its Applications 389 (2010) 4389. http://dx.doi.org/10.1016/j.physa.2010.02.024.
[223] T.M. Rocha Filho, A.E. Santana, J.R.S. Moura, M.A. Amato, A. Figueiredo, Dynamics and physical interpretation of quasi-stationary states in systems with long-range interactions. ArXiv e-prints arXiv:1305.2903.
[224] A. Figueiredo, T.M. Rocha Filho, A.E. Santana, M.A. Amato, Scaling of the dynamics of homogeneous states of one-dimensional long-range interacting systems. ArXiv e-prints arXiv:1305.4417.
[225] P.H. Chavanis, Kinetic theory of spatially homogeneous systems with long-range interactions: I. General results, The European Physical Journal Plus 127 (2012) 19. http://dx.doi.org/10.1140/epjp/i2012-12019-9.
[226] T.N. Teles, F.P.da C. Benetti, R. Pakter, Y. Levin, Nonequilibrium phase transitions in systems with long-range interactions, Physical Review Letters 109 (2012) 230601. http://dx.doi.org/10.1103/PhysRevLett.109.230601.
[227] D. Lee, G. Grinstein, Strings in two-dimensional classical XY models, Physical Review Letters 55 (5) (1985) 541–544. http://dx.doi.org/10.1103/PhysRevLett.55.541.
[228] F.C. Poderoso, J.J. Arenzon, Y. Levin, New ordered phases in a class of generalized XY models, Physical Review Letters 106 (6) (2011) 067202. http://dx.doi.org/10.1103/PhysRevLett.106.067202.
[229] R. Pakter, Y. Levin, Non-equilibrium dynamics of an infinite range *XY* model in an external field, Journal of Statistical Physics 150 (3) (2013) 531. http://dx.doi.org/10.1007/s10955-012-0576-9.
[230] A. Patelli, S. Gupta, C. Nardini, S. Ruffo, Linear response theory for long-range interacting systems in quasistationary states, Physical Review E 85 (2) (2012) 021133. http://dx.doi.org/10.1103/PhysRevE.85.021133.
[231] C. Tsallis, Introduction to Nonextensive Statistical Mechanics, Springer, 2009.
[232] L.A. Aguilar, D. Merritt, The structure and dynamics of galaxies formed by cold dissipationless collapse, The Astrophysical Journal 354 (1990) 33. http://dx.doi.org/10.1086/168665.

Chapter 8

Final considerations and conclusions

Systems with long-range interactions present peculiarities in their dynamical and equilibrium properties, with respect to the short-range interacting systems that are typically treated by statistical mechanics. From a dynamical perspective, the predominance of the mean-field results in a collisionless relaxation process which leads to long-lived quasi-stationary states that do not have a Maxwell-Boltzmann velocity distribution. These quasi-stationary states depend not only on the mean energy (or temperature, or other typical thermodynamic variables), but on the explicit form of the initial distribution. For example, initial distributions of the WB type whose ratio of mean kinetic and potential energy is not virialised can lead to a core-halo configuration. The formation of such structures depends on wave-particle resonances, a dynamical feature which cannot be taken into account by traditional statistical mechanics. If, on the other hand, the initial state satisfies the virial theorem, then oscillations are minimal and there is little halo formation. This had been demonstrated for several LRI systems. We showed that it is also valid for the HMF model, after determining a generalized virial condition based on the envelope equation technique of plasma physics.

The quasi-stationary states correspond to stationary solutions of the Vlasov (collisionless) dynamics, which is valid in the limit $N \to \infty$. However, for finite-size systems, the Vlasov dynamics is only the zero-order approximation. The kinetic equations resulting from the next order —the quasi-linear approximation— are the Landau and the Lenard-Balescu equations. They give the secular evolution of the one-particle distribution function, with terms that scale at least as $\mathcal{O}[1/N]$. These terms are responsible for driving the distribution to thermodynamic equilibrium, but only on timescales $\tau_R \sim N^\delta$ where $\delta > 0$ depends on the LR interaction. Once the equilibrium state is achieved, equilibrium statistical mechanics can be used to describe it. Even so, features such as ensemble inequivalence may be observed near phase transitions.

In this thesis, we have approached the statistical description of systems with long-range interactions through several of these aspects: first, by characterizing the quasi-stationary states using approaches based on opposing assumptions to see which best represents the dynamics in the QSS. The first approach, Lynden-Bell statistics, takes advantage of the

incompressibility of the Vlasov flow to perform a Boltzmann-counting of phase density elements in a discretized phase space. Thus, it is is possible to define a coarse-grained entropy. To find the QSS distributions, this entropy should be maximized respecting the appropriate constraints. The second approach is that of uncoupled, self-consistent particle dynamics: the integrable model. It consists of noninteracting particles evolving under a static potential, which phase-mix over constant energy orbits. The static potential is self-consistently calculated according to the stationary distribution after phase-mixing. The opposing assumptions of both approaches are ergodicity and efficient mixing (LB statistics) and integrability (IM dynamics).

These methods were applied to both the HMF model and to three-dimensional self-gravitating systems. For the HMF model, we expanded our generalized virial condition for multilevel WB distributions. Comparing LB and IM results, we show that the distributions obtained from the IM are a much better match with molecular dynamics than LB statistics.

For the self-gravitating system, we generalized the IM from the uncoupled pendula of de Buyl *et al*, where the only unknown to be determined self-consistently is the field H, to the gravitational IM, where the self-consistent potential has to be determined as a function of r. This led to very good results compared with molecular dynamics as well, providing a direct and simple method for determining the marginal distributions of spherically-symmetric self-gravitating systems that are close to virial equilibrium.

These results, together with the previous success of the core-halo distribution in describing QSS resulting from strong mean-field oscillations, indicate that the QSS is more integrable than ergodic. The topic of ergodicity breaking, however, is still active; other works which use quantitative measures of ergodicity such as comparison of time and ensemble averages and sojourn times show differing results. If a system is nonergodic, ensemble and time averages will differ, and sojourn times (the time the system spends in a given state) will follow a distribution with a power-law tail. For the HMF model, ergodicity is established after times that scale with N, so in the limit $N \to \infty$ it is broken [113]. For two-dimensional self-gravitating systems, the timescale is very long compared to a short-range interacting system, but does not depend on N [114]. The relation of these quantitative measures with our results, which are based on characterizing the QSS with models that imply nonergodicity, is a topic that can be investigated.

Second, after focusing on the QSS, we examined the relaxation to equilibrium. We proposed a short-range coupling between two HMF systems to see how the coupling intensity could affect the timescale of relaxation τ_R as well as the presence of chaotic orbits. In the mean-field limit, with a stationary magnetization, the HMF model should not present chaos. With a coupling between two degrees of freedom, however, chaotic orbits may arise. We showed a correlation between the presence of chaotic orbits and the decrease in the exponent δ of the timescale $\tau_R \sim N^\delta$, but only for very weak coupling.

Our second work on relaxation to equilibrium was focused on the kinetic equations themselves. Based on the Landau and Lenard-Balescu equations in action-angle variables proposed

by Chavanis, we calculated theoretical diffusion coefficients for the associated Fokker-Planck equations. The two kinetic equations result in different diffusion coefficients, seeing as the Landau one neglects collective effects while the Lenard-Balescu equation preserves them (through a dielectric function). We proposed a method of removing collective effects from the molecular dynamics of the HMF model by having test particles interact with a bath who is subject to a stationary magnetization. In this way, the bath does not have collective effects, since its internal perturbations do not affect its dynamics. Then, comparing diffusion coefficients obtained from the bath molecular dynamics setup and the full HMF molecular dynamics with their theoretical counterparts (obtained from the Landau and Lenard-Balescu equations, respectively), we saw that they match very well, for several different distributions. We showed that the inclusion of collective effects is very important in the HMF model, due to the qualitative and quantitative difference between the Landau and Lenard-Balescu diffusion coefficients.

Finally, the third aspect of this thesis concerns the equilibrium states themselves. We introduced a long-range version of an XY model with ferromagnetic and nematic coupling, the GHMF model, and calculated its equilibrium variables in the microcanonical and canonical ensembles. Using these results, we constructed phase diagrams and showed regions of negative specific heat and inequivalence between the two ensembles. These phase diagrams also differ significantly from a nonequilibrium phase diagram of the same system, published in a different work. In order to predict the transition lines of the nonequilibrium diagram, we analyzed the dynamical stability of the homogeneous state; since it is nonequilibrium and refers to phases of the QSS, equilibrium statistical mechanics does not apply.

Through these three aspects, we have made a broad examination of several phenomena peculiar to LRI systems. Many branches have also been opened to be explored in the future. For example, a theory is still needed to describe the core-halo configurations of the multilevel WB distributions used in our work with the HMF model. Regarding the collisional relaxation, our calculation of the diffusion coefficients now allows us to apply them in numerical integration of the Fokker-Planck equation in action-angle variables for the inhomogeneous HMF, or its associated Langevin equation. We may also apply our calculations to other one-dimensional potentials and verify if the collective effects remain as important as they are for the HMF model, or if it is an anomaly. Another interesting prospect is to continue our study of chaos and relaxation, by constructing other systems with chaotic orbits in the smooth, mean-field limit, to shed light on our results with the HMF-ladder model. One possibility is Schwarzschild's method of constructing triaxial mass distributions that obey Jeans' theorem (and so are stable) [115], to study their relaxation timescale compared with symmetric distributions. By these advances, we hope to have provided a good basis for continuing research on both the QSS and its characterization, as well as the relaxation processes.

Appendix A

Numerical simulation

The results presented in this thesis relied heavily on molecular dynamics simulations and numerical computations. The programs were developed in the languages Fortran 90 and C/CUDA. In this appendix, I present an outline of the methods used in each work.

A.1 Molecular dynamics

Molecular dynamics consists in integrating the equations of motion of N particles and following their evolution. Almost all the systems studied have time-independent Hamiltonians, with the exception of the test particles used in sections 4.1 and 4.4. Therefore, the molecular dynamics was carried out in the microcanonical ensemble, with the total energy conserved up to a desired tolerance dependant on the system and integration method.

The basic outline of all molecular dynamics programs is

1. Read input with simulation parameters; most importantly, number of particles N and desired initial distribution;
2. Generate initial values of position θ and momentum p for every particle according the desired initial distribution;
3. Calculate the total force on each particle;
4. Integrate the equations of motion of each particle for a time step Δt;
5. At certain time intervals, print output (usually, phase space coordinates of the N particles, total energy (to ensure the integrator conserves energy at a desired precision), etc.
6. Return to step 3 until final simulation time is achieved.

A.1.1 Initial particle distributions

In the Fortran 90 programs, the initial position q_i^0 and momentum p_i^0 of the ith particle is determined by the random number generator ran2, available in Reference [116]. The generator ran2 gives a real number x following a uniform probability distribution for $x \in [0,1]$. For an initial waterbag distribution in one dimension,

$$f_{wb}^{1d} = \frac{1}{4q_m p_m}\Theta(q_m - |q|)\Theta(p_m - |p|), \tag{A.1}$$

q_i^0 and p_i^0 are obtained from x simply by expanding the uniform probability range from [0,1] to $[-q_m,q_m]$ and $[-p_m,p_m]$, respectively. The limits q_m and p_m must be determined by the desired initial potential and kinetic energy. For example, in the HMF model (see chapter 4, the position coordinate is $q = \theta$, and the limit θ_m is given by the initial magnetization $M_0 = \langle\cos\theta\rangle_0 = \int \mathrm{d}p\mathrm{d}\theta \cos\theta f_{wb}^{1d}(\theta,p) = \sin\theta_m/\theta_m$. The magnetization determines the initial potential energy. Then, given a mean energy and initial magnetization, we also know the initial kinetic energy, and therefore p_m: $\mathcal{K} = \frac{1}{2}\int \mathrm{d}\theta\mathrm{d}p p^2 f_{wb}^{1d}(\theta,p) = p_m^2/6$.

In three dimensions, more care must be taken to generate the waterbag distribution,

$$f_{wb}^{3d} = \frac{1}{16\pi^2 r_m^3 v_m^3}\Theta(r_m^2 - r^2)\Theta(v_m^2 - v^2). \tag{A.2}$$

The coordinates $\mathbf{r}_i = (x_i,y_i,z_i)$ are then generated in the following way, for each i:

1. Generate three numbers $\alpha_i,\beta_i,\gamma_i \in [0,1]$ using the ran2 function;
2. Calculate $a_i = r_m^3\alpha_i$, $b_i = 2\beta_i - 1$ and $c = 4_i\pi * \gamma_i$;
3. Calculate the Cartesian coordinates $x_i = a_i^{1/3}\sqrt{1-b_i^2}\cos c_i$, $y_i = a_i^{1/3}\sqrt{1-b^2}\sin c_i$, $z_i = a_i^{1/3}b_i$.

The same is done for the velocity $\mathbf{v}_i = (v_{x,i},v_{y,i},v_{z,i})$.

More complicated distributions were generated using different methods. The rejection method was used for the parabolic-type distribution $f_p^{3d}(r,v) = \eta(r_m^2 - r^2)\Theta(r_m^2 - r^2)\Theta(v_m^2 - v^2)$ used in section 6.1. For the Gaussian distributions used in section 4.4, the Ziggurat algorithm was used, described in reference [117] with source code available in the website [118] under the GNU LGPL license.

For the molecular dynamics programs written using C, the same methods were used, replacing the random number generator ran2 with the C function rand(). This function gives an integer in the range [0,RAND_MAX], so each generated number must be transformed into floating point and divided by RAND_MAX to give a real number $x \in [0,1]$.

A.1.2 Integrating the equations of motion

After generating the phase space coordinates $\left(\{\mathbf{q}_i\}_{i=1}^N,\{\mathbf{p}_i\}_{i=1}^N\right)$, the evolution of the system is determined by integrating the equations of motion

$$\dot{q}_i^\alpha = \frac{p_i^\alpha}{m}, \tag{A.3}$$

$$\dot{p}_i^\alpha = -\frac{\partial \mathcal{H}}{\partial q_i^\alpha}, \tag{A.4}$$

where $\alpha = 1,\ldots,d$ and d is the spatial dimension (for example, in $d = 3$, $q^1 = x$,$q^2 = y$,$q^3 = z$).

In the Fortran 90 programs, numerical integrators available online were used. For the HMF model (chapter 4), integration was performed using the GNI_COMP algorithm described in reference [119] and made available in the website [120]. This method integrates second-order differential equations. In the case of the HMF and GHMF models,

$$\begin{aligned} \ddot{\theta}_i &= -M\sin\theta_i, \\ M &= \frac{1}{N}\sum_{i=1}^N \cos\theta_i \end{aligned} \tag{A.5}$$

if M is taken as symmetric around $\theta = 0$ or

$$\begin{aligned} \ddot{\theta}_i &= -M_x\sin\theta_i + M_y\cos\theta_i, \\ M_x &= \frac{1}{N}\sum_{i=1}^N \cos\theta_i, \\ M_y &= \frac{1}{N}\sum_{i=1}^N \sin\theta_i \end{aligned} \tag{A.6}$$

if the center of mass of the particles is allowed to fluctuate. The latter case is only used in the "MD(full)" simulations described in section 4.4.

Molecular dynamics of the three-dimensional self-gravitating systems were performed in two different ways: the first was using the "shell" method, in which we consider that each particle corresponds to a mass m uniformly distributed over a spherical shell with radius r_i, where i is the index of the particle. The hamiltonian in spherical coordinates is

$$\mathcal{H} = \frac{1}{2m}\sum_{i=1}^N \left(p_{r_i}^2 + \frac{p_{\theta_i}}{r_i^2} + \frac{p_{\phi_i}^2}{r_i^2\sin^2\theta_i}\right) + \frac{1}{2}\sum_{i=1}^N \psi(r_i) \tag{A.7}$$

where $\psi(r_i) = \sum_{j=1,j\neq i} Gm^2/|\mathbf{r}_i - \mathbf{r}_j|$. By Gauss' law and spherical symmetry, the force on a shell at radius r_i will depend only on the shells with radius $r < r_i$. Furthermore, the angular

momentum $\ell^2 = p_{\theta_i}^2 + p_{\phi_i}^2 / \sin^2\theta$ is conserved, so the relevant equation of motion is for r,

$$v_{r_i} = \frac{v_\ell^2}{r_i^3} - \frac{GM(r < r_i)}{r_i^2}, \tag{A.8}$$

where $v_\ell = \ell/m$ and $M(r < r_i)$ is the total mass of all shells with radius $r < r_i$. Since the mass of each shell is $1/N$, this is simply the number of shells with $r < r_i$ divided by N.

To integrate equation (A.8), the "dverk" subroutine was used, which is an adaptive step-size Runge-Kutta algorithm available online [121].

The second method for integrating the three-dimensional self-gravitating systems was full N-body simulation, without the shell approximation described above. In this case, each mass is a point particle of mass $m = 1/N$, located at $\mathbf{r}$. To simulate the evolution of the system, we integrate

$$\dot{\mathbf{v}}_i = -\frac{1}{N} \sum_{j \neq i} \frac{\mathbf{r}_i - \mathbf{r}_j}{|\mathbf{r}_i - \mathbf{r}_j|^3}. \tag{A.9}$$

The acceleration on each particle is calculated in parallel on GPUs using NVIDIA's CUDA language, based on the algorithm for N-body systems described in Ref [122]. To avoid time spent during data transfer between the GPU and CPU, the actual integration of equation (A.9) was also done on the GPU, using an implementation of the symplectic algorithm of Yoshida [123].

A.2 Other numerical methods

To obtain the diffusion coefficients in action-angle variables for the HMF model, described in section 4.4, it was necessary to evaluate elliptic integrals, integrals involving poles and principal values. In this case, all integrals were calculated numerically using routines available in the Gnu Scientific Library (GSL) for the C programming language.

Bibliography

[1] D. Ruelle, *Statistical Mechanics: Rigorous Results*. The Mathematical Physics Monograph Series, W. A. Benjamin Inc, 2 ed., 1974.

[2] H. B. Callen, *Thermodynamics and an Introduction to Thermostatics*. John Wiley & Sons, 2nd ed., 1985.

[3] A. Campa, T. Dauxois, and S. Ruffo, "Statistical mechanics and dynamics of solvable models with long-range interactions," *Physics Reports*, vol. 480, 2009.

[4] Y. Y. Yamaguchi, J. Barré, F. Bouchet, T. Dauxois, and S. Ruffo, "Stability criteria of the Vlasov equation and quasi-stationary states of the HMF model," *Physica A*, vol. 337, no. 1-2, pp. 36–66, 2004.

[5] V. Latora, A. Rapisarda, and S. Ruffo, "Superdiffusion and out-of-equilibrium chaotic dynamics with many degrees of freedoms," *Physical Review Letters*, vol. 83, no. 11, p. 2104, 1999.

[6] V. Latora, A. Rapisarda, and S. Ruffo, "Chaotic dynamics and superdiffusion in a Hamiltonian system with many degrees of freedom," *Physica A*, vol. 280, no. 1–2, p. 81, 2000.

[7] J. Barré, D. Mukamel, and S. Ruffo, "Inequivalence of Ensembles in a System with Long-Range Interactions," *Physical Review Letters*, vol. 87, no. 3, p. 030601, 2001.

[8] A. Lederhendler and D. Mukamel, "Long-Range Correlations and Ensemble Inequivalence in a Generalized ABC Model," *Physical Review Letters*, vol. 105, no. 15, p. 150602, 2010.

[9] O. Cohen and D. Mukamel, "Ensemble inequivalence: Landau theory and the ABC model," *Journal Statistical Mechanics: Theory and Experiment*, vol. 2012, p. P12017, 2012.

[10] W. Thirring, "Systems with Negative Specific Heat," *Zeitschrift für Physik*, vol. 235, no. 4, p. 339, 1970.

[11] D. Lynden-Bell, "Negative specific heat in astronomy, physics and chemistry," *Physica A*, vol. 263, p. 293, 1999.

[12] F. Bouchet and J. Barré, "Classification of Phase Transitions and Ensemble Inequivalence, in Systems with Long Range Interactions," *Journal of Statistical Physics*, vol. 118, no. 516, p. 1073, 2005.

[13] Y. Y. Yamaguchi, "Strange scaling and relaxation of finite-size fluctuation in thermal equilibrium," *Physical Review E*, vol. 94, p. 012133, 2016.

[14] T. Padmanabhan, "Statistical mechanics of gravitating systems," *Physics Reports*, vol. 188, 1990.

[15] P.-H. Chavanis and F. Bouchet, "On the coarse-grained evolution of collisionless stellar systems," *Astronomy & Astrophysics*, vol. 430, no. 3, p. 771, 2005.

[16] M. Joyce and T. Worrakitpoonpon, "Quasi-stationary states in the self-gravitating sheet model," *Physical Review E*, vol. 84, no. 1, p. 011139, 2011.

[17] Y. Elskens and D. F. Escande, *Microscopic Dynamics of Plasmas and Chaos*. CRC Press, 2002.

[18] F. Bouchet and A. Venaille, "Statistical mechanics of two-dimensional and geophysical flows," *Physics Reports*, vol. 515, 2012.

[19] M. Chalony, J. Barré, B. Marcos, A. Olivetti, and D. Wilkowski, "Long-range one-dimensional gravitational-like interaction in a neutral atomic cold gas," *Physical Review A*, vol. 87, no. 1, p. 013401, 2013.

[20] D. O'Dell, S. Giovanazzi, G. Kurizki, and V. M. Akulin, "Bose-Einstein Condensates with $1/r$ Interatomic Attraction: Electromagnetically Induced "Gravity"," *Physical Review Letters*, vol. 84, no. 25, p. 5687, 2000.

[21] P. Richerme, Z.-X. Gong, A. Lee, C. Senko, J. Smith, M. Foss-Feig, S. Michalakis, A. V. Gorshkov, and C. Monroe, "Non-local propagation of correlations in quantum systems with long-range interactions," *Nature*, vol. 511, p. 198, 2014.

[22] J. Barré, F. Bouchet, T. Dauxois, and S. Ruffo, "Large deviation techniques applied to systems with long-range interactions," *Journal of Statistical Physics*, vol. 119, no. 3, p. 677, 2005.

[23] D. Mukamel, "Statistical mechanics of systems with long range interactions," in *Dynamics and Thermodynamics of Systems with Long-Range Interactions: Theory and Experiments*. (A. Campa, A. Giansanti, G. Morigi, and F. Sylos Labini, eds.), vol. 31 of *AIP Conference Proceedings*, pp. 22–38, 2008.

[24] C. Villani, "Particle systems and nonlinear Landau damping," *Physics of Plasmas*, vol. 21, p. 030901, 2014.

[25] J. Barré, D. Métivier, and Y. Y. Yamaguchi, "Trapping scaling for bifurcations in the Vlasov systems," *Physical Review E*, vol. 93, p. 042207, 2016.

[26] T. Dauxois, S. Ruffo, and L. F. Cugliandolo, eds., *Long-Range Interacting Systems*, vol. 90 of *Lecture Notes of the Les Houches Summer School*. Oxford University Press, 2008.

[27] Y. Levin, R. Pakter, F. B. Rizzato, T. N. Teles, and F. P. C. Benetti, "Nonequilibrium Statistical Mechanics of Systems with Long-Range Interactions," *Physics Reports*, vol. 535, 2014.

[28] J. Binney and S. Tremaine, *Galactic Dynamics*. Princeton University Press, 2 ed., 2008.

[29] A. Gabrielli, M. Joyce, and B. Marcos, "Quasistationary States and the Range of Pair Interactions," *Physical Review Letters*, vol. 105, no. 21, p. 210602, 2010.

[30] A. Gabrielli, M. Joyce, B. Marcos, and F. Sicard, "A Dynamical Classification of the Range of Pair Interactions," *Journal of Statistical Physics*, vol. 141, no. 6, p. 970, 2010.

[31] M. E. Fisher, S.-k. Ma, and B. Nickel, "Critical exponents for long-range interactions," *Physical Review Letters*, vol. 29, no. 14, p. 917, 1972.

[32] A. Domínguez, M. Oettel, and S. Dietrich, "Dynamics of colloidal particles with capillary interactions," *Physical Review E*, vol. 82, p. 011402, 2010.

[33] W. B. Colson, "Theory of a free electron laser," *Physics Letters A*, vol. 59, no. 3, p. 187, 1976.

[34] R. Bonifacio, C. Pellegrini, and L. M. Narducci, "Collective instabilities and high-gain regime in a free electron laser," *Optics Communications*, vol. 50, no. 6, p. 373, 1984.

[35] J. Barré, T. Dauxois, G. De Ninno, D. Fanelli, and S. Ruffo, "Statistical theory of high-gain free-electron laser saturation," *Physical Review E*, vol. 69, no. 4, p. 045501, 2004.

[36] R. Bachelard, T. Manos, P. de Buyl, F. Staniscia, F. Cataliotti, G. De Ninno, D. Fanelli, and N. Piovella, "Experimental perspectives for systems based on long-range interactions," *Journal of Statistical Mechanics: Theory and Experiments*, vol. 2010, no. 06, p. P06009, 2010.

[37] T. Walker, D. Sesko, and C. Wieman, "Collective behavior of optically trapped neutral atoms," *Physical Review Letters*, vol. 64, p. 408, 1990.

[38] P. Jurcevic, P. Hauke, C. Maier, C. Hempel, B. P. Lanyon, R. Blatt, and C. F. Roos, "Spectroscopy of Interacting Quasiparticles in Trapped Ions," *Physical Review Letters*, vol. 115, p. 100501, 2015.

[39] T. Konishi and K. Kaneko, "Clustered motion in symplectic coupled map systems," *Journal of Physics A: Mathematical and General*, vol. 25, no. 23, p. 6283, 1992.

[40] C. Pichon, *Dynamics of self-gravitating disks*. PhD thesis, University of Cambridge, 1994.

[41] S. Inagaki and T. Konishi, "Dynamical stability of a simple model similar to self-gravitating systems," *Publications of the Astronomical Society of Japan*, vol. 45, no. 5, p. 733, 1993.

[42] M. Antoni and S. Ruffo, "Clustering and relaxation in Hamiltonian long-range dynamics," *Physical Review E*, vol. 52, no. 3, pp. 2361–2374, 1995.

[43] D. Lee and G. Grinstein, "Strings in two-dimensional classical XY models," *Physical Review Letters*, vol. 55, no. 5, pp. 541–544, 1985.

[44] F. C. Poderoso, J. J. Arenzon, and Y. Levin, "New Ordered Phases in a Class of Generalized XY Models," *Physical Review Letters*, vol. 106, no. 6, p. 067202, 2011.

[45] M. Kac, "On the Partition Function of a One-Dimensional Gas," *Physics of Fluids*, vol. 2, no. 1, pp. 8–12, 1959.

[46] M. Kac, G. E. Uhlenbeck, and P. C. Hemmer, "On the van der Waals Theory of the Vapor-Liquid Equilibrium. I. Discussion of a One-Dimensional Model," *Journal of Mathematical Physics*, vol. 4, no. 2, p. 216, 1963.

[47] K. Huang, *Statistical Mechanics*. John Wiley & Sons, 2nd ed., 1987.

[48] R. Balescu, *Equilibrium and nonequilibrium statistical mechanics*. Wiley-Interscience, 1975.

[49] P.-H. Chavanis, "Kinetic theory of spatially inhomogeneous stellar systems without collective effects," *Astron. Astrophys.*, vol. 556, 2013.

[50] F. Bouchet, S. Gupta, and D. Mukamel, "Thermodynamics and dynamics of systems with long-range interactions," *Physica A*, vol. 389, p. 4389, 2010.

[51] P. H. Chavanis, "Kinetic theory of spatially homogeneous systems with long-range interactions: I. General results," *The European Physical Journal Plus*, vol. 127, 2012.

[52] W. Braun and K. Hepp, "The Vlasov dynamics and its fluctuations in the 1/N limit of interacting classical particles," *Commun. Math. Phys.*, vol. 56, 1977.

[53] E. Caglioti and F. Rousset, "Quasi-Stationary States for Particle Systems in the Mean-Field Limit," *Journal of Statistical Physics*, vol. 129, 2007.

[54] T. M. Rocha Filho, A. Figueiredo, and M. A. Amato, "Entropy of Classical Systems with Long-Range Interactions," *Physical Review Letters*, vol. 95, no. 19, p. 190601, 2005.

[55] R. Clausius, "On a Mechanical Theorem Applicable to Heat," in *The Kinetic Theory of Gases* (S. G. Brush and N. S. Hall, eds.), History of Modern Physical Sciences, Imperial College Press, 2003.

[56] D. Lynden-Bell, "Statistical mechanics of violent relaxation in stellar systems," *Monthly Notices of the Royal Astronomical Society*, vol. 136, pp. 101–121, 1967.

[57] F. P. C. Benetti, T. N. Teles, R. Pakter, and Y. Levin, "Ergodicity Breaking and Parametric Resonances in Systems with Long-Range Interactions," *Physical Review Letters*, vol. 108, 2012.

[58] L. D. Landau, "On the vibrations of the electronic plasma," *J. Phys.(USSR)*, 1946.

[59] T. Teles, Y. Levin, and R. Pakter, "Statistical mechanics of 1D self-gravitating systems: the core-halo distribution," *Monthly Notices of the Royal Astronomical Society*, vol. 417, pp. L21–L25, 2011.

[60] T. Teles, R. Pakter, and Y. Levin, "Emittance growth and halo formation in the relaxation of mismatched beams," *Physical Review Special Topics - Accelerators and Beams*, vol. 13, no. 11, pp. 1–8, 2010.

[61] Y. Levin, R. Pakter, and T. N. Teles, "Collisionless Relaxation in Non-Neutral Plasmas," *Physical Review Letters*, vol. 100, no. 4, p. 040604, 2008.

[62] Y. Levin, R. Pakter, and F. B. Rizzato, "Collisionless relaxation in gravitational systems: From violent relaxation to gravothermal collapse," *Physical Review E*, vol. 78, no. 2, p. 021130, 2008.

[63] L. Reichl, *A Modern Course In Statistical Physics.* Wiley-Interscience, second ed., 1998.

[64] F. Hohl and J. W. Campbell, "Statistical Mechanics of a Collisionless Self-Gravitating System," *The Astronomical Journal*, vol. 73, no. 7, p. 611, 1968.

[65] S. Goldstein, S. Cuperman, and M. Lecar, "Numerical Experimental Check of Lynden-Bell Statistics for a Collisionless One-Dimensional Stellar System," *Monthly Notices of the Royal Astronomical Society*, vol. 143, p. 209, 1969.

[66] S. Cuperman, S. Goldstein, and M. Lecar, "Numerical experimental check of Lynden-Bell statistics-II. The core-halo structure and the role of the violent relaxation," *Monthly Notices of the Royal Astronomical Society*, vol. 146, pp. 161–169, 1969.

[67] Y. Y. Yamaguchi, "One-dimensional self-gravitating sheet model and Lynden-Bell statistics," *Physical Review E*, vol. 78, no. 4, p. 041114, 2008.

[68] T. N. Teles, Y. Levin, R. Pakter, and F. B. Rizzato, "Statistical mechanics of unbound two-dimensional self-gravitating systems," *Journal of Statistical Mechanics: Theory and Experiment*, vol. 2010, 2010.

[69] A. Antoniazzi, D. Fanelli, J. Barré, P.-H. Chavanis, T. Dauxois, and S. Ruffo, "Maximum entropy principle explains the quasistationary states in systems with long-range interactions: The example of the Hamiltonian mean-field model," *Physical Review E*, vol. 75, p. 011112, 2007.

[70] B. B. Kadomtsev and O. P. Pogutse, "Collisionless Relaxation in Systems with Coulomb Interactions," *Physical Review Letters*, vol. 25, p. 1155, 1970.

[71] D. Sagan, "On the physics of Landau damping," *American Journal of Physics*, vol. 62, no. 5, p. 450, 1994.

[72] R. Pakter and Y. Levin, "Core-Halo Distribution in the Hamiltonian Mean-Field Model," *Physical Review Letters*, vol. 106, p. 200603, 2011.

[73] A. C. Ribeiro-Teixeira, F. P. C. Benetti, R. Pakter, and Y. Levin, "Ergodicity breaking and quasistationary states in systems with long-range interactions," *Physical Review E*, vol. 89, 2014.

[74] A. J. Lichtenberg and M. A. Lieberman, *Regular and Chaotic Dynamics.* Applied Mathematical Sciences, Springer New York, 1992.

[75] P. de Buyl, D. Mukamel, and S. Ruffo, "Statistical mechanics of collisionless relaxation in a non-interacting system.," *Philos. Trans. R. Soc. London, Ser. A*, vol. 369, no. 1935, pp. 439–52, 2011.

[76] P. de Buyl, D. Mukamel, and S. Ruffo, "Self-consistent inhomogeneous steady states in Hamiltonian mean-field dynamics," *Physical Review E*, vol. 84, p. 061151, 2011.

[77] F. P. C. Benetti, A. C. Ribeiro-Teixeira, R. Pakter, and Y. Levin, "Nonequilibrium Stationary States of 3D Self-Gravitating Systems," *Physical Review Letters*, vol. 113, p. 100602, 2014.

[78] T. M. Rocha Filho, A. E. Santana, M. A. Amato, and A. Figueiredo, "Scaling of the dynamics of homogeneous states of one-dimensional long-range interacting systems," *Physical Review E*, vol. 90, 2014.

[79] S. Chandrasekhar, "The time relaxation of stellar systems," *Astrophy. J.*, vol. 93, 1941.

[80] D. Heggie and P. Hut, *The Gravitational Million-Body Problem.* Cambridge University Press, 2003.

[81] M. Joyce and T. Worrakitpoonpon, "Relaxation to thermal equilibrium in the self-gravitating sheet model," *Journal of Statistical Mechanics: Theory and Experiment*, vol. 2010, no. 10, p. P10012, 2010.

[82] B. Marcos, "Collisional relaxation of two-dimensional self-gravitating systems," *Physical Review E*, vol. 88, 2013.

[83] T. M. Rocha Filho, M. A. Amato, A. E. Santana, A. Figueiredo, and J. R. Steiner, "Dynamics and physical interpretation of quasistationary states in systems with long-range interactions," *Physical Review E*, vol. 89, p. 032116, Mar 2014.

[84] J. Heyvaerts, "A Balescu-Lenard-type kinetic equation for the collisional evolution of stable self-gravitating systems," *Monthly Notices of the Royal Astronomical Society*, vol. 407, 2010.

[85] S. J. Aarseth, M. Hénon, and R. Wielen, "A comparison of numerical methods for the study of star cluster dynamics," *Astronomy and Astrophysics*, vol. 37, p. 183, 1974.

[86] A. P. Lightman and S. L. Shapiro, "The distribution and consumption rate of stars around a massive, collapsed object," *Astrophysical Journal*, vol. 211, 1977.

[87] H. Cohn, "Numerical integration of the Fokker-Planck equation and the evolution of star clusters," *Astrophysical Journal*, vol. 234, p. 1036, 1979.

[88] P. Valageas, "Relaxation of a one-dimensional gravitational system," *Physical Review E*, vol. 74, no. 1, p. 1, 2006.

[89] J. Barré, A. Olivetti, and Y. Y. Yamaguchi, "Dynamics of perturbations around inhomogeneous backgrounds in the HMF model," *Journal of Statistical Mechanics: Theory and Experiment*, vol. 2010, p. P08002, 2010.

[90] P.-H. Chavanis, "Kinetic theory of long-range interacting systems with angle-action variables and collective effects," *Physica A*, vol. 391, p. 3680, 2012.

[91] A. J. Kalnajs, "Dynamics of Flat Galaxies," *Astrophysical Journal*, vol. 166, p. 275, 1971.

[92] M. Weinberg, "Self-gravitating response of a spherical galaxy to sinking satellites," *Monthly Notices of the Royal Astronomical Society*, vol. 239, p. 549, 1989.

[93] S. Chandrasekhar, "Stochastic Problems in Physics and Astronomy," *Reviews of Modern Physics*, vol. 15, no. 1, pp. 1–89, 1943.

[94] D. Mukamel, "Notes on the Statistical Mechanics of Systems with Long-Range Interactions," *arXiv:0905.1457v1*, 2009.

[95] R. S. Ellis, H. Touchette, and B. Turkington, "Thermodynamic versus statistical nonequivalence of ensembles for the mean-field blume-emery-griffiths model," *Physica A*, vol. 335, p. 518, 2004.

[96] M. Costeniuc, R. S. Ellis, and H. Touchette, "Complete analysis of phase transitions and ensemble equivalence for the curie-weiss-potts model," *Journal of Mathematical Physics*, vol. 46, p. 063301, 2005.

[97] E. Caglioti, P. L. Lions, C. Marchioro, and M. Pulvirenti, "A special class of stationary flows for two-dimensional Euler equations: a statistical mechanic description," *Communications in Mathematical Physics*, vol. 143, p. 501, 1992.

[98] M. Kiessling and T. Neukirch, "Negative specific heat of a magnetically self-confined plasma torus," *Proceedings of the National Academy of Sciences of the USA*, vol. 100, no. 4, p. 1510, 2003.

[99] P. Hertel and W. Thirring, "A soluble model for a system with negative specific heat," *Annals of Physics*, vol. 63, no. 2, p. 520, 1971.

[100] M. Kastner, "Nonequivalence of Ensembles for Long-Range Quantum Spin Systems in Optical Lattices," *Physical Review Letters*, vol. 104, p. 240403, 2010.

[101] H. Touchette, "Equivalence and Nonequivalence of Ensembles: Thermodynamic, Macrostate, and Measure Levels," *Journal of Statistical Physics*, vol. 159, p. 987, 2015.

[102] D. Mukamel, S. Ruffo, and N. Schreiber, "Breaking of Ergodicity and Long Relaxation Times in Systems with Long-Range Interactions," *Physical Review Letters*, vol. 95, p. 240604, 2005.

[103] F. Bouchet, T. Dauxois, D. Mukamel, and S. Ruffo, "Phase space gaps and ergodicity breaking in systems with long-range interactions," *Physical Review E*, vol. 77, no. 1, p. 011125, 2008.

[104] T. N. Teles, F. P. C. Benetti, R. Pakter, and Y. Levin, "Nonequilibrium phase transitions in systems with long-range interactions," *Physical Review Letters*, vol. 109, 2012.

[105] A. Pikovsky, S. Gupta, T. N. Teles, F. P. C. Benetti, R. Pakter, Y. Levin, and S. Ruffo, "Ensemble inequivalence in a mean-field XY model with ferromagnetic and nematic couplings," *Physical Review E.*, vol. 90, 2014.

[106] T. Dauxois, V. Latora, A. Rapisarda, S. Ruffo, and A. Torcini, *Dynamics and Thermodynamics of Systems with Long-Range Interactions*, vol. 602 of *Lecture Notes in Physics*, ch. The Hamiltonian Mean Field Model: From Dynamics to Statistical Mechanics and Back, pp. 458–487. Springer, 2002.

[107] D. O'Dell, S. Giovanazzi, and G. Kurizki, "Rotons in Gaseous Bose-Einstein Condensates Irradiated by a Laser," *Physical Review Letters*, vol. 90, no. 11, p. 110402, 2003.

[108] A. J. Kalnajs, "Dynamics of Flat Galaxies II Biorthonormal Surface Density-Potential Pairs for Finite Disks," *Astrophysical Journal*, vol. 205, p. 745, 1976.

[109] J. B. Fouvry, C. Pichon, and P. H. Chavanis, "Secular diffusion in discrete self-gravitating tepid discs: I. Analytic solution in the tightly wound limit," *Astronomy & Astrophysics*, vol. 581, p. A139, 2015.

[110] S. Ogawa, "Spectral and formal stability criteria of spatially inhomogeneous stationary solutions to the vlasov equation for the Hamiltonian mean-field model," *Physical Review E*, vol. 87, p. 062107, 2013.

[111] R. Pakter, B. Marcos, and Y. Levin, "Symmetry Breaking in d-Dimensional Self-Gravitating Systems," *Physical Review Letters*, vol. 111, 2013.

[112] T. M. Rocha Filho, A. E. Santana, M. A. Amato, and A. Figueiredo, "Scaling of the dynamics of homogeneous states of one-dimensional long-range interacting systems," *Physical Review E*, vol. 90, p. 032133, 2014.

[113] A. Figueiredo, T. M. Rocha Filho, M. A. Amato, Z. T. Oliveira Jr., and R. Matsushita, "Truncated Lévy flights and weak ergodicity breaking in the hamiltonian mean-field model," *Physical Review E*, vol. 89, p. 022106, 2014.

[114] C. Silvestre and T. Rocha Filho, "Ergodicity in a two-dimensional self-gravitating many-body system," *Physics Letters A*, vol. 380, p. 337, 2016.

[115] M. Schwarzschild, "A numerical model for a triaxial stellar system in dynamical equilibrium," *Astrophysical Journal*, vol. 232, p. 236, 1979.

[116] W. H. Press, S. A. Teukolsky, W. T. Vetterling, and B. P. Flannery, *Numerical Recipes: The Art of Scientific Computing*. Cambridge University Press, 2 ed., 1992.

[117] "The Ziggurat Method For Generating Random Variables," *Journal of Statistical Software*, vol. 5, 2000.

[118] J. Burkardt, "Fortran 90 software," 2010.

[119] E. Hairer, C. Lubich, and G. Wanner, *Geometric Numerical Integration: Structure-Preserving Algorithms for Ordinary Differential Equations*. Springer, 2 ed., 2006.

[120] E. Hairer, "Fortran and Matlab Codes," 2004. http://www.unige.ch/~hairer/software.html.

[121] K. R. Jackson. http://www.netlib.no/netlib/ode/dverk.f.

[122] H. Nguyen, *Gpu gems 3*. Addison-Wesley Professional, 2007.

[123] H. Yoshida, "Construction of higher order symplectic integrators," *Phys. Lett. A*, vol. 150, no. 5-7, p. 262, 1990.